RICE UNIVERSITY

Novel Exogenous Agents for Improving Articular Cartilage Tissue Engineering

by

Donald Joseph Responte

A THESIS SUBMITTED
IN PARTIAL FULFILLMENT OF THE
REQUIREMENTS FOR THE DEGREE

Doctor of Philosophy

APPROVED, THESIS COMMITTEE:

Kyriacos Athanasiou, Ph.D., Thesis Director
Distinguished Professor
Department of Biomedical Engineering
University of California, Davis

Antonios Mikos, Ph.D., Committee Chair
Louis Calder Professor
Department of Bioengineering
Rice University

Jun Lou, Ph.D.
Assistant Professor
Department of Mechanical Engineering
Rice University

HOUSTON, TEXAS
OCTOBER 2011

ABSTRACT

Novel Exogenous Agents for Improving Articular Cartilage Tissue Engineering

by

Donald Joseph Responte

This thesis demonstrated the effects of exogenous stimuli on engineered articular cartilage constructs and elucidated mechanisms underlying the responses to these agents. In particular, a series of studies detailed the effects of chondroitinase-ABC (C-ABC), hyaluronic acid (HA), and TGF-β1 on the biochemical and biomechanical properties of self-assembled articular cartilage. Work with C-ABC showed that this catabolic agent can be employed to improve the tensile properties of constructs. When constructs were cultured for 6 weeks, treating with C-ABC at 2 weeks enhanced the tensile stiffness. Furthermore, treating at 2 and 4 weeks synergistically increased tensile properties and allowed compressive stiffness to recover to control levels. Another study showed that combining C-ABC and TGF-β1 synergistically enhanced the biochemical and biomechanical properties of neotissue. Microarray analysis demonstrated that TGF-β1 increased MAPK signaling in self-assembled neocartilage whereas C-ABC had minimal effects on gene expression. SEM analysis showed that C-ABC increased collagen fibril diameter and fibril density, indicating that C-ABC potentially acts via a biophysical mechanism. Constructs treated with C-ABC and TGF-β1 also showed stability and maturation *in vivo*, exhibiting a tensile stiffness of 3.15±0.47 MPa compared to a pre-implantation stiffness of 1.95±0.62 MPa. To

assess the response to HA application, studies were conducted to optimize HA administration and examine its effects in conjunction with TGF-β1. Applying HA increased the compressive stiffness 1-fold and increased GAG content by 35%, with these improvements depending on HA molecular weight, application commencement time, and concentration. Microarray and PCR analyses showed that HA also influenced genetic signaling, up-regulating multiple genes associated with the TGF-β1 pathway. In addition to genetic effects, the enhanced GAG retention due to HA treatment could increase the fixed charge density of the matrix and thereby increase resistance to compressive loading. Additive effects were observed when HA was applied in conjunction with TGF-β1, with the combined treatment increasing compressive stiffness and GAG content by 150% and 65%, respectively. In general, results demonstrated mechanisms underlying C-ABC, HA, and TGF-β1 treatments and showed how these agents can be applied to improve cartilage regeneration efforts.

Acknowledgments

This dissertation depended on the contributions of many individuals both within and outside of our laboratory. A wide spectrum of people, from undergraduates to seasoned faculty members, made this thesis project possible. I would like to acknowledge all of these individuals for their personal and academic support over the past four years.

First I would like to thank Dr. Athanasiou for providing guidance and support throughout the entire process over the years. I would also like to acknowledge my other committee members, Dr. Tony Mikos and Dr. Jun Lou, for their assistance during graduate school. Additionally, Dr. Jerry Hu has provided a wealth of scientific knowledge. The guidance of these individuals has added considerable perspective to work described in this thesis.

My primary mentor upon joining the lab was Dr. Roman Natoli; I credit him with teaching me the fundamentals of laboratory work and, more importantly, introducing me to the conduct of good science. The early morning starts with our esteemed undergraduate Ben Lu also taught me the sacrifices needed to get data! The projects and ideas explored during those early years eventually became a large portion of my current work; in many ways, my experience in the Roman Legion formed the foundation of this thesis.

Several current colleagues in the lab also contributed greatly to my thesis work. Dena Wiltz and Sriram Eleswarapu helped me navigate the Athanasiou lab shortly after I started graduate school and have provided continual support

throughout the process. Dr. Eleftherios Makris, Michael Higashioka, and Gordon Peng have worked with me on various HPLC projects as we established this new assay. Dr. Boaz Arzi has assisted extensively with *in vivo* work that provided some exciting additions to our conventional assays. Jeni Lee, in addition to gracing our office with stellar baked goods, did an outstanding job working on substantial review papers and contributing to our SHG collaboration soon after starting in the lab. All of these individuals and the other members of the Athanasiou lab have provided invaluable assistance.

Last but not least, I would like to thank family and friends who have helped me over the years. This support has been crucial during the ups and downs of graduate school, particularly in light of the lab move to California, and it has been vital to my successes over the past several years. Your academic and personal encouragement has played a pivotal role in my graduate school career.

Table of Contents

List of Tables

List of Figures

Introduction and background

Articular cartilage: basic biology

Articular cartilage is a hyaline cartilage that lines the articulating surface of bones that is devoid of vasculature, nerves, and lymphatics.[1] Articular cartilage consists of a solid phase and a fluid phase. Water, along with dissolved solutes, forms the fluid phase that accounts for 60-85% of the total cartilage weight.[2] The solid phase primarily includes collagen, proteoglycans, and chondrocytes. Chondrocytes, the only cell type within cartilage, comprise only 1-5% of the tissue by volume.[1] Because cartilage lacks vasculature, chondrocytes receive nutrients by diffusion or imbibition and exudation during loading. The organization and presence of cells and matrix components exhibit depth-dependence within cartilage.

Although chondrocytes represent a small fraction of articular cartilage, they are crucial because they synthesize the matrix that imparts mechanical integrity to the tissue. After chondrogenic differentiation of mesenchymal stem cells, chondrocytes produce the matrix that forms the bulk of cartilage. Hypertrophic chondrocytes near the bone contribute to matrix calcification whereas cells in other zones produce the collagen and proteoglycan matrix. As the chondrocytes mature, they cease proliferation. This results in a largely acellular tissue with a substantial extracellular matrix.

One key component of articular cartilage matrix is an extensive fibrillar collagen network. Collagen molecules are comprised of three polypeptide chains that form a unique triple helical structure. These polypeptides contain high numbers of the repeating peptide sequence glycine–X–Y, where X and Y are frequently proline and hydroxyproline. This sequence helps stabilize the triple helix structure. Additionally, there are two short extrahelical telopeptides on each polypeptide chain which have neither the repeating peptide sequence nor a triple helical conformation. The most common types of collagen are the fibrillar molecules that assemble into fibrils; examples of fibrillar collagens include collagens I, II, and XI. The major collagen source within articular cartilage is a heteromer of collagen types II, IX, and XI, which is over 90% collagen II.[3,4] This heteromer forms the fibrillar network that provides articular cartilage with is tensile strength and stiffness. Both the orientations and sizes of the fibrils change as the tissue matures. Collagen VI is localized around the chondrocytes and contributes to the mechanical properties of the pericellular matrix, as well as cell signaling. Several types of collagen, namely collagens I and X, are rarely expressed in normal articular cartilage but are present during development and certain pathologies.

The other major components of cartilage matrix are proteoglycans, which are proteins with bound glycosaminoglycan (GAG) chains. The major proteoglycan of cartilage, aggrecan, is comprised of hyaluronic acid (HA) that aggregates with a protein core with many bound chondroitin sulfate and keratan sulfate chains. Because these GAGs create a highly negative matrix, cartilage

exhibits increased water content. GAGs contribute extensively to the compressive strength of cartilage by their bulk presence in the matrix and due to the swelling of the retained water. Additionally, proteoglycans can sequester bioactive molecules such as growth factors.[5] Several small proteoglycans including lumican, decorin, and fibromodulin also interact with collagen. These interactions can regulate fibril diameter, fibril-fibril interactions, and susceptibility to degradation.[6] For instance, knocking out perlecan, a heparan sulfate proteoglycan, reduced the size and density of collagen fibrils.[7,8] These various roles of proteoglycans illustrate their contributions to the functional properties of cartilage.

Articular cartilage disease and repair

Articular cartilage has a low repair capacity due to its lack of vasculature, lymphatics, and cells.[9] Cartilage injury produces a mechanically inferior repair fibrocartilage,[10,11] which prevents recovery of cartilage functionality. In particular, increased collagen I and decreased GAG content within fibrocartilage alters the tissue's mechanical properties. This repair tissue eventually degenerates and contributes to osteoarthritis.

Osteoarthritis is a significant global health problem that impacts millions and creates a serious economic burden. In the United States alone, expenditures for arthritis and other rheumatic conditions exceeded $320 billion in 2003.[12] Osteoarthritis is particularly problematic within the elderly population; for example, it has been estimated that 10% of people over age 60 have osteoarthritis.[13] The primary symptoms are inflammation of the joint and joint

pain; in severe cases, these symptoms can impair physical function and adversely impact the patient's lifestyle. The prevalence and severity of osteoarthritis provides a strong impetus for engineering articular cartilage.

The lack of an effective clinical treatment for osteoarthritis and the limited regenerative capacity of cartilage make tissue engineering a particularly promising approach. Due to the limited regenerative capacity and physiological importance of articular cartilage, any damaged or diseased tissue needs to be replaced. Tissue engineering has the potential to substantially improve the treatment of cartilage defects. The hydrated matrix of cartilage, composed primarily of proteoglycans and collagen, creates the mechanical integrity of the tissue. The importance of the matrix in cartilage biomechanics, and its ability to withstand a demanding mechanical environment, necessitates producing a suitable matrix in tissue engineered constructs. Ultimately, creating neotissue with the same biomechanical properties as native tissue will help create a viable cartilage repair method.

Unfortunately, an acceptable cartilage replacement treatment does not currently exist, so physicians are typically limited to treating patients symptomatically.[14] To provide a more effective treatment, several techniques have been developed to promote cartilage repair including microfracture, osteochondral grafts, and autologous chondrocyte implantation. However, current cartilage repair methods have achieved limited clinical success, particularly due to their dependence on tissue harvested from a non-weight

bearing portion of the knee.[15] Additionally, using xenogenic or allogenic cells can pose immunogenicity problems.

Several repair treatments are currently employed, but disadvantages have prevented any methods from becoming a widely accepted treatment. Microfracture repair has shown some success clinically, but it is only appropriate for a fraction of patients.[15,16] Although osteochondral grafting avoids immunogenicity problems, it requires multiple surgical sites and subsequently makes it a more invasive treatment.[17-19] Many studies have also focused on suspended chondrocyte implantation. Allogenic suspended chondrocytes pose immune rejection problems, which has precluded widespread clinical use.[20] A more common suspended chondrocyte technique is autologous chondrocyte implantation, which has an established clinical record. For instance, autologous grafts have maintained their durability even in a nine year study.[21] Despite various studies showing promising results for autologous chondrocyte implantation, there have also been concerns such as the presence of fibrocartilage in the replacement tissue.[22] In general, these current replacement methods have all achieved some clinical success, but the need for a more effective solution still exists.

Exogenous stimuli for cartilage tissue engineering

Many external agents have shown promise for cartilage engineering. For example, growth factors increase matrix synthesis and promote chondrogenic differentiation, making them useful for improving tissue engineered constructs. Additionally, administering HA has been shown to influence the matrix structure

and composition of chondrocyte cultures. Chondroitinase-ABC (C-ABC), an enzyme that depletes GAG content, has also been used to improve the functional properties of constructs. These external stimuli will be discussed in more detail below.

Growth factors

The TGF-β superfamily, which includes forms of TGF-β and the bone morphogenic proteins (BMPs), has been extensively investigated for its beneficial effects on cartilage. This class of growth factors is known to contribute to both embryonic cartilage development[23] and chondrogenic differentiation of mesenchymal progenitor cells.[24-27] Furthermore, TGF-β1 has been shown to improve *in vivo* cartilage repair.[28] Administering TGF-β to tissue engineered constructs has also been extensively studied. For instance, administering TGF-β increased GAG deposition in three-dimensional cultures of equine chondrocytes,[29] rabbit auricular chondrocytes,[30] and bovine articular chondrocytes.[31] Other studies have shown that BMP-2 increases GAG deposition in explant cultures[32] and engineered cartilage.[33] Many BMPs have also been shown to promote collagen synthesis. For instance, BMP-2[34] and BMP-7[35] have been employed to increase collagen deposition. The prevalence of exciting TGF-β superfamily results has made it one of the most widely applied classes of anabolic agents for *in vitro* cartilage regeneration.

Another well-characterized growth factor for *in vitro* cartilage culture is insulin growth factor-1 (IGF-1). IGF-1 treatment has been shown to increase GAG production in both explants[36] and tissue engineered constructs.[37,38] In self-

assembled constructs, treatment with BMP-2 and IGF-1 resulted in a 118% increase in compressive stiffness and a 54% increase in GAG production.[39] Additionally, combining IGF-1 treatment with direct compression increased protein and proteoglycan synthesis by 180% and 290%, respectively.[40] For bovine articular chondrocytes cultured on alginate beads, IGF-1 increased collagen gene expression and deposition,[41] but it did not impact the number of crosslinks.[42] These studies showed the ability of IGF-1 to improve *in vitro* cartilage culture.

Despite many studies that demonstrated the role of growth factors, the responses to a growth factor have not been consistent in many cases. For example, members of the TGF-β superfamily have been shown to increase or decrease collagen deposition depending on the experimental system.[29,37,42-44] In addition to the variation in culture systems, the developmental stage of the cell,[30,45] zone of cell source,[41] and the amount of extracellular matrix already deposited[44] also influenced the response to the growth factor. Synergism between growth factors also altered their impact.[39] The complexity of the growth factor response complicated the generalization of an optimal treatment regimen.

Chondroitinase-ABC

Chondroitinase-ABC (C-ABC) is a GAG lyase that selectively degrades chondroitin and dermatan sulfates,[46] which has been shown to influence the biochemical and biomechanical properties of both explants and tissue engineered constructs. For instance, when C-ABC was used to treat cartilage explants that were then cultured for 2 weeks, GAG levels recovered and the

tissue exhibited increased tensile properties.[47] Additionally, treating agarose encapsulated chondrocytes with C-ABC resulted in increased collagen concentration.[48] These results are highly relevant to tissue engineering because tissue engineered constructs tend to overproduce GAGs and subsequently create an imbalance in matrix components.[49,50] C-ABC could improve the quality of neotissue matrix by countering this GAG overproduction.

Compared to GAG content and compressive properties, collagen and tensile properties of engineered articular cartilage have remained inferior. A recent study has shown that C-ABC treatment of self-assembled constructs increases their tensile properties.[51] Self-assembled constructs were treated with C-ABC at 2 weeks, followed by an additional 2 weeks of culture. At 4 weeks, the ultimate tensile strength and tensile modulus of C-ABC treated constructs increased by 121% and 80%, respectively. The GAG content increased from 2 to 4 weeks; the compressive stiffness of C-ABC treated constructs also increased, but did not recover to control values. This study showed the potential of C-ABC for increasing the tensile properties of tissue engineered articular cartilage.

Biomechanical stimuli

In addition to the biochemical stimuli described above, mechanical stimulation has also been investigated to improve the functional properties of constructs. Mechanical loading of diarthrodial joints results in direct compression of chondrocytes, and chondrocytes also experience hydrostatic pressure due to compression of synovial fluid inside the joint capsule. Recapitulating the mechanical environment of native chondrocytes is important due to the extreme

forces that these cells endure, which have been shown to influence their phenotype.[52] Some of the stimulation methods that have been employed to promote *in vitro* chondrocyte culture include hydrostatic pressure and direct compression.

Direct compression has been used to modulate matrix composition and concomitantly influence construct properties. Direct compression at various frequencies and strain levels has been shown to increase collagen deposition.[53,54] By applying dynamic compression to medial meniscal explants, it was shown that aggrecan was up-regulated by 108%.[55] The beneficial effects of dynamic compression have also been observed in self-assembled constructs: applying 17%, 0.1 Hz compression increased the aggregate modulus by 70%. These results have shown the potential of direct compression to further improve tissue engineered constructs.

Although there has not been extensive examination of hydrostatic pressure for tissue engineering, several studies have shown promise for this type of stimulation. Hydrostatic pressure has also been shown to increase collagen gene transcription,[56] collagen production,[57,58] and construct tensile properties.[59] For instance, applying 10 MPa hydrostatic pressure to self-assembled constructs at 1 Hz for 4 hours per day and 5 days a week increased collagen content.[57] Additionally, the combination of hydrostatic pressure and growth factor treatment was found to produce synergistic increases in collagen content and additive increases in both Young's modulus and the aggregate modulus.[59] These findings were exciting as coupling hydrostatic pressure stimulation with growth factor

application allowed for the formation of tissue engineered constructs with biomechanical and biochemical properties spanning native tissue values. Studies on PGA meshes have shown that hydrostatic pressure can increase matrix production.[60,61] Despite these promising results, hydrostatic pressure has also been shown to be deleterious. In particular, applying hydrostatic pressure above physiological levels exhibited harmful effects and led to decreased matrix production and increased expression of inflammatory signaling cytokines such as interleukin-6 and tumor necrosis factor.[62] These studies showed the potential of hydrostatic pressure to improve construct biomechanical and biochemical properties by choosing an appropriate stimulation regimen.

Cell sources for cartilage engineering

A readily available cell source that does not dedifferentiate is crucial for any tissue engineering strategy. Although animal sources pose potential immunogenicity problems, their accessibility makes them preferable for initial tissue engineering studies. Fully differentiated chondrocytes can be harvested from various animals and then used to engineer neotissue. Alternatively, progenitor cells such as mesenchymal stem cells and human embryonic stem cells (hESCs) can be differentiated and then used to engineer tissue. Each cell source has distinct advantages and disadvantages.

The most plentiful cell source is hESCs. The high proliferation capacity of these cells makes them an unlimited cell source if they are cultured such that undesired differentiation is prevented. Because hESCs are totipotent, they can be differentiated into any cell type including the chondrocyte. Ethical concerns

have limited the use of stem cells, but new technologies such as induced pluripotent stem cells may avoid these issues. Although hESCs have great potential for tissue engineering, their use is still limited because chondroinduction protocols are still being developed.

Mesenchymal stem cells (MSCs) can differentiate into mesenchymal tissues such as bone, cartilage, and muscle. Unlike hESCs, MSCs are present in adults and are therefore easier to isolate and expand. Chondrogenic differentiation of MSCs has been examined in high-density pellet culture.[24] Additionally, MSCs have been studied for cartilage engineering in various types of scaffolds.[63-65] Despite strides toward achieving chondroinduction *in vitro*, MSC culture in chondrogenic medium often resulted in chondrocyte hypertrophy.[66,67] This problem will need to be addressed prior to using MSCs for tissue engineering.

Primary chondrocytes can be obtained by harvesting tissue from articular cartilage and then enzymatically digesting the matrix. Because immature chondrocytes exhibit higher metabolic activity, they are often preferred for tissue engineering studies.[68] Passaging chondrocytes can be used to expand these cells. However, primary cells are preferred due to potential dedifferentiation during monolayer culture.[69] To avoid these complications, only primary chondrocytes will be used for the experiments described in this proposal.

Tissue engineering approaches

The pressing clinical need for cartilage replacement therapy has resulted in various tissue engineering strategies. Although many methods have been

employed, most can be categorized as scaffold-based or scaffoldless approaches.

Scaffold-based

Scaffold-based tissue engineering uses a synthetic and/or natural polymer to create a temporary matrix for the cells to populate. This matrix degrades over time as the chondrocytes proliferate and deposit new matrix. To ensure effective neotissue formation, the scaffold needs to degrade without toxic byproducts and promote chondrocyte proliferation and biosynthesis.

Collagen has been extensively employed as a scaffold for cartilage engineering due to its natural biocompatibility, porosity, and low immunogenicity. Collagen matrices have also been found to have the proper molecular cues to stimulate collagen production.[70] The prevalence of collagen in the articular cartilage matrix makes collagen particularly attractive for cartilage tissue engineering applications; however, as with many natural biomaterials, collagen poses a risk for pathogen transmission. In particular, concerns have been raised about the increased frequency of prion diseases, which may be associated with collagen scaffolds.[71]

Hyaluronic acid (HA) has also been examined as a potential scaffold. One of the most thoroughly studied forms of HA for tissue engineering is the HA benzyl ester HYAFF©11. By modulating the degree of esterification, the degree of HA solubility and degradation can be controlled. The biocompatibility of these esterfied polymers has been established in various studies[72,73] and they have been shown to produce hyaline-like cartilage in rabbit osteochondral defects.[64]

Furthermore, the clinical product Hyalograft C©, which is based on HYAFF© 11, has shown positive clinical outcomes in various studies.[74-76] HA has also been incorporated into many conventional biomaterials such as alginate gels,[77] collagen gels,[78] and PLGA scaffolds.[79]

Fibrin has been investigated as a tissue engineering scaffold because of its crucial role as a provisional matrix during wound healing. During the clotting response, the protein fibrinogen is cleaved into fibrin. For example, using fibrin scaffolds to treat full thickness defects in horses significantly increased aggrecan levels and the proportion of collagen II.[80] Fibrin has also been employed clinically to treat osteochondral fractures.[81,82] The rapid degradation of fibrin can be advantageous for wound healing, but reduce the mechanical integrity of the scaffold and thus pose problems for longer-term applications. Modulating parameters such as the fibrinogen concentration can be used to alter the mechanical properties of the scaffold.[83]

Alginate is a highly biocompatible hydrogel derived from algae. A key advantage of alginate is its ability to be polymerized *in situ*, which minimizes the invasiveness of the implantation procedure. Alginate generally exhibits minimal inflammatory responses during in vivo studies, which provides a key advantage over agarose.[84,85] For instance, bovine chondrocytes in alginate disks that were implanted in nude mice for 12 weeks exhibited gross cartilage formation.[86] Alginate also appears to prevent dedifferentiation in long term culture: chondrocytes cultured for 8 months in alginate gels continued to produce

collagen II and aggrecan without synthesizing collagen I.[87] However, some have raised toxicity concerns regarding alginate.[88]

Various synthetic materials have also been investigated for cartilage tissue engineering. poly(glycolic acid) (PGA), poly(lactic acid) (PLA) and copolymers of these two polymers.[89,90] PLA, which is more hydrophobic, degrades more slowly than PGA. Hydrogels such as poly(ethylene oxide) (PEO) provide many of the benefits of natural hydrogels like alginate. Another study showed that implanting bovine chondrocytes in PEO in nude mice for 12 weeks resulted in neotissue with significantly higher matrix deposition and cell proliferation than controls.[91] These common biomaterials have been widely investigated for cartilage engineering applications.

Scaffoldless

There are various scaffoldless approaches including pellet culture,[92] aggregate culture,[93] and self-assembly.[94] The key advantage of these methods is increased cell-cell interaction, which has been shown to promote chondrocyte differentiation.[24,95,96] Although many variations of scaffoldless culture exist, most of the techniques depend on high density culture to foster cell-cell interactions and reduce the need for a scaffold.

One of the most common scaffoldless methods is pellet culture, which entails centrifuging chondrocytes to create a high density culture. Pellet culture has been applied to a wide range of chondrocytes including growth plate chondrocytes[97] and hyaline chondrocytes.[93] This culture method has been used to produce collagen networks that have the same composition and fibril sizes as

explant cultures.[98] Additionally, pellet culture has been employed to induce cartilage differentiation of human adult stem cells.[99] Pellet culture has also been studied in combination with other stimuli such as cyclic compression[100] and growth factors[101] However, a key limitation of this culture method is that it yields only one small pellet per centrifugation tube. This scaffoldless approach has been somewhat successful at reproducing the cartilage phenotype, but the restricted sizes and shapes of the constructs limits the versatility of pellet cultures. Self-assembly, which is scaffoldless methodology focus of this proposal, is described in the following section.

Self-assembly

A novel chondrocyte self-assembly has recently been developed for cartilage tissue engineering.[94,102] When chondrocytes are cultured at high density in non-adherent wells, the cells aggregate to form constructs with functional properties approaching native values. For example, on a dry weight basis these tissue-engineered constructs contained two thirds more GAG than native tissue. Collagen reached one third the level of native tissue, and the stiffness reached more than one third that of native tissue.[94] Increases of N-cadherin expression during neotissue formation suggests that differential adhesion mediates self-assembly.[103] After extensive scaffold research in articular cartilage engineering, our group decided to develop a methodology that avoids the complications associated with scaffolds. Self-assembly provides numerous advantages over scaffolds including increased retention of phenotype, increased cell-cell contact, and lack of degradation products.

A variety of mechanical and biochemical stimuli have been investigated to enhance self assembly. For instance, growth factors,[104] hydrostatic pressure,[57,105] and combinations of these stimuli[59] have been shown to improve the biochemical and biomechanical properties of constructs. Although self-assembly has improved tremendously in recent years, work still needs to be undertaken to achieve native tissue properties. This proposal aims to enhance self-assembly by applying exogenous agents that modulate the matrix composition and subsequently enhance functional properties.

Thesis aims

This thesis aims to improve self-assembly for articular cartilage tissue engineering. Self-assembly is a novel process that involves high-density seeding of chondrocytes in non-adherent molds that allows cells to form constructs. The global hypotheses that motivated this thesis are 1) exogenous catabolic and anabolic agents can be applied to modulate matrix composition and subsequently enhance the functional properties of self-assembled articular cartilage, and 2) administering these agents individually or in combination will produce differential gene expression indicative of pathways related to enhanced structure-function relationships in engineered constructs.

These hypotheses were assessed by analyzing the biochemistry and biomechanics of constructs. In particular, creep indentation and tensile testing were employed to evaluate biomechanics. Immunohistochemistry, histology, and quantitative biochemistry of DNA, collagen, and glycosaminoglycans (GAGs) were used to determine the matrix composition of constructs. To evaluate gene expression,

microarray analysis was conducted. The following aims were employed to test the overall hypotheses of this proposal:

1. To examine the effects of application frequency and TGF-β1 administration on chondroitinase ABC (C-ABC) treatment of self-assembled articular cartilage.
2. To investigate the effects of exogenously adding hyaluronic acid (HA) to self-assembled constructs.
3. To examine the mechanisms underlying the response to HA, C-ABC, and TGF-β1 in self-assembled articular cartilage.

Chapters 1-2 include studies for Aim 1. Studies for Aim 2 are described in Chapters 3-4. Mechanistic information for C-ABC and TGF-β1 is contained in Chapter 2; investigation of the HA mechanism of action is included in Chapter 3. Chapters 5-6 contain additional original research studies and Chapters 7-8 are review articles.

Chapter 1: Effects of multiple chondroitinase ABC applications on tissue engineered articular cartilage*

Abstract

Increasing tensile properties and collagen content is a recognized need in articular cartilage tissue engineering. This study tested the hypothesis that multiple applications of chondroitinase ABC (C-ABC), a glycosaminoglycan (GAG) degrading enzyme, could increase construct tensile properties in a scaffold-less approach for articular cartilage tissue engineering. Developing constructs were treated with C-ABC at 2 wks, 4 wks, or both 2 and 4 wks. At 4 and 6 wks, construct sulfated GAG composition, collagen composition, and compressive and tensile biomechanical properties were assessed, along with immunohistochemistry (IHC) for collagens type I, II, and VI, and the proteoglycan decorin. At 6 wks, the tensile modulus and ultimate tensile strength of the group treated at both 2 and 4 wks were significantly increased over controls by 78% and 64%, reaching values of 3.4 and 1.4 MPa, respectively. Collagen concentration also increased 43%. Further, groups treated at either 2 wks or 4 wks alone also had increased tensile stiffness compared to controls. Surprisingly, though GAG was depleted in the treated groups, by 6 wks there were no significant differences in compressive stiffness. IHC showed abundant collagen type II and VI in all groups, with no collagen type I. Further, decorin staining was

* Chapter published in Journal of Orthopaedic Research: Natoli RM, Responte DJ, Lu BY, Athanasiou KA. Effects of multiple chondroitinase ABC applications on tissue engineered articular cartilage. J Orthop Res. 27(7): 949-56, 2009.

reduced following C-ABC treatment, but returned during subsequent culture. The results support the use of C-ABC in cartilage tissue engineering for increasing tensile properties.

Introduction

Degeneration of articular cartilage poses a significant clinical problem. The low regenerative capacity of cartilage limits healing, making the need for replacement tissue important. The primary goal of cartilage tissue engineering is to produce neotissue with sufficient mechanical properties to, when implanted, function in the native environment.

Self-assembly of chondrocytes has shown promise for cartilage tissue engineering.[94,102] In this process, chondrocytes are cultured in non-adherent agarose wells, and inter-cellular adhesion directs self-assembly through an N-cadherin binding process.[103] Other scaffold-less systems, such as pellet and aggregate culture, have also been used in cartilage tissue engineering.[92,93,106] Collectively, these approaches provide potential benefits over traditional scaffold-based strategies, including increased biocompatibility and a lack of exogenous degradation products. Self-assembly has been studied with growth factors[107,108] and mechanical stimulation,[57,107] but efforts to-date have not produced constructs with tensile properties in the range of native tissue. Engineered constructs generally have significantly less collagen than native tissue,[109-112] and an insufficient collagen network reduces construct functionality by impairing their tensile stiffness and resistance to proteases.[113] One way to improve upon this

limitation is application of exogenous agents that modulate the matrix of the developing tissue.

One potential exogenous agent is the glycosaminoglycan (GAG) degrading agent chondroitinase ABC (C-ABC). In a recent study, C-ABC treatment of cartilage explants followed by 2 wks of culture resulted in reconstitution of GAG content and increased tensile properties.[47] Moreover, C-ABC treatment of agarose encapsulated chondrocytes increased collagen concentration.[48] Cartilage grown *in vitro* tends to lack maturational growth and overproduces GAGs, resulting in an imbalance between GAG and collagen content that reduces tissue tensile properties.[49,50] Thus, using C-ABC, which selectively degrades chondroitin and dermatan sulfates,[46] could benefit the matrix by restoring the balance between GAG and collagen content.

The purpose of the present study was to elucidate the temporal effects of multiple C-ABC treatments on self-assembled articular cartilage constructs. To investigate this, constructs were treated with C-ABC at 2 wks, 4 wks, or both 2 and 4 wks, with construct assessment at 4 and 6 wks. We hypothesized that a single C-ABC treatment would increase tensile mechanical properties, and that multiple treatments would further enhance tensile properties. Additionally, by allowing additional culture time post-treatment, it was expected that constructs treated at 2 wks would regain GAG content and compressive stiffness similar to untreated controls.

Methods

Chondrocyte isolation and culture

Bovine chondrocytes were isolated and self-assembled as previously described.[94] Cartilage from the distal femur and patellofemoral groove of male calves (Research 87, Boston, MA) was digested in collagenase type II for 24 hrs. Cells were counted using a hemocytometer and then frozen at -80°C in DMEM containing 20% FBS and 10% DMSO. Within days, cells were thawed and counted. Chondrocyte viability was >90% upon thawing. Cells were then seeded at ~5 million cells in 100 □L of media into 5 mm diameter cylindrical agarose wells. An additional 400 μL of media was added 4 hrs later. Chondrogenic medium composed of DMEM with 4.5 mg/mL glucose and L-glutamine (Biowhittaker/Cambrex, Walkersville, MD), 100 nM dexamethasone (Sigma, St. Louis, MO), 1% fungizone, 1% penicillin/streptomycin, 1% ITS+ (BD Scientific, Franklin Lakes, NJ), 50 □g/mL ascorbate-2-phosphate, 40 □g/mL L-proline, and 100 □g/mL sodium pyruvate (Fisher Scientific, Pittsburgh, PA) was used for seeding and subsequent media changes. This chondrogenic medium formulation contains no FBS and no stimulatory factors other than those listed above. The 500 □L of media were changed daily throughout the experiment. At 10 days, all constructs were transferred to tissue culture plates in which only the bottom of the wells was coated with a thin layer of agarose[114] and randomly assigned to one of the four treatment groups. Of note, separate harvests were used for the 4 and 6 wk experiments. In the 4 wk experiment, cells from 3 distinct calves were used. Based on the promising results at 4 wks, a 6 wk study was then conducted. Cells from 4 distinct calves were used in the 6 wk study. Separate batches of agarose wells were also fabricated for each experiment.

C-ABC treatment and construct processing

In the 4 wk experiment, constructs were treated with C-ABC at 2 wks (early), 4 wks (late), or 2 and 4 wks (combined). For treatment, constructs were exposed to C-ABC (Sigma or Associates of Cape Cod, Falmouth, MA) at an activity of 2 U/mL in chondrogenic media for 4 hrs at 37°C, followed by five washes in 400 µL chondrogenic media. At 4 wks, samples were prepared for histology, quantitative biochemistry, and mechanical testing. Hence, the late and combined groups did not have any recovery time post-treatment in the 4 wk experiment. In the 6 wk experiment, constructs were treated early, late, or combined, but culture duration was lengthened to 6 wks, at which time samples were prepared for histology, quantitative biochemistry, and mechanical testing. Separate groups served as untreated controls for both experiments. Just prior to mechanical testing, constructs were removed from culture and processed. A 3 mm diameter core was removed from the construct's center with a biopsy punch for creep indentation testing. The remaining outer ring was portioned ~60% for biochemical analysis and ~40% for tensile testing. This method of tissue processing tests tensile properties and assays the biochemical content of the outer annulus, which is presumably representative of the entire construct. However, any inhomogeneities that are specific to the annulus of tissue engineered constructs may bias the results. Indeed, inhomogeneities in tissue engineered articular cartilage have been observed at similar time points to those investigated in this study.[115] However, as all specimens are prepared similarly, any bias is not likely to affect inter-group comparisons.

Gross morphology, histology, and immunohistochemistry (IHC)

Construct diameter was measured from digital photographs using ImageJ (National Institutes of Health, Bethesda, MD). For histology, constructs were cryoembedded and sectioned at 14 μm. Some sections were fixed in 10% phosphate buffered formalin and stained with Safranin O/fast green for GAG content. For IHC, slides were first fixed with acetone at 4°C for 20 min. For collagens type I, II, and VI, slides were rinsed with IHC buffer, quenched of peroxidase activity, and blocked with horse serum for collagen type I and goat serum for collagens type II and VI (Vectastain ABC kit, Vector Labs, Burlingame, CA). Sections were then incubated for 1 hr with either mouse anti-collagen type I diluted 1:1000 (Accurate Chemicals, Westbury, NY), rabbit anti-collagen type II diluted 1:300 (Cedarlane Labs, Burlington, NC), or rabbit anti-collagen type VI diluted 1:300 (US Biological, Swampscott, MA). The secondary antibody, made by adding one drop of stock solution is added to 10 mL of buffer in the mixing bottle (anti-mouse or anti-rabbit IgG, Vectastain ABC kit), was then applied for 30 min, and color was developed using the Vectastain ABC reagent and 5 min exposure to DAB. For decorin, whole rabbit serum (LF-94) was a generous gift from the laboratory of Dr. Larry W. Fisher.[116] Following fixation in cold acetone and peroxidase quenching, sections were treated with 0.2 U/mL protease free C-ABC (Associates of Cape Cod) in a solution of 0.01 M Tris, 0.01 M NaCl, and 0.012 M NaAc containing 0.1% bovine serum albumin (BSA) for 1 hr at 37°C to expose the core protein. Sections were then blocked with goat serum and incubated overnight at 4°C in the presence of LF-94 diluted 1:500 in tris-buffered

saline (TBS) containing 1% BSA. Finally, the secondary antibody, made as described above (anti-rabbit IgG, Vectastain ABC kit), was applied for 1 hr, and color was developed using the Vectastain ABC reagent and 5 min exposure to DAB. In addition to IHC staining of experimental groups, bovine articular cartilage was used as a positive control for collagen type II, collagen type VI, and decorin and as a negative control for type I collagen. Bovine tendon and bone were used as positive controls for collagen type I. As additional negative controls, tissues were stained for each protein as described above, but without application of the appropriate primary antibody.

Biochemical analysis

The portion of the sample assigned to biochemical analyses was weighed wet, lyophilized for 48 hrs, weighed dry, and subjected to a sequential pepsin-elastase digestion previously described.[108] Briefly, samples were re-suspended in 0.8 mL of 0.05 M acetic acid containing 0.5 M sodium chloride. To this suspension, 0.1 mL of a 10 mg/ml pepsin (Sigma) solution in 0.05 M acetic acid was added, and the suspension was mixed at 4ºC for 96 hrs. Next, 0.1 ml of 10x TBS buffer was added along with 0.1 ml pancreatic elastase (1 mg/ml dissolved in 1x TBS buffer). This suspension was mixed at 4ºC overnight. Following this protocol, no residual neo-tissue remained. DNA content was assessed with the Quant-iT™ PicoGreen® dsDNA Assay Kit (Invitrogen, Carlsbad, CA). Following hydrolysis with 4N NaOH for 20 min at 110ºC, collagen content of the samples was quantified with a modified chloramine-T hydroxyproline assay.[117] Finally, sulfated

GAG content was quantified using the Blyscan Glycosaminoglycan Assay kit (Accurate Chemical and Scientific Corp., Westbury, NY).

Creep indentation testing

Compressive mechanical properties were determined by creep indentation testing of the central 3 mm core biopsy assuming a linear biphasic model.[118] Thickness was measured using a micrometer, and specimens were attached to a flat stainless steel surface with a thin layer of cyanoacrylate glue. The attached specimen was then placed into the creep indentation apparatus, which was used to automatically load and unload the specimens while monitoring specimen creep and recovery. In the 4 wk experiment, the late and combined treatment groups were tested using a 0.05 g tare followed by a 0.27 g test load. These lighter loads allowed control over excessive deformation that resulted immediately following GAG removal. All other specimens were tested with a tare load of 0.2 g followed by a test load of 0.7 g. The loads were applied to the specimens through a 0.8 mm diameter, flat-ended, porous tip. To determine construct mechanical properties, a semi-analytical, semi-numerical, linear biphasic model was employed,[119] followed by a non-linear finite element optimization (FEO) to refine the solution and obtain values for the aggregate modulus, permeability, and Poisson's ratio.[120] To assess the appropriateness of the biphasic model for assessment of self-assembled tissue engineered constructs, a goodness-of-fit test was performed. The coefficient of determination from the FEO output and experimental displacement data was calculated using the following equation:

$$r^2 = 1 - \frac{\sum_{i=1}^{n}\left(y_i^{\exp} - y_i^{FEO}\right)^2}{\sum_{i=1}^{n}\left(y_i^{\exp} - y_{avg}^{\exp}\right)^2}$$

In this equation, y_i^{exp} are the experimental displacement data, y_i^{FEO} are the theoretical values obtained from the FEO, and y_{avg}^{exp} is the average of the experimental displacement data. This method has been used before to assess the appropriateness of several biomechanical models for articular cartilage.[121]

Tensile testing

The portion of each sample assigned to tensile testing was cut into a dog-bone shape and glued to paper tabs.[122] This procedure prepares specimens with slightly curved lateral edges from the outer annulus, which may introduce artifact into the testing. However, as all specimens were prepared in the same manner, this potential artifact would be evenly distributed. ImageJ was used to determine sample gauge length and width from photographs. Gauge length was defined as the distance between the paper tabs. Thickness was measured with a micrometer. Tensile tests were performed at a strain rate of 1% gauge length per second on a mechanical testing system (Instron Model 5565, Canton, MA). There was no pre-conditioning of the specimens. The Instron monitors and records displacement, which when combined with gauge length, allows strain to be calculated. Young's modulus was determined by linear regression of the linear portion of the stress-strain curve based on initial cross-sectional area. The ultimate tensile strength (UTS) was taken to be the maximal stress prior to failure.

Statistical analyses

Each group consisted of n = 8 samples. Two samples were randomly assigned for histology and IHC. The remaining six were used in the biochemical, compression, and tension tests. At each time point, a 2-way ANOVA based on main factors of treatment at 2 wks or treatment at 4 wks was performed to investigate additive or synergistic effects.[123] Where warranted, the ANOVA was followed by a Student-Newman-Keuls post-hoc test on a cross of the main factors. Significance was set at $p < 0.05$. All data are presented as mean ± standard deviation (S.D.).

Results

4 wk experiment

Figure 1-I shows results from histology and IHC. At 4 wks, Safranin-O/fast green staining for GAGs showed GAG presence in the control and early treatment groups, and verified GAG removal in the late and combined treatment groups. Staining for collagens type II and VI (data not shown for type VI) was evident in all constructs. With respect to collagen type VI, pericellular staining was present, but it was not exclusive. There was also diffuse staining throughout the construct. Constructs did not stain for collagen type I. Decorin stained intensely throughout constructs in the control and early treatment groups, but stained only on the perimeter of constructs in the late and combined treatment groups.

One-time treatment at 2 wks or 4 wks was a significant factor for diameter, wet weight (WW), and thickness. Further, with respect to decreasing WW, the interaction term was significant ($p = 0.03$). For diameter, each group was significantly different from the others, except for early and combined treatments

being similar. Diameters measured 6.02 ± 0.17, 5.45 ± 0.07, 5.71 ± 0.18, and 5.31 ± 0.07 mm for the control, early, late, and combined groups, respectively. For thickness, each group was significantly different from the others, except for late treatment being similar to early and combined. Thicknesses measured 0.45 ± 0.04, 0.36 ± 0.03, 0.34 ± 0.05, and 0.30 ± 0.03 mm for the control, early, late, and combined groups, respectively. For WW, each group was significantly different from the others, except for early and late treatments being similar. WWs measured 14 ± 1.7, 9.2 ± 0.8, 8.3 ± 1.2, and 5.5 ± 0.6 mg for the control, early, late, and combined groups, respectively. In terms of DNA content, treatment at 4 wks was a significant factor. Post-hoc testing showed the combined treatment group had significantly less DNA than control (30 ± 5.6 μg per construct compared to 21 ± 1.8 μg). The early group had 28 ± 5.2 μg and the late group had 26 ± 6.5 μg.

Turning to extracellular matrix (ECM) content, for both GAG/WW and collagen/WW treatment at 2 wks or treatment at 4 wks was a significant factor. Table 1-I shows GAG/WW and collagen/WW. Post-hoc testing of GAG/WW showed each group was significantly different from the others, except for late treatment being similar to combined. Post-hoc testing of collagen/WW showed the combined treatment group was significantly different from all others. GAG or collagen per construct can be obtained by multiplying the WW% by the total wet weight. Post-hoc testing of GAG/construct was identical to GAG/WW. Post-hoc testing of collagen/construct showed the combined treatment group was significantly different from control and the late treatment groups.

Compressive and tensile mechanical properties were also measured. Treatment at 2 wks or treatment at 4 wks was a significant factor for compressive stiffness. The interaction term was also significant (p = 0.012). Further, treatment at 4 wks was as significant factor for permeability. All treatment groups were significantly less stiff in compression compared to control (Fig. 1-2A). Post-hoc testing of permeability showed an increasing trend with treatment. Permeabilities measured 3.11 ± 1.73, 9.35 ± 5.92, 75.5 ± 64.6, and 86.8 ± 85.9 x 10^{-15} $m^4/N{\cdot}s$ for the control, early, late, and combined groups, respectively. Post-hoc testing of Poisson's ratio showed combined treatment was significantly greater than early or late treatment. Poisson's ratio measured 0.093 ± 0.095, 0.035 ± 0.028, 0.054 ± 0.039, and 0.172 ± 0.097 for the control, early, late, and combined groups, respectively. Goodness-of-fit was assessed by calculating the coefficient of determination (r^2). There were no significant differences in r^2 among the groups. The r^2 values were calculated to be 0.890 ± 0.046, 0.908 ± 0.041, 0.917 ± 0.033, and 0.910 ± 0.065 for the control, early, late, and combined groups, respectively.

In terms of tensile properties, treatment at 2 wks or at 4 wks was a significant factor for UTS, and treatment at 2 wks was a significant factor for Young's modulus The interaction term was also significant for Young's modulus (p = 0.0008). All treatment groups had significantly greater UTS than control (Fig. 2B). Post-hoc testing of Young's modulus showed all groups were significantly different from each other except control and early treatment. Young's modulus measured 1299 ± 101, 1308 ± 257, 950 ± 284, and 1689 ± 159 kPa for the control, early, late, and combined groups, respectively.

6 wk experiment

In the 6 wk experiment, histology and IHC results were similar to the 4 wk experiment, except GAG and decorin were present in the late and combined treatment groups (Fig. 1-1). Treatment at 4 wks was a significant factor for diameter, WW, and thickness. Further, with respect to decreasing diameter, the interaction term was significant (p = 0.046). For diameter, each group was significantly different from the others, except for late and combined treatment being similar. Diameters measured 5.27 ± 0.10, 5.14 ± 0.07, 4.99 ± 0.09, and 5.00 ± 0.07 mm for the control, early, late, and combined groups, respectively. For thickness, late and combined treatments were significantly different than both control and early treatment, though the differences were small. Thicknesses measured 0.29 ± 0.03, 0.31 ± 0.03, 0.25 ± 0.04, and 0.24 ± 0.02 mm for the control, early, late, and combined groups, respectively. For WW, late and combined treatments were significantly different than both control and early treatment. WWs measured 5.9 ± 0.4, 5.7 ± 0.5, 4.9 ± 0.3, and 4.7 ± 0.3 mg for the control, early, late, and combined groups, respectively. DNA content at 6 wks showed a similar trend to 4 wks. Post-hoc testing showed the late and combined treatments had significantly less DNA than both control and early treatment.

In terms of ECM content and mechanical properties, treatment at 4 wks was a significant factor for both GAG/WW and collagen/WW. Further, with respect to decreasing GAG/WW, the interaction term was significant (p = 0.02). Late or combined treatment resulted in significantly decreased GAG/WW compared to control or early treatment, while late or combined treatment resulted

in significantly increased collagen/WW compared to control (Table 1-1). Post-hoc testing of GAG/construct showed each group was significantly different from the others, except for late treatment being similar to combined. There were no significant differences in collagen/construct.

In terms of compressive properties, treatment at 4 wks was a significant factor (p = 0.048) for compressive stiffness (Fig. 1-3A). There were no significant differences in aggregate modulus among the four groups. Post-hoc testing of permeability and Poisson's ratio also showed no significant differences among the groups. Permeabilities measured 19.7 ± 19.8, 17.6 ± 16.9, 15.7 ± 8.5, and 20.7 ± 12.7 x 10^{-15} $m^4/N{\cdot}s$ for the control, early, late, and combined groups, respectively. Poisson's ratio measured 0.138 ± 0.110, 0.085 ± 0.119, 0.072 ± 0.033, and 0.133 ± 0.112 for the control, early, late, and combined groups, respectively. As seen at 4 wks, there were no significant differences among the groups for r^2 values, which were 0.936 ± 0.031, 0.930 ± 0.028, 0.911 ± 0.054, and 0.907 ± 0.094 for the control, early, late, and combined groups, respectively.

For tensile properties, treatment at 2 wks or at 4 wks was a significant factor for Young's modulus, and treatment at 4 wks was a significant factor for UTS. All treated groups had significantly greater Young's modulus than control (Fig. 1-3B). Additionally, the combined treatment group was greater than early or late treatment. Post-hoc testing of UTS showed the control and early treatment group were not significantly different, and the late and combined treatment groups were not significantly different. All other comparisons were significantly

different. UTS measured 881 ± 181, 984 ± 143, 1343 ± 169, and 1441 ± 184 kPa for the control, early, late, and combined groups, respectively.

Discussion

In this study, we examined the effects of multiple C-ABC applications on self-assembled tissue engineered articular cartilage constructs. Results showed that the group treated at both 2 and 4 wks (combined) had significantly greater tensile properties (ultimate tensile strength and Young's modulus) than control in both the 4 and 6 wk experiments, reaching a stiffness of 3.4 MPa at 6 wks. Further, treating at 2 wks (early) or at 4 wks (late) alone resulted in significantly greater ultimate tensile strength at 4 wks, and significantly greater Young's modulus at 6 wks, compared to controls at these time points. Though compressive stiffness of all treatment groups was less than control in the 4 wk experiment, there were no significant differences at 6 wks. These results support our hypotheses that multiple C-ABC treatments would further enhance tensile properties compared to a single treatment, and, given longer culture time post-treatment, the early treatment group would not have a significantly different compressive stiffness compared to untreated controls.

An interesting result of this study is that the compressive properties of all C-ABC treated groups were not significantly different from controls at 6 wks. Furthermore sulfated GAG returned following depletion in the early treatment group over 4 wks of culture. Additionally, though given only 2 wks of culture post-treatment, compressive stiffness at 6 wks of the late and combined treatment groups was not significantly different from controls, despite significantly

decreased sulfated GAG content. This is potentially explained by the significantly increased collagen content in these groups compared to control, reaching 23% by WW. Indeed, collagen has been shown to have a role in the compressive behavior of articular cartilage. One study performed confined compression with the expectation that compressions greater than 5% would lead to the full load being borne by the proteoglycan osmotic pressure, evidenced by equal stresses in the axial and radial directions. However, it was found that the axial and radial stresses were not equal, highlighting a role for the collagen network in compression.[124] Williamson *et al.*[125] examined bovine cartilage compressive properties as a function of age, showing that the compressive modulus increased 180% from fetus to adult. This increase correlated with increased collagen during development, as GAG content changed negligibly. These findings underscore the concept that construct material properties reflect the balance of ECM components, and both collagen and GAG contribute to compressive stiffness.

Analysis of compressive testing data also revealed that the liner biphasic theory well predicts the compressive behavior of self-assembled articular cartilage constructs. This claim is supported by the relatively high coefficients of determination that were calculated by comparing the experimental displacement data to the theoretical output of the FEO. The lowest r^2 calculated was 0.89. This is surprisingly good considering the relative simplicity of the linear biphasic theory. More complicated theories for the biomechanical behavior of articular cartilage, such as the biphasic-CLE-QLV model,[121] have achieved r^2 values of 0.95 and 0.97 for confined and unconfined compression testing, respectively. It is

likely that these models would also better predict the behavior of self-assembled tissue engineered articular cartilage; however, it is not yet clear if self-assembled cartilage exhibits non-linear behavior for the same reasons or in the same proportions that native tissue articular cartilage does. As the permeability in linear biphasic theory captures these behaviors, the permeability values should be interpreted in this light, and not necessarily as the intrinsic permeability of the engineered constructs, which can only be properly measured through direct permeation experiments. As self-assembled constructs are further studied and become more robust, more detailed assessments of their biomechanical behavior can be made.

Moreover, the results of this study show C-ABC treatment increases construct tensile properties. At 4 wks, the increase in tensile properties may be attributed to substantially decreased construct size (e.g., thickness) resulting from loss of GAG and its associated water or to increased ability of collagen to rearrange in the absence of a pre-stress generating swelling pressure.[126,127] However, as GAG returns, differences in construct size at 6 wks were markedly reduced. This suggests increased collagen concentration could be responsible for the increased tensile properties. Kempson *et al.*[128] have shown that the tensile properties of articular cartilage are correlated to collagen content. However, another interesting possibility raised by results from this study is a role for the small proteoglycan decorin. Decorin is known to interact with type II collagen and has key roles in collagen fibrillogenesis, such as limiting fiber diameter.[6,129] For example, fibroblasts seeded onto collagen scaffolds from

decorin knockout mice have been shown to increase scaffold tensile properties compared to wild-type cells.[130] The decrease in decorin evident by IHC staining shown immediately post-treatment in the present study may allow larger diameter collagen fibers to be formed or previously blocked interactions between neighboring collagens to take place, both of which could lead to a more functional collagen network and increased tensile properties. This proposition is similar to a recently described mechanism whereby selective knockdown of the small proteoglycan lumican led to increased collagen deposition and fibril diameter in a polyglycolic acid scaffold based approach to cartilage engineering employing bovine nasal chondrocytes.[110] In addition to decorin and lumican, aggrecan and biglycan have a role in the observed changes. Selective modulation of small, regulatory matrix molecules could be an important consideration for future articular cartilage tissue engineering experiments.

In addition to self-assembly, other scaffold-less culture systems for engineering cartilage replacement tissue have been studied.[131-136] One study showed that human articular chondrocytes grown in serum free conditions exhibit an age-dependent ability to produce neo-tissue.[131] However, mechanical properties were not assessed. Fedewa et al.[132] plated rabbit articular chondrocytes at a concentration of 2 million cells per 25 cm^2 and cultured them for up to 10 wks. Chondrocytes grew into cell sheets up to 130 μm thick and produced collagens type II, IX, and XI, indicating that cell phenotype was not affected. At 10 wks, the engineered tissue's tensile stiffness was 1.3 MPa. Stiffness was further increased to 3.4 MPa by treatment with interleukin-1β, but

the cell sheet thickness decreased to only 38 μm. Using the same culture system, it was shown that increased construct tensile stiffness correlated with greater collagen volume fraction[136] and that bonds formed among collagen fibrils.[135] In the present study, greater construct collagen concentration was also related to increased tensile stiffness. Further, it is possible that interfibrillar collagen bonds formed upon GAG depletion with C-ABC. This possibility should be assessed in future studies.

Another study used the plated chondrocyte culture system to assess the effects of proteoglycans on construct tear toughness.[134] C-ABC was used to remove GAG from the cell sheets at 8 wks, followed by tensile tear testing. C-ABC treatment decreased the thickness of grown tissue, and material tear toughness was increased upon GAG removal, but not when adjusted for collagen content. The authors concluded that proteoglycans were not a determining factor of the grown tissue's fracture toughness. Finally, Gemmiti and Guldberg[133] demonstrated that exposure of scaffold-less grown engineered cartilage to fluid flow-induced shear stress causes increased total and type II collagen. These increases in collagen were mirrored by increased tensile properties, reaching a stiffness of 2.28 MPa at 17 days. Despite these efforts, the tensile stiffness of engineered articular cartilage remains low compared to native tissue. Further research into methods for increasing tensile properties of scaffold-less grown tissue engineered cartilage remains necessary.

In summary, C-ABC treatment is a promising approach for increasing tensile properties of self-assembled tissue engineered cartilage, perhaps by

inducing maturational instead of expansive growth,[47] whereby construct size changes minimally while ECM continues to be deposited. A potential limitation to scaffold-free approaches is less control over construct thickness, which is further affected by C-ABC treatment. However, construct size could be increased before treatment by using more cells[137] or allowing additional culture time before C-ABC application. Using the self-assembly process, our laboratory has grown constructs greater than 1 mm thick,[107] though there is considerable biological variability. In conclusion, as hypothesized, treatment with C-ABC at both 2 and 4 wks resulted in further enhancement of tensile properties compared to a single treatment at 2 or 4 wks. Future experiments should probe more deeply into the mechanism as to how temporary proteoglycan depletion affects the collagen network of tissue engineered constructs by examining aspects such as fiber size and degree of cross-linking.

Table 1-1: Construct GAG and collagen content normalized to wet weight.

	4 wks		6 wks	
Group	GAG / WW (%)	Collagen / WW (%)	GAG / WW (%)	Collagen / WW (%)
Control	6.9 ± 1.8^{a}	8.9 ± 2.1^{a}	6.3 ± 0.6^{A}	16 ± 2.1^{A}
C-ABC @ 2 wks	4.4 ± 0.8^{b}	19 ± 3.1^{a}	5.5 ± 1.1^{A}	$20 \pm 4.3^{A,B}$
C-ABC @ 4 wks	3.1 ± 1.7^{c}	17 ± 3.4^{a}	2.7 ± 0.5^{B}	24 ± 3.9^{B}
C-ABC @ 2 & 4 wks	1.6 ± 0.8^{c}	38 ± 15^{b}	3.3 ± 0.4^{B}	23 ± 2.0^{B}

Values in table are mean ± S.D. (n = 6). WW = wet weight. Separate statistical analyses were run on each column. Within a column, groups not sharing a similar letter are significantly different from one another ($p < 0.05$ by Student-Newman-Keuls post-hoc test). At 6 wks, the groups that had been treated at 4 wks contained significantly less sulfated GAG/WW, but significantly more collagen/WW, than control.

Figure 1-1: Histology and IHC

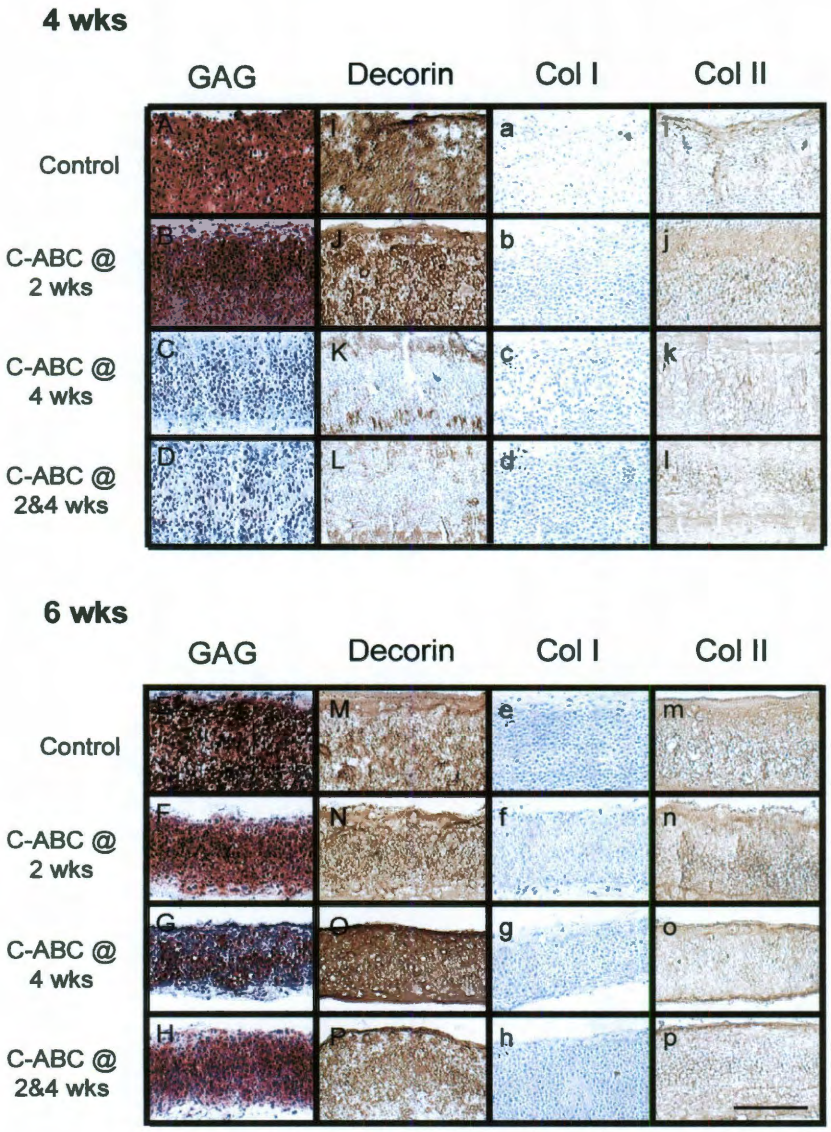

A-H) Safranin-O/fast green stain for GAGs, I-P) IHC for decorin, a-h) IHC for collagen type I, and i-p) IHC for collagen type II. At 4 wks, note the absence of GAG and substantially decreased decorin staining immediately following C-ABC treatment in the group treated at 4 wks and group treated at both 2 and 4 wks (C, D, K, and L, respectively). GAG and decorin staining returned in these groups by 6 wks (G, H, O, and P, respectively). Scale bar in P is 200μm.

Figure 1-2: Four week biomechanical properties

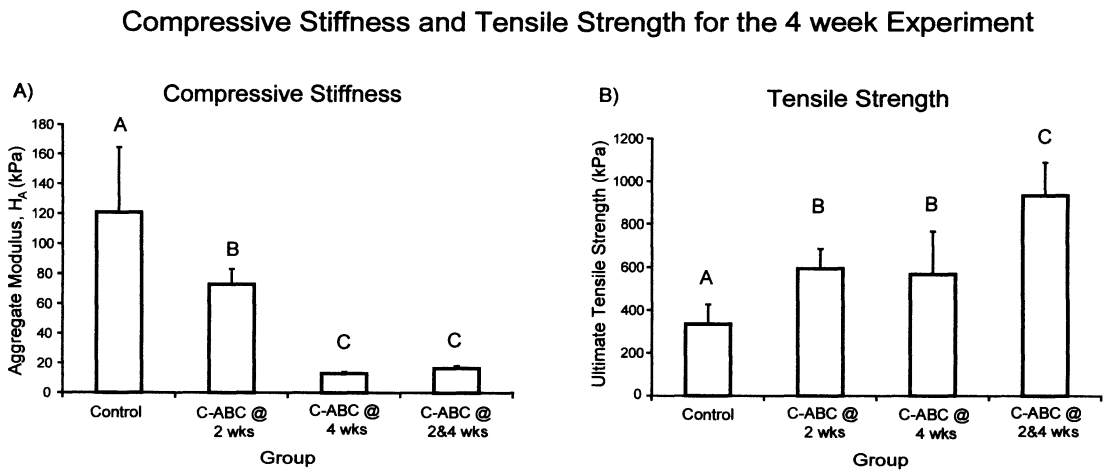

A) Compressive stiffness and B) ultimate tensile strength. Bars represent mean ± S.D. Groups not connected by the same letter are significantly different. The aggregate modulus of all treated groups was significantly less than control. The ultimate tensile strength of all treated groups was significantly greater than control, reaching 931 ± 155 kPa in the combined group. The group treated at both 2 and 4 wks was significantly greater than the groups treated at only 2 or 4 wks.

Figure 1-3: Six week biomechanical properties

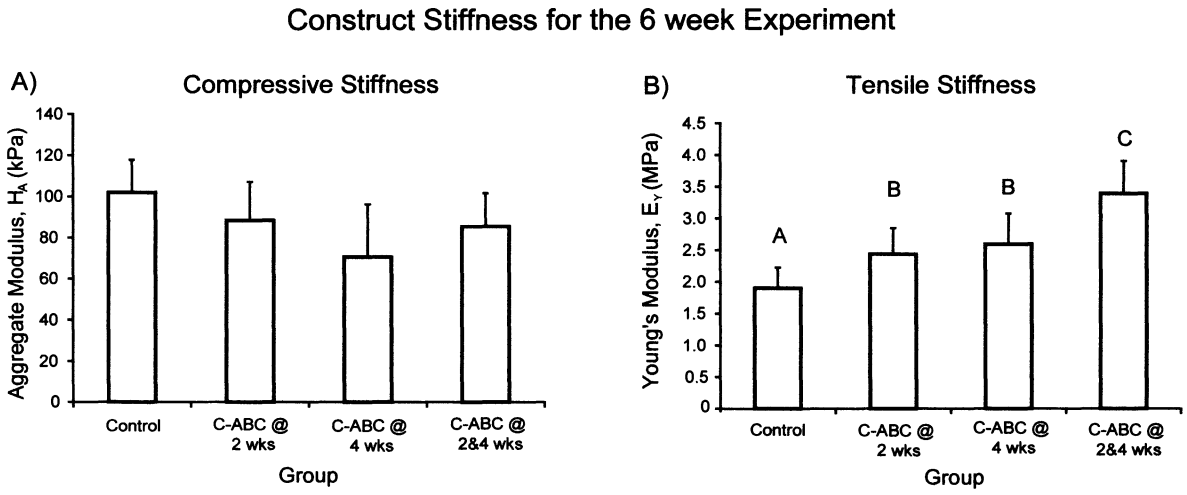

A) Compressive stiffness and B) tensile stiffness. Bars represent mean ± S.D. Groups not connected by the same letter are significantly different. There were no significant differences in aggregate modulus. Young's modulus of all treated groups was significantly greater than control, reaching 3.4 ± 0.5 MPa in the combined group. Further, the group treated at both 2 and 4 wks was significantly greater than the groups treated at only 2 or 4 wks, which measured 2.4 ± 0.4 and 2.6 ± 0.5 MPa, respectively.

Chapter 2: Mechanisms underlying the synergistic enhancement of self-assembled neocartilage treated with chondroitinase-ABC and TGF-β1*

Abstract

Developing a platform for *in vitro* cartilage formation would enhance the study of cartilage development, pathogenesis, and regeneration. Promoting maturational growth of the matrix and achieving native biomechanical properties are major challenges of current i*n vitro* cartilage growth efforts. To improve neocartilage formation, our group developed a novel self-assembly process for articular chondrocytes, which has been improved in this study using a novel combination of catabolic and anabolic agents. TGF-β1 was applied in conjunction with the enzyme chondroitinase-ABC (C-ABC) to additively increase tensile properties and synergistically enhance collagen content. Additionally, microarray analysis indicated that TGF-β1 up-regulated MAPK signaling in contrast to C-ABC, which did not enrich genetic pathways. The lack of genetic signaling spurred investigation of the biophysical role of C-ABC, which showed that C-ABC treatment increased collagen fibril diameter and density. After four weeks of culture in nude mice, neocartilage treated with C-ABC and TGF-β1 exhibited stability and maturation. This study illustrates an innovative strategy for improving *in vitro* and *in vivo* articular cartilage formation and elucidated mechanisms

* Responte DJ, Natoli RM, Athanasiou KA. Synergistic effects of chondroitinase ABC and TGF-β1 on tissue engineered articular cartilage. Nature Biotechnology (in preparation)

underlying TGF-β1 and C-ABC treatment based on genetic pathways and biophysical mechanisms, respectively.

Introduction

Articular cartilage is crucial to proper joint function, providing a wear-resistant, low-friction surface covering the articulating surfaces of bones. Cartilage is largely acellular and relies on its extracellular matrix, which is predominantly composed of collagen and glycosaminoglycans (GAGs), to provide mechanical integrity. The matrix of cartilage contains aggrecan complexes with GAGs and an organized collagen network, both of which contribute to the tissue's biomechanics. Recapitulating the biomechanical and biochemical properties of native tissue has remained elusive despite decades of research. An effective method for *in vitro* grown cartilage would greatly advance the study of cartilage disease, regeneration, and development.

A novel self-assembly approach, which uses high density cell culture to promote chondrocyte aggregation, recapitulates cartilage development and produces robust neocartilage.[94,102] Various strategies have been employed to overcome deficiencies of *de novo* cartilage such as overabundance of GAGs[49,50] and tensile properties below those of native tissue.[138] For instance, applying exogenous stimuli such as growth factors,[104] hydrostatic pressure,[57,105] and combinations of these stimuli[59] has improved the functional properties of self-assembled neocartilage. These developments highlight the potential of employing exogenous stimuli to enhance the self-assembly process.

The enzyme chondroitinase-ABC (C-ABC), which depletes glycosaminoglycans (GAGs), provides an innovative method for inducing maturational growth. Because *in vitro* cartilage generally overproduces glycosaminoglycans (GAGs),[49,50] C-ABC has been investigated as a method of promoting matrix maturation. For example, treating cartilage explants with C-ABC and culturing for an additional 2 weeks increased tensile properties.[47] C-ABC treatment of chondrocytes seeded on agarose hydrogels increased the collagen concentration and tensile properties of constructs.[139] Furthermore, both single[11,12] and multiple[140] C-ABC treatments have been employed to increase the tensile properties of self-assembled neotissue without compromising compressive properties. These results suggest that C-ABC is an exciting new method for improving *in vitro* cartilage growth.

TGF-β1 has also been investigated for its beneficial effects on cartilage growth. For instance, administering TGF-β increased GAG deposition in three-dimensional cultures of equine chondrocytes,[29] rabbit chondrocytes,[30] and bovine articular chondrocytes.[31] Additionally, administering TGF-β1 to self-assembled cartilage enhanced GAG and collagen production and concomitantly increased compressive and tensile properties.[39] TGF-β1 has also been employed in conjunction with hydrostatic pressure[59] and direct compression[141] to enhance the functional properties of neocartilage. These studies illustrate the ability of TGF-β1 to enhance both the matrix composition and biomechanical properties of *in vitro* cartilage.

This study used a combination of C-ABC and TGF-β1 treatments to integrate anabolic and catabolic strategies for enhancing cartilage formation. The objectives of this study were to 1) assess the effects of combining TGF-β1 and C-ABC treatment on self-assembled neocartilage, 2) investigate potential mechanisms underlying the response to these stimuli, and 3) evaluate the *in vivo* response of neotissue treated with TGF-β1 and C-ABC. This study tested the hypotheses that 1) TGF-β1 administration will act synergistically with C-ABC to increase tensile properties and collagen content of self-assembled neotissue, 2) C-ABC and TGF-β1 will up-regulate functionally-relevant molecular signaling pathways, and 3) self-assembled neocartilage will exhibit stability and maturation *in vivo*. To test these hypotheses, we employed a full factorial design of factor C-ABC (no treatment, treatment at 2 weeks) and factor TGF-β1 (no treatment, treatment during weeks 1&2 (continuous), treatment during weeks 1&3 (intermittent). The biomechanics, biochemical content, gene expression, collagen ultrastructure, and *in vivo* properties of neotissue were assessed.

Results

C-ABC and TGF-β1 treatments maintain native cartilage phenotype

Neocartilage was assessed at 4 weeks via histology and morphology to assess the gross properties and composition of the neotissue (Fig. 1). All constructs, which originated from 5 mm wells, showed no contraction and exhibited the following diameters: 5.97±0.16, 5.10±0.08, 5.32±0.11, and 5.03±0.09 mm for control, C-ABC, TGF-β1, and combined treatments, respectively. Both treated

and control neotissue exhibited uniform staining for GAGs and total collagen. Additionally, IHC showed that all constructs stained positive for collagen II but negative for collagen I. The presence of collagen II, GAGs, and total collagen but not collagen I demonstrates that both control and treated groups maintained normal cartilage phenotype.

Combining C-ABC and TGF-β1 treatment synergistically enhances collagen content

To investigate maturational growth of the matrix, the amount of collagen and GAGs was quantified at 4 weeks. GAG content (Fig. 2d) was highest for growth factor only groups, which exhibited values of 7.0±0.8%, 8.5±0.5%, and 9.2±0.8% for control, continuous TGF-β1, and intermittent TGF-β1, respectively. Groups treated with C-ABC had lower GAG contents except for the intermittent TGF-β1 group, which was not statistically different than the control value. Combined treatment synergistically increased collagen content (Fig. 2c), reaching 18.6±1.9% and 16.2±1.1% for continuous and intermittent TGF-β1 treatment, respectively. These results showed that combining TGF-β1 and C-ABC synergistically promotes maturation of matrix composition.

Combined treatment additively increases tensile properties and promotes recovery of compressive stiffness

To quantify the influence of C-ABC and TGF-β1 on biomechanics, the aggregate modulus in compression and Young's modulus (E_Y) in tension were determined. The compressive stiffness was highest for groups treated with intermittent TGF-

β1 (Fig. 2b), which attained values of 170±22 kPa and 190±45 kPa when treated with and without C-ABC, respectively. The aggregate modulus was lower for continuous TGF-β1 treatment and lowest for groups receiving no TGF-β1 treatment. The higher compressive stiffness for intermittent TGF-β1 treatment suggested that week 3 growth factor administration aided the recovery of compressive properties following C-ABC treatment, which initially results in negligible residual compressive stiffness following treatment due to GAG depletion. Enhanced mechanical properties reflected the observed changes in biochemical composition.

Tensile testing showed that combining C-ABC and TGF-β1 treatments additively increased the tensile stiffness. Tensile stiffnesses were 0.89±0.22, 1.33±0.23, 1.51±0.29, and 1.40±0.12 MPa for control, C-ABC, continuous TGF-β1, and intermittent TGF-β1 treatments, respectively. Young's moduli were highest for combined treatments, which reached 1.95±0.21 MPa and 1.83±0.38 MPa for continuous and intermittent treatment, respectively (Fig. 2a). The tensile stiffnesses for C-ABC in combination with TGF-β1 showed additive increases when compared to individually applied stimuli.

Construct properties are on par with native tissue

A functionality index (FI) was developed to quantify the similarity between neocartilage and native tissue, which was also tested as a positive control. As shown in Eq. 1, the FI equally weights the compressive stiffness (E^C), tensile

stiffness (E^T), GAG content (G), and collagen content (C). The subscripts 'nat' and 'sac' represent values for native and self-assembled cartilage, respectively.

$$FI = \frac{1}{4}\left(\left(1-\frac{(G_{nat}-G_{sac})}{G_{nat}}\right)+\left(1-\frac{(C_{nat}-C_{sac})}{C_{nat}}\right)+\left(1-\frac{(E^T_{nat}-E^T_{sac})}{E^T_{nat}}\right)+\left(1-\frac{(E^C_{nat}-E^C_{sac})}{E^C_{nat}}\right)\right) \quad (1)$$

The FI yields a score of 1 when neocartilage properties are equivalent to those of native tissue. FI values were 0.41, 0.52, 0.78, and 0.84 for control, C-ABC, intermittent TGF-β1, and combined treatments, respectively. These FI values suggest that combined treatment produces neotissue closest to native cartilage.

TGF-β1 up-regulates MAPK signaling

To elucidate the mechanisms underlying the effects of C-ABC and TGF-β1 on cartilage formation, microarray analysis was conducted at 2 weeks for control, C-ABC, continuous TGF-β1, and combined treatment. The number of differentially expressed genes relative to control neotissue was 191, 548, and 537 for C-ABC, TGF-β1, and combined treatments, respectively. To understand gene expression changes on a more functional level, we used these differentially expressed gene lists to determine if any genetic pathways were enriched.

For both TGF-β1 treatments, the only significantly enriched pathway was MAPK signaling, which was observed for TGF-β1 treatment (19 genes, p = 0.0003) and combination treatment (19 genes, p = 0.00005). There was substantial overlap between the MAPK genes differentially regulated by TGF-β1 and combination treatments, with each group only having one distinct gene (Table 1). Both groups showed up-regulation of MAPK intermediates relating to p38 signaling including MAPKK3, MAP3K5, MAP3K6, and MAPK13. In addition,

in both groups receiving TGF-β1 treatment TGF-β1 was up-regulated, while TGF-β3 and TGF-β receptor type II were down-regulated. The differential regulation of TGF-β1 and its receptor could suggest a feedback mechanism in response to TGF-β1 treatment. The enriched MAPK signaling observed for both groups receiving growth factor treatment could play a role in the observed increases in matrix production, which could subsequently enhance the mechanical properties of the neocartilage.

In contrast to TGF-β1 administration, C-ABC treatment did not significantly enrich genetic pathways. The number of differentially regulated genes was also substantially lower for C-ABC treatment, which only altered the expression of approximately 35% as many genes as TGF-β1 application. Furthermore, the TGF-β1 and combined treatments had nearly identical gene expression patterns, both in terms of the number of genes and specific genes that were differentially expressed. The lower number of differentially expressed genes and lack of enriched pathways suggested that C-ABC did not influence gene expression significantly, in contrast to the response to the TGF-β1 treatments.

To validate microarray data, real time PCR was employed to quantify the expression of intermediates involved in MAPK signaling including MAP3K5, MAPK13, protein tyrosine phosphatase (PTP), and MAP2K3 (Fig. 3). Both TGF-β1 alone and combination treatments increased the expression of MAPK13, protein tyrosine phosphatase (PTP), and MAP2K3 while down-regulating MAP3K5. Additionally, the relative gene expression values were significantly lower for C-ABC, suggesting that TGF-β1 treatment altered the expression of

MAPK intermediates more so than C-ABC. These expression trends mirrored the microarray data.

C-ABC plays a biophysical role

The lack of genetic effects due to C-ABC treatment prompted further investigation of the role of C-ABC. It was hypothesized that C-ABC acted via a biophysical mechanism to influence tensile properties. Specifically, because collagen plays a major role in the tensile properties of cartilage, we considered that C-ABC was modulating the collagen network at the biophysical level, subsequently enhancing tensile properties. Several aspects of the collagen network contribute to its mechanics including fibril organization, fibril diameter, and post-translational modifications such as pyridinoline crosslinking. Polarized light microscopy showed that C-ABC did not produce any detectable collagen organization (data not shown). Because C-ABC did not appear to be promoting collagen orientation, we decided to also investigate collagen fibril diameters.

Our previous work showed that C-ABC treatment depletes the small proteoglycan decorin,[138] which inhibits fibril growth, so it was hypothesized that C-ABC application would increase collagen fibril diameter. Control, intermittent TGF-β1, C-ABC, and combined treatments were imaged using SEM at 4 weeks (Fig. 4a). SEM image analysis showed that mean fibril diameters were 43.3±8.6 nm, 40.1±6.2 nm, 64.4±7.8 nm, and 59.2±4.3 nm for control, TGF-β1, C-ABC, and combined treatments, respectively (Fig. 4b). These values corresponded to a 50% increase in fibril diameter due to C-ABC treatment. TGF-β1 treatment alone

did not significantly alter fibril diameter. Similar trends were observed for the density of fibrils, which was computed as the percent area occupied by collagen. Fibril density increased by 36% and 29% following C-ABC and combined treatments, respectively. These results indicated that C-ABC treatment was increasing fibril diameter and density, while TGF-β1 treatment did not have a significant influence.

Constructs treated with C-ABC and TGF-β1 exhibit in vivo stability and maturation

To assess any changes in morphological, biochemical, or biomechanical properties following *in vivo* culture, neotissue (grown for 4 weeks *in vitro* and treated with C-ABC and intermittent TGF-β1) and native cartilage controls were implanted subcutaneously in athymic mice. Mice were sacrificed at 4 weeks after implantation (8 weeks total neotissue growth) and all samples were removed without complications. Both neocartilage and explants exhibited a cartilage phenotype as evidenced by histological analysis (Fig. 5a). Although both constructs and explants had the same diameters upon implantation, explants showed lower diameters and increased thicknesses post-sacrifice. Post-sacrifice diameters were 4.9±0.16 mm and 5.8±0.09 mm for explants and neocartilage, respectively. Respective thicknesses for explants and neocartilage were 1.82±0.14 mm and 1.25±0.07 mm.

Neocartilage constructs exhibited both biochemical and biomechanical maturation *in vivo*. Post-sacrifice explant tensile stiffness decreased (p=0.02) and

the aggregate modulus remained unchanged (Fig. 5b, 5d). For constructs, tensile stiffness was significantly higher post-sacrifice (p=0.01), exhibiting 3.15±0.47 MPa compared to 1.95±0.62 MPa (Fig. 5b). Increased collagen content (Fig. 5c) paralleled the increased tensile properties: collagen/ww was 12.5±1.8% and 19.0±2.3% for pre-implantation post-sacrifice groups, respectively. Although GAG content and compressive stiffness did not increase for explants, post-sacrifice neocartilage exhibited enhanced GAG content (Fig. 5e) and increased compressive stiffness (Fig. 5d). These results showed that self-assembled neocartilage matures *in vivo*, further enhancing the effects noted *in vitro*.

Discussion

This is the first study to examine the mechanisms underlying dual anabolic and catabolic treatments for enhancing articular cartilage formation. Results confirmed our hypothesis that combining these agents (C-ABC and TGF-β1) would further enhance tensile properties compared to either treatment acting alone. Novel contributions of this study include demonstrating 1) C-ABC and TGF-β1 can be applied to synergistically enhance neotissue formation, 2) TGF-β1 can be applied to aid the recovery of compressive stiffness following C-ABC treatment, 3) TGF-β1 increases MAPK signaling in self-assembled neocartilage, 4) C-ABC treatment increases collagen fibril diameter and density, and 5) neocartilage exhibits stability and maturation *in vivo*.

Neotissue treated with both TGF-β1 and C-ABC exhibited *in vitro* maturation, attaining biochemical and biomechanical properties approaching native values. This is particularly exciting for collagen content and tensile

properties, which are typically lower for *in vitro* cartilage.[142] For combined treatment groups, the collagen content spanned adult values for both human and bovine cartilage,[21,22] indicating that TGF-β1 and C-ABC help recapitulate cartilage development. The additive increase of Young's modulus coupled with synergistic increases in collagen content showed the promise of applying TGF-β1 and C-ABC in combination. Collectively, these results indicated that dual treatment promoted *in vitro* cartilage development, producing neocartilage on par with native tissue, as evidenced by the higher functionality index.

Growth factor treatment during week 3 also promoted the recovery of compressive stiffness following C-ABC treatment, which was a concern from prior work.[51,138] In addition, intermittent TGF-β1 treatment combined with C-ABC treatment expedited the recovery of compressive properties and supplemented improvements to construct collagen content and tensile properties seen with C-ABC treatment alone. The contribution of TGF-β1 to compressive recovery following C-ABC treatment showed how an anabolic agent can be employed to overcome one of the challenges associated with C-ABC. This reinforced the benefits of combining anabolic and catabolic agents during neotissue formation.

Microarray analysis showed that TGF-β1 up-regulated MAPK signaling via p38, suggesting that this is the primary mechanism of TGF-β1 signaling in self-assembled neocartilage. Other work has shown that inhibiting p38 MAPK signaling in chondrocytes represses TGF-β1 gene expression in a dose-dependent manner.[27] Similarly, inhibiting p38 MAPK activity reduced TGF-β-induced proteoglycan synthesis in articular chondrocytes,[143] showing that p38

signaling influences biosynthesis. Various studies also showed the role of p38 signaling in chondrogenesis, which was suppressed by p38 inhibition.[144] Furthermore, inhibition of chondrogenesis using epidermal growth factor[145] or retinoic acid[146] both corresponded with reduced p38 activity, reinforcing the role of p38 in cartilage development. These studies highlight the developmental and biosynthetic role of p38 signaling in chondrocytes, which could explain the increased GAG and collagen contents observed in self-assembled neotissue treated with TGF-β1.

C-ABC has been employed to induce maturational growth during cartilage formation,[51,138,139] but its mechanism has not been previously interrogated. Unlike TGF-β1, C-ABC treatment does not appear to enrich functionally relevant pathways, suggesting that it did not significantly alter gene expression. The similarity between the gene expression profiles of TGF-β1 and combined treatments reinforced the minimal influence of C-ABC on genetic signaling. Although it is conceivable that C-ABC could indirectly alter gene expression by modulating the bioavailability of signaling molecules or reducing the abundance of matrix molecules that interact with chondrocytes, these effects did not appear to be predominant in self-assembled constructs. Increased tensile properties due to C-ABC treatment without gene expression changes suggested that C-ABC could have a biophysical mechanism.

Indeed, SEM analysis identified a potential biophysical mechanism underlying C-ABC treatment by illustrating increased collagen fibril diameters. The increased fibril diameters noted with C-ABC treatment, which parallel the

fibril growth that occurs as cartilage matures,[142] show that C-ABC promotes maturation of the collagen network. Fibril diameters of C-ABC treated constructs, which were 59±4.3 nm, are on par with the native tissue values of 30-80nm.[147,148] In addition, fibril diameter has been shown to influence the stiffness of collagen fibers,[149] which supports the hypothesis that the increased Young's modulus following C-ABC administration relates to fibril diameter, in addition to increased collagen content. This finding also suggests that exciting new strategies such as altering decorin expression could be employed to alter the collagen network. It is well known that small leucine-rich proteoglycans impact collagen fibrillogenesis, so they offer a rich new area of research for improving neocartilage.

This study also was the first to show that self-assembled cartilage can mature *in vivo*. Interestingly, explant tensile properties decreased while neocartilage properties increased. Other work has shown that cartilage explants can swell and subsequently demonstrate reduced tensile properties,[150] which could explain why the explants were less stiff and had increased thicknesses. The improved neocartilage properties could result from the nutrient rich environment that *in vivo* environments provide, which has been shown to improve the properties of implanted engineered tissue.[151] Because the neocartilage was significantly more cellular than native tissue, it could have had a more pronounced response to *in vivo* nutrients and growth factors. The increased biochemical and biomechanical properties, without concomitant swelling or contraction, suggest that self-assembled cartilage can develop *in vivo*.

This study showed how anabolic and catabolic agents can be combined to promote *in vitro* and *in vivo* neocartilage maturation. TGF-β1 application increased MAPK signaling, which could be responsible for increased biosynthesis and the observed increases in matrix composition. Additionally, this is the first study to identify a potential mechanism for the effects of C-ABC on enhanced cartilage formation. The two distinct mechanisms underlying C-ABC and TGF-β1 treatments could help explain the synergistic effects of combining these agents. Based on the maturation that constructs displayed when implanted in mice, *in vivo* culture presents an exciting opportunity for improving *de novo* cartilage formation. Future experiments could further investigate the mechanisms underlying the effects of these stimuli and examine the response of self-assembled neocartilage in larger animal models.

Methods

Neocartilage culture

Immature bovine chondrocytes were harvested and cultured as described previously.[94] For C-ABC treatment, constructs were treated with C-ABC (Sigma) at an activity of 2 U/ml in chondrogenic medium for 4 hours.[47] TGF-β1 (Peprotech) was administered daily media at 30 ng/ml. At 4 weeks, constructs were prepared for biochemistry, histology, and biomechanics.[138]

Quantitative biochemistry

Samples were frozen at -20°C for 24h and then lyophilized for dry weight determination. Subsequently, a pepsin and elastase protocol[138] was used to

digest each sample. A Blyscan Glycosaminoglycan Assay kit (Accurate Chemical and Scientific Corp.) was used to quantify sulfated GAG content. Collagen abundance was determined using chloramine-T based assay.[117]

Histology

Samples were cryoembedded and sectioned at 12 μm. Histology samples were fixed in formalin and then stained with Safranin-O/fast green and Picrosirius Red as described previously.[138] For IHC, samples were fixed in 4°C acetone and stained for collagen II or collagen I.[138]

Mechanical testing

A creep indentation apparatus[152] was used to quantify compressive properties. Samples were tested as described previously[138] using a semi-analytical, semi-numeric, biphasic model[118] and finite element optimization[153] to yield each sample's aggregate modulus. For tensile testing, dermal punches were used to create dog-bone shaped samples.[122] A material testing system (Instron Model 5565) was used to apply uniaxial tension.[138] The slope of the linear portion of each stress-strain curve was reported as the Young's modulus (E_Y).

Scanning electron microscopy (SEM)

SEM was performed for control, intermittent TGF-β1, C-ABC, and combined intermittent TGF-β1 and C-ABC groups. Samples were fixed in 3% glutaraldehyde for 12h at 4°C and then dehydrated in an ascending series of

ethanol. Samples were subsequently critical point dried and sputter coated with gold prior to imaging. Three locations were used for each sample and n=3. For each image, a 4x4 grid was drawn and three squares were randomly chosen from each image for diameter quantification using ImageJ. To quantify density, the ImageJ threshold function was used to set threshold limits. The measure function was then used to compute the area percentage corresponding to fibrils, which was reported as density.

RNA isolation and microarray hybridization

RNA was isolated at 2 wks for control, C-ABC, continuous TGF-β1, and C-ABC combined with continuous TGF-β1 (n=3). Isolation was performed 4h following the administration of C-ABC and/or TGF-β1 using a Qiagen RNeasy Lipid Tissue Mini Kit. RNA was analyzed using a nanodrop to determine RNA purity and concentration; an Agilent bioanalyzer was employed to ensure RNA was not degraded. 400ng of RNA was hybridized to bovine microarrays (Agilent) based on the manufacturer's one color gene expression protocol. Arrays were imaged using an Agilent high-resolution C scanner; images were processed using Agilent's Feature Extraction Software 10.5.

Microarray analysis

Entrez Gene IDs were cross-referenced with HomoloGene build 65 (ftp://ftp.ncbi.nih.gov/pub/HomoloGene/build65/) to determine human orthologs. Normalized intensities of each gene were used to determine differentially

expressed genes relative to control samples (n=3 for each group). The Benjamini-Hochberg multiple testing correction was applied to generate adjusted p-values; data were filtered based on adjusted p-values < 0.005 and a minimal 2 fold change. Enriched pathways were determined based on $p < 0.001$.

PCR

The primer for GAPDH was synthesized as described previously.[69] Other primers including MAP3K5, MAPK13, protein tyrosine phosphatase (PTP), and MAP2K3 were purchased from Invitrogen. RT was performed by incubating 500 ng of RNA with SuperScript III (Invitrogen) as recommended by the manufacturer. Real-time PCR was done using SYBR Green mastermix and 1 μM primers on a Rotor-gene 3000 real-time PCR machine (Corbett Research). A 10 min denaturing step was employed, followed by 45 cycles of 95°C (15s) and 60°C (60s). The take-off cycle (C_T) for each gene of interest (GOI) was compared to the housekeeping gene GAPDH. Relative gene expressions were calculated using the $2^{-\Delta\Delta CT}$ method.

In vivo study

Four male athymic mice, age 6-8 weeks were utilized under the approval of the Animal Use and Care Administrative Advisory Committee, University of California, Davis. Under general anesthesia, one construct (treated with C-ABC and intermittent TGF-β1) and one cartilaginous bovine explant were implanted in a subcutaneous pouch, one in each side of the thorax, in a random fashion. The

mice were humanely sacrificed at 4 weeks and the implanted tissues were harvested.

Statistical analysis

Biochemistry and mechanical testing data (n=6) were analyzed using a two-factor ANOVA of the factors C-ABC treatment or TGF-β1 treatment with $p<0.05$. Post-sacrifice and pre-implantation data were compared using an unpaired, one-tail t-test. PCR data (n=3) were analyzed using a one-factor ANOVA with $p<0.05$. SEM diameters were analyzed using repeated measures ANOVA, with 9 data points per sample (n=3). Student Newman–Keuls post-hoc test was applied when warranted. The interaction term of a two-factor ANOVA was used to test for additive or synergistic effects as described previously.[123] All data are shown as mean ± standard deviation.

Acknowledgements

The authors acknowledge funding support from NIAMS R01AR053286 and thank Kevin Lockwood, James Cravotta, and Jamie Amaral for assistance during *in vivo* procedures.

Table 2-1: Differentially expressed genes in the MAPK pathway.

	TGF-β1		C-ABC + TGF-β1	
Gene	FC	Regulation	FC	Regulation
RAS p21 activator 2	2.1	up	2.2	Up
Dual specificity phosphatase 4	2.8	up	2.5	Up
FGF 2	4.0	up	4.1	up
MAPK 8 interacting protein 1	4.6	up	3.9	up
MAP2K 3	4.1	up	3.9	up
protein tyrosine phosphatase, type 7 (PTP)	5.5	up	3.3	up
TGF-β1	6.6	up	6.9	up
calcium channel, β3 subunit	2.2	down	2.5	down
FGF 13	3.2	up	3.4	up
FGF 18	2.3	up	3.2	up
MAPK 13	3.2	up	2.1	up
MAP3K 5	3.2	down	2.6	down
MAP3K 6	5.1	up	5.4	up
p21 protein-activated kinase 1	2.6	up	2.8	up
PDGF receptor	3.2	down	3.6	down
tyrosine phosphatase - receptor type 5	14.4	up	13.7	up
TGF-β receptor II	2.6	down	2.7	down
TGF-β3	2.4	down	2.1	down
RAS guanyl releasing protein 4	4.5	up	-	-
MAPK serine/threonine kinase 1	-	-	2.3	up

Microarray analysis was used to determine genes that were differentially expressed in 2 week self-assembled neocartilage treated with TGF-β1 (during weeks 1&2) or with chondroitinase-ABC (C-ABC) and TGF-β1. These differentially expressed genes significantly enriched the MAPK pathway. Fold changes are relative to control values. Dashes represent no differential expression for that gene.

Figure 2-1: Histology and gross morphology at 4 weeks.

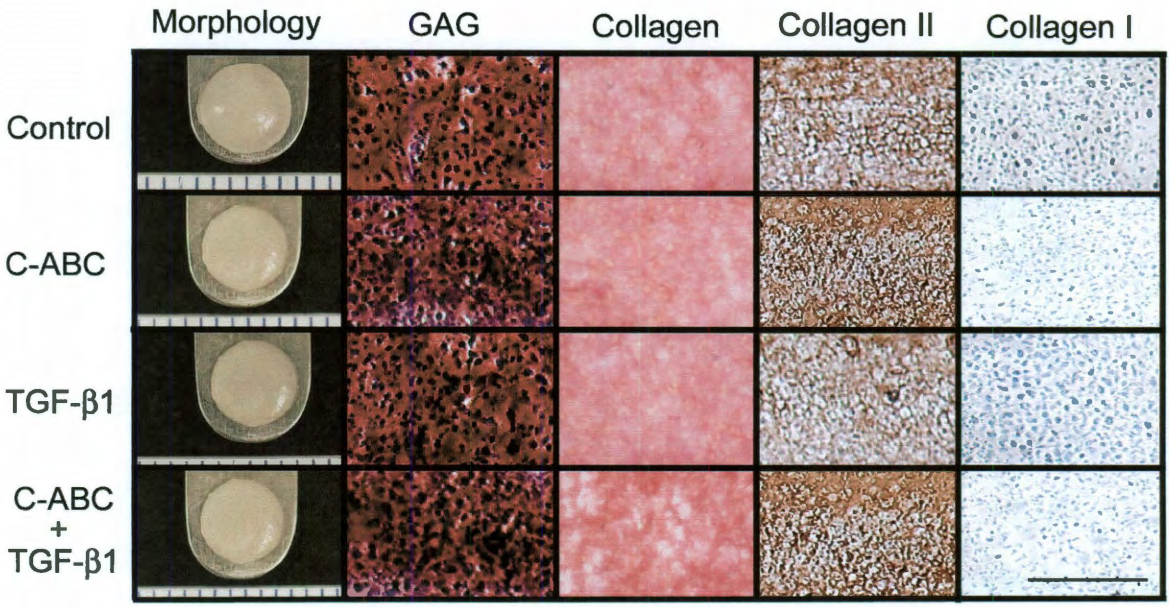

Neocartilage treated with chondroitinase-ABC (C-ABC), intermittent TGF-β1, or C-ABC combined with TGF-β1. Histology showed that control and treated constructs had uniform distributions of glycosaminoglycans (GAGs), total collagen, and collagen II without exhibiting collagen I staining. Picrosirius Red was used to stain total collagen and Saf-O/fast green was used for GAG staining. IHC was employed to assess collagen I and collagen II distributions. Scale bar is 200 μm for histology images and gross morphology markings are 1 mm.

Figure 2-2: Biomechanical and biochemical properties at 4 weeks.

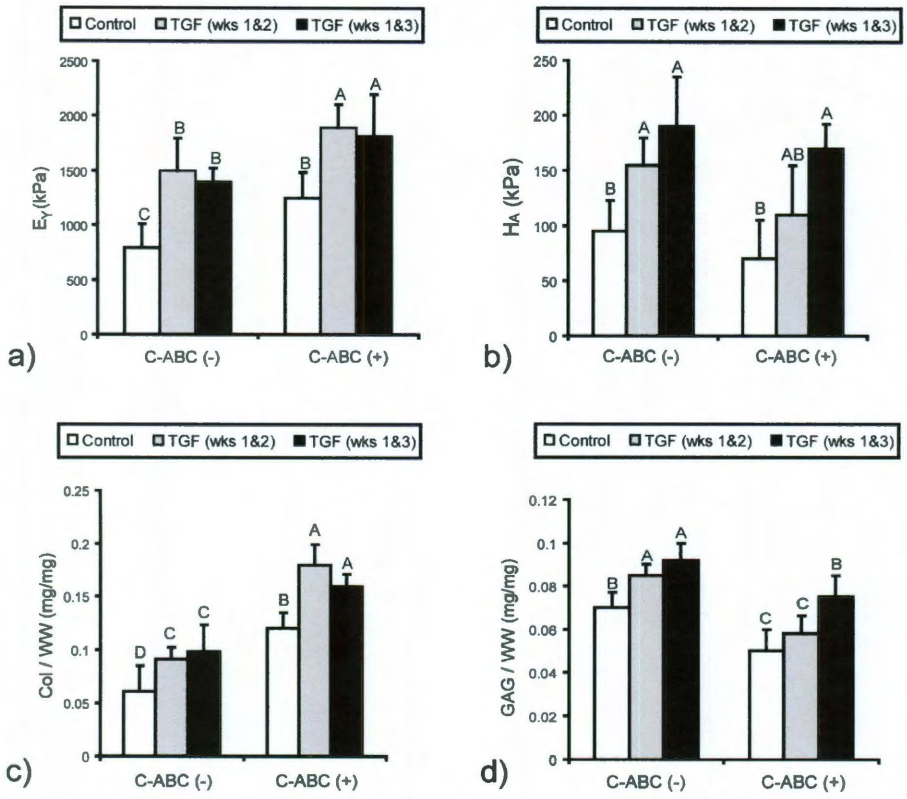

Neocartilage was treated with chondroitinase-ABC (C-ABC), TGF-β1, or C-ABC and TGF-β1. (a) Tensile stiffness was enhanced by C-ABC and TGF-β1 treatments and additively increased for combined treatment groups. (b) Compressive stiffness was highest for groups treated with intermittent TGF-β1. (c) Combined C-ABC and TGF-β1 treatment synergistically increased collagen content. (d) GAG content was highest for groups treated with TGF-β1. Bars labeled with different letters exhibit significant differences ($p < 0.05$).

Figure 2-3: PCR of MAPK signaling gene expression in neocartilage

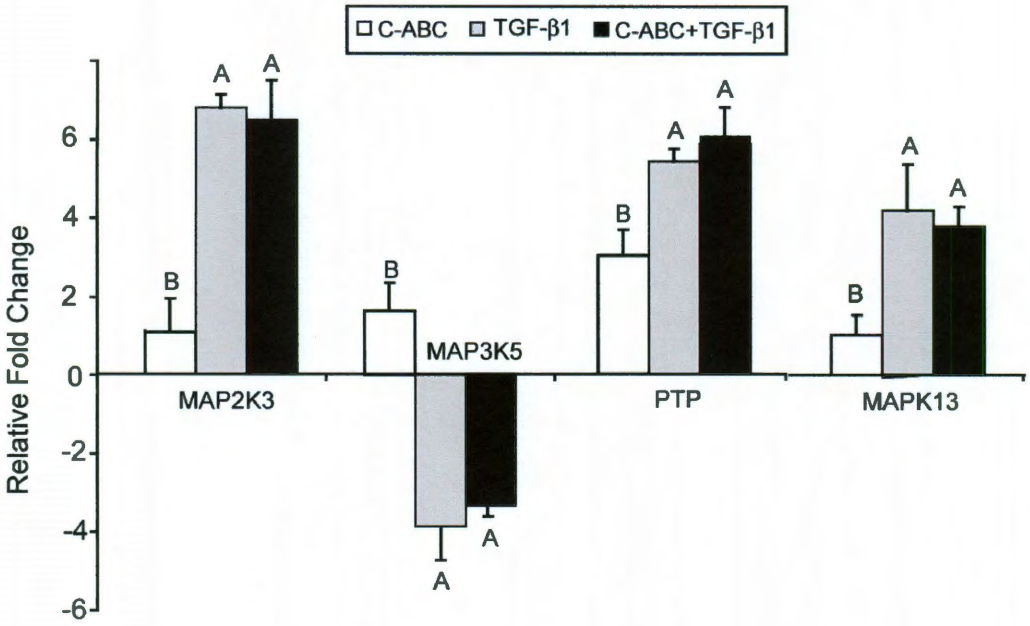

Gene expression levels for MAP3K5, MAPK13, protein tyrosine phosphatase (PTP), and MAP2K3 were normalized to control values. Combined treatments and TGF-β1 treatments generally had gene expression levels that were not statistically distinct. Negative values reflect down-regulation in relation to control. Bars labeled with different letters exhibit significant differences ($p < 0.05$).

Figure 2-4: SEM analysis of neotissue at 4 weeks.

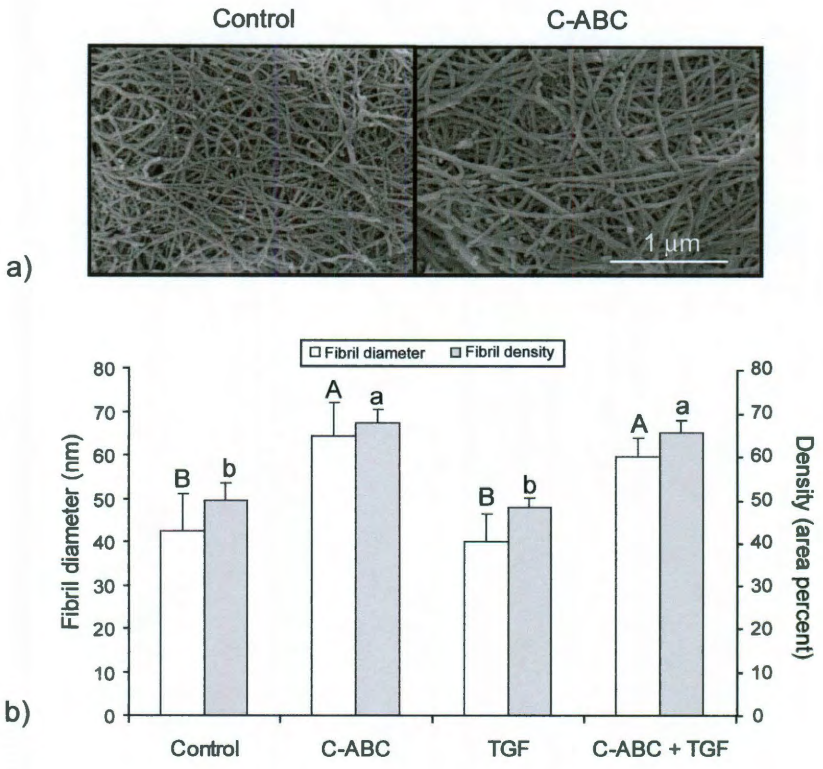

(a) Representative SEM images of control neotissue and neocartilage treated with chondroitinase-ABC (C-ABC). (b) Quantification of fibril diameters based on image analysis of 3 locations on each neotissue sample with n=3. Bars labeled with different letters exhibit significant differences ($p < 0.05$).

Figure 2-5: Properties of constructs post-sacrifice

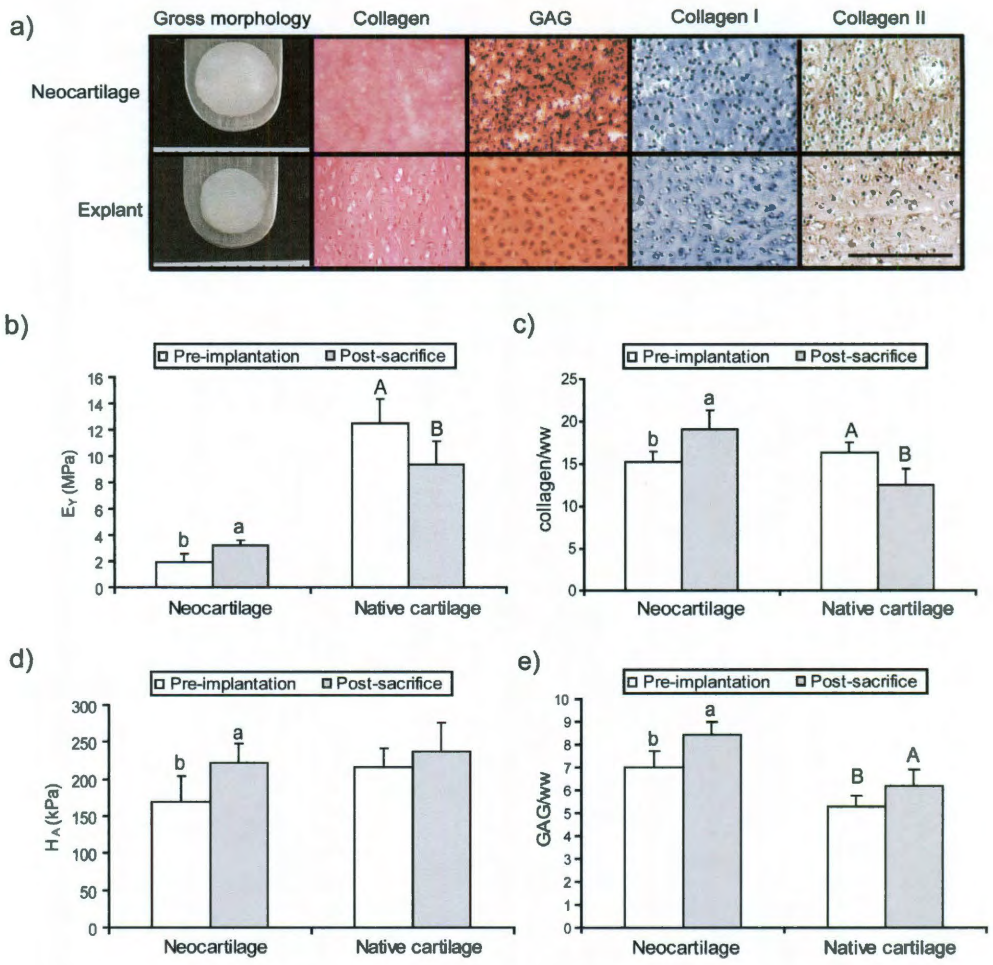

Self-assembled articular cartilage was cultured for 4 weeks with TGF-β1 treatment during weeks 1&3 and chondroitinase-ABC (C-ABC) administration at day 14. Neocartilage was then implanted in nude mice for 4 weeks with condylar cartilage explants as controls (n=4). (a) Gross morphology and histology using Picrosirius Red for collagen, Safranin-O/fast green for glycosaminoglycans, and immunohistochemistry for collagen I and collagen II. Scale bar is 200 μm. (b) Post-sacrifice tensile stiffness increased for neocartilage while explant stiffness

decreased. (c) Collagen content increased for constructs post-sacrifice while it decreased for native cartilage. (d) Compressive stiffness increased for constructs but did not significantly change for explants. (e) Glycosaminoglycan (GAG) content increased for both native tissue and neocartilage post-sacrifice. Bars labeled with different letters exhibit significant differences ($p < 0.05$).

Chapter 3: Identification of potential biophysical and molecular signaling mechanisms underlying hyaluronic shows that acid enhancement of cartilage formation*

Abstract

This study exogenous hyaluronic acid (HA) acts via both biophysical and genetic mechanisms to enhance biomechanical and biochemical properties of self-assembled neocartilage. The influence of HA commencement time, concentration, application duration, and molecular weight was assessed. HA treatment of developing neocartilage increased compressive stiffness 1-fold and increased glycosaminoglycan (GAG) content by 35%. Additionally, applying HA increased GAG retention within self-assembled neotissue, indicating that HA could enhance compressive stiffness by increasing the osmotic pressure that negatively charged GAGs create. To investigate the influence of HA administration on gene expression, microarray analysis was conducted and validated with PCR. HA administration up-regulated 503 genes, including multiple genes associated with TGF-β signaling, revealing a potential mechanism for altering matrix composition. This study is the first to show that exogenous HA application can enhance biochemical and biomechanical properties during cartilage formation, illustrating the potential use of HA to improve future cartilage regeneration efforts and better understand cartilage development.

---

* Responte DJ, Natoli RM, Athanasiou KA. Identification of potential biophysical and molecular signaling mechanisms underlying hyaluronic shows that acid enhancement of cartilage formation. *Nat. Commun.* (submitted)

Articular cartilage lines the articulating surface of bones and provides a low-friction, load-bearing surface. Developing an effective *in vitro* method for cartilage formation could provide a platform technology for investigating novel regeneration strategies, studying cartilage pathogenesis, and examining cartilage development. However, numerous problems including chondrocyte de-differentiation[70] and difficulty reproducing the cartilage matrix[109-112] have hindered the development of effective *in vitro* cartilage growth models.

Recent efforts have focused on developing *in vitro* neocartilage that recapitulates the biochemical composition and biomechanical properties of native tissue. The primary matrix constituents of cartilage are glycosaminoglycans (GAGs) and collagen, which confer tensile and compressive integrity to the tissue. Aggrecan, the major proteoglycan of cartilage, binds negatively charged GAGs and subsequently increases the fixed charge density of the tissue, increasing resistance to compressive loading.[154] Collagen contributes primarily to tensile mechanics; both the amount and organization of collagen in articular cartilage correlate with tensile properties.[128,155] Because the extracellular matrix (ECM) contributes extensively to cartilage biomechanics, modulating the composition, organization, and interactions between matrix molecules is a central goal of *in vitro* cartilage development.

Our laboratory has pioneered a novel self-assembly approach for scaffoldless cartilage formation[94,102] based on high density chondrocyte culture. Self-assembly avoids many of the problems associated with biomaterial scaffolds such as decreased retention of phenotype,[70] limit cell-cell communication,[58,156]

and potential toxicity of degradation byproducts.[157] This process also mimics cartilage development,[103] providing a platform for investigating *in vitro* cartilage formation. Surprisingly, a recent study showed that self-assembled constructs lacked hyaluronic acid (HA),[103] a high molecular weight polysaccharide present in the ECM that acts a scaffold for proteoglycans,[158] suggesting that it may be necessary to exogenously add HA to reproduce native cartilage formation.

Applying HA to chondrocyte cultures has been shown to increase biosynthesis in various experimental models. For instance, HA application to monolayer cultures has been observed to increase proteoglycan synthesis in equine articular cartilage,[159] rabbit chondrocytes,[160,161] and bovine articular cartilage.[162] Furthermore, exogenous HA administration has been shown to promote the expression of adhesion-related molecules such as integrin receptors, paxillin, focal adhesion kinase, and mitogen-activated protein kinase, suggesting that HA application could modulate chondrocyte-matrix interactions.[163] These studies show that HA has a significant signaling role that could influence the functional properties of neotissue, but there have not yet been studies on how exogenous HA treatment influences biomechanical properties.

In this paper, we present a series of studies evaluating the effects of exogenous HA application on the *de novo* formation of self-assembled articular cartilage and potential mechanisms underlying these effects, which have implications for both developmental biology and regenerative medicine. The influence of HA application time, concentration, and molecular weight on the

biochemical and biomechanical properties of neocartilage were investigated. Our hypotheses were that exogenous HA treatment would 1) increase GAG content, 2) enhance compressive stiffness, 3) differentially regulate functionally-relevant genetic pathways, and 4) increase GAG retention. To interrogate these hypotheses, HA was administered to neotissue in three sequential phases to examine the effects of HA commencement time (phase I), HA concentration and duration (phase II), and HA molecular weight (phase III).

Results

HA-treated neotissue resembles native cartilage phenotype

In all experiments in this paper (except gene expression analysis), self-assembled neocartilage was cultured for 4 weeks. The diameter of HA-treated constructs was not statistically different from the control value of 5.8±0.2 mm. Wet weight was significantly greater for HA treatment, with values of 14±2 and 20±1 mg for control and HA-treated groups, respectively. Histological analysis (Fig. 3-1) showed that neocartilage produced collagen and GAG uniformly. Immunohistochemistry indicated that both control and treated samples stained positive for collagen II, while only HA-treated constructs stained positive for HA. Additionally, HA-treated neotissue produced matrix that reflected native articular cartilage phenotype: uniform distribution of GAGs, total collagen, collagen II, and HA.

HA increases GAG content and compressive stiffness when applied at seeding

In phase I, the effects of application commencement time were studied. Neotissue was treated with 1 mg/ml HA at seeding (day 0) or at day 4, with subsequent continual HA exposure through media changes. To assess the effects of HA application on biochemical composition, GAG and collagen contents were quantified. Treated neotissue did not exhibit statistically different collagen contents normalized to wet weight (col/ww) from the control value of 9.5±2.3%. However, GAG/ww was statistically higher for the day 0 group, which had a GAG/ww of 8.5±1.4% compared to the control value of 6.5±0.9% at 4 weeks (Fig. 2b). The effects of HA on construct biomechanical properties were quantified by measuring Young's modulus (E_Y), ultimate tensile strength (UTS), and aggregate modulus (a measure of compressive stiffness). For tensile properties, no group was statistically different from the control group, which had a UTS of 370±155 kPa and E_Y of 641±370 kPa. The aggregate modulus was significantly higher for constructs treated with HA: the group treated at seeding reached 181±50 kPa while the control group was 65±33 kPa (Fig. 2a).

Intermediate HA concentration enhances compressive stiffness

In phase II, we carried forward the application of HA at seeding and then performed a full-factorial examination of the treatment duration (weeks 1-2, weeks 1-4) and HA concentration (0.1 mg/ml, 1 mg/ml, and 5 mg/ml). Neocartilage was again cultured for a total of 4 weeks. Constructs treated with 5 mg/ml HA did not self-assemble, probably due to the high viscosity of the solution. GAG results (Fig. 2d) showed differences only for the 1 mg/ml group; no

significant differences were observed for the 0.1 mg/ml groups or between the two application durations. For the 1 mg/ml HA treatment, GAG content reached 8.3±0.9%, which was 38% greater than the control value. Collagen contents for treated groups were not significantly different than the control value of 8.9±0.5%. Biomechanical properties of neotissue treated with 1 mg/ml paralleled phase I results. Treating with HA at 1 mg/ml increased the aggregate modulus by approximately 40% (Fig. 3-2c); however, the 0.1 mg/ml group did not exhibit significantly higher compressive stiffness. Neither the 0.1 mg/ml group nor the 1 mg/ml group had tensile properties that statistically differed from control values of 748±97 and 362±117 kPa for the E_Y and UTS, respectively. Thus, the effects of HA treatment depended on concentration, but did not depend on whether application duration was 2 weeks or 4 weeks.

HA molecular weight influences biomechanical and biochemical properties

A range of HA molecular weights exist in native cartilage, varying between $3x10^5$ Da and $2x10^6$ Da,[164] and HA size has profound influences on its biological function. To examine the influence of HA size, we assessed the effects of five different molecular weights: $5.1x10^3$ Da, $1.2x10^4$ Da, $3.1x10^4$ Da, $1.7x10^6$ Da, and $2.7x10^6$ Da, all at concentrations of 1 mg/ml. Treatment commenced at seeding and was continuous for the first 2 weeks of culture based on phase II results. Constructs were assessed after 4 weeks of culture. Neocartilage had significantly higher GAG content (Fig. 2f) when treated with $1.7x10^6$ Da or $2.7x10^6$ Da HA (p = 0.023). GAG/ww values were 6.0±0.9%, 6.5±0.7%,

5.9±1.0%, 5.5±1.3%, 7.4±0.9%, and 7.2±0.5% for the control, $5.1x10^3$ Da, $1.2x10^4$ Da, $3.1x10^4$ Da, $1.7x10^6$ Da, and $2.7x10^6$ Da groups respectively. The $1.7x10^6$ Da and $2.7x10^6$ groups both showed increased compressive stiffness with values of 163±33 kPa and 136±37 kPa, respectively (Fig. 3-2e). Hence, only higher molecular weight HA had the ability to enhance the biochemical and biomechanical properties of neocartilage.

HA promotes GAG retention

Increasing GAG retention, which would increase the fixed charged density of the neotissue, could provide a biophysical mechanism for enhanced compressive properties. Thus, after 4 weeks of culture, GAG retention was assessed by incubating control and HA-treated constructs in PBS for 1h, 2h, 4h, 6h, or 8h and quantifying the GAG content of each construct (Fig. 3-3). HA-treated neotissue had $1.6x10^6$ Da HA applied at 1 mg/ml from seeding for the first 2 weeks of culture. GAG content was not statistically different for the first hour, but then began to decrease by 2h. By 8h, GAG content for control constructs had decreased to 3.7% of the initial amount. HA treatment promoted significant GAG retention compared to control based on a 2-way ANOVA (p = 0.034) of the factors duration and HA treatment. For instance, after 8h of incubation in PBS total GAG content of the HA-treated was three times higher than that of the control (0.15±0.12 μg and 0.05±0.04 μg, respectively).

Neocartilage properties are on par with native tissue

To quantitatively compare the properties of neocartilage to native tissue, we employed a functionality index (FI) by giving equal weight to the GAG content (G), collagen content (C), compressive stiffness (E^C), and tensile stiffness (E^T) (see Eq. 1). The subscripts 'nat' and 'sac' denote native and self-assembled construct values, respectively.

$$FI = \frac{1}{4}\left(\left(1-\frac{(G_{nat}-G_{sac})}{G_{nat}}\right)+\left(1-\frac{(C_{nat}-C_{sac})}{C_{nat}}\right)+\left(1-\frac{(E^T_{nat}-E^T_{sac})}{E^T_{nat}}\right)+\left(1-\frac{(E^C_{nat}-E^C_{sac})}{E^C_{nat}}\right)\right) \quad (1)$$

The FI is structured such that a score of 1 represents a construct with properties equivalent to those of native cartilage. Treating with 1 mg/ml, $1.6x10^6$ Da HA beginning at seeding for a total of 2 weeks resulted in a FI of 0.85, producing a considerable improvement over the control FI of 0.56.

Microarray and PCR analyses show that HA enriches functional gene pathways

To investigate possible genetic mechanisms underlying the changes in functional properties, microarray analysis comparing the gene expression profiles of control constructs and HA-treated constructs was performed. For these experiments, neocartilage was treated with 1 mg/ml, $1.6x10^6$ Da HA beginning at seeding. Gene expression was analyzed at 4 days based on prior data showing elevated levels of surface receptors on day 4.[103] Results showed that HA application differentially regulated 794 genes: 503 genes were up-regulated and 291 genes were down-regulated. HA treatment up-regulated several genes relating to chondrocyte phenotype[165] including collagen II, collagen XI, and chondroadherin. HA treatment down-regulated collagen I, which is associated with chondrocyte de-differentiation. The up-regulation of cartilage-specific genes and concomitant

decrease in collagen I expression suggested that HA administration promoted cartilage phenotype.

As summarized in Table 3-1, genes only enriched pathways relating to TGF-β signaling (9 genes, p = 0.003) and ECM-receptor interactions (11 genes, p = 0.0001). The ECM-receptor pathway included the upregulation of several collagen molecules (collagen II, III, and XI) and surface receptors (syndecan-4 and integrin α7), suggesting that HA could modulate chondrocyte interactions with the surrounding ECM. The TGF-β pathway list included several well established downstream intermediates of TGF-β signaling including protein phosphatase and the transcription factors Myc and E2F4. These enriched pathways showed that exogenous HA administration modulated functionally-relevant gene expression, which could contribute to the observed biochemical and biomechanical results.

Quantitative real time PCR was used to validate microarray results. Gene expression values for collagen II, collagen I, Myc, E2F4, and protein phosphatase were quantified (Fig. 4). HA treatment increased the expression of collagen II, Myc, E2F4, and protein phosphatase by 13.2±2.1, 12.1±1.9, 7.1±1.4, and 9.0±4.3 fold, respectively. Additionally, HA treatment down-regulated collagen I expression 7.0±3.0 fold. These results paralleled the fold changes observed with microarray results.

Discussion

This study has shown that exogenous HA application improves the biochemical and biomechanical properties of neocartilage and also enriches pathways relating to TGF-β signaling and ECM-receptor signaling. Through several phases, an HA administration regimen was identified that enhances the biochemical and biomechanical properties of developing neocartilage. Subsequent study revealed potential mechanisms to explain the observed results. The experiments of this study confirmed the hypotheses that exogenous HA treatment 1) increases GAG content, 2) enhances compressive stiffness, 3) differentially regulates functionally-relevant genetic pathways, and 4) increases GAG retention. This is the first study to show that HA can be applied exogenously to improve the biochemical and biomechanical properties of tissue engineered cartilage. This work also demonstrates potential biophysical and genetic mechanisms that could produce these enhancements.

Diffusion limitations could be underlying the observed dependence on commencement time but not application duration. Other studies have documented increased diffusion limitations during cartilage construct culture. For instance, 3 kDa dextran showed decreased diffusion as constructs were cultured; the authors attributed this reduced diffusion to increased matrix deposition.[166] Time-dependent diffusion limitations could decrease HA penetration at later time points and explain why HA application at seeding had a larger effect than when it was applied at day 4. The lack of dependence on application duration implies that the HA effects are maximized at the earlier stages of self-assembly, which

also makes sense in light of likely diffusion limitations. Previous diffusion studies and the effects observed in this study suggest that HA must be applied in the early stages of neocartilage formation to enhance construct properties.

This study also showed that higher molecular weight HA can increase compressive stiffness by 75% and increase GAG content by 30%, which builds upon other studies that have shown the importance of HA molecular weight. In general, larger molecular weight HA is considered to be chondroinductive[167] whereas smaller fragments, such as HA hexamers, are generally associated with inflammatory events and disruption of pericellular matrix formation.[168] HA molecular weight could influence signaling because HA size alters how many CD44 receptors it can bind, which in turn changes the signaling events related to CD44 receptor clustering.[169] These results suggest that HA molecular weight has a profound impact on its biological function, and imply that modulating chain length may be a powerful tool for altering the effects of HA applied *in vitro*. In particular, this study suggests that only higher molecular weight HA increases the GAG content and compressive stiffness of self-assembled neocartilage.

The GAG retention results suggest that the effects of HA are also mediated by a biophysical mechanism. Because negatively charged GAGs create a large fixed charge density in the matrix, enhanced GAG retention could increase osmotic pressure and subsequently increase resistance to compressive loading.[158] Thus, increasing GAG retention could increase the osmotic pressure of neocartilage and subsequently enhance its compressive properties. Exogenous HA has been shown to suppress proteoglycan release from

chondrocyte cultures[170,171] and reduce *in vivo* GAG release from canine joints.[172] Interactions between HA and other matrix molecules increase the viscosity of the matrix,[173] which could decrease GAG release. Because increased GAG retention could increase compressive stiffness, this presents an exciting potential biophysical mechanism underlying the enhanced mechanical properties.

In addition to biophysical effects, microarray and PCR results suggest that HA application has a molecular signaling role. Because HA up-regulated chondrogenic genes such as collagen II and down-regulated collagen I, it could be a potent chondrogenic agent for cartilage formation. Furthermore, the observed up-regulation of chondroadherin, which increases ERK signaling,[174] could create secondary signaling effects. Increased expression of syndecan-4, which binds to TGF-β1 via its heparan sulfate chains,[175] also suggests that TGF-β1 and HA could potentially be applied simultaneously to produce synergistic effects. These findings illustrate that HA administration increased the expression of key surface molecules such as syndecan-4 and integrin-α7 and matrix constituents including collagen II and collagen XI, which collectively could influence chondrocyte-matrix interactions.

In addition to the differential expression of matrix molecules, up-regulation of intracellular signaling intermediates, such as the transcription factors Myc and E2F4 as well as protein phosphatase, suggests that HA may induce a Smad cascade. Although there is not a well-established mechanism regarding CD44 signaling in chondrocytes,[176] data from this study indicate that HA may primarily signal using the TGF-β pathway in self-assembled neocartilage (Fig. 3-5). This

supports previous work showing that HA activates the TGF-β receptor and subsequently induces Smad protein phosphorylation.[177] Based on our previous investigations of direct TGF-β treatment,[59,178] signaling via the TGF-β pathway could up-regulate matrix synthesis and thus improve biochemical and biomechanical properties.

The observed changes in gene expression are probably mediated by the surface receptor CD44, which has been shown to bind the cytoplasmic domain of the TGF-β receptor and influence signaling.[177] However, conflicting results exist that show CD44 as a positive[177] and negative[179] regulator of the TGF-β signaling pathway. Interestingly, while anti-CD44 antibodies completely inhibit HA binding to chondrocytes, HA-mediated gene expression is not completely blocked.[180] This result shows that factors in addition to CD44 signaling play a role in HA-induced gene expression changes. Signaling via TGF-β intermediates could supplement the biophysical effects to enhance the functional properties of cartilage neotissue.

In summary, this study has shown that exogenous HA could act via both biophysical and genetic mechanisms to enhance the biomechanical and biochemical properties of self-assembled neocartilage. Although exogenous HA application has been studied in monolayer chondrocyte culture, this study has been the first to illustrate how HA can be applied exogenously to influence functional-relevant genetic pathways, and also improve biochemical and biomechanical properties during *in vitro* cartilage formation. Future studies could block CD44 to further investigate how HA influences intracellular signaling, apply

HA in conjunction with other agents such as TGF-β1 to synergistically improve construct functionality, and probe the biophysical mechanism of HA-induced GAG retention.

Materials and methods

Chondrocyte isolation and culture

Bovine chondrocytes were isolated and cultured described previously.[94] For HA treatment, $1.7x10^6$ Da HA (Sigma) was dissolved in chondrogenic media[94] by stirring at 4°C for 48h and applied daily during construct feeding. For phase III, HA polymers with molecular weights of $5.1x10^3$, $1.2x10^4$, $3.1x10^4$, $1.7x10^6$, and $2.7x10^6$ Da (Lifecore Biosciences) were employed.

Construct processing

All experiments except for gene expression analyses were 4 weeks in duration. At 4 weeks, samples were prepared for histology, quantitative biochemistry, and mechanical testing. A 3 mm diameter punch was removed from the construct's center for creep indentation testing. The outer region was divided to create samples for biochemical assays and tensile testing.

Histology and immunohistochemistry

At 4 weeks, samples were cryoembedded and frozen at -20°C for at least 24 hours prior to cryosectioning at 14 μm. Some of these sections were fixed in formalin and stained with Safranin-O/fast green and Picrosirius Red to show GAG and collagen distributions, respectively. Other sections were fixed in 4°C

acetone and processed for collagen II IHC as described previously.[138] For HA IHC, sheep anti-HA (Abcam) was diluted 1:100 followed by an anti-sheep IgG Vectastain ABC kit applied for 30 min.

Quantitative biochemistry

Samples were frozen at -20ºC for at least 24 hours and then lyophilized for 48 hours to obtain dry weights. Subsequently, each sample was digested using pepsin and elastase as described previously.[138] Sulfated GAG content was assayed using the Blyscan Glycosaminoglycan Assay kit (Accurate Chemical and Scientific Corporation). Total collagen content was determined using a chloramine-T hydroxyproline assay.[117] To assess GAG retention, constructs were incubated in PBS at 37°C and removed at 1h, 2h, 4h, 6h, or 8h.

Creep indentation testing

The aggregate modulus of each sample was determined using a creep indentation apparatus.[152] A tare load of 0.2 g followed by a test load of 0.7 g was applied via a 0.8 mm porous indentation tip. Material properties were determined using a semi-analytical, semi-numeric biphasic model.[119,153]

Tensile testing

Samples were cut into dog-bone shapes and glued to paper tabs for gripping.[122] Prior to positioning the samples on the paper, pictures were taken and then analyzed using ImageJ to determine the width and gauge length. A micrometer

was used to determine sample thicknesses. Tensile tests were conducted at a strain rate of 1% of the gauge length per second on a materials testing system (Instron Model 5565). Young's modulus was calculated as the slope of the linear region of the stress-strain curve; the maximum stress was reported as ultimate tensile strength.

RNA isolation and microarray hybridization

RNA was isolated at 4 days (n=3) for control constructs and HA-treated constructs (4h following the application of HA) using a Qiagen RNeasy Lipid Tissue Mini Kit. To assess RNA purity and concentration, RNA was analyzed using a nanodrop. An Agilent bioanalyzer was employed to assess the quality of the RNA. Bovine microarrays were acquired from Agilent. 400ng of total RNA were processed according to Agilent's one color gene expression protocol. The arrays were scanned on Agilent's high-resolution C scanner and analyzed using Agilent's Feature Extraction Software 10.5.

Microarray data analysis

Current annotations for the microarray probes were obtained from Agilent technologies (https://earray.chem.agilent.com/earray). The Entrez Gene IDs from the Agilent annotation were cross-referenced with HomoloGene build 65 (ftp://ftp.ncbi.nih.gov/pub/HomoloGene/build65/) to find the gene names for the corresponding human orthologs. Changes in gene expression were assessed between control and HA treatment based on the normalized intensities of each

gene. Genes with adjusted p-values < 0.01 were considered to be differentially expressed. Differentially expressed genes were entered into the Database for Annotation, Visualization and Integrated Discovery to determine enriched Kyoto Encyclopedia of Genes and Genomes (KEGG) pathways.[181] Enriched pathways were defined as $p < 0.005$ and a minimal 5 genes appearing among the differentially expressed genes.

Real time PCR

Primers for GAPDH, COL2, and COL1 were synthesized as described previously;[69] other primers (Myc, E2F4, protein phosphatase) were purchased from Invitrogen. RT was performed by incubating 500 ng of RNA with SuperScript III (Invitrogen) as recommended by the manufacturer. Real-time PCR was done with a Rotor-gene 3000 real-time PCR machine (Corbett Research). SYBR Green mastermix was used with primers at a concentration of 1 μM. A 10 min denaturing step was employed, followed by 45 cycles of 95°C (15s) and 60°C (60s). The take-off cycle (C_T) for each gene of interest (GOI) was compared to the housekeeping gene GAPDH. Relative gene expressions were computed as $2^{-\Delta\Delta CT}$, where $\Delta\Delta C_T = (C_{T,GOI} - C_{T,GAPDH})_{HA} - (C_{T,GOI} - C_{T,GAPDH})_{control}$.

Statistical analysis

Biochemistry and biomechanics samples (n=6) were analyzed using a one-factor ANOVA in phases I and III. For phase II and GAG retention, a two-factor ANOVA

was employed. When warranted, Tukey's post hoc testing was performed to determine significant differences. Significance was defined as $p < 0.05$.

Table 3-1: Differentially expressed genes of pathways enriched by HA.

TGF-β pathway targets

Gene	Fold change	Regulation
Activin	6.82	up
inhibitor of DNA binding 1	8.57	down
inhibitor of DNA binding 2	4.67	up
Myc transcription factor	5.34	up
E2F4 transcription factor	4.78	up
protein phosphatase	3.47	up
thrombospondin 1*	4.92	up
thrombospondin 2*	8.22	up
thrombospondin 3*	4.26	up
thrombospondin 4*	6.82	up

ECM receptor pathway targets

Gene	Fold change	Regulation
chondroadherin	13.42	up
Collagen, type I, alpha 1	4.92	down
Collagen, type II, alpha 1	4.47	up
Collagen, type III, alpha 1	3.42	up
Collagen, type XI, alpha 2	5.01	up
integrin, alpha 7	4.07	up
syndecan 4	5.52	up

HA treatment enriched only pathways relating to TGF-β signaling and ECM-receptor interactions. Fold changes represent the gene expression of neotissue at 4 days treated HA (1 mg/ml, 1.6×10^6 Da HA) relative to control values. Targets marked with an asterisk were differentially expressed in both the TGF-β signaling and ECM-receptor interactions pathways.

Figure 3-1: Histology and IHC for HA treatment.

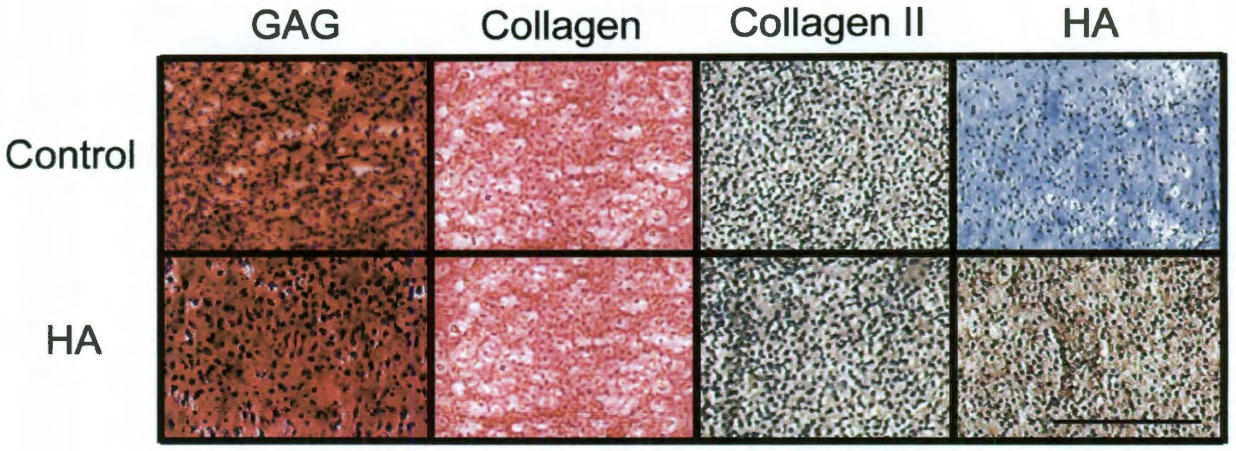

Photomicrographs of Safranin-O/fast green staining for glycosaminoglycans (GAGs), Picrosirius Red for collagen, and immunohistochemistry for collagen II and hyaluronic acid (HA). Sections were prepared after 4 weeks of culture. All images are shown at 10X magnification. Scale bar represents 200 μm.

Figure 3-2: Biomechanical and biochemical properties.

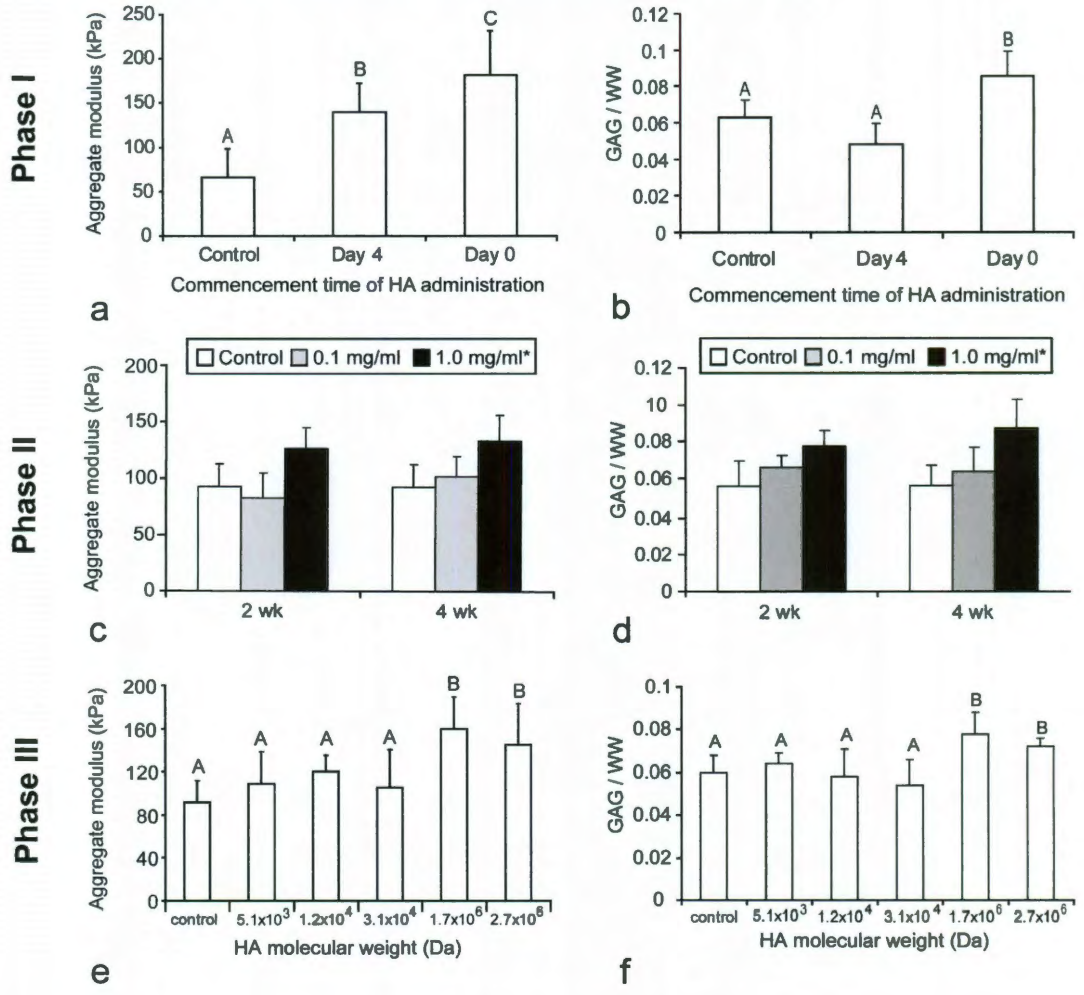

Phase I: (a) Day 0 hyaluronic acid (HA) application significantly increased the aggregate modulus. (b) Application of HA at day 0 resulted in a significantly higher glycosaminoglycan (GAG) content. Phase II: (c) 1 mg/ml HA administration enhanced compressive stiffness. (d) Application duration did not have a significant effect on GAG content, though HA application at 1 mg/ml significantly increased GAG content. Phase III: (e) High molecular weight HA also enhanced the aggregate moduli of constructs. (f) HA with higher molecule weights resulted in higher GAG content.

Figure 3-3: GAG retention effects of HA treatment

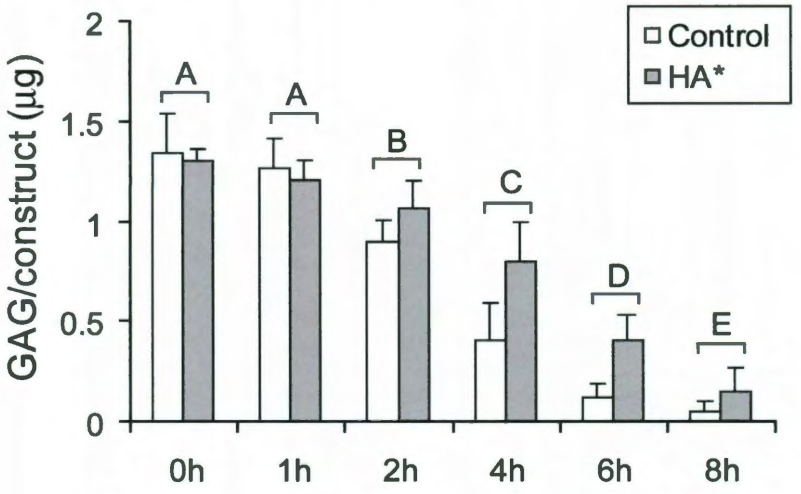

The GAG retention was compared between control constructs and constructs treated with 1 mg/ml hyaluronic acid (HA) for 2 weeks. To assess GAG retention, total GAG content was quantified after various incubation periods in PBS following 4 weeks of culture. HA administration increased GAG retention for HA-treated constructs based on a 2-way ANOVA of the factors duration and HA treatment. Data are presented as means with standard deviation error bars, n=6 per bar. Groups marked with distinct letters significant different ($p < 0.05$).

Figure 3-4: PCR results for neocartilage treated with hyaluronic acid.

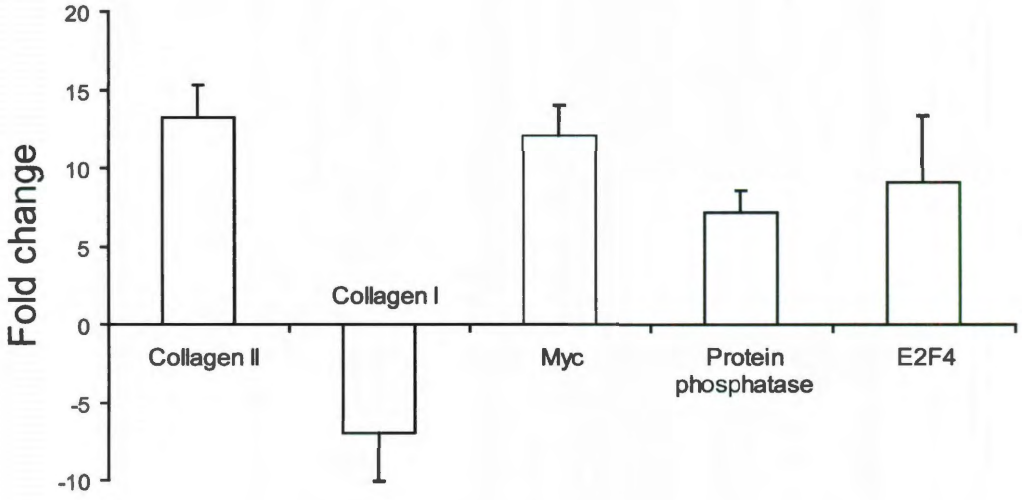

All reported values are gene expression values of HA neocartilage normalized to control expression levels computed using the $2^{-\Delta\Delta CT}$ method. Data are presented as means with standard deviation error bars, n=3 per bar.

Figure 3-5: Potential hyaluronic acid signaling pathway

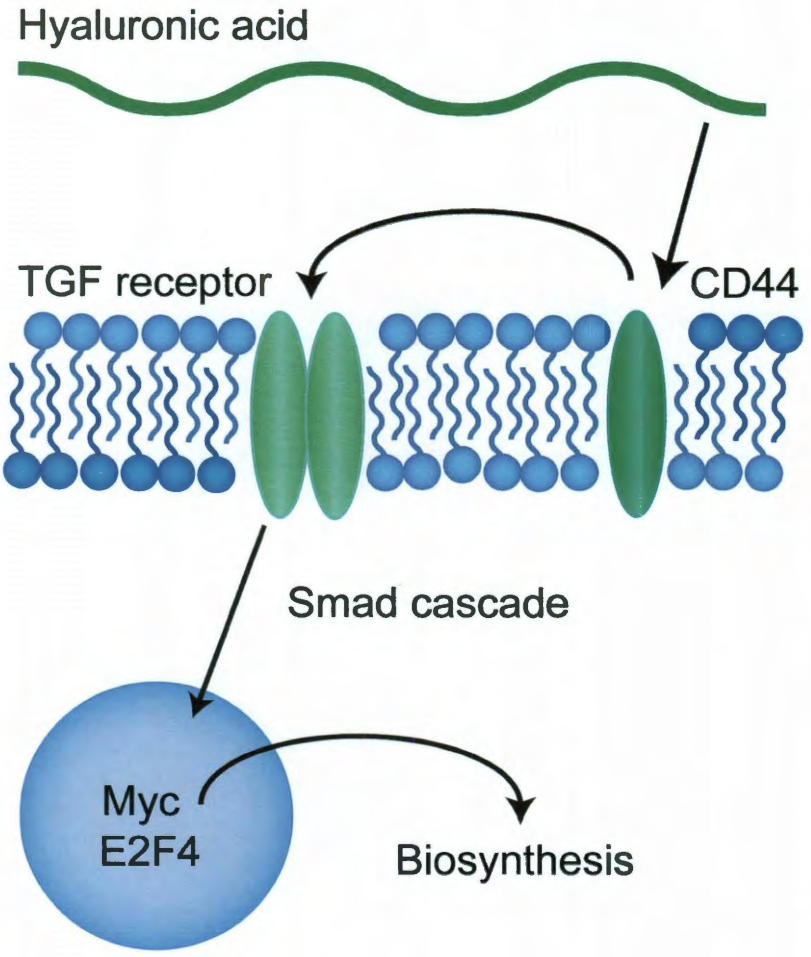

Microarray and PCR analysis showed that several TGF-β intermediates, including the transcription factors Myc and E2F4, are up-regulated following HA treatment. HA-induced signaling may be mediated by HA binding to CD44, which is known to bind to and activate the TGF-β receptor.

Chapter 4: Additive effects of exogenous hyaluronic acid and TGF-β1 on tissue engineered articular cartilage*

Abstract

This study examines the application of hyaluronic acid (HA) and TGF-β1, applied individually and in combination, to improve the functional properties of self-assembled cartilage constructs. Constructs were assessed after 4 weeks using biochemistry, histology, and biomechanics. Histology and IHC showed that both treatments promoted articular cartilage phenotype, demonstrating the expression of glycosaminoglycans (GAGs) and collagen II but not collagen I. HA and TGF-β1 significantly increased the GAG content and compressive stiffness of constructs, and applying HA in conjunction with TGF-β1 additively increased the GAG content and compressive properties. Combined HA and TGF-β1 treatment produced neocartilage with a compressive stiffness of 230±34 kPa and a GAG content of 10.7±0.5%, which were respective increases of 150% and 65% above control values. This study demonstrated that HA and TGF-β1 can be applied in combination to further enhance the increased biochemical and biomechanical properties resulting from treatment with either agent applied individually.

* Responte DJ, Athanasiou KA. Additive effects of exogenous hyaluronic acid and TGF-β1 on tissue engineered articular cartilage. *JOR* (in preparation)

Introduction

Articular cartilage damage and degeneration create a tremendous clinical burden, with 67 million individuals projected to be diagnosed by 2030.[182] Osteoarthritis (OA) is particularly problematic within the elderly population, with 10% of people over age 60 exhibiting OA.[13] OA is associated with poor quality of life issues including joint inflammation and pain; in severe cases, these symptoms can impair physical function and adversely impact the patient's lifestyle. The prevalence and severity of OA provide a strong impetus for developing new strategies to promote articular cartilage regeneration. Unfortunately, cartilage has an intrinsically limited healing capacity, so novel technologies are needed to produce repair tissue.

Cartilage regeneration efforts have focused on recapitulating the biochemical composition and biomechanical properties of native cartilage. The primary matrix constituents of cartilage are collagen and glycosaminoglycans (GAGs), which confer tensile and compressive integrity to the tissue. Mechanical properties are crucial because constructs should be able to function in the demanding joint environment, which can impose forces of 20 MPa on cartilage.[183] Various tissue engineering strategies have been investigated to produce neocartilage that can withstand this strenuous environment.

One particularly promising regeneration approach is a self-assembly process that recapitulates cartilage development[103] and produces constructs with biochemical and biomechanical properties on par with those of native

tissue.[94] Self-assembly has been improved by applying various biochemical and biomechanical stimuli including hydrostatic pressure,[57,105] growth factors,[39] and the enzyme chondroitinase-ABC.[51,140] In addition to examining the effects of individual stimuli, self-assembly has been improved by combining stimuli to synergistically enhance construct properties. For instance, combining hydrostatic pressure and TGF-β1 treatment has been shown to additively increase the aggregate modulus by 164% and the Young's modulus by 231%. Additionally, the combined treatment had a synergistic effect on collagen content, increasing it by 173%.[59] Despite these exciting developments, recent work has shown that self-assembled constructs do not contain hyaluronic acid (HA),[103] suggesting that his matrix component may need to be added exogenously.

HA is a large, unsulfated glycosaminoglycan comprised of repeating units of glucuronic acid and N-acetylglucosamine. High molecular weight (10^5-10^7 Da) HA forms the core of aggrecan, a major constituent of cartilage matrix. HA has also been implicated in native cartilage development due to its presence in embryonic mesenchymal tissue and promotion of chondrogenesis.[168,184] HA contributes to *in vitro* matrix organization by promoting the development of pericellular matrices that resemble those of native chondrocytes.[185] Additionally, HA application increases proteoglycan biosynthesis[160,186] and protein production in equine articular cartilage,[159] rabbit chondrocytes,[161] and bovine articular cartilage.[162] The key role of HA in development and biosynthesis suggests that HA has important implications for *in vitro* cartilage formation.

TGF-β1 is an anabolic agent that is known to improve cartilage biosynthesis and improve the properties of cartilage constructs. This class of growth factors is known to contribute to both embryonic cartilage development[23] and chondrogenic differentiation of mesenchymal progenitor cells.[24-27] Furthermore, TGF-β1 has been shown to improve *in vivo* cartilage repair.[28] Administering TGF-β to tissue engineered constructs has also been extensively studied. For instance, administering TGF-β increased GAG deposition in three-dimensional cultures of equine chondrocytes,[29] rabbit auricular chondrocytes,[30] and bovine articular chondrocytes.[31]

HA application to self-assembled constructs has not yet been investigated in combination with TGF-β1. Thus, the objective of this study was to investigate the effects of combining HA with TGF-β1. This study examined the hypotheses that HA and TGF-β1 administration would 1) increase biochemical and biomechanical properties and 2) further enhance construct properties when applied in combination. To test these hypotheses, a full factorial design was employed with the factors HA (no treatment, treatment of 1 mg/ml) and TGF-β1 (no treatment, treatment during weeks 1&2 (continuous), treatment during weeks 1&3 (intermittent)).

Materials and methods

Chondrocyte isolation and culture

Bovine chondrocytes were isolated as previously described.[94] Cartilage tissue was isolated from the distal femur and patellofemoral groove of three 1 week old

male calves (Research 87, Boston, MA) and digested in collagenase type II (Worthington Biochemical Corp., Lakewood, NJ) for 24 hours in a 0.20% solution. Cells were counted with a hemacytometer and subsequently frozen at -80°C at a concentration of 30 million cells per ml. Cells were thawed and seeded in 5 mm diameter non-adherent, cylindrical wells made of 2% agarose. 5.5 million cells in 100 µl medium were placed into each well; an additional 400 µL of medium was added to each well after 4 hours. The constructs were removed from the cylindrical molds at 10 days and cultured in well plates coated with 2% agarose.[114]

For the entire culture duration, constructs were fed with chemically-defined medium consisting of DMEM with 4.5 mg/ml glucose and L-glutamine (Biowhittaker/Cambrex, Walkersville, MD), 1% fungizone, 1% penicillin/streptomycin, 50 µg/ml ascorbate-2-phosphate, 100 nM dexamethasone (Sigma, St. Louis, MO), 1% ITS+ (BD Scientific, Franklin Lakes, NJ), 40 µg/ml L-proline, and 100 µg/ml sodium pyruvate (Fisher Scientific, Pittsburgh, PA). Media was changed daily. For HA treatment, HA with a molecular weight of $1.6x10^6$ Da (Sigma) was applied at 1 mg/ml in chondrogenic media. Growth factor groups were treated daily with TGF-β1 at 30 ng/ml suspended in chondrogenic media used for daily feeding.

Construct processing

Constructs were processed at 4 wks for evaluation of histology, quantitative biochemistry, and mechanics. A 3 mm biopsy punch was used to remove the

centers of the constructs, which were used for compressive testing. The outer rings of constructs were divided and used for tensile assessment, quantitative biochemistry, and histology.

Histology and immunohistochemistry (IHC)

Samples were assessed for distribution of GAG, collagen, collagen I, and collagen II. At 4 weeks, samples were cryoembedded and frozen at -20ºC for at least 24 hours and then were cryosectioned at 14 µm. Some of these sections were fixed in formalin and stained with Safranin-O/fast green and Picrosirius Red to show GAG and DNA distributions, respectively. Other sections were analyzed using IHC for collagen I or collagen II. Samples were prepared using a Vectastain ABC kit (Vector Labs) according to the manufacture's instructions. Primary detection was achieved with mouse anti-collagen type I diluted 1:1000 (Accurate Chemicals) or rabbit anti-collagen type II diluted 1:300 (Cedarlane Labs). The secondary antibody (anti-mouse or anti-rabbit IgG, Vectastain ABC kit) was then added for 30 min and developed using the Vectastain ABC reagent and DAB. Immature bovine tendon was employed as a positive control for collagen I. Articular cartilage was used as a positive control f for collagen type II and a negative control for collagen I.

Quantitative biochemistry

Samples were frozen at -20ºC for at least 24 hours and then lyophilized, weighed dry, and digested using a papain solution.[187] DNA content was determined with

the PicoGreen® dsDNA Assay Kit (Invitrogen), and cell numbers were inferred assuming 7.8 pg of DNA per cell. Sulfated GAG content was assayed using the Blyscan Glycosaminoglycan Assay kit (Biocolor), which is based on 1,9-dimethylmethylene blue binding (Accurate Chemical and Scientific Corp., Westbury, NY). Total collagen content was assayed using a modified chloramine-T hydroxyproline assay.[117]

Creep indentation testing

Compressive mechanical properties were determined using a creep indentation apparatus.[152] The properties were obtained based on a linear biphasic model[118] that was used to compute each sample's aggregate modulus, Poisson's ratio, and permeability. A tare load of 0.2 g followed by a test load of 0.7 g was employed for all other samples. The loads were applied via a 0.8 mm porous indentation tip. Material properties were determined using a semi-analytical, semi-numeric biphasic model was used.[119] These results were subsequently refined using finite element optimization.[153]

Tensile testing

Samples were cut into dog-bone shapes and glued to paper tabs for gripping.[122] Prior to positioning the samples on the paper, pictures were taken and then analyzed using ImageJ to determine the width and gauge length. A micrometer was used to determine sample thicknesses. Tensile tests were conducted at a strain rate of 1% of the gauge length per second on a materials testing system

(Instron Model 5565). The Young's modulus was calculated from the slope of the linear region of the stress-strain curve; the ultimate tensile strength was recorded as the maximum stress from the curve.

Results

Histology and gross morphology

Histology results are summarized in Fig. 4-1. Histology demonstrated that all samples stained uniformly positive for total collagen and GAGs. In addition, IHC showed the presence of collagen II but not collagen I throughout the constructs. The absence of collagen I and presence of collagen II and GAGs suggested that all treatments promoted a cartilage phenotype.

For all groups, chondrocytes self-assembled to form uniform discs. Analysis of gross morphology showed that TGF-β1 treatments altered construct diameter. Control construct diameters increased to 6.07±0.19 mm compared to the original 5 mm diameter, whereas diameters for growth factor groups did not change. Diameter values were 5.10±0.15, 5.31±0.11, 5.05±0.08, and 4.97±0.12 mm for intermittent TGF-β1, continuous TGF-β1, HA with intermittent TGF-β1, and HA with continuous TGF-β1, respectively. Treatment groups did not have significantly different amounts of DNA than the control group, which had 38.1 ± 4.7 μg per construct, which corresponded to 4.9 million cells. Groups treated with TGF-β1 demonstrated significantly reduced thicknesses with values of 0.48 ± 0.04, 0.31± 0.06, 0.37 ± 0.03, 0.34 ± 0.05, and 0.30 ± 0.03 mm for control,

intermittent TGF-β1, continuous TGF-β1, HA with intermittent TGF-β1, and HA with continuous TGF-β1, respectively.

Biochemistry

As shown in Fig. 4-2b, all treatment groups had higher GAG contents than the control group, with the combined treatment groups exhibiting the highest GAG abundances. GAG/ww reached 10.7±0.5% and 10.3±0.8% for HA in conjunction with continuous TGF-β1 and intermittent TGF-β1, respectively. These reflected additive increases over the other groups, which exhibited GAG contents of 6.5±0.5%, 8.1±0.8%, 8.4±0.7%, and 8.6±1.0% for control, HA, continuous TGF-β1, and intermittent TGF-β1, respectively.

Collagen contents of HA-treated groups were not significantly different than the control value of 7.7±0.7% (Fig. 4-3b). For groups treated with TGF-β1, collagen/ww was significantly greater than control and HA groups, exhibiting collagen abundances of 9.9±0.7%, 10.2±0.7%, 10.7±0.5%, and 10.0±0.7% for continuous TGF-β1, intermittent TGF-β1, HA with continuous TGF-β1, and HA with intermittent TGF-β1, respectively.

Mechanical testing

Compressive properties were quantified by determining the aggregate modulus, Poisson's ratio, and permeability. The aggregate modulus was significantly higher for individual HA and TGF-β1 treatments and additively increased following combination treatment. The compressive stiffness was highest for

combined treatment groups (Fig. 4-2a), which exhibited aggregate moduli of 230±34 kPa and 221±37 kPa when treated with continuous and intermittent TGF-β1, respectively. These increases in compressive stiffness paralleled the enhanced GAG contents for treatment groups. Permeabilities were 20.4 ± 10.1, 9.1 ± 0.3, 10.4 ± 6.2, and 8.1 ± 8.6 x 10^{-15} $m^4/N \cdot s$ for control, HA alone, HA with continuous TGF-β1, and HA with intermittent TGF-β1. Post-hoc testing demonstrated that HA-treated groups had lower permeability values and that growth factor treatment alone did not significantly alter the permeability. Poisson's ratios for treatment groups were not significantly different than the control value of 0.047 ± 0.038.

Tensile testing showed that TGF-β1 treatment significantly increased tensile stiffness (Fig. 4-3a). Tensile stiffnesses were 614±158, 1206±172 and 1163±137, 1033±72, and 1271±167 kPa for control, continuous TGF-β1, and intermittent TGF-β1, HA with continuous TGF-β1, and HA with intermittent TGF-β1, respectively. The Young's moduli for the HA groups were not statistically different than control. UTS values was significantly higher for constructs treated with growth factors, with values of 437±47, 750±65, 747±83, 728±65, 773±92 kPa for control, continuous TGF-β1, and intermittent TGF-β1, HA with continuous TGF-β1, and HA with intermittent TGF-β1, respectively. In general, collagen and GAG contents mirrored the trends in tensile and compressive stiffness, respectively.

Construct properties are on par with native tissue

To quantitatively compare the treatment groups and native cartilage, a functionality index (FI) was employed. The FI compares native cartilage with engineered tissue based on the compressive stiffness (E^C), tensile stiffness (E^T), GAG content (G), and collagen content (C) as shown in Eq. 1. Native tissue and engineered cartilage are denoted by the subscripts 'nat' and 'sac,' respectively.

$$FI = \frac{1}{4}\left(\left(1-\frac{(G_{nat}-G_{sac})}{G_{nat}}\right)+\left(1-\frac{(C_{nat}-C_{sac})}{C_{nat}}\right)+\left(1-\frac{(E^T_{nat}-E^T_{sac})}{E^T_{nat}}\right)+\left(1-\frac{(E^C_{nat}-E^C_{sac})}{E^C_{nat}}\right)\right) \quad (1)$$

An FI value of 1 corresponds to engineered cartilage properties that equal those of native tissue. FI values were 0.41, 0.54, 0.73, and 0.88 for control, HA, intermittent TGF-β1, and combined treatments, respectively. The higher FI value for the combined treatment group indicates that combining HA and TGF-β1 most effectively reproduces the properties of native cartilage.

Discussion

This study employed HA and TGF-β1 treatments to assess the effects of combining these exogenous agents. Novel contributions of this study include showing that 1) HA does not interfere with TGF-β1 signaling in self-assembled cartilage and 2) HA and TGF-β1 can be applied to additively improve the biochemical and biomechanical properties of cartilage constructs.

The application of 30 ng/ml and 1 mg/ml HA resulted in additive increases in the biochemical and biomechanical properties of constructs. Results supported the hypothesis that combining HA and TGF-β1 would further improve biochemical and biomechanical properties compared to treating with either agent individually. The combination treatment increased the GAG content and

compressive stiffness by 64% and 151%, respectively. Results supported the hypothesis that combining HA and TGF-β1 would further improve biochemical and biomechanical properties compared to treating with either agent individually.

The results highlight an important structure-function relationship in cartilage neotissue, particularly the relationship between GAG content and compressive properties. Significant increases in compressive stiffness due to both individual and combined treatments mirrored GAG content. GAG have been shown to be the influence compressive properties by creating a large fixed charge density and subsequently increasing the osmotic pressure of the tissue,[188] which increases resistance to compressive loading. Although the role of GAGs in compressive mechanics has been well-established, the collagen network also plays a crucial role. For example, collagen fiber organization[189] and collagen content[125] have been shown to contribute to the compressive properties of cartilage. Thus, modulating the collagen network could provide a strategy for further improving the compressive properties of cartilage constructs.

The increased compressive stiffness observed following HA treatment could be mediated by enhanced GAG retention. Applying HA exogenously has been shown to decrease GAG release from both *in vitro* chondrocyte cultures[170,171] and the *in vivo* joint space.[172] This suppressed GAG release could be caused by the extensive interactions between HA and other ECM components,[173] which could increase the viscosity of the matrix. Increasing GAG retention could increase compressive properties by increasing the fixed charge density and osmotic pressure of the ECM, which consequently increased

compressive properties.[158] The increased osmotic pressure related to GAG content could explain the increase compressive stiffness that was observed following HA and TGF-β1 treatments.

In addition to the effects of HA and TGF-β1, it is likely that HA sequesters TGF-β1 in matrix. The large negative charge of HA and positive charge of growth factors like TGF-β1 results in the formation of ionic complexes,[190] which could sequester TGF-β1 in the matrix. This increased growth factor retention could increase the effective growth factor dosage compared to soluble TGF-β1 administration. Similar effects were observed by tethering TGF-β1 to PEG hydrogels, which increased matrix production more so than soluble TGF-β1 treatment.[191] The ability of both biomaterials and anionic natural polymers to localize growth factors provides a strategy for controlling the spatial localization of TGF-β1 in the matrix.

HA has also been shown to influence the response to other growth factors applied to engineered cartilage. For instance, adding HA to alginate and embedding chondrocytes showed that IGF-1 can become entrapped within the matrix and therefore interfere with the delivery of IGF-1 to chondrocytes.[192] HA sequestered IGF-1 in the matrix, which was assessed by observing gene expression relating to IGF-1 signaling. Exogenous HA also increased IGF-1 retention in cartilage explants and concomitantly increased proteoglycan synthesis, suggesting that HA promotes IGF-1 signaling in native cartilage.[193] Considering the formation of ionic complexes between growth factors and HA

discussed earlier, it is likely that HA will promote the retention of various signaling molecules and subsequently alter signaling.

This study has shown that exogenously applying HA and TGF-β1 additively increases the GAG content and compressive stiffness of self-assembled cartilage. HA administration did not appear to interfere with TGF-β1 signaling, and could have enhanced TGF-β1 retention in the matrix via electrostatic interactions. Because other work has shown beneficial effects of combining mechanical stimuli with growth factor treatment,[59,141] future studies should examine how TGF-β1 and HA can be combined with mechanical stimuli.

Figure 4-1: Histology and gross morphology

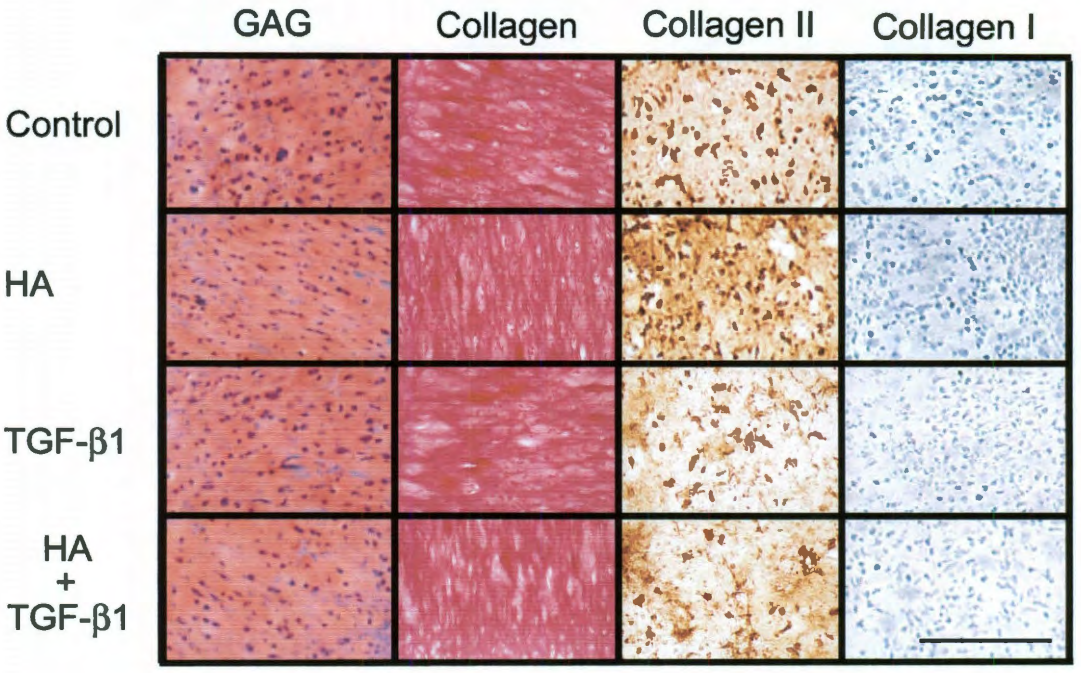

Constructs were treated with hyaluronic acid (HA), TGF-β1, or HA and TGF-β1. Total collagen was stained with Picrosirius Red and GAGs were stained using Safrainin-O/fast green. Immunohistochemistry was used to assess the abundance and distribution of collagen I and collagen II. Both control and treated constructs exhibited uniform distributions of glycosaminoglycans (GAGs), total collagen, and collagen II without expression collagen I. Scale bar represents 200 μm.

Figure 4-2: Compressive stiffness and glycosaminoglycan (GAG) content

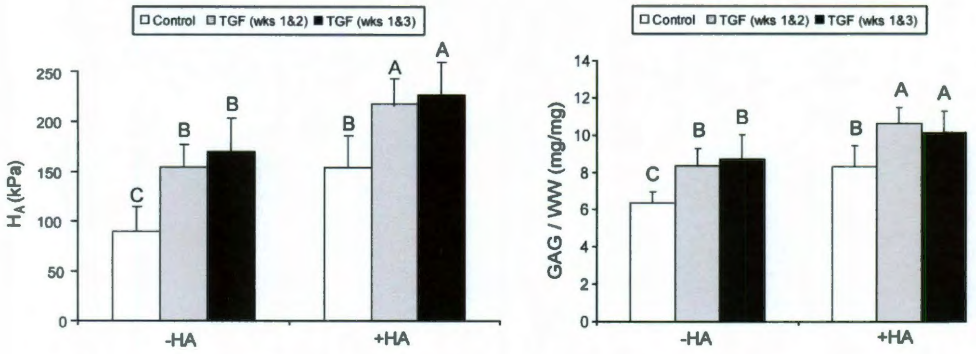

Constructs were treated with hyaluronic acid (HA), TGF-β1, or HA and TGF-β1. (a) Compressive stiffness was additively increased following combined HA and TGF-β1 treatment. (b) Combined HA and TGF-β1 treatment additively increased GAG content. Bars labeled with different letters exhibit significant differences ($p < 0.05$).

Figure 4-3: Tensile stiffness and collagen content

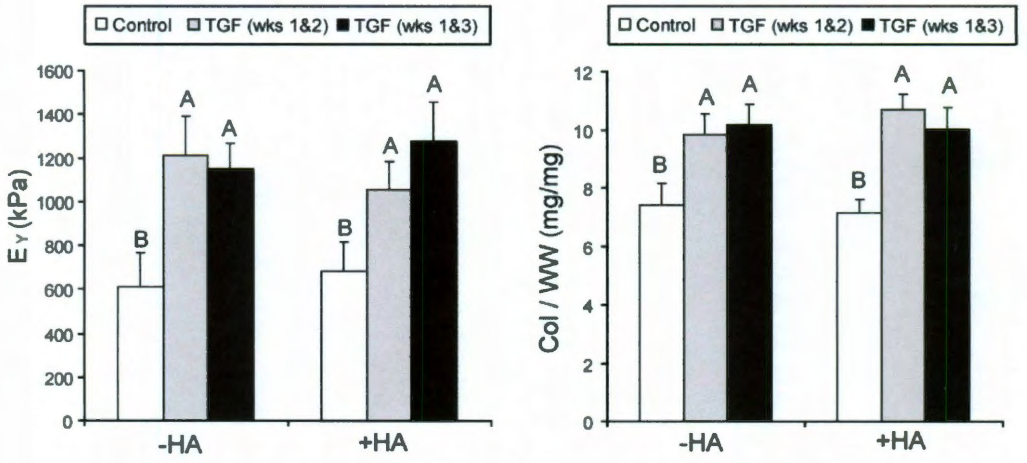

(a) Tensile stiffness (b) TGF-β1 treatment significantly increased the tensile stiffness. Bars labeled with different letters exhibit significant differences ($p < 0.05$).

Chapter 5: Tensile properties and collagen network characterization of connective tissues of the immature knee joint*

Abstract

Background: The major connective tissues of the knee joint act in concert during locomotion to provide joint stability, smooth articulation, shock absorption, and distribution of mechanical stresses. These functions are largely conferred by the intrinsic material properties of the tissues, which are in turn determined by their biochemical composition. A thorough understanding of the structure-function relationships of the connective tissues of the immature knee joint is needed in order to provide design parameters for efforts in tissue engineering.

Methodology/Principal findings: The objective of this study was to perform a comprehensive characterization of the tensile properties, collagen content, and pyridinoline crosslink abundance of condylar cartilage, patellar cartilage, medial and lateral menisci, cranial and caudal cruciate ligaments (analogous to anterior and posterior cruciate ligaments in humans, respectively), medial and lateral collateral ligamen[1]ts, and patellar ligament from immature bovine calves. Tensile stiffness and strength were greatest in the menisci and patellar ligament, and lowest in the hyaline cartilages and cruciate ligaments; these tensile results were reflected in the results for collagen content. Pyridinoline crosslinks were found in

* Eleswarapu SV,* Responte DJ,* Athanasiou KA. Interplay of collagen content and crosslinking with tensile mechanics of musculoskeletal tissues of the immature bovine joint. PLoS ONE (accepted)

every tissue despite the relative immaturity of the joints, and significant differences were observed among tissues.

Conclusions/Significance: Results from this investigation reinforce the interplay of tissue biomechanics and biochemical content and provide preliminary design parameters for future efforts concerned with connective tissue engineering for joint repair.

Introduction

The major connective tissues of the knee joint act in concert during locomotion to provide joint stability, smooth articulation, shock absorption, and distribution of mechanical stresses.[194-196] These functions are largely conferred by the intrinsic material properties of the tissues, which are in turn determined by their biochemical compositions. Based on structure-function relationships, each connective tissue of the knee joint can be conceptualized along a continuum from hyaline to fibrocartilaginous to fibrous (Figure 1). These tissues have received considerable attention in both basic science and clinical literature, but much work remains to be done to elucidate the contributions of particular biochemical components to important mechanical parameters, especially with respect to applications in tissue engineering. Approaches in tissue engineering are guided heavily by the interplay of native tissue structures and their corresponding functional correlates. To better understand these relationships, this study examines the biochemical composition and tensile properties of the major connective tissues of the immature bovine knee joint.

The knee is a pivotal hinge joint that permits flexion, extension, and limited rotation through coordinated action of its hyaline, fibrocartilaginous, and fibrous connective tissues. Hyaline cartilage is found at the condylar surfaces of the femur and tibia, as well as on the posterior aspect of the patella. Hyaline cartilage provides a smooth surface for low-friction gliding of the femoral and tibial condyles and the patella during knee flexion and extension. Fibrocartilage comprises the medial and lateral menisci, which are crescent-shaped structures interposed between the femoral and tibial condyles. The two menisci bear dynamic loads applied by the femoral condyles during joint compression and relaxation, thereby playing a role in shock absorption and stress distribution over the tibial condyles. Fibrous tissue makes up the major ligaments of the knee joint, in particular the patellar ligament, the collateral ligaments, and the cruciate ligaments. The patellar ligament originates from the apex of the patella and inserts at the tibial tuberosity below; together with the tendon of the quadriceps femoris, the patellar ligament provides stability to the patella as it glides over the patellofemoral groove and femoral condyles. The medial and lateral collateral ligaments (MCL and LCL) are extracapsular ligaments that protect the medial and lateral sides of the knee from a contralateral outside or inside bending force, respectively. The anterior and posterior cruciate ligaments (ACL and PCL) are intracapsular ligaments that stabilize the knee during rotation and bending. Relative to the femur, the ACL prevents anterior transposition of the tibia, while the PCL prevents posterior transposition. Together, these tissues contribute significantly to normal knee function.

The connective tissues of the knee joint are known to derive their mechanical properties from their biochemical compositions, but precise structure-function relationships remain elusive beyond general notions of the role of the extracellular matrix (ECM). Structurally, each of these tissues is hypocellular and possesses an ECM rich in collagen, with varying amounts of glycosaminoglycans (GAGs).[197,198] In general, collagen is known to be largely responsible for the tensile integrity of these tissues, while GAGs, predominant in hyaline cartilage and sparse in fibrous tissues, contribute to compressive strength.[199] In addition to total collagen content, the amount of crosslinking present in the collagen network has been shown to play an important role in tissue tensile properties.[200] In examining tissue tensile properties, two important measures of tensile integrity are Young's modulus and ultimate tensile strength (UTS). Young's modulus is a measure of a material's tensile stiffness; it is defined as the slope of the linear portion of the stress-strain curve describing a material's behavior during uniaxial loading in tension. The UTS is the maximum stress a material can withstand and is determined as the highest point of the stress-strain curve. Though collagen content and crosslinking are known to play a role in tensile mechanics, their precise structure-function relationships with respect to Young's modulus and UTS remain unclear. In particular, pyridinoline crosslinks have been shown to correlate with both tensile strength and stiffness in bovine articular cartilage,[49] but there is a dearth of literature describing the contribution of pyridinoline crosslinks to the mechanical behavior of other bovine joint tissues.

In humans, conditions afflicting the connective tissues of the knee, such as traumatic injury and osteoarthritis, contribute to substantial healthcare costs and work-related disability. The prevalence and severity of these conditions result in annual direct costs of $510 billion, which is expected to increase as the population ages.[201] For arthritis alone, which can arise as a result of injury to any of these tissues[202], it is projected that 67 million individuals will be diagnosed by 2030[182]. Surgical treatments such as total joint replacement are highly invasive, require extensive recovery and rehabilitation times, and may often involve costly revision surgeries.[203] Biological treatments such as autografts and allografts present additional challenges such as secondary surgeries, immunogenicity,[204] and limited cell sources.

The field of tissue engineering aims to improve orthopedic medicine by providing functional replacements for damaged or diseased joint tissues. Recent tissue engineering efforts have focused on major connective tissues such as hyaline cartilage,[53,94] meniscus,[187,205] tendon,[206,207] and ligament.[208] Although various approaches have been employed to engineer these tissues, it has been difficult to reproduce native collagen organization and attain native mechanical properties. Various types of mechanical[53-55,58] and biochemical[33,51] stimuli have been studied to improve construct properties, and both scaffold-free[94,99,209] and scaffold-based[90,210] approaches have been investigated for connective tissue engineering applications.

An important consideration in these tissue engineering efforts has been the cell source used to produce constructs. Comparisons of cell types have

shown that immature cells exhibit increased biosynthesis[211], making them promising candidates for tissue engineering. Immature cells have been used to produce constructs with clinically relevant dimensions[94] and mechanical properties on par with native tissue. To make informed cell source choices, it is necessary to establish a comprehensive understanding of the physiology of immature joint tissues. Moreover, while studies on the knee joint are well represented in the literature, it is important to note that much of what is known about the structure-function relationships of these tissues comes from assessments of adult rather than immature joints, whether human or animal. Given the prevalence of knee injuries in the pediatric population[212], along with a greater push towards using immature tissues as cell sources for tissue engineering, a thorough elucidation of the biochemistry of immature knee joint tissues, not just adult tissues, is warranted. An understanding of immature joint physiology may also yield insight into tissue development by providing a reference to which adult tissues can be compared, as well as informing a general understanding of factors at play in pediatric joint injury. Additionally, because orthopaedic explant and tissue engineering studies are relying more readily on bovine tissues, it is imperative that a full assessment of the bovine joint be undertaken.[55,94,213-215]

The objective of this study was to perform a comprehensive characterization of the tensile properties, collagen content, and pyridinoline crosslink abundance of the major connective tissues of the immature bovine knee joint. Tissues of interest were femoral condylar and patellar cartilage,

medial and lateral menisci, cranial and caudal cruciate ligaments (analogous to the ACL and PCL in humans, respectively), medial and lateral collateral ligaments, and patellar ligament. It was hypothesized that trends in tensile properties would reflect those in collagen content; that tensile properties and collagen content would be higher in fibrocartilaginous and ligamentous tissues than in hyaline tissues; and that pyridinoline crosslinks would be found in all tissues, in spite of the immaturity of the tissues. It was further hypothesized that pyridinoline crosslinks would be found to contribute preferentially to Young's modulus rather than UTS. Results from this investigation reinforce the interplay of tissue biomechanics and biochemical content and provide preliminary design parameters for future efforts concerned with connective tissue engineering for joint repair.

Material and methods

Tissue harvest and specimen preparation. Tissue specimens were harvested from the knee joints of 6 one-week-old male bovine calves (Research 87, Boston, MA) shortly after slaughter. To normalize variability among animals, each leg came from a different animal. Hyaline femoral condylar cartilage (CC), hyaline patellar cartilage (PC), medial meniscus (MM), lateral meniscus (LM), cranial cruciate ligament (CraCL), caudal cruciate ligament (CauCL), medial collateral ligament (MCL), lateral collateral ligament (LCL), and patellar ligament (PL) were taken. For CC and PC specimens, the cartilage was separated from subchondral bone with a scalpel. For MM and LM specimens, the femoral and tibial surfaces, as well as the inner 1/3 and outer 1/3 portions of the annulus, were sliced away,

leaving the approximate interior circumferential portion of the specimen for assessment. CraCL, CauCL, MCL, LCL, and PL were taken whole from their attachments.

From each freshly harvested specimen, a 3 mm dermal biopsy punch was used to obtain samples for histology, quantitative biochemistry, and high performance liquid chromatography (HPLC). The remainder of each specimen was then prepared for tensile testing. Tensile specimens were stored for a maximum of 24 h in phosphate buffered saline with protease inhibitors at 4°C and were allowed to equilibrate to room temperature prior to testing.

Histology. Samples were cryo-embedded and sectioned at 14 μm. Sections were fixed in formalin for 10 min and then stained with either picrosirius red or safranin O/fast green as described previously.[94] Samples were dehydrated in an ascending series of ethanol and mounted with coverslips prior to imaging.

Quantitative biochemistry. Biochemistry samples were weighed wet, frozen, lyophilized for 48 h, and then digested in a phosphate buffer with 125 μg/mL papain (Sigma) for 18 h at 65°C. A chloramine-T hydroxyproline assay was employed to quantify total collagen content after 2 N NaOH hydrolysis for 20 min at 110ºC [117]. Total collagen was normalized to tissue wet weight.

High performance liquid chromatography (HPLC). HPLC was performed to quantify the abundance of pyridinoline crosslinks. Samples were weighed wet, digested in 800 μL of 6 N HCl at 100°C for 20 h, and then dried using a vacuum concentrator. Samples were re-suspended in 50 μL of an aqueous solution containing 10 nmol pyridoxine/mL and 2.4 μmol homoarginine/mL and then

diluted fivefold with an aqueous solution of 0.5% HFBA acetonitrile in 10% acetonitrile. 10 μL of each sample was injected into a 25 mm C18 column (Shimadzu, Columbia, MD) and eluted using a solvent profile described previously.[216] To quantify the amount of crosslink in each sample, pyridinoline standards (Quidel, San Diego, CA) were employed to create a calibration curve.

Tensile testing. Each specimen was cut into a dog-bone shape with a 1-mm-long gauge length. The specimen was photographed alongside a ruler, and ImageJ software was used to determine the width and thickness. A uniaxial electromechanical materials testing system (Instron Model 5565, Canton, MA) was employed to determine tensile properties with a 50 N (CC and PC only) or 5 kN load cell (all other tissues). CC and PC specimens were affixed with cyanoacrylate glue to paper tabs outside of the gauge length for gripping; all other specimens were gripped directly outside of the gauge length. MM and LM specimens were tested in the circumferential direction. CraCL, CauCL, MCL, LCL, and PL specimens were tested in the longitudinal direction. Tensile tests were performed until failure within the gauge length at a strain rate of 1% of the gauge length per second. Force-displacement curves were generated, and stress-strain curves were calculated by normalizing data to specimen dimension. The apparent Young's modulus, a measure of specimen tensile stiffness, was determined by least squares fitting of the linear region of the stress-strain curve. The ultimate tensile strength (UTS) was determined as the maximum stress reached during a test.

Statistical analysis. All biochemical, HPLC, and tensile assessments were made using n=5-6. To compare among tissues, a single-factor analysis of variance was employed, and a Fisher least significant difference post hoc test was used when warranted. Significance was defined as $p<0.05$.

Results

Histology. Representative histology for hyaline cartilage, meniscus, and ligament are shown in Figure 2. Staining for collagen was observed in all tissues, though hyaline cartilage exhibited less extensive collagen staining compared to either meniscus or ligament. Extensive staining for GAG was observed in the hyaline cartilage specimens, but was not qualitatively observed in meniscus or ligament specimens.

Collagen content. The collagen/wet weight for CC, PC, MM, LM, CraCL, CauCL, MCL, LCL, and PL were 6.7±2.6%, 5.1±1.4%, 22.7±5.3%, 26.7±7.5%, 4.6±0.9%, 2.8±1.2%, 19.4±4.6%, 20.9±0.3%, and 21.2±3.5%, respectively (Figure 3). Fibrocartilage tissues (MM and LM) had the highest collagen content; the fibrocartilage tissues averaged together had 4.1x the collagen content in the hyaline tissues averaged together and 6.7x the collagen content in the cruciate ligaments averaged together. Among just the fibrous tissues, the collateral ligaments (MCL and LCL) and PL had higher collagen content than the cruciate ligaments (CraCL and CauCL); in particular, the collateral ligaments averaged together had 5.4x the collagen content in the cruciate ligaments averaged together. The cruciate ligaments were not significantly different from the hyaline cartilage tissues (CC and PC) in collagen content.

Pyridinoline crosslink content. Pyridinoline was resolved as one peak for all samples. Pyridinoline normalized to tissue wet weight (pyd/ww) for CC, PC, MM, LM, CraCL, CauCL, MCL, LCL, and PL were 0.303±0.101, 0.174±0.049, 0.498±0.160, 0.534±0.115, 0.374±0.087, 0.565±0.204, 0.414±0.123, 0.422±0.067, and 0.585±0.069 nmol/mg, respectively (Figure 4a). Pyd/ww was highest in PL, while CauCL, LM, and MM samples trended higher compared to all other tissues. The hyaline cartilages (CC and PC) had the lowest pyd/ww. The fibrocartilage tissues averaged together had a pyd/ww 2.16x the hyaline cartilages averaged together, and all of the ligament tissues averaged together had a pyd/ww 1.98x the hyaline cartilages averaged together.

Pyridinoline normalized to collagen content (pyd/col) for CC, PC, MM, LM, CraCL, CauCL, MCL, LCL, and PL were 5.69±3.85, 3.68±1.59, 2.28±0.88, 2.17±0.92, 8.32±2.12, 16.08±4.53, 2.22±0.85, 2.02±0.34, and 2.80±0.42 nmol/mg, respectively (Figure 4b). Statistically, CauCL had the highest pyd/col and CraCL the second highest, followed by the hyaline cartilages. The collateral and patellar ligaments and both menisci were not statistically different from each other and were less than the cruciate ligaments and the hyaline cartilages. CauCL had a pyd/col 1.93x CraCL, 3.43x the hyaline cartilages averaged together, 7.22x the fibrocartilage tissues averaged together, and 7.59x the collateral ligaments averaged together.

Tensile properties. The Young's moduli for CC, PC, MM, LM, CraCL, MCL, LCL, and PL were 8.4±4.1, 4.6±1.8, 25.9±7.0, 21.6±6.2, 2.1±1.0, 11.6±5.9, 13.2±5.8, 16.9±4.07, 27.5±2.8 MPa, respectively (Figure 5a). The UTS for CC,

PC, MM, LM, CraCL, MCL, LCL, and PL were 7.0±2.2, 3.9±0.7, 15.1±4.5, 24.6±2.0, 1.4±0.6, 7.4±5.9, 10.1±6.4, 14.9±3.9, and 15.7±3.3 MPa, respectively (Figure 5b). MM, LM, and PL exhibited significantly higher stiffnesses (Young's moduli) and strengths (UTS) compared to the other tissues, while CC, PC, CraCL, and CauCL were among the softest and weakest in tensile properties. Also of note, among the cruciate ligaments, CauCL was significantly stiffer and stronger than CraCL: Young's modulus and UTS for CauCL were both 5.4x CraCL.

Discussion

This study examined the major connective tissues of the immature bovine knee joint, motivated by a need to understand the interplay of biomechanics and biochemistry in immature connective tissues, as well as to establish design parameters for in vitro tissue engineering efforts. In the present study, differences were found across tissue types with respect to histology, collagen content, pyridinoline crosslink abundance, and tensile properties. In addition to reinforcing orthopaedic structure-function relationships, to our knowledge, this study is the first to examine these parameters in a direct head-to-head comparison between all of the major connective tissues of the knee, the first to assess pyridinoline crosslink abundance in all the tissues of a bovine joint, and the first to report results for pyridinoline crosslink abundance that suggest a preferential structure-function relationship to tensile stiffness rather than strength.

In the present study, tissues of interest were first examined histologically for the presence of collagen and GAGs to infer qualitative structural differences

underlying the biomechanical distinctions between these different tissues. Meniscus and ligament specimens appeared nearly identical, exhibiting extensive staining for collagen with no observable GAG staining (Figure 2). Hyaline cartilage, by contrast, exhibited less collagen staining than either meniscus or ligament, but also significant GAG staining. These histological trends correspond to the notion of knee joint connective tissues spanning a continuum between hyaline tissue (high collagen, high GAG) and fibrous tissue (high collagen, low GAG) (Figure 1). These qualitative histological differences relate to the functional roles of these tissues: fibrous tissues (ligaments and tendons) and fibrocartilage tissues (menisci) experience tremendous tensile stresses during locomotion, while hyaline cartilage experiences a balance of both tensile and compressive stresses, though preferentially the latter.

Tissue tensile properties, especially in connective tissues, are largely understood to derive from collagen content,[199] so it was hypothesized that trends in tensile properties would reflect trends in collagen content. In this study, collagen content was quantified in each tissue and normalized to tissue wet weight (Figure 3). It was found that the menisci had the highest collagen content, followed by the patellar ligament and the collateral ligaments. Collagen content was lowest in the hyaline cartilages and the two cruciate ligaments. As expected, the tensile properties (Figure y-5) do appear to reflect the general trends observed in collagen content. In particular, it was found that the menisci and patellar ligament exhibited significantly higher stiffness (Young's moduli) and strength (UTS) values compared to the other tissues, while the hyaline cartilages

and the cruciate ligaments were among the softest and weakest in tensile properties.

The differences in tensile properties among the ligament tissues (high in patellar ligament, medium in collateral ligaments, and low in cruciate ligaments) may reflect the anatomical development of these tissues, since the stiffer/stronger tissues are extracapsular ligaments, and the softer/weaker tissues are intracapsular ligaments. In particular, the patellar ligament arises from fibers of the quadriceps muscle attaching inferiorly to the tibial tuberosity (hence the term "patellar tendon" often used interchangeably with patellar ligament, given the tendinous origin), the cruciate ligaments arise posteriorly from the articular interzone, and the collateral ligaments form independently of the joint capsule (LCL) or from mesenchymal condensation in the joint capsule (MCL).[217] Furthermore, of particular interest was the finding that CraCL (analogous to the ACL in humans) is significantly softer and weaker than CauCL (analogous to the PCL in humans). Clinically, ACL injuries are more commonly diagnosed than PCL injuries, both in children and adults; the apparent softness and weakness of the CraCL compared to the CauCL supports the idea that the CraCL, and thus the ACL in humans, may be more prone to injury. Taken together, the tensile data described above contribute important information about the tensile properties of immature tissues, especially in light of the increasing incidence of knee joint injuries among youths.[212] Additionally, these tensile properties may serve as important benchmarks to determine success criteria for in vitro engineering of the major knee joint connective tissues, all of which play important

roles in mechanical function. Tissue engineering efforts aimed at recapitulating native tissue structures should strive to reproduce native tissue biomechanical properties, as well.

Crosslink analysis with HPLC showed that the different joint tissues had varying pyridinoline abundances that contributed to tensile stiffness. The data showed that the hyaline cartilages and the cruciate ligaments exhibited the highest pyridinoline levels (Figure 4). Both the patellar ligament and CauCL exhibited higher tensile stiffness values that paralleled pyridinoline content but not the amount of collagen. Although pyridinoline has been shown to correlate with tensile strength and stiffness in bovine articular cartilage,[49] this is the first study to show that pyridinoline also contributes to the mechanical properties of other bovine joint tissues. These results also corroborate structure-function relationships in other species. For example, a study of the rat tendon demonstrated that pyridinoline was a better indicator of ultimate stress than collagen content.[218] These structure-function relationships illustrate the importance of crosslinking in a variety of joint tissues.

Pyridinoline content is known to generally increase as tissues matures, but this study provides comprehensive, quantitative benchmarks that can be compared to adult tissue values. For instance, the observed pyridinoline abundances for condylar cartilage and meniscus fibrocartilage are approximately 50% and 70% of the mature values, respectively.[49,219] These pyridinoline results can inform future tissue engineering efforts that aim to reproduce the biochemical composition of native tissues. Because engineered cartilage has shown less

collagen crosslinking than native tissue, strategies such as increasing lysyl oxidase expression[220] may be needed to increase pyridinoline formation. Other stimuli such as TGF-β1 have been shown to increase pyridinoline content in articular cartilage[221] and could potentially be beneficial for enhancing crosslinking in engineered tissue as well. Considering the role of pyridinoline in tissue mechanics[49,50] and the inherently mechanical nature of knee joint connective tissues, crosslinking should be a central focus of future tissue engineering approaches.

This study provides comprehensive biochemical and biomechanical data describing hyaline, fibrocartilaginous, and fibrous tissues of the immature bovine knee joint. These data may serve as important design parameters for future efforts in tissue engineering, particularly with respect to pyridinoline crosslink abundance. This work also advances an understanding of structure-function relationships in immature connective tissues. Future work may expand on this study by examining temporal development and maturation of the collagen network and tensile properties, or by making direct comparisons in pyridinoline crosslink abundance between immature and adult tissues. Finally, an assessment of these parameters in disease states such as osteoarthritis or traumatic injury models such as ligament rupture may shed light on predisposing factors.

Figure 5-1: Continuum of knee joint connective tissues.

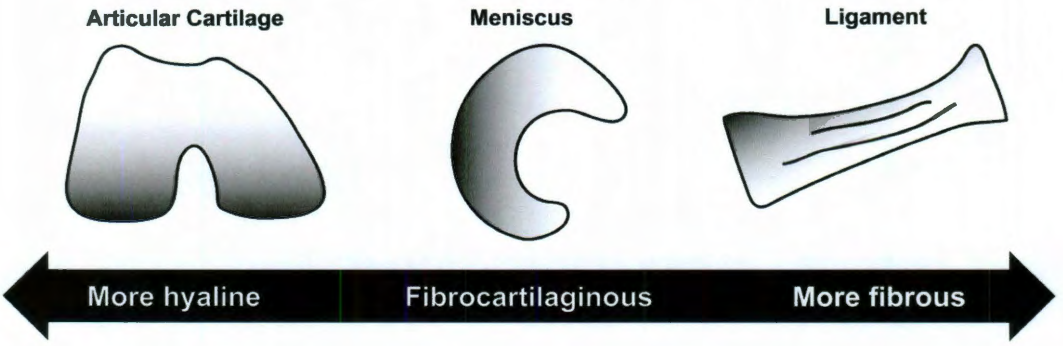

Based on their structural compositions, the major connective tissues of the knee joint can be conceptualized along a continuum from hyaline (condylar and patellar cartilage), to fibrocartilaginous (meniscus), to fibrous (ligament).

Figure 5-2: Histology of representative joint tissues

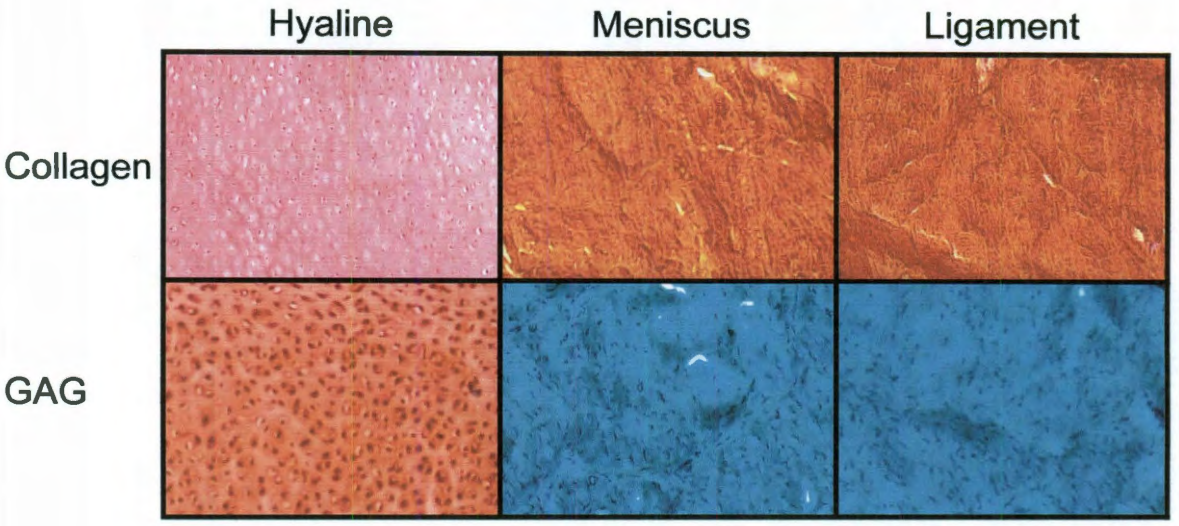

Picrosirius red staining for collagen showed that hyaline cartilage, meniscus, and ligament all had significant collagen content. The meniscus and ligament samples stained more intensely for collagen than hyaline cartilage. Safranin O/fast green staining for GAG showed that hyaline cartilage had significant GAG content; meniscus and ligament did not exhibit GAG staining.

Figure 5-3: Collagen content normalized to wet weight

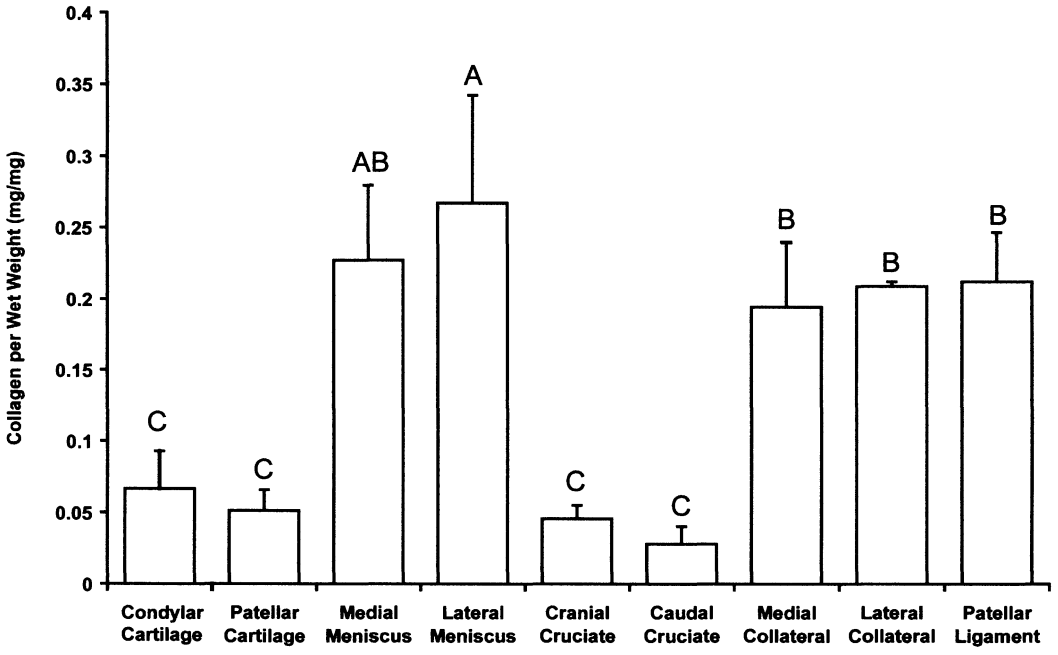

Collagen content was significantly higher for menisci, collateral ligaments, and patellar ligament. Groups denoted by different letters are significantly different ($p<0.05$).

Figure 5-4: Pyridinoline content of joint tissues

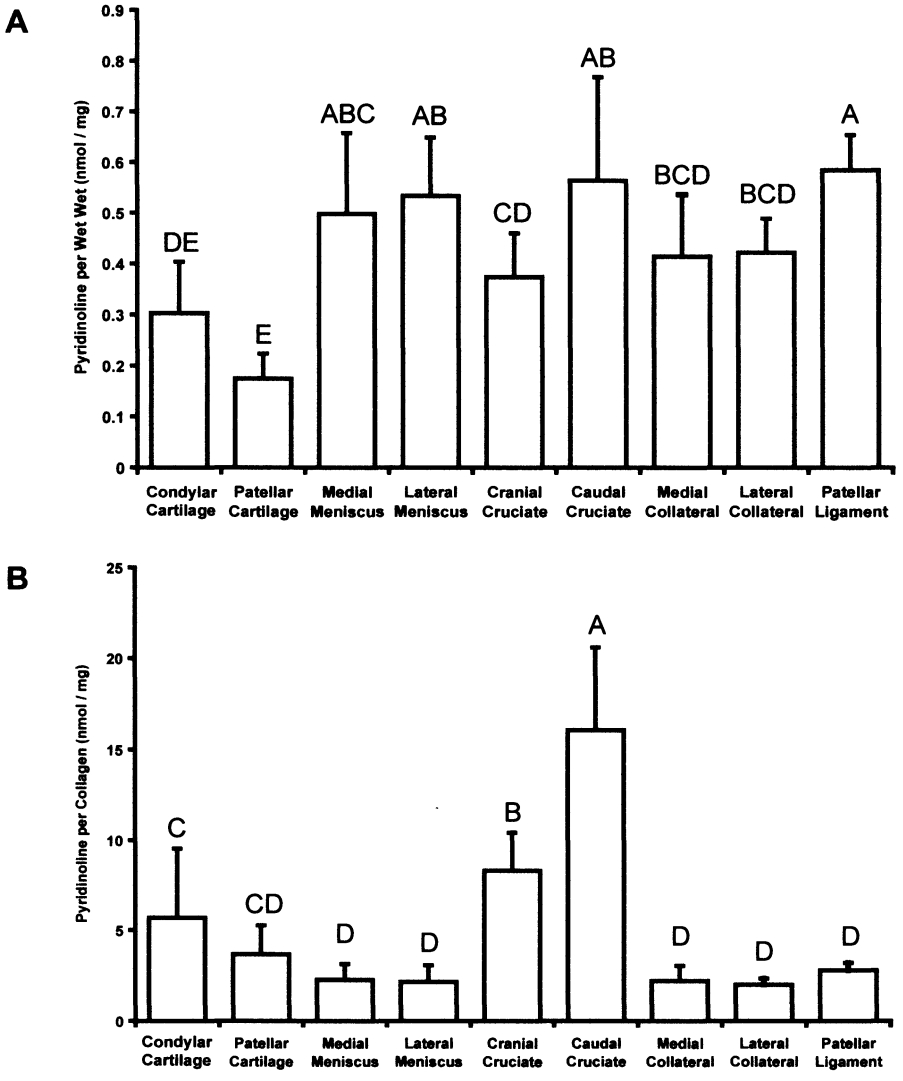

(a) Pyridinoline normalized to wet weight was highest for menisci, patellar ligament, and the caudal cruciate ligament. Crosslink content was lowest for patellar cartilage. (b) Pyridinoline normalized to collagen was highest for hyaline cartilages and cruciate ligaments. Groups denoted by different letters are significantly different ($p<0.05$).

Figure 5-5: Tensile properties of joint tissues

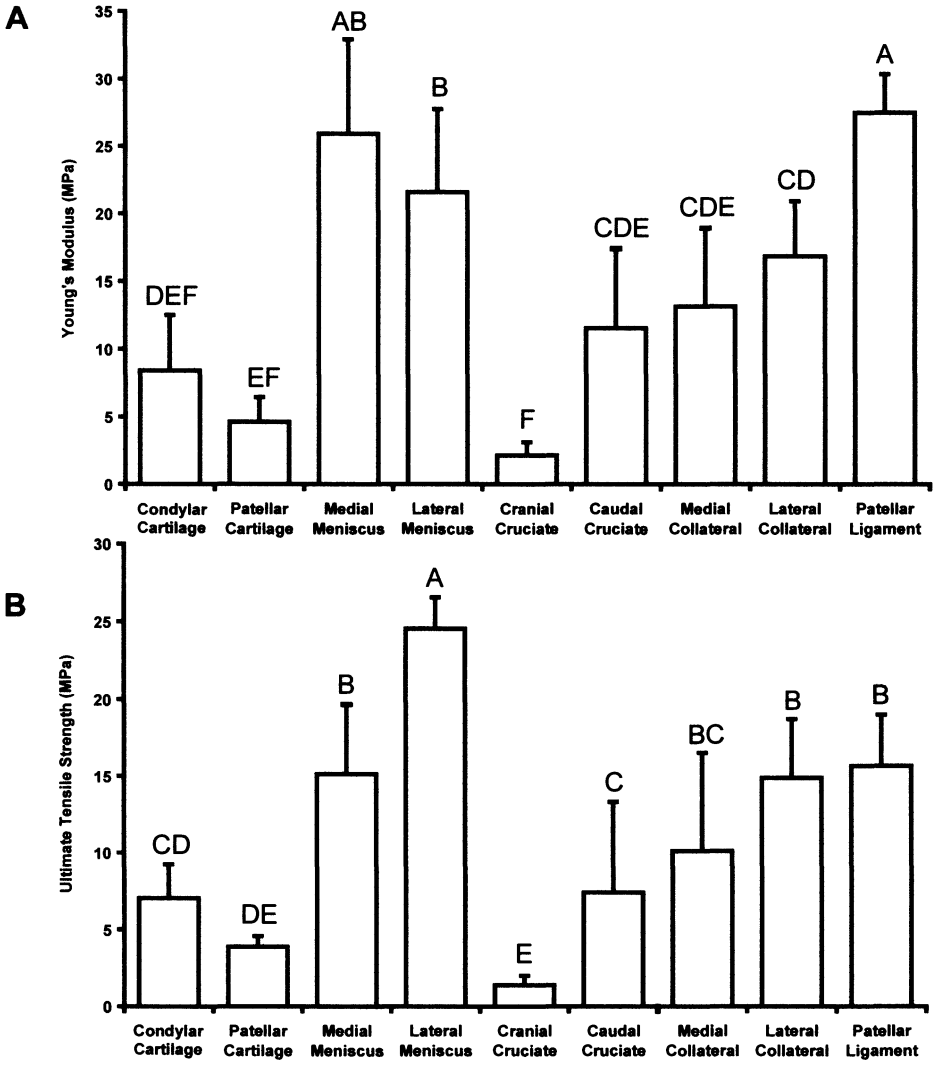

(a) Young's modulus was highest for the menisci and patellar ligament and lowest for the cranial cruciate ligament. (b) Ultimate tensile strength was also higher for the patellar ligament and the menisci. Groups denoted by different letters are significantly different ($p<0.05$).

Chapter 6: Noninvasive evaluation of bioengineered articular cartilage using time-resolved fluorescence spectroscopy*

Abstract

A bimodal technique integrating time-resolved fluorescence spectroscopy (TRFS) and ultrasound backscatter microscopy (UBM) was used to evaluate self-assembled bioengineered articular cartilage samples. Using a prototype system of combined TRFS and UBM, we compared the biochemical changes in cartilage samples treated with three types of exogenous agents (collagenase, C-ABC, and ribose) with a control group through fluorescence lifetime and spectral measurements. The microstructure and the thickness of the engineered cartilage samples were characterized by UBM. The optical and ultrasound results were validated against those acquired via conventional techniques including collagen and glycosaminoglycan (GAG) quantification and mechanical measurement of construct stiffness. Current results have demonstrated that a set of optical parameters (e.g., average fluorescence lifetime and decay constants) showed significant correlation ($p < 0.05$) with biochemical and mechanical data, and high resolution ultrasound images provided complementary cross-section information of the cartilage samples with deeper penetration depth. Therefore, the technique was capable of noninvasively evaluating the composition of extracellular matrix and the microstructure of engineered tissue, demonstrating great potential as an alternative to traditional destructive assays.

---

* Sun Y, Responte DJ, Xie H, Liu J, Hu J, Athanasiou KA, Marcu L. Noninvasive evaluation of tissue engineered articular cartilage with combined time-resolved fluorescence spectroscopy and ultrasonic backscatter microscopy. Tissue Eng Part C (submitted)

Introduction

Self-assembled cartilage: Cartilage degeneration is a serious problem in orthopedic medicine and afflicts millions worldwide. For instance, osteoarthritis affects an estimated 10% of people over age 60.[13] The acellularity and avascularity of cartilage contribute to its limited healing capacity, which has created a pressing need for novel tissue regeneration strategies. One tissue engineering approach, self-assembly, entails culturing chondrocytes at high density in agarose molds to produce cartilage constructs with properties approaching those of native tissue.[94] Several anabolic[59,178] and catabolic[51,138] exogenous agents have been investigated to modulate the matrix composition of constructs and subsequently alter their biomechanical and biochemical properties.

Non-invasive evaluation technology for tissue engineering: The success in developing a useful engineered tissue construct relies heavily on evaluating its structural and biochemical properties both before and after implantation. Traditional destructive methods such as biochemistry assays and mechanical testing are a clear impediment to such a setting and are highly inefficient in time and cost. Destructive measurements are undesirable in tissue engineering because cell culturing and differentiation are expensive and time consuming. Additionally, conventional methods demonstrate high variability and do not allow dynamic measurements that are important for long term tissue studies. Thus, there is a clear need for non-invasive, non-destructive tissue characterization

methodology that allows ongoing evaluation of tissue during development or analysis of matrix modified by exogenous agents.

Fluorescence based techniques have the potential to measure biochemical changes in tissue in relation to clinical diagnosis.[222] Auto-fluorescence of structural proteins (collagen and elastin), co-enzyme factors (the reduced form of nicotinamide adenine dinucleotide, NADH), amino acids (tryptophan, tyrosine), lipids and vitamins allow label free compositional analysis of samples.[223] Laser induced fluorescence has been widely employed in characterizing skin tumors, urinary bladder tumors and head and neck cancer[224] and myocardial tissue.[225] However, techniques based on the analysis of intensity and spectral distribution of fluorescence are often hampered by challenges in resolving the broad emission spectra and spectrally overlapping of the endogenous fluorophores. Time-resolved fluorescence spectroscopy (TRFS) techniques take into account the decay characteristics of the fluorescence emission thus providing better differentiation between fluorophores with overlapping spectra.[226,227] Additionally, the fluorescence decay characteristics allow description of biological microenvironment of the fluorophore. This makes TRFS a more robust method for non-destructive tissue analysis. The use of auto-fluorescence in tissue engineering, however, is fairly recent. Previous work includes non-invasive in situ evaluation of osteogenic differentiation with time-resolved fluorescence spectroscopy,[228] and TRFS and ultrasound evaluation of cartilage constructs cultured in scaffolds.[229] Collagen, glycosaminoglycans (GAG), and NADH are major endogenous fluorophores of engineered tissue that can be analyzed using

fluorescence spectroscopy. Formation or degradation of collagen, collagen crosslinks and changes in relative concentration of other fluorophores will change the overall tissue fluorescence emission.

Ultrasound imaging is well recognized as a viable tool for studying the structure and morphology of biological tissue.[230,231] Moreover, ultrasound backscatter microscopy (UBM) that employs high frequencies transducers (>40 MHz), has been used to characterize atherosclerotic lesions,[232] connective tissue network[233] and collagen fiber distribution in human dermis.[234] It provides a spatial resolution of tens of microns and sufficient penetration depth of 5-6 mm. We have previously demonstrated the use of UBM in atherosclerotic plaque characterization studies.[235,236] High frequency ultrasound was also used to assess the morphologic acoustic, and mechanical properties of articular cartilage.[237]

The overall objective of this study is to evaluate the ability of an experimental system combining TRFS and UBM modalities for non-destructive analysis of self-assembled cartilage constructs properties. Experiments were conducted in constructs where the extracellular matrix (ECM) protein is biochemically altered in a manner that affect the ECM content as well as the mechanical properties of the construct. Specifically, the goals of this study are (1) to determine whether changes induced in tissue constructs via a set of anabolic or catabolic agents known to affect the ECM composition can be detected using non-destructive bimodal TRFS-UBM measurements; and (2) to determine the correlation between optical and ultrasonic parameters of the constructs and biochemical,

biomechanical properties measured using conventional assays and mechanical tests.

Methods

Tissue fluorophores: To understand the overall fluorescence emission (intensity, peak, emission, decay characteristics or lifetime) originated from the engineered cartilage tissue, TRFS measurements were performed in all major intrinsic fluorophores within the sample. These included collagen type II (major collagen type in week 4 cartilage sample), GAG (providing mechanical integrity to the tissue), aggrecan (backbone of the protein-sugar complex proteoglycan), and NADH (expressed in the cells). These measurements served as references. The measurements were conducted in pure powder form for collagen, GAG (chondroitin sulfate)and aggrecan and in 1 mMPBS solution for NADH. All the chemicals were extracted from tissues or cells and purchased from Sigma-Aldrich.

Cartilage sample preparation and treatments: Bimodal TRFS and UBM measurements were performed on the self-assembled articular cartilage samples generated as follows. Chondrocytes were harvested from the patellofemoral groove and distal femur of immature bovine legs (Research 87, Boston, MA) and isolated as described previously.[94] Cells were thawed and seeded in 5 mm diameter agarose wells to form constructs. Constructs were cultured at 37ºC, 10% CO_2 and were fed daily with a chemically-defined medium.[94] All exogenous agents were administered in chondrogenic media and constructs were cultured at

37°C, 10% CO_2 for the duration of each respective treatment. Chondroitinase-ABC (C-ABC) treated constructs were each treated with 500 µl of a 2U/ml C-ABC solution for 4 hours. For the collagenase treatment, constructs were exposed to 0.2% collagenase for 30 min. Ribose treatment was performed for 4 hours at a concentration of 30mM.Collagenase is responsible for the degradation of the collagen components while C-ABC is effective for GAG digestion resulting in an increase of collagen concentration. Ribose can nonspecifically oxidize the collagen crosslinks. At 4 weeks, constructs were assessed using non-invasive assessments and then processed for biochemical and biomechanical testing. The central 3 mm regions of the constructs were used for compressive evaluation and the outer ring was used for biochemical assays and tensile evaluation.

TRFS-UBM system and measurements: The hybrid TRFS-UBM system consists of four primary modules: TRFS sub-system, UBM sub-system, hybrid probe, and control unit (Fig. 1).

TRFS sub-system: A pulsed nitrogen laser (337 nm, 0.7 ns, 30 Hz) provided the excitation light through an optical fiber (600 µm core diameter, NA = 0.22), which was positioned perpendicular to the sample and directed light onto the sample. Sample autofluorescence was collected throughthe same fiber and a beam splitter, and dispersed by a spectrophotometer after which scattered excitation light was removed by the use of a long-pass filter (340 nm). The fluorescence signal was detected with a gated multichannel plate photomultiplier

tube (MCP-PMT, rise time of 180 ps),and amplified by a wideband preamplifier (1.5 GHz bandwidth), recorded by a fast digitizer (2.5GHz bandwidth, 20G samples/s). The fluorescence decay pulsesfrom each sample were obtained by scanning of the spectrophotometer across a spectral range of 360-600nm (steps of 5 nm). The laser output energy was measured at the end of the optical fiber and was adjusted to 2 μJ/pulse. Measurements were taken from fourlocations on each sample, with the probe placed in direct contact with the sample. Reflected laser pulses from the sample were measured following the fluorescence measurements for the deconvolution of the system response from the measurements.

UBM subsystem:A high-voltage pulser generating a wideband pulse (200V peak-to-peak) was used to drive the ultrasound transducer. The received radiofrequency (RF) echoes were amplified with a 30 dB low-noise amplifier and filtered with a bandpass filter (24–90 MHz). A 12-bit digitizer with a sampling rate of 400M samples/s was employed to record the RF. A linear positioning stage (1 μm positioning resolution) allowed for scanning and forming a UBM image. The measurements were conducted with a customized 40MHz press-focused single element transducer (aperture size of 3.75mm, 63% bandwidth, 6mm focal depth) made available by the Ultrasonic Transducer Resource Center, University of Southern California, Los Angeles, CA. The optical fiber for TRFS measurements was inserted in the center channel (0.9 mm diameter) of the transducer. The UBM system with this transducer provided an axial and lateral resolution of 30 and 65 μm, respectively.

Biochemical, histological, and mechanical testing: For biochemical analysis, samples were frozen at -20°C and lyophilized for 48 hours to determine dry weights. Lyophilized samples were digested using pepsin-elastase as described previously.[138] DNA content was determined using PicoGreen®dsDNA Assay Kit (Invitrogen, Carlsbad, CA). Sulfated GAG content was assayed using the Blyscan Glycosaminoglycan Assay kit (Biocolor) and collagen content was quantified using a chloramine-T hydroxyproline assay.[117] For histology, samples were cryo-embedded and then sectioned at 14 μm. Sections were fixed in formalin and stained with safranin-O/fast green and picrosirius red.

Compressive properties were quantified using a creep indentation apparatus.[119,152]A 0.8 mm porous indentation tip was used to apply a tare load of 0.2 g followed by a test load of 0.7 g. For tensile testing, samples were cut into dog-bone shapes and glued to paper tabs for testing. Tensile assessments were conducted at a strain rate of 1% of the gauge length per second on a materials testing system (Instron Model 5565, Canton, MA). The slope of the resulting stress-strain curve yielded the Young's modulus and the maximum stress was reported as the ultimate tensile strength.

Fluorescence and ultrasonic data processing: Fluorescence system response was fully characterized by the shape of its fluorescence decay profile, h(k) for k = 0...K-1, where k was the index for the (k+1)th time sampling point with a sampling rate of 20 G samples/s(δ_t = 0.05 ns).The fluorescence decay

functionh(k) was assumed to follow a bi-exponential (BE) decay model[26], whereh(k) was a weighted average of two exponential decay functions with two time constants, τ_1 and τ_2 [Equation (1)]:

$$(k) = \sum_{j=1}^{2} \alpha_i e^{-\frac{(\delta t)\cdot k}{\tau_i}}, \qquad for\ k = 0 \ldots K-1 \tag{1}$$

α_1 and $\alpha_2$were the amplitude of the components at t = 0, and τ_1 and τ_2 were estimated from time-resolved fluorescence responses. However, we must emphasize that, with bi-exponential model, we did not implicitly assume that the fluorescence system under study was composed of two distinct fluorescent species. Rather, the choice of number of exponential decay components was merely justified by the goodness of fit. The time constants for the two components were considered as averaged time scales for fast components and slow components in the fluorescence system respectively.

The average lifetime can be calculated as Equation (2),

$$\tau_{avg} = \frac{\delta t \cdot \sum_k k\boldsymbol{h}(k)}{\sum_k \boldsymbol{h}(k)} \tag{2}$$

Incidentally, for bi-exponential model with decay profile in (1), Equation (3) gives,

$$\tau_{avg}^{BE} = \frac{\alpha_1\tau_1^2 + \alpha_2\tau_2^2}{\alpha_1\tau_1 + \alpha_2\tau_2} \tag{3}$$

The fractional contribution for each time constant to the average lifetime was defined as Equation (4):

$$A_1 = \frac{\alpha_1\tau_1}{\alpha_1\tau_1 + \alpha_2\tau_2}, \qquad A_2 = \frac{\alpha_2\tau_2}{\alpha_1\tau_1 + \alpha_2\tau_2} \tag{4}$$

The fluorescence spectrum was obtained by integration of the measured fluorescence decay curves over time. The fluorescence spectra were normalized by maximum fluorescence intensity along the entire emission wavelength.

The ultrasound image was formed by subtracting the DC offset from the ultrasonic radiofrequency (RF) data, and a band-pass filter with frequency range of 24 to 75 MHz was used to remove high frequency noise. The Hilbert transform was applied to the filtered RF signals to detect the envelopes, followed by a logarithmical compression. The processed data for each line of sight were displayed as a gray-scale B-mode ultrasound image showing the reconstruction of the cross section of the tissue constructs.

Statistical and correlation analysis: Six samples were assessed with conventional biochemical and biomechanical tests, as well as noninvasive optical and ultrasonic measurements for each group. A one-way ANOVA test was used to analyze the data and Tukey's post-hoc test was used when warranted. Significance was defined as $p<0.05$. All the data were presented as mean ± standard deviation. Pairwise comparisons were generated between all optical and conventional parameters and correlation coefficients with $p<0.05$ were considered significant. Correlation coefficients are reported in the results.

Results

TRFS of tissue fluorophores: The fluorescence emission characteristics obtained from the major intrinsic fluorophores in cartilage tissue are presented in Fig. 2. Collagen showed significantly stronger fluorescence intensity than all other

fluorescent components (Fig. 2a). While the fluorescence spectral shape of GAG (chondroitin sulfate) strongly overlapped (emission peak at ~400 nm) that of collagen (Fig. 2b), the intensity of GAG was significantly lower by 6.5 times. Both aggrecan and NADH had red-shifted emission peaks at ~450 nm and ~465 nm, respectively (Fig. 2b). Collagen exhibited the longest lasting emission among all fluorophores as demonstrated by both the average lifetime values (~5.6 ns at 400 nm) (Fig. 2c) and the slow decay time component τ_2 value (~6.7 ns at 400 nm) (Fig.2d) that accounted for ~80% of the overall decay (Fig. 2e). GAG presented also a relative long lasting emission with an average lifetime slightly lower than collagen (~4.3 ns at 400 nm) and a slightly different decay dynamics characteristics (~5.0 nsτ_2 and ~83% A_2). Aggrecan presented a faster decay dynamics (~3.1 ns $\tau_{average}$, ~4.4 ns τ_2 and ~65% A_2at 400 nm) when compared with both collagen and GAG. The NADH in free form presented a very fast decay dynamics with an average lifetime in sub-nanosecond range (~0.38 ns at 465 nm) as previously reported.[12]

TRFS of cartilage constructs: The time-resolved fluorescence spectrum of the four groups of cartilage samples (control, collagenase, C-ABC, and ribose,) can be fully described by various combinations of spectroscopic parameters as a function of wavelength (Fig. 3). The cartilage samples treated with collagenase had degraded collagen contents and presented a significantly lower intensity by 33% compared to the control group which showed the highest intensity in the 400-460 nm spectral range (Fig. 3a). The emission spectra of all groups were

largely overlapped (peak at ~430 nm), except for the control group that showed a slightly blue-shifted peak emission (~415 nm)(Fig. 3b). Major changes of the average lifetimes of all the groups occurred at the wavelength band of 400/40 nm instead of the fluorescence emission peak of 430 nm. The average lifetimes were elevated at 400/40 nm and then decreased when the wavelength increased (Fig. 3c). The control and C-ABC groups with higher collagen concentration (C-ABC deleted GAG therefore increased GAG concentration) exhibited the longer lasting emission compared to other groups as demonstrated by the average lifetime values of ~ 2.8 ns(Fig. 3c)and the dynamics characteristics (~3.8 ns τ_2 and ~70% A_2)(Fig. 3dand 3e).The samples of the collagenase group with degraded collagen contents showed a fast decay dynamics (~2.4 ns$\tau_{average}$ at 400/40 nm, ~3.4 ns τ_2,and ~65% A_2). There was no significant difference for the fast decay components τ_1 for all the groups obtained from multiexponential deconvolution (0.7 ns at 400 nm) (Fig. 3d). The fractional contribution of the slow decay A_2 contributed more to the average lifetime and showed more difference between groups (Fig. 3e).

A set of time-resolved parameters were analyzed statistically for each group and summarized in Fig. 4. If the mean value of average lifetimes was calculated over the whole wavelength range from 360-600 nm, the lifetime value of the C-ABC group was significantly longer the lifetime of the control group (Fig. 4a). The average lifetime at 400/40 nm (this band was picked at the area with the major changes of decay dynamics) of the collagenase group was significantly lower than the control and C-ABC group (Fig. 4b) but no significant difference was

shown between the C-ABC and control group. Information at longer wavelength also helped with differentiation between groups by comparing Fig. 4a and 4b. For the slow decay constant τ_2 at the wavelength band of 400/40 nm, the τ_2 value of the constructs treated by C-ABC was significantly increased by 12% than the τ_2 of the collagenase group which related to the increase of the collagen concentration (Fig. 4c). The slow decay constant $\tau_2$contributed to the overall fluorescence emission greater than 60% regardless of the treatments(Fig. 4d). The fractional contribution of the slow decay constant A_2 of the collagenase also showed significantly lower than the control and C-ABC group (Fig. 4d). The combination of τ_2 and A_2resulted in a significant faster decay and shorter average lifetime for the collagenase group compared to the control and C-ABC group.

UBM images of cartilage constructs: UBM images of the cross section of the cartilage samples from the four treatment groups are shown in Fig. 5. The surface of the sample was well defined with a homogeneous region within the margins (Fig. 5a). The thickness of each sample was determined from the top and bottom surfaces of the UBM images at ten different locations and the average thickness was compared between groups (Fig. 5b). The collagenase group was found to have a significantly lower thickness of 0.22±0.02 mm compared to the thickness of 0.41±0.04 mm for the control group, decreasing 46% compared to the thickness of the control group.

Histology: Histology results are summarized in Fig. 6. Picrosirius red staining showed decreased collagen abundance in collagenase-treated samples, whereas the other two treatment groups exhibited similar staining intensities as control(Fig. 6a). Saf-O/fast green stained the control and ribose groups more than the collagenase or C-ABC treatment groups(Fig. 6b). Collagenase deleted collagen fibers such that GAG compositions were not held in the network and were washed out.C-ABC administration resulted in less GAG staining than collagenase treatment.

Biochemical and biomechanical results: Biochemical and biomechanical assessments are shown in Fig. 7. Collagen content decreased significantly following collagenase treatment and increased significantly for neotissue treated with C-ABC (Fig. 7a). Ribose treatment did not statistically alter collagen content. GAG abundance decreased for constructs treated with collagenase and C-ABC, resulting in GAG/WW values of 5.1% and 3.1% for collagenase and C-ABC treatments, respectively(Fig. 7b).E_Y significantly decreased after collagenase treatment. In contrast, tensile strength increased following both C-ABC and ribose treatments, increasing by 72% and 49%, respectively(Fig. 7c). Compressive stiffness decreased significantly for both collagenase and C-ABC treatment groups. Aggregate modulus values were 70 kPa and 36 kPa for the collagenase and C-ABC treatment groups, respectively. Ribose treatment did not significantly alter the compressive stiffness (Fig. 7d).

Correlation with optical, biochemistry, and biomechanical properties: Parameters between technologies (optical, biochemistry, and biomechanical methods) with high and significant correlation were selected. The time-resolved parameters such as τ_{390}, τ_{450}, τ_{1-390}, τ_{1-450},showed high correlation (r>0.45) and significant correlation with collagen/ww and Young's modulus (E_Y). Significant and high correlation was observed for collagen/ww with E_Y (r=0.67), and collagen/wwwtih average lifetime over all the wavelengths (r=0.7) (Fig. 8a). In comparison, significant and high correlation was observed for GAG/ww with H_A(r=0.67). However, no significance was shown between GAG/ww and the average lifetime over all the wavelengths (r=-0.35) (Fig. 8b). Correlation analysis was also performed for the average lifetime from the wavelength band of 400/40 nm. High and significant correlation was observed for collagen/ww and average lifetime at 400/40 nm with r=0.69 and no significant correlation was observed between GAG/ww and the average lifetime at 400/40 nm.

Discussion

Biochemical compositions and TRFS results: Given the biochemical content of cartilage tissue constructs, the most likely auto-fluorescent biomolecules in these constructs are the constituents of the extracellular matrix (collagen type II, crosslinks, and GAGs) and the NADH in cells. The fluorescence emission of these biological fluorophores was studied (Fig. 2) and found consistent with values in literature.[8,27]While GAG demonstrated a peak fluorescence emission at about 400 nm, similar to emission peak of collagen, GAG emission measured in tissue extracts for the same excitation fluence rate was found more than six times weaker than that of collagen (Fig. 2a). This

suggested that (1) GAG had less contribution to the overall fluorescence emission due to the weak emission intensity and (2) the collagen emission characteristics were most likely to dominate the whole emission when both collagen and GAG molecules are present. The fluorescence spectrum of the aggrecan composition showed an emission peak of 450 nm, close to the emission peak of the spectrum of the cartilage sample (420-430 nm), demonstrating the contribution of aggrecan to the cartilage autofluorescence (Fig. 2a). To our best knowledge, this is the first time to report the time-resolved fluorescence spectroscopic data for GAG and aggrecan.

Current TRFS results obtained for cartilage constructs showed that blue-shifted increased fluorescence intensity and longer average lifetime values at 400 nm. In addition, most of the changes of the decay dynamics, such as τ_2 and A_2, happened at ~400 nm (Fig. 3). Mature collagen presents a blue-shifted peak emission at about 390-400 nm with and a lifetime greater than5 ns. Moreover, the TRFS revealed statistically significant decreases in average fluorescence lifetime values (400/40 nm) as a function of collagen content, ranging from 2.65 ns in control samples to 2.37 ns in collagen-depleted samples (Fig. 4b). This was further demonstrated by the correlation in Fig. 8 where collagen/ww showed significant and high correlation with the average lifetime (r=0.7), but the correlation between GAG/ww and average lifetime was not significant. Therefore, all the results above confirmed that (1) collagen dominated the fluorescence emission of cartilage constructs and (2) if collagen contents were increased by endogenous agents, fluorescence intensity and average lifetime were both increased and the changes occurred at ~ 400 nm. The emission peak of the

spectrum of the cartilage constructs was ~430 nm (not 400 nm) due to the contribution of aggrecan and NADH.

Combination of multiple time-resolved fluorescence parameters: Time-resolved fluorescence parameters were robust for the characterization of tissue fluorescence emission due to the independence of the excitation intensity and light excitation-collection geometries. These parameters including the decay constants τ_1, τ_2, fractional contribution A_2, and average lifetime at specific wavelength bands, allowed full characterization of the fluorescence dynamics originated from tissue constructs (Fig. 4). For example, average lifetime gave an estimation of the mixture of different biochemical compositions, but the fast and slow decay constants and the fractional contribution of each decay constants gave a more detailed description of the decay dynamics (Fig. 2, 3, 4). The combination of a set of time-resolved parameters provided a more stable and sensitive detection of biochemical compositions.

Potential optical quantification of collagen crosslinks: The crosslinks 3-hydroxypyridinoline and pyridinoline present a peak fluorescence emission around 390nm and are identified as abundant components of cartilage collagen. Thus, this crosslink is most likely to dominate the fluorescence of mature collagen type II. Crosslink between collagen fibers has an important impact in cell and tissue mechanics and tissue engineering. Cartilage specifically forms hydroxylysyl and lysylpyridinoline crosslinks that exhibit an emission peak around

400nm when excited with 325nm light.[238] Our future work is geared towards optical characterization of collagen crosslinks using time resolved fluorescence spectroscopy. We hope to study collagen gels with controlled crosslink and correlate HPLC,[216] mechanical and biochemical assay results to fluorescence intensity and lifetime results in these gels. Results may shine light upon the feasibility of developing a non-invasive optical assay for monitoring cartilage development in-vitro by tracking collagen crosslink.

Possible tissue characterization with UBM RF data: Optical coherence tomography (OCT)was used to quantify optical surface reflection and surface roughness of articular cartilage,[239] providing high resolution images (~10 □m) but limited penetration depth (~1 mm). In clinical study, the modalities for osteoarthritis diagnosis include x-ray,[240] arthroscopy,[241] and magnetic resonance imaging (MRI).[242] However, all these techniques have some limitations. X-ray and arthroscopy are invasive approaches, and MRI is limited by resolution and expensive. Here, we determined that UBM measurements successfully complemented the optical methods by providing morphological information of the cross section of the sample with greater penetration depth. In its current configuration, UBM can reach a penetration depth of 5–6mm, which is more than 10 times deeper than attainable for the optical techniques applied here (<250 μm). The analysis of the ultrasound RF signals facilitates a direct visualization of the sample but may also allow for evaluating mechanical information.[243]

Feasibility of non-invasive evaluation with the combined TRFS/UBM: The tissue characterization techniques, TRFS and UBM, successfully detected changes in tissue construct composition that correlated strongly with standard biochemical and mechanical analysis. The tissue samples with collagenase treatment showed significantly shorter lifetime at 400/40 nm compared to other groups since the collagen contents were depleted by collagenase (Fig. 4b). C-ABC treatment depleted GAG and therefore increased the concentration of collagen, resulting in an increase of average lifetime (Fig. 4a). The collagenase group gave the weakest fluorescence intensity and also the shortest average lifetime because the collagenase not only degraded the collagen network but also decreased the GAG content. UBM provided parallel information in terms of the growth of the constructs with different types of treatments. The reduced thickness of the collagenase group and C-ABC group samples was attributed to the depletion of the collagen and GAG respectively (Fig. 5). These observations were validated by biochemical results where the collagen/ww of the collagenase group was lowest among the groups and the GAG/ww was lowest for the C-ABC group (Fig. 7). In summary, a set of optical parameters (such as average lifetime at specific wavelength bands, decay constants, and fractional contribution) could be used to infer the biochemical and biomechanical properties of engineered tissues.

Conclusions

This paper presented a novel technique to evaluate tissue engineered articular cartilage using combined optical and ultrasound techniques. The

approach allowed characterizing a cartilage construct's collagen composition and structure in a nondestructive manner. Significant and high correlations were found between Young's modulus and collagen/ww, as well as aggregate modulus and GAG/ww. Moreover, significant and high correlation was observed between optical parameters and collagen/ww, but not GAG/ww. Each modality examined in this study demonstrated the ability to discriminate between changes in constructs treated with exogenous agents. Correlations of optical parameters with results from traditional assays demonstrated the potential of this bimodal technique in non-invasive evaluation of tissue engineered cartilage. Our future work will be focused on using the system to quantitate more subtle changes involved in *in vitro* differentiation such as collagen crosslinks.

Acknowledgments

This work was funded by the NIH Grant R01-HL67377. The authors also would like to acknowledge Dr. K. Kirk Shung, Dr. Jonathan M. Cannata, and Hao-Chung Yang of the University of Southern California for providing the ultrasonic transducer used in the study. We would also like to thank Dr. Jennifer Phipps and Dr. Abhijit J. Chaudhari for their help on data and imaging processing, Dr. Grace Zhang, Dr. Yinghua Sun, and Matthew Lam for helping with the initial experiments.

Figure 6-1: Schematic diagram of the combined TRFS-UBM system.

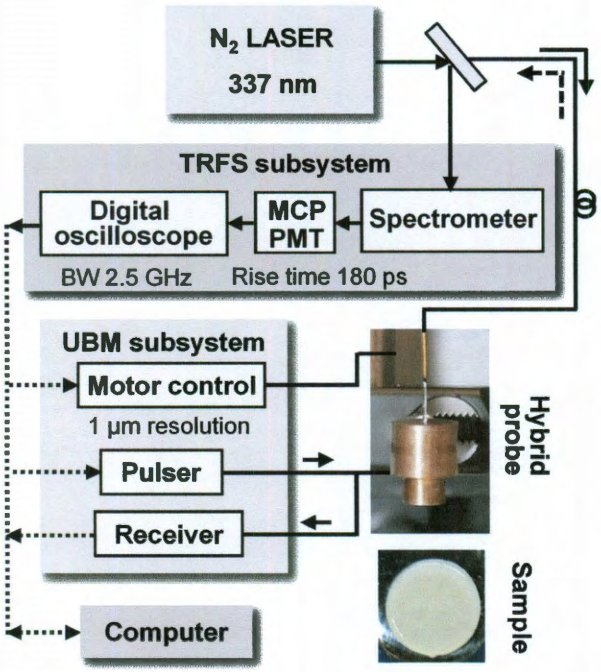

System includes laser source module, TRFS subsystem, UBM subsystem, and the combined probe (transducer+fiberoptics). A tissue engineered cartilage sample (at t=week 4) is shown.

Figure 6-2: Fluorescence spectroscopic data.

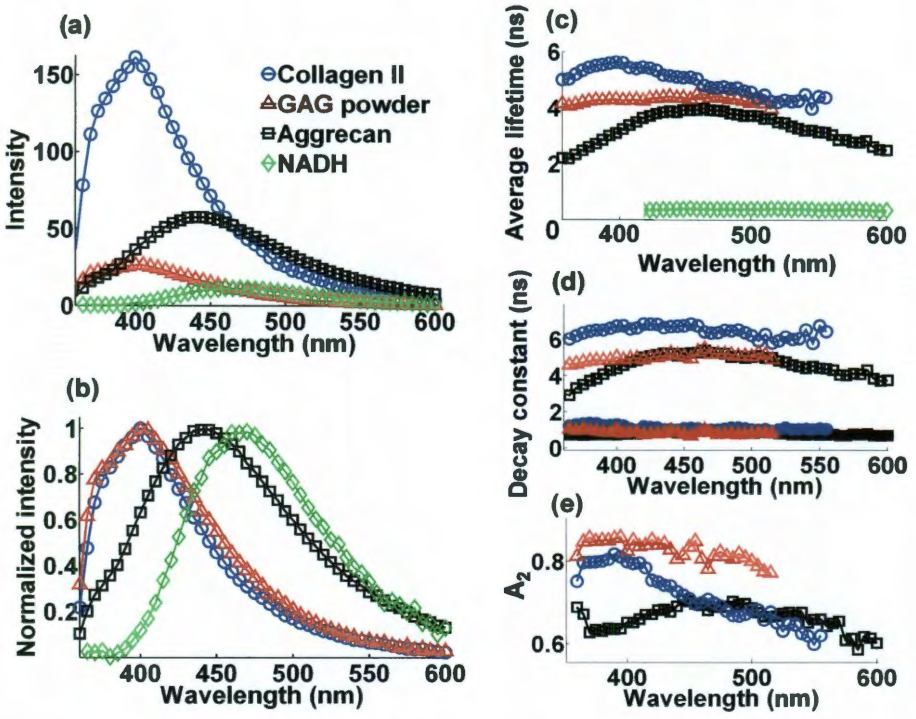

Data were acquired from the major endogenous fluorophores in the cartilage samples, including collagen type II, GAG powder, aggrecan, and NADH in cells. The time-resolved fluorescence parameters were retrieved with bi-exponential deconvolution. (a) Plots of fluorescence spectrum, (b) normalized spectrum, (c) average lifetime, (d) fast decay constant τ_1 (filled symbols) and slow decay constant τ_2 (open symbols) for collagen, GAG, and aggrecan(since NADH has only one exponential component, NADH was not included here),and (e)the fractional contribution of the slow decay component A_2.

Figure 6-3: Fluorescence spectroscopic data of constructs

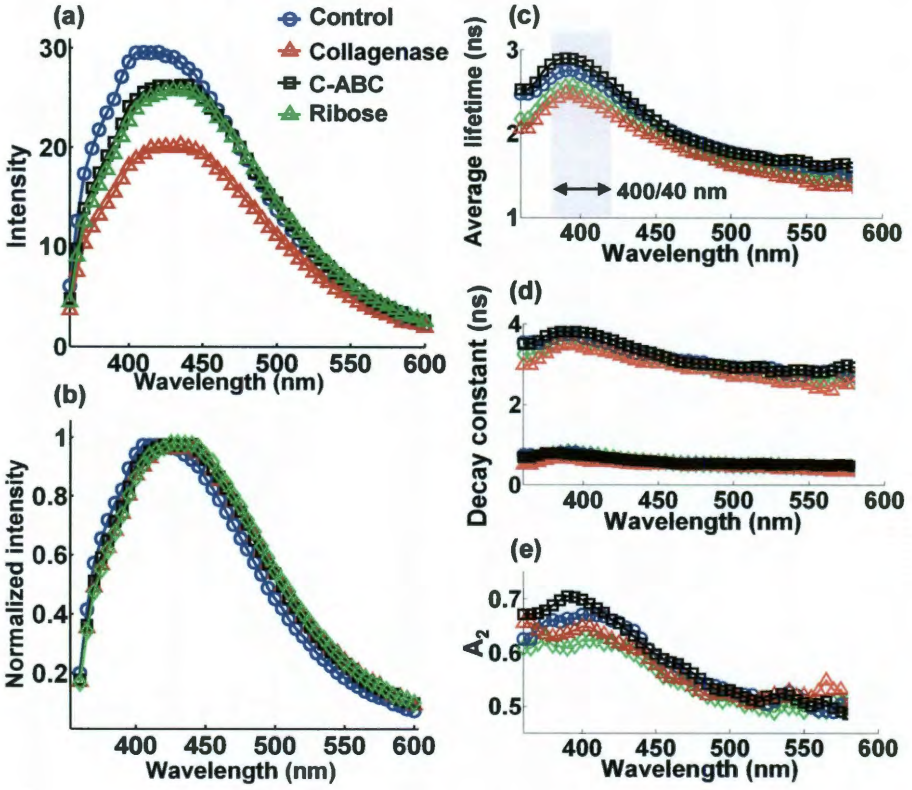

Fluorescence data were acquired from four groups of cartilage samples with different types of treatment (control, collagenase, C-ABC, and ribose). The time-resolved fluorescence parameters were retrieved with bi-exponential deconvolution. (a) Fluorescence emission spectrum, (b) normalized spectrum, (c) average lifetime, (d) fast decay constant τ_1 (filled symbols) and slow decay constant τ_2 (open symbols), (e) fractional contribution of the slow decay component A_2.

Figure 6-4: Quantification of the time-resolved fluorescence parameters

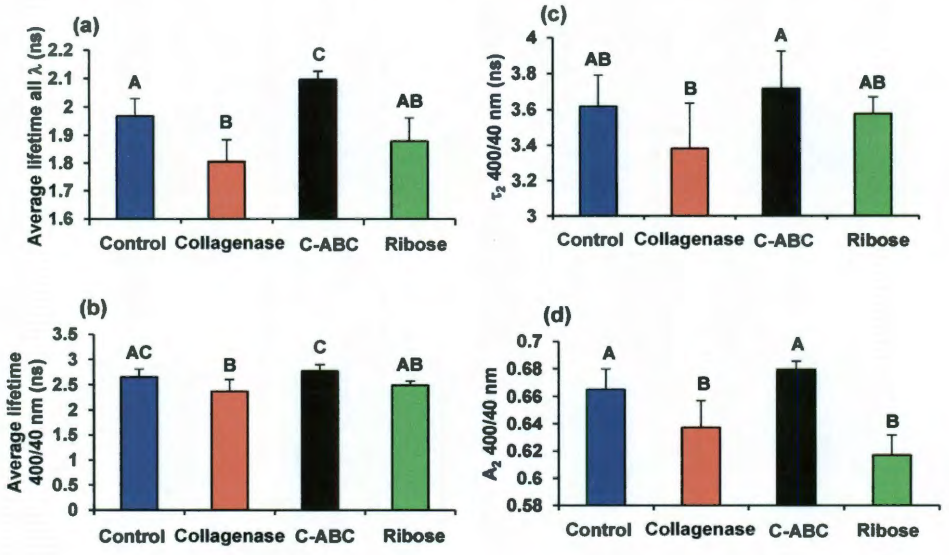

(a) the mean value of the average lifetime from 360 nm to 600 nm, (b) average lifetime at 400/40 nm, (c) slow decay constant $\tau_2$at 400/40 nm, (d) andfractional contribution of the slow decay component A_2.

Figure 6-5: Ultrasound imaging of constructs

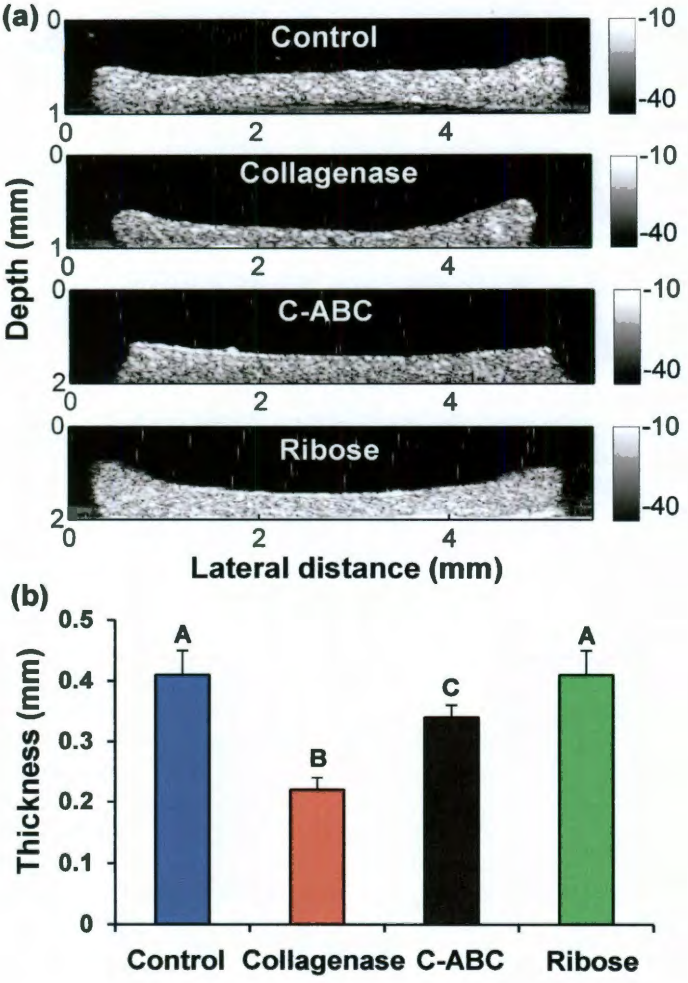

(a) UBM images of the cartilage samples from the four groups. (b) Thickness measurements of samples for each group.

Figure 6-6: Histology results

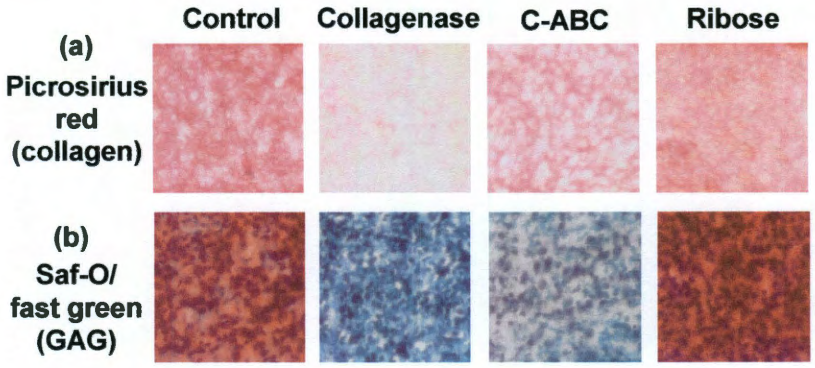

(a) Picrosirius Red for collagen and (b) Saf-O/fast green for GAG. Both stain were positive for control and ribose groups, but C-ABC and collagenase treatments decreased GAG staining. Collaganese treatment also decreased collagen staining intensity.

Figure 6-7: Biochemistry and biomechanics results

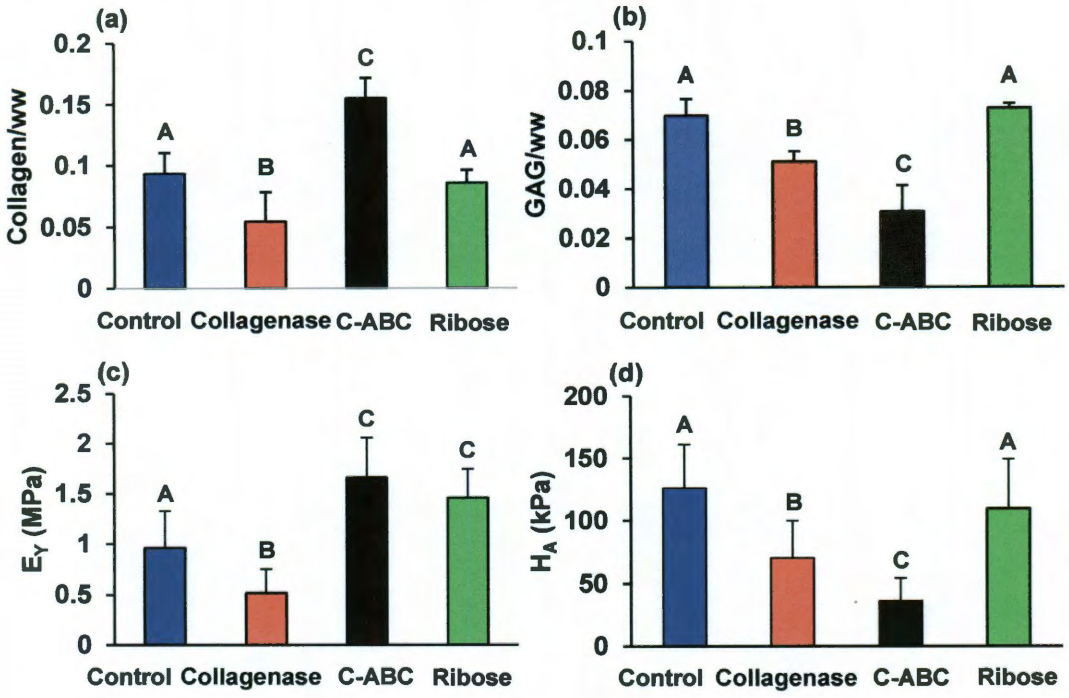

(a) collagen content and (b) GAGcontent normalized by wet weight of the sample. Biomechanical results for (c) Young's modulus and (d) aggregate modulus for the four groups.

Figure 6-8: Correlation between optical and conventional assessments

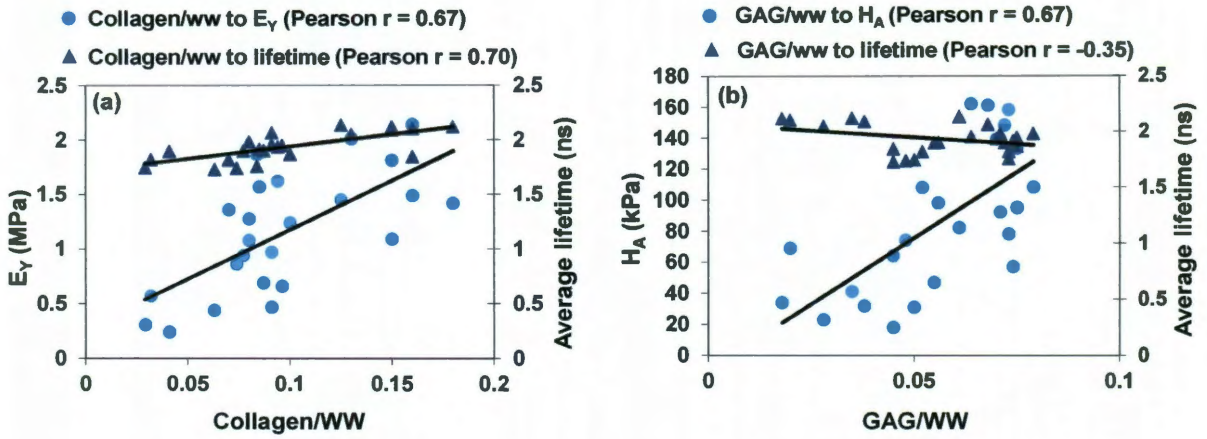

(a) Correlations between collagen/ww and E_Y (Pearson r=0.67, p=0.0003), collagen/ww and mean value of the average lifetime over the whole wavelength range from 360 to 600 nm (Pearson r=0.70, p=0.0001). (b) Correlations between GAG/ww and H_A (Pearson r=0.67, p=0.0003), GAG/ww and the average lifetime (Pearson r=-0.35, p=0.09).

Chapter 7: Collagens of articular cartilage: structure, function, and importance in tissue engineering*

Abstract

Collagen is a crucial matrix component of articular cartilage. Because articular cartilage is a load bearing tissue, developing mechanical integrity is a central goal of tissue engineering. The significant role of collagen in cartilage biomechanics necessitates creating a collagen network in tissue engineered constructs. An extensive network of collagen fibrils provides cartilage with mechanical integrity, but developing strategies to replicate this collagen network remains a challenge for articular cartilage tissue engineering efforts. To study the structure and biomechanics of the collagen network, many experimental and computational methodologies have been developed. However, despite extensive cartilage tissue engineering research, few studies have assessed collagen type, crosslinks, or fibril orientation. Further study of the collagen network, both within native tissue and engineered neotissue, will enable more robust constructs to be developed. This review focuses on the biology and biomechanics of the collagen network, relevant experimental methods for assessing the collagen network, and articular cartilage tissue engineering studies that have examined collagen.

---

* Chapter published as Responte DJ, Natoli RM, Athanasiou KA. Collagens of articular cartilage: structure, function, and importance in tissue engineering. Critical Reviews in Biomedical Engineering. 35(5): 363-411, 2009.

Motivation

Articular cartilage

Articular cartilage is a hyaline cartilage that lines the articulating surface of bones that is devoid of vasculature, nerves, and lymphatics.[1] Articular cartilage consists of a solid phase and a fluid phase. Water, along with dissolved solutes form the fluid phase, accounts for 60-85% of the total cartilage weight.[2] The solid phase primarily includes collagen, proteoglycans, and chondrocytes. Chondrocytes, the only cell type within cartilage, comprise only 1-5% of the tissue by volume.[1] Because cartilage lacks vasculature, chondrocytes receive nutrients by diffusion or imbibition and exudation during loading. The organization and presence of cells and matrix components exhibit depth-dependence within cartilage.

Cartilage injury and disease

The avascular, aneural, alymphatic, and largely acellular nature of cartilage hinders tissue repair.[9] Cartilage injury produces a mechanically inferior repair fibrocartilage,[10,11] which prevents recovery of cartilage functionality. In particular, increased collagen I and decreased glycosaminoglycan content within fibrocartilage alters the tissue's mechanical properties. The repair tissue ultimately breaks down, resulting in continual degeneration leading to osteoarthritis.

Osteoarthritis is a significant problem worldwide, especially in developed countries, resulting in a great economic burden. In western nations, it is estimated that up to 2.5% of the GNP is spent on arthritis,[244] and in the United

States, expenditures for arthritis and other rheumatic conditions exceeded $320 billion in 2003.[12] It is estimated that 10% of the world's population aged 60 years or more has osteoarthritis,[13] making it a leading cause of disability.[245] Osteoarthritis is also associated with some of the poorest quality of life issues,[244] particularly in terms of pain and physical function. The prevalence and severity of cartilage degeneration provides a strong impetus for engineering articular cartilage.

Collagen and tissue engineering

Due to the limited regenerative capacity and physiological importance of articular cartilage, damaged or diseased tissue needs to be replaced. Tissue engineering has the potential to substantially improve treatment of cartilage defects. The hydrated matrix of cartilage, composed primarily of proteoglycans and collagen, creates the mechanical integrity of the tissue. The importance of the matrix in cartilage biomechanics, and its ability to withstand a demanding mechanical environment, necessitates producing a suitable matrix in tissue engineered constructs.

The structure of the collagen network contributes extensively to the mechanical integrity of cartilage, particularly to the tensile properties.[128] Collagen comprises 60-85% of adult articular cartilage by dry weight,[2] making it a significant component of the extracellular matrix. Several types of collagen form a fibrillar network within the tissue. Many experimental methods exist to study the composition, structure, and crosslinking of this network. In addition, theoretical and computational models have been developed to analyze the role of collagen

in articular cartilage biomechanics. Despite extensive research, tissue engineered articular cartilage tends to have significantly less collagen than native tissue.[246-248] Strategies for improving this shortcoming will be needed to move closer to functional tissue engineered cartilage. This review covers the biology and mechanics of the collagen network in articular cartilage, pertinent experimental methods for studying collagen, and results from articular cartilage tissue engineering studies. In doing so, methods and directions for advancing engineering of the articular cartilage collagen network are highlighted and identified.

Biology of articular cartilage collagens

Types of collagen

Collagen molecules are comprised of three polypeptide chains that form a unique triple helical structure. These polypeptides contain high numbers of the repeating peptide sequence glycine–X–Y, where X and Y are frequently proline and hydroxyproline. This sequence helps stabilize the triple helix structure. Additionally, there are two short extrahelical telopeptides on each polypeptide chain which have neither the repeating peptide sequence nor a triple helical conformation. The most common types of collagen are the fibrillar molecules that assemble into fibrils; examples of fibrillar collagens include collagens I, II, and XI. The major collagen source within articular cartilage is a heteromer of collagen types II, IX, and XI, which is over 90% collagen II.[3,4] This heteromer forms the fibrillar network that provides articular cartilage with is tensile strength and stiffness. As shown in Fig. 1, these fibrils have a hierarchical organization.

Collagen VI is localized around the chondrocytes and contributes to mechanical properties of the pericellular matrix, as well as cell signaling. Several types of collagen, namely collagens I and X, are rarely expressed in normal articular cartilage but are present during development and certain pathologies. The following provides a brief synopsis of the collagens commonly studied in articular cartilage.

Collagen II

Collagen II is only found in articular cartilage and the vitreous humor of the eye, and it accounts for the majority of collagen in hyaline cartilage.[249] As the predominant collagen of the heterofibril, collagen II is a primary indicator of hyaline cartilage differentiation. Although collagen II accounts for 75% of fetal collagen, as the tissue matures the collagen II proportion increases to 90%.[3] Collagen II has been shown to be expressed at higher levels by proliferating human fetal chondrocytes.[250] Furthermore, creating transgenic mice that did not express collagen II resulted in chondrocyte apoptosis,[251] indicating the necessity of collagen II in articular cartilage.

Collagen IX

Collagen IX forms covalent links between other collagen IX molecules and also crosslinks collagen II molecules as shown in Fig. 1B.[252] Because collagen IX is only found in cartilage and a few other tissues such as the vitreous humor and developing cornea,[253] it can be used as a marker for cartilage differentiation. The upregulation of collagen IX during maturation also suggests it has a role in

development.[254] *In vivo* studies have shown that collagen IX plays a structural role in the development and integrity of articular cartilage. For instance, collagen IX knockout mice displayed irregular integrin immunostaining and abnormal columnar arrangement of chondrocytes. However, these developmental problems largely attenuated as the mice aged.[255] Other *in vivo* studies have shown the roles of collagen IX to include development of the cartilage growth plate[256] and prevention of multiple epiphyseal dysplasia.[257]

Collagen XI

Collagen XI is a fibrillar collagen that associates with collagen II. Type XI collagen comprises 10% of fetal cartilage collagen, but only 3% of adult tissue.[3] Collagen XI molecules crosslink primarily with other collagen XI molecules within the heterofibril.[252] Additionally, collagen XI has also been shown to limit fibrillogenesis by inhibiting the growth of collagen II fibrils, which could be attributed to steric hindrance or interaction with other matrix molecules.[258] This inhibition has been confirmed *in vivo* with collagen XI knockout mice that showed increased collagen fibril diameters.[259]

Collagen VI

Collagen VI is localized in the matrix immediately surrounding chondrocytes, a region referred to as the pericellular matrix.[260] Type VI collagen contains the sequence Arg-Gly-Asp that binds to chondrocyte receptors.[261] It has been hypothesized that the close interactions between collagen VI and chondrocytes contribute to mechanotransduction,[262] so replicating the collagen VI structure

may be important for creating an appropriate microenvironment for chondrocytes. Moreover, collagen VI mRNA is barely detectable in dedifferentiated chondrocytes, but starts to increase only six hours following differentiation.[263] Development also entails localization of collagen VI in the pericellular region; it is more widely distributed throughout the matrix prior to birth.[264] Collagen VI comprises less than 1% of adult collagen.[3]

Collagen I

Collagen I is produced in many different connective tissues of the body, but it is not typically expressed in hyaline articular cartilage. Study of the rabbit knee joint has shown that collagen I is expressed at the articular surface early in development, but disappears by six weeks after birth.[265] However, collagen I is abundant in tissues such as ligament, tendon, temporomandibular joint disc, and the meniscus. Type I collagen also appears in repair fibrocartilage that fills defects in damaged articular cartilage.[266] Because repair cartilage is mechanically inferior to native hyaline cartilage,[267] collagen I expression is undesirable for tissue engineered articular cartilage. Culturing chondrocytes *in vitro* can result in dedifferentiation and collagen I production.[69,268] Thus, collagen I can act as a marker for the differentiation status of chondrocytes for tissue engineering procedures.

Collagen X

As with collagen I, collagen X is not expressed natively in hyaline cartilage. Generally, collagen X is only found near the bone, as immunohistological studies

have shown that collagen X is localized in the zone of hypertrophic and calcifying cartilage.[269] In addition, collagen X is expressed by some cells at the articular surface of maturing cartilage[264] and in osteoarthritic cartilage.[270,271] Collagen X has been shown to be localized at the lower growth plate of both chick embryo[272] and human fetal cartilage.[250] The appearance of collagen X in tissue engineered constructs can indicate hypertrophic chondrocytes.

Collagen crosslinks

The various types of collagen discussed above interconnect with one another via crosslinks. The enzyme lysyl oxidase mediates normal crosslinking[273] and can form several types of crosslinks, including pyridinoline (Fig. x2-1C) and ketoimine linkages. In native articular cartilage, there are significantly more pyridinoline than ketoimine crosslinks, with a mean ratio of ~12 to 1.[274] Crosslinks can also be formed non-enzymatically when collagen amines react with sugars to form advanced glycation endproducts (AGEs).[275] Many different sugars, including glucose, ribose, and threose, can play a role in AGE formation. For instance, adding ribose increased the formation of AGEs in the matrix of adult bovine chondrocytes.[276] In human articular cartilage, the formation of AGEs increases with advancing age.[277] Increased AGE-mediated crosslinking contributes to increasingly stiff, brittle cartilage that may predispose cartilage to degeneration and osteoarthritis.[278]

Furthermore, the number and types of crosslinks change as the tissue matures. For example, as human cartilage matures, the number of crosslinks increases.[249,279] Crosslinks increase with age in animal models as well. In bovine

explants, the number of collagen crosslinks per wet weight is 730% greater in adult cartilage relative to fetal cartilage.[49] AGE crosslinks also show maturation dependence, increasing linearly with age after reaching maturity.[278] After lysyl oxidase oxidizes a lysine residue, several intermediate structures form prior to forming a pyridinoline crosslink. Comparing the number of pyridinoline crosslinks to the number of crosslink intermediates provides one way of assessing tissue maturation.[274] These results indicate that a tissue engineered construct may need the proper proportion of pyridinoline crosslinks to reflect native tissue.

Crosslinks play several important functional roles in cartilage. In addition to effects on tissue mechanics, crosslinks increase collagen retention, which could impact cell signaling. Fewer crosslinks can also increase collagen susceptibility to proteases.[280] These various functions of crosslinks show the necessity of recapitulating suitable crosslinking in tissue engineered constructs.

Collagen fibrillogenesis

Fibrillogenesis is a sequential process that begins when individual collagen molecules are extruded from chondrocytes. After extrusion, the collagen molecules fuse, either laterally or linearly, to form larger fibrils. Initially, this process produces small fibrils with uniform diameters that eventually interconnect to form fibrils. As the tissue matures, the diameters of the fibrils increase and the fibril size becomes less uniform as depicted in Figure x2-2. Throughout this process, various mechanisms, such as growth inhibition and fibril degradation regulate fibril formation. The growth of fibrils is modulated at fibril interfaces by the binding of small proteoglycans.[281] Diffusion limitations can also inhibit fibril

growth.[282] Additionally, chondrocytes produce collagenases that degrade collagen molecules. Various collagenases that chondrocytes produce provide a way to finely control collagen degradation.[254,283] In particular, cleaving regions involved in crosslinking could destabilize fibrils. Modulation of fibril formation and degradation of fibrils control the development of the collagen network.

Ultrastructure of articular cartilage

Organization of collagen

Articular cartilage has several structurally distinct regions known as the superficial, middle, deep, and calcified zones, and the properties of the collagen network vary significantly between zones (Table 1). In native tissue, collagen concentration is highest in the superficial zone and decreases farther from the articular surface,[284] yielding an inhomogeneous distribution (Fig. 2). Additionally, the organization of the collagen fibrils varies depending on the zone, and was first characterized by Benninghoff in 1925.[285] The superficial zone has fibrils oriented parallel to the articular surface. Beneath the superficial zone lies the middle zone that has larger fibrils that form interweaving arches. The deep zone contains the largest fibrils, which are oriented perpendicularly to the articular surface. The calcified layer contains the transition from the hyaline cartilage into the subchondral bone. This zonal variation can be attributed to the force distribution that cartilage experiences *in vivo*,[286,287] yielding an anisotropic arrangement in native tissue. Generally, the fibrils have smaller diameters near the surface, with a mean fibril diameter of 30-35 nm in the superficial zone and

40-80 nm in the deep zone.[147,148] Because collagen largely dictates the tensile properties, zonal variation of collagen fibril orientation and collagen content are important to consider when evaluating tensile properties of tissue samples.

Within each zone, several types of matrix exist: the pericellular matrix, the interterritorial matrix, and the territorial matrix. The territorial matrix is farthest from the chondrocytes and has less aligned collagen fibrils. Closer to the chondrocytes, the interterritorial matrix has more oriented collagen fibers with larger diameters. The pericellular matrix immediately surrounds the chondrocytes and buffers the mechanical forces that the chondrocytes experience.[288-291] The pericellular matrix can also impact cell-cell communication by sequestering soluble signaling molecules.[292]

Although the zonal organization of cartilage has been identified, considerable structural variation exists. Studies have shown differences in collagen ultrastructure based on factors like age, anatomical origin of the sample (e.g., joint and location within a joint), and variations in individual anatomy and physiology.[284,293,294] Although collagen organization of the superficial zone is widely confirmed, conflicting results pertaining to the intermediate and deep zones have been reported. Scanning electron microscopy (SEM) analysis has shown that fibrils in the intermediate zone actually form overlapping lamellae rather than interweaving arches.[295] Some studies of the deep zone have also shown divergences from the classic Benninghoff model of perpendicularly oriented fibrils. Traverse fibrils[296] and fibrils with random orientations[148] have been observed, in addition to the predominant perpendicular arrangement.

However, the Benninghoff model characterizes the majority of the fibrils in articular cartilage.

While the Benninghoff model describes collagen orientation through the depth of the tissue, split-lines illustrate the collagen orientation in the plane of the tissue surface. Pricking cartilage with a pin dipped in ink produces lines that correspond to fibril orientation in the superficial zone (Fig. 3). Electron microscopy has been used in various studies to show the correspondence between split-lines and collagen orientation.[296,297] Within areas of cartilage that experience the most loading, split-line patterns are highly consistent between samples.[298] Tensile properties have been shown to correspond to split-lines orientation.[128,155] Split-lines show the importance of considering the in-plane collagen ultrastructure, in addition to the vertical variation.

Ultrastructure development

Studies in rabbit knee joints have shown that the organization of collagen depends on age, with initial organization in tibial plateau cartilage occurring within two weeks after birth. In particular, the orientation of collagen fibrils correlates with the acquisition of full mobility.[299] As the animal matures, collagen fibrils acquire increasingly vertical orientations in deeper layers (Fig. 2), resulting in lower tensile strength parallel to the surface.[300] The factors that control development of collagen orientation have not been fully elucidated, but mechanical loading appears to govern this process.[301]

Mechanical loading on the tissue has been frequently proposed as the primary stimulus for collagen orientation.[301] Additionally, theoretical modeling of

cartilage development based on a loading stimulus reproduces native collagen structure.[302] Although the loading hypothesis for ultrastructure development has not been fully confirmed, some experimental evidence exists. For instance, fibroblast-seeded collagen gels subjected to 2.5% cyclic strain develop fiber alignment and mechanical anisotropy.[303] Various studies have also shown that loading of cartilage lowers the susceptibility of collagen to enzymatic degradation.[304,305] This selective degradation has been proposed as a mechanism underlying mechanical stimulation of collagen orientation, but alternate mechanisms could also play a role.

Collagen interactions with other matrix molecules

Although the collagen network directly influences the mechanics of cartilage, interactions with other components of the matrix are also crucial. Various proteoglycans interact with collagen and, in many cases, regulate the assembly of fibrils. Reduced aggrecan deposition in mice has been shown to increase fibril diameter and alter banding patterns, suggesting interplay between aggrecan and collagen.[306] Several small proteoglycans including lumican, decorin, and fibromodulin also interact with collagen. These interactions can regulate fibril diameter, fibril-fibril interactions, and susceptibility to degradation.[6] Knocking out perlecan, a heparan sulfate proteoglycan, reduced the size and density of collagen fibrils.[7,8] This is in contrast to decorin and lumican knockout models, in which fibril size is increased. Molecules other than proteoglycans can also influence the collagen network. For example, cartilage oligomeric matrix protein (COMP) stabilizes fibrils by binding to collagen triple helices.[307,308] The

interactions between the collagen and various matrix components play a large role in governing the size and stability of collagen fibrils.

Collagen-cell interactions

Collagen also interacts directly with chondrocytes to influence cellular function. For example, interaction with collagen II increased chondrocyte aggregation and reduced the level of chondrocyte apoptosis.[251] In contrast, degrading collagen caused 45% of chondrocytes to apoptose; exogenous addition of intact collagen back to the culture reversed these apoptosis effects.[309] Similarly, administering caspase inhibitors has been shown to mitigate chondrocyte apoptosis induced by removal of collagen from the matrix.[310] In addition to preventing apoptosis, the collagen network influences biosynthesis. For instance, inhibiting collagen crosslinking increased collagen levels by 100%, indicating a feedback mechanism between the collagen network and chondrocytes.[311] Collagen's influence on the survival and biosynthesis of chondrocytes shows the integral role of collagen-cell interactions in cartilage physiology.

Although the cellular interactions with collagen are not fully elucidated, many of them have been attributed to integrin-β1[309] and annexin V.[312] Annexin V has been shown to regulate mineralization of growth plate cartilage; it may have a role in pathological mineralization as well.[313] Studies have suggested that annexin V influences growth plate chondrocytes by altering calcium transport across cell membranes.[314] Knocking out integrins created abnormal chondrocyte shape and reduced chondrocyte proliferation by 35%.[315] The integrin receptor also mediates the differentiation of chondrocytes and appears to be critical for

joint development.[316] These various collagen-chondrocyte interactions play a critical role in cartilage development and homeostasis.

Conclusions

The collagen network of articular cartilage is primarily composed of fibrils of collagens II, IX, and XI. In addition to collagen IX crosslinking, enzymatic (lysyl oxidase mediated) and non-enzymatic (AGE formation) crosslinks interconnect the fibrils. Crosslinks can impact cartilage biomechanics, collagen retention, and collagen susceptibility to proteases. As the tissue matures, collagen molecules fuse laterally or linearly to form larger fibrils and, ultimately, fibers. Collagen exhibits zonal variation within cartilage, both in terms of amount and orientation. Additionally, several distinct levels of collagen organization exist around chondrocytes with a pericellular matrix, territorial matrix, and interterritorial matrix.

Collagen mechanics: theoretical, computational, and experimental insights

As discussed above, collagen in native articular cartilage is inhomogeneously dispersed and anisotropically arranged. Further, cartilage has been shown to possess tension-compression non-linearity[121,317,318] due to the increased stiffness of collagen in tension. These features complicate theoretical and computational approaches. In this section, we will examine mechanical properties of collagen, mechanical models of articular cartilage specifically incorporating features of the collagen network, and experimental findings elucidating the varied roles of collagen in articular cartilage biomechanics.

Fibrillar and molecular stiffness of collagen

Any effort to incorporate features of the collagen network into mechanical models of articular cartilage must be informed by the mechanical properties of collagen itself. Researchers have investigated collagen mechanical properties within tissue and at the single molecule level. At the single molecule level, material properties of collagen type II have been measured using optical tweezers, yielding an average persistence length of 11.2 nm.[319] Assuming a solid rod with circular cross section of diameter d, an estimate of the Young's modulus (E_Y) from the persistence length (L_P) is given by $E_Y = (64k_BTL_P)/(\pi d^4)$, where k_B is Boltzmann's constant and T is the temperature.[320] At room temperature (23°C), and assuming a diameter of 1 nm, $E_Y \approx 0.93$ GPa. Other investigators have also found the stiffness of the collagen molecule to be in the range of a few GPa by X-ray diffraction and Brillouin light scattering.[321-323]

In an early study on collagenous tissue, Haut and Little[324] proposed a quasi-linear viscoelastic constitutive equation for collagen fibers from rat tails and measured the material properties via tensile stress-relaxation tests. They then used the measured material properties to predict the tissue's behavior under constant strain-rate, hysteresis loop, and dynamic tests, finding good experimental agreement with all but the latter. The value of the material property corresponding to the elastic nature of collagen fibers was found to be 11.5 GPa. Quasi-linear viscoelasticity of collagen fibers has more recently been examined in articular cartilage. Using tensile step-wise stress relaxation testing, the instantaneous fibrillar modulus was found to be ~2.2 times the relaxed modulus

($E_{relaxed}$), the latter of which depended on applied strain (ε), as $E_{relaxed}$ = 0.5 + 250ε MPa.[325] Another study suggests that collagen type II has an elastic modulus of 7 GPa.[326] It is important to know the stiffness of collagen fibers for implementation in mechanical models of articular cartilage, a topic which we will now discuss.

Theoretical and computational models of articular cartilage incorporating the effects of collagen

Fiber reinforced continuum models

While there are several ways to incorporate features of the collagen network in material models of articular cartilage, fiber reinforced continuum models (Fig. 4A) have been the most common approach.[127,136,327-341] However, it must be noted that the presence of fibers within a composite does not guarantee that the mechanical behavior of the bulk material will be different than it is without the fibers. As Aspden[342,343] points out with respect to cartilage, a collagen fiber must exceed a critical aspect ratio to have a sufficient interaction force with the rest of the extracellular matrix to effectively transfer stress to the fiber. While collagen fibers in native tissue satisfy this aspect ratio, fiber aspect ratio may be an important consideration in tissue engineering efforts.

At the most basic level, fiber reinforced models include fibers distributed throughout the solid matrix that are predominantly active in tension (Fig. 4B). In an early study, Schwartz et al.[127] related the stiffness at the continuum level to the microstructure of articular cartilage. Their microstructural model consisted of bilinear elastic fibers embedded in an elastic matrix. The fibers, representing collagen, were given a tensile modulus of 150 MPa and a compressive modulus

of 2 MPa. They also allowed the fibers to have random orientation throughout the tissue. An interesting finding, which has also borne out in subsequent studies, is that re-orientation of the fibers during loading leads to increased stiffness in the direction of the applied load and a non-linear tensile stress-strain curve. Elastic fibers have also been incorporated into the linear biphasic model[118] to overcome difficulties the homogeneous biphasic model has in fitting unconfined compression experiments.[339] It was found that a fiber Young's modulus of 11 MPa best fit unconfined stress relaxation experiments. Additionally, it was discovered that different constituents in the model (e.g., fibers or the matrix) can experience substantially different stresses in a region of identical strain. This feature is not present in homogeneous models.

The elastic fiber reinforced biphasic model has been improved upon to include cartilage inhomogeneities through the incorporation of depth-dependent material properties and anisotropy, by orienting the collagen fibers differently through the depth of the tissue.[332] This model was also used to investigate the strain-rate dependent stiffness of articular cartilage, which was attributable to "self-stiffening" of fibers, with little contribution from the rest of the solid matrix.[344] In a recent study, the anisotropic nature of the collagen network was also accounted for by orienting the fibers according to their zonal structure: parallel to the articular surface in the superficial zone, random in the middle zone, and perpendicular to the subchondral bone in the deep zone.[338] It was shown that deep vertical collagen fibers increase tissue stiffness in the transient period of loading, which the authors postulate may be mechano-protective against damage

to the underlying bone. Collagen fibers in biphasic fiber reinforced models have also been treated as viscoelastic.[330,340,341,345] These studies have also shown that collagen network architecture is important in determining the tissue's mechanical behavior. One study used sample-specific data for the tissue's composition,[330] demonstrating the degree of specificity that can be incorporated into these models. Finally, this line of inquiry has even been extended to include hyperelastic fibers in a viscohyperelastic matrix within a biphasic framework, thereby creating a model that accounts for the non-linear nature of finite deformations.[329]

Other models incorporating features of the collagen network

Other methods for including aspects of the collagen network into mechanical models include transversely isotropic theories,[346,347] conewise linear elasticity,[318,348] and microstructural models taking into account collagen distribution, orientation, or crosslinking.[349-351] (Fig. 4A) With respect to articular cartilage, planes parallel to the articular surface are the transversely isotropic planes. Thus, the tissue's material properties are different perpendicular to the surface compared to parallel to the surface. It was demonstrated that a transversely isotropic, transversely homogeneous model was able to predict non-uniform behavior of the tissue, whereas the isotopic homogeneous model could not.[347] To account for the tension-compression non-linearity of cartilage material properties, Soltz and Ateshian[318] developed a conewise linear elastic model within a biphasic framework. Though developed at the level of an orthotropic material, due to experimental considerations, they reduced the model to cubic

symmetry. Good agreement was found between theory and experiment for both confined and unconfined compression experiments and torsional shear testing. On average, articular cartilage was ~21 times stiffer in tension than compression.

In an interesting study, Quinn and Morel[351] generated a model for articular cartilage mechanics using only one material property, an elastic modulus of 70 MPa for the collagen fibrils. The rest of the model was generated taking into account the molecular orientation and distribution of collagen fibers and their interaction with the proteoglycan gel. Scaling up the model allowed prediction of continuum level mechanical properties in reasonable agreement with previous experimental measurements. The model also predicts novel matrix interactions at low compressive strains (~1%) where current experimental data are limited. Lastly, two studies have initiated investigation into connections within the collagen network[349,350] (e.g., crosslinking), one of which suggests substantial differences between collagen modeled as a network than when modeled as moving in an affine manner.

Experimental findings

Effects of collagen amount, orientation, and intrinsic viscoelasticity on tensile properties

Turning now to predominantly experimental work, as early as 1973 the tensile properties of articular cartilage were shown to be related to collagen amount, as well as to its anisotropic and inhomogeneous arrangement within the tissue.[128] Specifically, it was shown that cartilage is stiffer in the superficial zone compared to deeper zones (Table 1) and also stiffer when pulled parallel to the predominant

fiber orientation (determined by split-lines, Fig. 3) compared to when pulled perpendicularly. Woo et al.[155] found similar results to the aforementioned study by employing an exponential stress-strain law (equivalent Young's modulus ranged 1.65 to 3.5 MPa) as opposed to simply fitting the linear portion of the stress-strain curve. Results from both of these studies were additionally related to the preferred direction of collagen fibers determined by polarized light microscopy or SEM.

More recently, tension-compression non-linearity (i.e., the disparity between tensile and compressive moduli measured in articular cartilage) and flow-independent viscoelasticity of the solid matrix (i.e., that part of the viscous behavior due solely to the solid matrix and not flow of fluid within the matrix) have been examined experimentally.[121,317,352] Huang and associates[121,317] employed the biphasic-conewise linearly elastic quasi-linear viscoelasticity model (B-CLE-QLV) during confined and unconfined stress-relaxation compression tests of articular cartilage at both slow and fast strain rates, finding an average aggregate modulus in tension of 8.8 MPa. The B-CLE-QLV was able to simultaneously describe the tensile and compressive behavior, performing better than the preceding biphasic-conewise linear elastic and biphasic poroviscoelastic models of articular cartilage. These findings suggest tension-compression non-linearity and flow-independent matrix viscoelasticity, both attributable to collagen, are important contributors to the transient mechanical behavior of articular cartilage. Another study examined the tensile properties as a function of strain rate, finding similar Young's moduli and ultimate tensile strengths at 1, 20, and 50% strain s^{-1},

but significantly increased properties at 70% strain s^{-1}. The authors suggest this may be a protective mechanism for cartilage to withstand sudden traumatic loads.[352]

Effects of collagen crosslinking on tensile properties

While collagen content, anisotropy, and inhomogeneity are important in determining cartilage tensile properties, another important aspect is the amount of crosslinking present in the collagen network.[200] Williamson et al.[49,50] studied changes in collagen content and pyridinoline crosslinking as a function of age in a bovine model and related them to tissue tensile properties. They found that both increasing collagen amount and pyridinoline crosslinking correlated with increases in equilibrium and dynamic tensile stiffness and tensile strength. As an alternative approach, one study inhibited crosslink formation by treatment with β-aminopropionitrile (BAPN), an inhibitor of the crosslinking enzyme lysyl oxidase, and measured tensile properties. Results showed that treated explants had significantly less crosslinking and decreased tensile properties.[353] In addition, administering sugars exogenously increased the formation of AGEs and, subsequently, increased the stiffness of the tissue.[276] The biomechanical role of AGEs is unclear, if not controversial. Increased AGEs may be a way in which cartilage attempts to mitigate the decrease in mechanical properties associated with aging or, by causing cartilage to become more brittle, be an explanation for why advanced age is a risk factor for the development of osteoarthritis. Regardless, these studies, and those mentioned above, underscore the

complicated role the collagen network plays with respect to the tensile mechanical properties of articular cartilage.

The role of collagen in compression

Though it is well accepted that the GAG content of articular cartilage is essential for its compressive properties, collagen has also been shown to have a role in governing compressive behavior and, interestingly, Poisson's ratio. In articular cartilage, the negatively charged GAGs lead to substantial hydration within the tissue that induces a swelling pressure able to resist compressive loads. The swelling pressure is balanced by tensile forces within the collagen network. Kovach and Athanasiou[189] showed that the spatial arrangement of collagen fibers is related to the aggregate modulus measured during creep indentation. In another study, confined compression was performed to various strain levels in the presence of different saline concentrations with the expectation that compressions greater than 5% would lead to the full load being borne by the proteoglycan osmotic pressure, which would be evidenced by equal stresses in the axial and radial directions. Contrary to the authors' expectations the axial and radial stresses were not equal, highlighting a role for the collagen network in compression.[124] It has demonstrated that the function of the stiffness of the collagen network is to maintain a high concentration of proteoglycans, which is then able to resist compressive forces.[354] Similar to their study of bovine cartilage tensile properties, Williamson et al.[125] examined compressive properties as a function of age. Results showed that the compressive modulus measured in confined compression increased 180%, while tissue permeability decreased

70%, from fetus to adult. These changes were correlated with increased collagen during development, since GAG changes during this period were negligible. Finally, Kiviranata et al.[355] demonstrated that Poisson's ratio is negatively correlated with collagen content (i.e., increased collagen, decreased Poisson's ratio) in bovine articular cartilage. An additional unique aspect of this study was that collagen content was measured with Fourier transform infrared (FTIR) spectroscopy. Further the effect of fiber and proteoglycan moduli on Poisson's ratio were parametrically assessed via finite element analysis, showing that the fiber modulus had far more of an effect on Poisson's ratio than the proteoglycan matrix modulus.

Conclusions

In summary, collagen plays an important and varied role in articular cartilage biomechanics that has been evidenced experimentally. Further, sophisticated theoretical and computational models of collagen's biomechanical functions have reproduced experimental findings and have predicted behavior that yet remains to be verified. From a basic science standpoint, future models should continue to increase in complexity. Special focus should be placed on models informed by detailed microstructural analyses that incorporate collagen orientations and distributions with molecular physics scaling up to the tissue level and models including collagen network crosslinking. This would be a daunting challenge. At the same time that more complicated models are developed, from a functional tissue engineering approach[356] we must recognize that such a level of

sophisticated understanding may not be necessary to evaluate whether a construct can adequately function in articular cartilage's native mechanical environment. Tissue engineers and biomechanicians alike need to continue to identify the salient mechanical characteristics of tissues and constructs that are necessary for cartilage regeneration and the structure-function relationships defining them. Further, standardized testing protocols should be followed so that mechanical properties can be compared from one study to another.

Experiment methods for collagen assessment

Due to the importance of collagen in cartilage, collagen composition and ultrastructure have been examined using various experimental methods. Many of these methods have also been used in tissue engineering studies to assess the collagen network within neotissue.

General collagen assessment

Several methods have been developed to measure collagen in articular cartilage without distinguishing among the different types of collagen. Hydroxyproline assays quantify the amount of collagen within cartilage based on the fact that hydroxyproline residues within biological tissue originate from elastin or collagen. Because articular cartilage contains negligible amounts of elastin, the amount of hydroxyproline can be used to infer the amount of collagen in the tissue. This method entails using chloramine-T to oxidize the hydroxyproline groups. Subsequently, adding Ehrlich's reagent (p-dimethyl-aminobenzaldehyde) produces a chromophore that can be quantified by assuming that 12.5% of the

collagen is hydroxyproline[357] or by employing a collagen standard. The hydroxyproline content varies by only 0.14% between collagen I and collagen II, indicating that either collagen type can be used as a standard.[358]

Another common method is collagen staining. Sirius red, dissolved in saturated picric acid, is an anionic dye that enables selective staining of collagen. When the dye binds to collagen via the dye's sulphonic acid groups, a change in birefringence occurs that can be visualized using polarized light microscopy.[359] Other staining protocols can be used as well, such as Gomori or Mallory trichromes, osmium tetroxide, periodic acid-Schiff, and Van Gieson. All of these methods readily verify the presence of collagen, but do not distinguish among the various collagen types.

Immunohistochemistry (IHC) and enzyme-linked immunosorbent assays (ELISAs)

IHC provides qualitative visualization of specific collagens within cartilage. Typically, a primary antibody is used to bind a particular collagen, followed by a secondary antibody binding the primary antibody. The secondary antibody can be conjugated to enzymes, like horseradish peroxidase or alkaline phosphatase, or fluorophores to produce a product that can be visualized. Employing a monoclonal antibody rather than a polyclonal antibody can increase the specificity of the antibody binding.[360] For tissue engineering applications, IHC can elucidate the localization of specific collagen types in a construct[361,362] and characterize the phenotype of neotissue.[363]

ELISAs can provide highly specific, quantitative determinations of the amount of collagen within a sample.[364] ELISAs rely on reporters (e.g., enzymes or fluorophores) conjugated to antibodies to produce color that can be quantified. For example, indirect ELISAs detect the amount of collagen in a well based on the number of primary antibodies that are retained (Fig. 5A). This can be disadvantageous if the collagen does not bind strongly to the well plate's surface. Sandwich ELISAs determine the quantity of collagen between two antibody layers (Fig. 5B). The use of two antibodies to bind collagen improves the specificity of sandwich ELISAs. Another ELISA variation is the competitive ELISA (Fig. 5C), which involves incubating samples with unlabeled antibodies. Then the antibodies are added to wells coated with collagen, but antibodies that have bound collagen from the sample will not be retained. Thus, higher collagen concentrations in the sample produce reduced color. This method can also be used for collagens that do not bind to the well. These numerous variations of ELISAs provide a versatile array of methods for quantifying collagen.

The convenience and high sensitivity of ELISAs make them the preferred method for quantifying levels of specific collagen types. ELISAs are commonly used to determine the proportions of collagens type I and II in cartilaginous neotissue.[280,365] The quantitative nature of ELISAs allows collagen levels to be statistically compared among treatment groups.

Electron microscopy

Electron microscopy can provide high resolution images of collagen fibril organization within cartilage. The two most common types are transmission

electron microscopy (TEM) and scanning electron microscopy (SEM), both of which create images based on detecting emitted electrons. Samples are typically stabilized by applying an oxidant (e.g., glutaraldehyde) to crosslink proteins. To more easily visualize the fibrils, bound proteoglycans are often removed with a short proteolytic digest.[366] Subsequently, heavy salts, such as osmium tetroxide and uranyl acetate, are applied to create contrast. Next, ethanol is used to dehydrate samples prior to embedding and sectioning. Finally, the sample is permeated by a resin and then fixed. Analysis of the ultrastructure can be performed in several ways. Analyzing cross-sections of tissue can show fibril diameters and distributions, while serial sectioning can give information about the entire length of the fibril.[367] In embryos, the small size of the fibrils has enabled analysis of entire fibrils, elucidating the fibrillogenesis process.[281]

Electron microscopy has the disadvantage of requiring samples to undergo substantial preparation prior to assessment, affecting the degree to which they retain their original collagen architecture. Common problems include structure distortion due to dehydration and loss of GAGs.[368] To minimize issues associated with chemical fixation, several other fixation methods have been developed. Microwave irradiation can be employed more quickly than conventional fixation to fix samples while preserving the collagen structure.[369] Additionally, freezing has been used to fix samples while avoiding extensive dehydration. Using high pressure or very rapid freezing can mitigate ice crystal formation during the freezing process.[368,370] Further, cryoprotectants can be added to reduce the formation of ice crystals. These methods provide

advantages over the traditional chemical fixation, which ultimately improve the accuracy electron microscopy images of collagen network.

Scanning electron microscopy (SEM)

SEM detects electrons that are emitted from the sample surface after the primary electrons interact with the sample. Various studies have employed SEM to examine the orientation and size of collagen fibrils within articular cartilage.[295,300,366,370,371] SEM has a lower resolution than TEM, but the depth of view is much greater. This enables SEM to provide a more three-dimensional representation of the collagen network. Cryofracture has been used to section the sample in two orthogonal planes and, subsequently, determine more about the three-dimensional collagen organization.[295] Prior to conducting SEM, samples must be coated with a conductive material. This coating, which is typically less than 20 nm thick, does not impair visualization of most collagen fibrils.

Transmission electron microscopy (TEM)

TEM creates images based on electrons that are transmitted through thin sections of a sample. The key advantage of TEM is its high resolution. TEM can show collagen fibril morphology, fibril orientation, and fibril diameter. Furthermore, the high resolution of TEM allows imaging of detailed fibril morphology, such as banding patterns of collagen fibrils.[372-374] The banding patterns indicate how the fibrils have packed together and can vary significantly, even within a single fibril. Although banding patterns reveal important structural

information, aspects such as collagen quantity and collagen type provide more functionally relevant information. Studies have employed TEM to study the collagen within cartilage and collagen fibrils grown *in vitro* to examine fibril diameter and pericellular matrix organization (see for example[112,375]).

Prior to conducting TEM, samples must be sliced into ultrathin sections approximately 50-100 nm thick. Because fibril organization is on the order of microns, TEM sections can be too thin to show tissue ultrastructure. Furthermore, treatment with heavy salts is sometimes applied to create additional contrast before microscopy. Lead citrate is commonly employed to stain biological samples for TEM (Fig. 6). Like other lead based stains, staining intensity is heavily dependent on pH, and the tissue fixation method can also impact the staining intensity.[376] Because the electron density depends primarily on the amount of bound uranyl acetate, the lead is thought to bind mostly to the uranyl acetate.[377] Additionally, conjugation of antibodies to gold particles can be used to visualize specific macromolecule localization.

Assessing collagen orientation

Polarized light microscopy

Polarized light microscopy measures birefringence of the sample to elucidate collagen alignment within cartilage. The polarization angle is a widely used method for quantifying collagen orientation. Additionally, orientation information can be used to infer thickness of the zones within a sample. When light passes through cartilage, it interacts with the valence electrons of collagen.[378] This

creates birefringence that can be detected by a polarized light microscope. In general, highly oriented fibers will increase the phase difference between the orthogonal components of the light.[379] Collagen orientation is then deduced from the directions of the optical axes at maximal birefringence. The optical retardance, which is linearly proportional to birefringence, can also be used to infer collagen orientation. Thus, larger polarization angles are indicative of the superficial zone, while smaller polarization angles are indicative of the deep zone. Other factors, including size of the fibrils and the sample's thickness, can influence this phase difference.[379] This technique has been used to determine collagen fibril orientation in many studies in both native tissue [285,379] and tissue engineered constructs.[114,380]

Diffusion tensor imaging (DTI)

Magnetic resonance can also be used to deduce the collagen fibril orientation. In particular, diffusion tensor imaging (DTI) has been applied to cartilage tissue.[293,381-383] DTI measures the movement of water molecules, which is related to constraining forces within the matrix.[293] The collagen distribution within cartilage produces an anisotropic constraint on the water, which allows DTI to be used to quantify collagen orientation. DTI has been shown to reproduce the results of polarized light microscopy,[293] suggesting that DTI can provide a viable alternative for examining collagen orientation. The non-destructive nature of DTI analysis provides a key advantage. Although DTI is a powerful tool, higher costs have limited its application in the research setting.

Quantifying anisotropy

Quantifying collagen anisotropy from micrographs can compliment methods like polarized light microscopy and DTI. Image analysis can be used to determine how fibril orientation varies with respect to depth, which can be used to quantify anisotropy of fibrils. For instance, conducting localized vector analysis of electron micrographs can quantify fibril anisotropy.[384] Additionally, a gradient detection algorithm has been employed to quantify orientation in confocal reflectance micrographs of collagen gels.[385] Some freely available programs such as Continuity (University of California-San Diego) can also be used to determine collagen fibril orientation.[386] In general, researchers use different computational methods to quantify orientation. The lack of a standard methodology for determining anisotropy makes it difficult to quantitatively compare the orientations between studies.

Assessing collagen inhomogeneity

FTIR involves detecting infrared radiation that is transmitted through a sample, the results of which can be used to quantify collagen distribution. FTIR is used to quantify the collagen content in tissue sections, providing spatial information that bulk assays such as hydroxyproline do not. This spatial resolution shows how collagen content varies with depth and location in a joint. FTIR has been used for examining collagen content in cartilage tissue.[330,355,387,388] The data FTIR provides have functional implications, such as a correlation between the fibril network modulus and collagen content.[330] Similarly, FTIR has been used to show

the distribution of collagen in tissue engineered cartilage.[388] The quantification and spatial resolution of FTIR makes it a valuable technique for assessing collagen orientation.

Crosslink assessment

Methods are available to examine collagen crosslinking in articular cartilage. The amount of crosslinks can be quantified using high performance liquid chromatography (HPLC). Generally, cartilage samples are first hydrolyzed to free the crosslink residues. Then the solution is passed through an HPLC column that can separate compounds based on factors like charge, size, and polarity. The fluorescence of the eluted sample can be used to quantify the number of crosslinks by excitation/detection at 295/400 nm for pyridinolines and 328/378 nm for pentosidines. Additionally, the specific type of pyridinoline link can be determined from the elution time at peak absorbance. The high sensitivity of HPLC allows detection at the picomolar level.[216] More recently, mass spectrometry has been applied to yield more detailed information about crosslinking chemistry, such as glycosylation state.[389] As an indirect measure, lysyl oxidase activity can be used to approximate the extent of crosslinking.[390,391] Because pyridinoline crosslinks play an important role in the mechanics of cartilage, quantifying them provides a powerful tool for assessing neotissue.

Conclusions

A wide variety of methods enable study of the structure and composition of collagen within cartilage samples. Techniques like IHC and histological staining

can qualitatively verify the presence of collagen, which can be quantified using methods such as hydroxyproline assays and ELISAs. Electron microscopy provides information about the collagen distribution and orientation, but requires extensive sample preparation. For examining collagen orientation, traditional polarized light microscopy has been complemented by newer methods such as DTI. Additionally, HPLC can quantify the number of crosslinks, providing more information about the structure of the collagen network. Collectively, these methods can thoroughly characterize collagen within both native tissue and engineered cartilage.

Role of collagen in tissue engineering

Significance of collagen in tissue engineering

To produce functional cartilage constructs, tissue engineering efforts will likely need to recapitulate the collagen network of native tissue. Because the matrix plays an important role in providing mechanical integrity, it is necessary to reproduce a collagen network with appropriate composition, orientation, and crosslinking. The overabundance of GAGs in tissue engineered cartilage makes it particularly important to improve the collagen network.[112,141,392] Despite various strategies, including scaffolds, biochemical agents, and mechanical stimulation, tissue engineered constructs generally have significantly less collagen than native tissue.[109,246-248] This lack of collagen is problematic because it compromises the mechanical integrity of the tissue.

Collagen scaffolds for tissue engineering

Collagen has been employed as a biomaterial scaffold to promote cartilage engineering due to its natural biocompatibility, porosity, and low immunogenicity. Collagen matrices have also been found to have the proper molecular cues to stimulate collagen production.[70] The prevalence of collagen in the articular cartilage matrix makes collagen particularly attractive for cartilage tissue engineering applications; however, as with many natural biomaterials, collagen poses a risk for pathogen transmission. In particular, concerns have been raised about the increased frequency of prion diseases, which may be associated with collagen scaffolds.[71]

Despite this concern, several tissue engineering studies have examined the potential of collagen scaffolds for articular cartilage tissue engineering. Much of this work has examined chondrocytes seeded on collagen scaffolds[393] or crosslinked collagen sponges.[394] Canine chondrocytes seeded on collagen II retained their chondrocytic phenotype more than cells seeded on collagen I, which is expected considering the predominance of collagen II in articular cartilage.[395] Collagen scaffolds have been shown to increase collagen synthesis more than other common biomaterials, such as copolymers of lactic acid and glycolic acid.[70] To more closely replicate the cartilage matrix, collagen has been combined with other matrix molecules (e.g., GAGs).[396] In addition to extensive *in vitro* work, various *in vivo* studies have been conducted with collagen scaffolds, including rabbit,[397,398] dog,[395,399] and horse[400] models. Similar to many other tissue engineering strategies, collagen scaffolds promote chondrocyte

phenotypes and matrix production without attaining native mechanical properties. For example, mesenchymal stem cells seeded on collagen gels implanted in rabbit osteochondral defects promoted hyaline cartilage formation, but failed to reproduce tissue with native mechanical values.[397,398] Despite extensive research, these deficiencies in mechanical properties suggest that other tissue engineering strategies will need to be pursued.

Engineering the collagen network

Collagen content

Culture conditions often have a profound impact on collagen production. Numerous studies have mechanical stimulation can be used to increase the collagen content of neotissue. For example, direct compression[53,54193] and shear[401] have been shown to increase collage deposition. Hydrostatic pressure has also been shown to increase collagen gene transcription,[56] collagen production,[57,58] and construct tensile properties.[59] However, relatively few studies have examined the collagen deposition in tissue engineered constructs that have been mechanically stimulated. Other conditions, like cell density,[365,402] scaffold porosity,[403] and cell source,[404,405] also modulate collagen production.

Tissue engineering studies have shown localization of collagen VI in the pericellular space. Human and bovine articular chondrocytes cultured *in vitro* exhibited chondron structures in regions displaying characteristics of hyaline cartilage.[406] Furthermore, confocal microscopy has shown that cultured chondrocytes sequestered type VI collagen in the pericellular space.[407] In self-assembled constructs, collagen VI localized in the pericellular region within four

weeks.[103] Type VI collagen also accumulated uniformly around cells embedded in agarose, with the rate of deposition slowing after two weeks. The production of the pericellular matrix may actually be excessive in some constructs, as agarose embedded chondrocytes have exhibited collagen VI expression levels 400% higher than native values.[408]

Exogenous application of bioactive agents also can be used to increase collagen content. For bovine articular chondrocytes cultured on alginate beads, IGF-1 increased collagen gene expression and deposition,[41] but it did not impact the number of crosslinks.[42] Further, TGF-β1 promoted collagen fibril formation[409] and increased the collagen weight fraction.[37] Many of the bone morphogenetic proteins (BMPs), which are part to the TGF-β superfamily, have also been shown to promote collagen synthesis. For instance, BMP-2[34] and BMP-7[35] have been employed to increase collagen deposition. Recently, small proteoglycans in tissue engineered constructs have been shown to decrease collagen deposition. By knocking out the small leucine-rich proteoglycan lumican, there was increased collagen II deposition and increased fibril diameters.[374] Similarly, when decorin was removed from tissue engineered constructs, increased tensile properties indicated a possible alteration of the collagen network.[392] Adding various bioactive molecules, individually or in combinations, provides many opportunities for altering collagen content.

Despite many studies that demonstrate the role of growth factors, the responses to a growth factor is often difficult to predict. This is particularly true with members of the TGF-β superfamily, which have been shown to increase or

decrease collagen deposition depending on the experimental system.[29,37,42-44] In addition to the variation in culture systems, the developmental stage of the cell,[30,45] zone of cell source,[41] and the amount of extracellular matrix already deposited[44] also influence the response to the growth factor. Synergism between growth factors can also alter their impact.[39] The complexity of the growth factor response makes it difficult to generalize an optimal treatment regimen.

Crosslinking

Studies have shown that crosslinks are generally less common in tissue engineered constructs than in native tissue. For a six week culture of bovine chondrocytes in a rotating bioreactor, the number of crosslinks was only 30% of native values.[280] Similarly, after four weeks of alginate bead culture, crosslinks reached only 22% of native values.[311] The inability to fully produce crosslinks in tissue engineered constructs presents a necessary area for improving tissue engineering efforts. The number of crosslinks has been found to depend on the cell source, with more crosslinks formed in constructs from full thickness cell sources compared to middle or deep zone sources.[404]

Various small molecules can be employed to modulate collagen crosslinking. For example, BAPN inhibits lysyl oxidase, thereby decreasing the extent of crosslinking. BAPN treatment of cartilage explants decreased tensile integrity, without altering the amounts of collagen or GAGs.[353] For bovine chondrocytes cultured on alginate beads, administering BAPN reduced the amount of collagen near chondrocytes and increased collagen synthesis.[311] In another study, chondrocytes seeded on alginate beads and treated with BAPN

for the first five weeks of a ten week culture exhibited increased collagen content and increased stiffness.[113]

In contrast to inhibition, several agents can be added to increase crosslinking. Oxidative agents can be used to increase collagen crosslinking, but these compounds are not specific like lysyl oxidase. The major disadvantage of commonly used crosslinking chemicals (e.g., glutaraldehyde) is cytotoxicity. Genipin, an extract from the gardenia plant, has recently been explored as a crosslinking agent. Applying genipin to bovine articular cartilage[410] and human intervertebral discs[411] did not increase cytotoxicity. In the intervertebral disc study, genipin treatment increased the mean circumferential yield stress and ultimate tensile strength by ~78%. Alternatively, adding sugars increased collagen crosslinking by inducing AGE formation.[276,412] Finally, though not in cartilage, applying exogenous lysyl oxidase to tissue engineered vascular constructs increased their tensile strength and elastic modulus.[220] Interestingly, collagen crosslinks can also contribute to compressive properties, such that the proportion of mature to immature crosslinks correlated with the equilibrium modulus in unconfined compression.[249]

Network organization

Engineering the anisotropic distribution of collagen poses another significant challenge. As a step forward, radial confinement of self-assembled constructs increased collagen organization perpendicular to the articular surface.[114] In addition to confining constructs, it is possible to control the cell distribution within neotissue and, consequently, alter collagen distribution. For example, creating

anisotropic pore architecture within a scaffold produced by 3D fiber deposition created zonal variation in collagen composition.[403] However, this approach produced collagen levels an order of magnitude less than native tissue.

The bacterially-derived enzyme chondroitinase-ABC (C-ABC) has also been used to alter the cartilage matrix. C-ABC selectively degrades GAGs,[46] which subsequently reduces stress on the collagen network. Applying C-ABC has been shown to increase the tensile properties of cartilage explants.[47,413] Additionally, Natoli et al.[392] have used C-ABC to increase tensile properties of self-assembled tissue engineered articular cartilage. Treating constructs at both two and four weeks resulted in a tensile stiffness of 3.4 MPa at six weeks. Treatment with C-ABC also reduced decorin staining, which subsequently recovered. Because decorin is known to reduce collagen fibril diameters, C-ABC mediated decorin reduction may contribute to increased tensile stiffness. Although the mechanism by which it increases tensile properties has not been characterized, it is possible that the reduced GAG content promotes crosslinking, larger fibril size, or altered fibril orientation.

V.D. Conclusions

Reproducing a collagen network in tissue engineered articular cartilage constructs with appropriate composition, orientation, and crosslinking has proven to be a difficult task. Several strategies, including mechanical stimulation and growth factor application, have been employed to alter the collagen composition of neotissue with some success. In general, crosslinks are less common in engineered neotissue than in native tissue. Although exogenous oxidative agents

can increase crosslinking, these crosslinks are not specific like lysyl oxidase mediated crosslinking. Ultimately, it will be necessary to develop improved methods for engineering network crosslinking and organization before neotissue replicates the structure of native cartilage. By further studying the collagen network in both native tissue and engineered cartilage, it will be possible to improve the quality of tissue engineered constructs.

Conclusions

Collagen forms a complex network within articular cartilage. The major component is the heterofibril of collagens II, IX, and XI. These fibrils are organized inhomogeneously and anisotropically within cartilage and provide mechanical integrity to the tissue. Various theoretical and computational models of cartilage biomechanics have been developed, but incorporating microstructural analyses will help improve these efforts. To better understand factors affecting the collagen network, many experimental methods are available. It is possible to readily assess the composition, crosslinking, and structure of the collagen network.

Successful articular cartilage tissue engineering will need to produce an appropriate collagen network. Studies have shown that tissue engineered cartilage generally lacks sufficient collagen, a problem that will need to be addressed. Cartilage tissue engineering studies have primarily examined the amount of collagen, with fewer studies assessing collagen type, crosslinks, or fibril orientation. By overlooking these aspects, many tissue engineering studies do not elucidate the mechanisms that underlie observed changes in mechanical

integrity. Furthermore, the interactions between collagen, proteoglycans, and chondrocytes need to be studied more extensively. Understanding properties and interactions of the collagen network will enable more robust constructs to be developed, and will subsequently improve the functionality of tissue engineered articular cartilage.

Table 7-1: Collagen fibril characteristics and zonal variation

	Superficial	**Deep**
Fibril diameter[147,148]	30-35 nm	40-80 nm
Fibril orientation[285]	Parallel	Perpendicular
Tensile modulus (parallel)[2]	42.2 MPa	2.6 MPa
Tensile modulus (perpendicular)[2]	15.6 MPa	1.1 MPa
Confined compressive modulus[414,415]	0.27-1.16 MPa	0.71-7.75* MPa

*7.75 MPa measured in region 1250-1500 μm depth from the surface bordering the transition zone to calcified cartilage

Figure 7-1: Hierarchical structure of a collagen fiber

A.

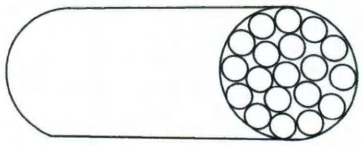

B.

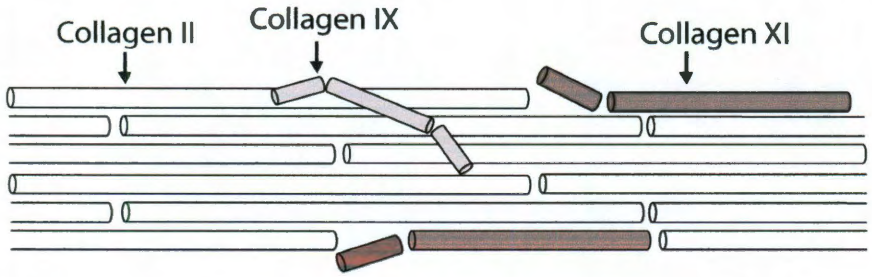

C.

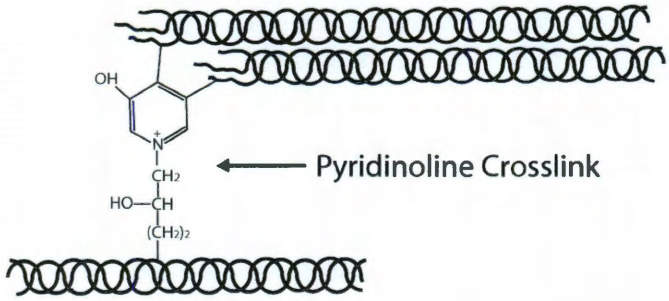

A) Collagen fiber. A fiber is a collection of many fibrils. B) The collagen II:IX:XI heterofibril. The fibril is formed by end-to-end and lateral fusion of collagen molecules. Collagen IX forms crosslinks between collagen molecules. C) The basic triple helix structure of the collagen type II molecule. Shown out of scale is the structure of a pyridinoline crosslink, which interconnects collagen triple helices through oxidation of lysine residues by lysyl oxidase.

Figure 7-2: Schematic representation anisotropic collagen arrangement

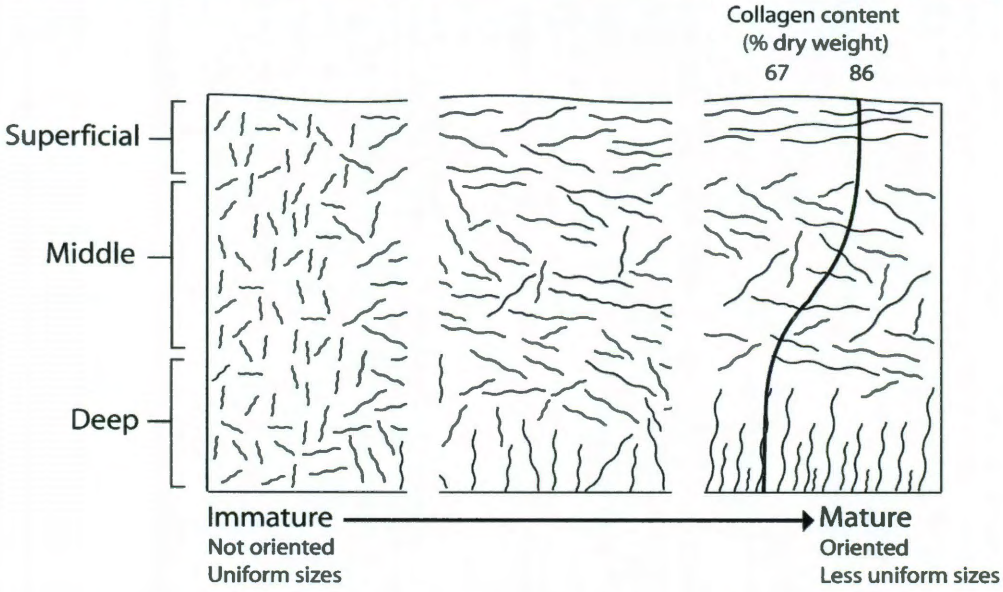

Immature tissue is composed of randomly oriented fibers with roughly uniform size. As the tissue matures, the characteristic collagen orientation begins to emerge. Mature tissue has horizontally oriented fibers in the superficial zone, randomly oriented fibers in the middle zone, and vertically oriented fibers in the deep zone. Mature tissue is also composed of fibers less uniform in size.

Figure 7-3: Demonstration of split-lines in articular cartilage

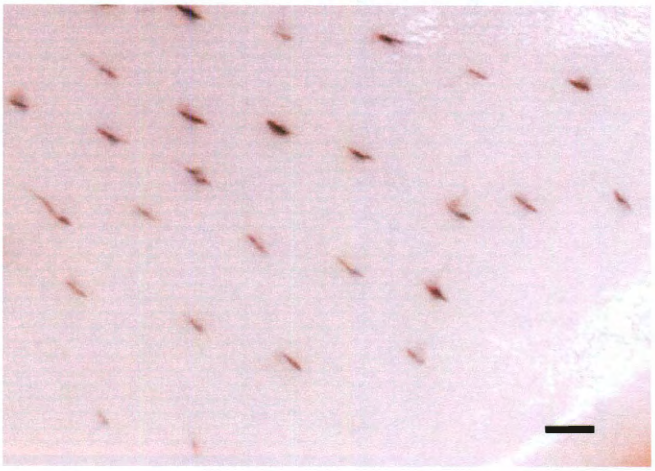

Split-lines show orientation of collagen fibers in the superficial zone. A small round pin was dipped in black ink and gently pressed into the tissue. The ink stains in direction parallel to collagen fibers. In this picture, split-lines are running from upper left to lower right. The image was taken on a Leica MZ6 dissection scope at 4X magnification. Scale bar = 1 mm.

Figure 7-4: Theoretical cartilage mechanics

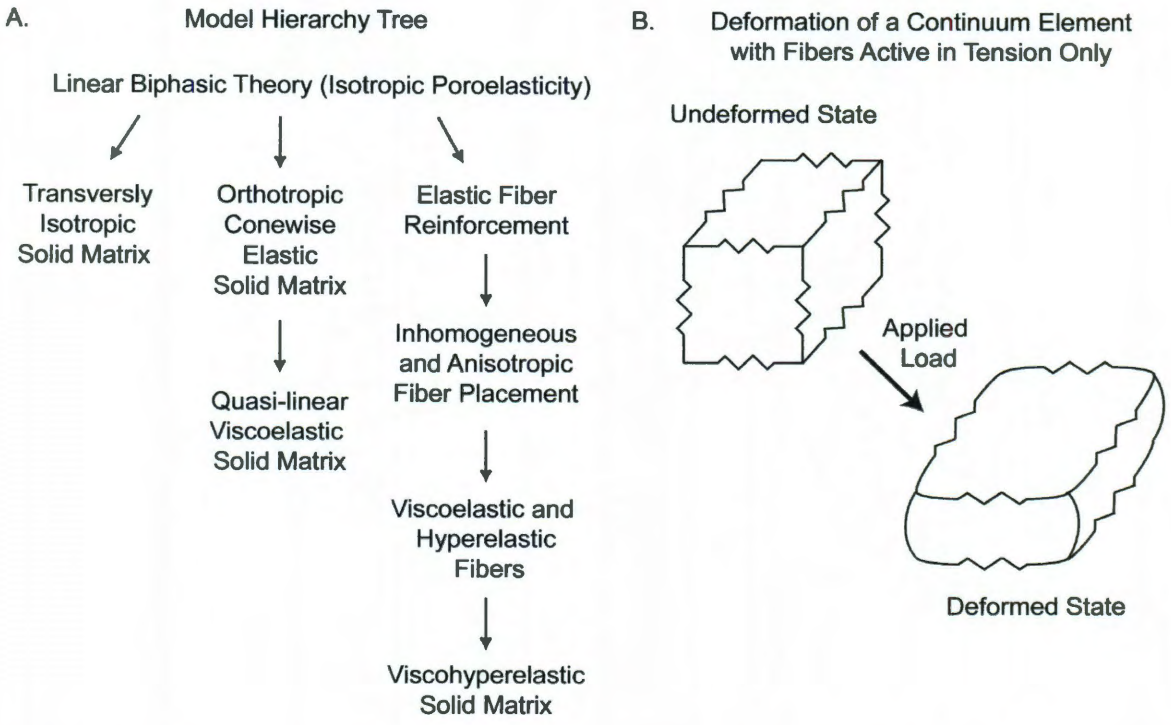

Fig 4: A) Hierarchy tree for models of articular cartilage incorporating features of the collagen network. The basic model for articular cartilage is the linear biphasic theory. As one moves down the branches, the models become more complex. Along a branch, each level incorporates all of the features from the models above it. The most developed branch is that which treats cartilage as a composite reinforced by collagen fibers. B) Representative deformation of a continuum element reinforced by collagen fibers active only in tension. An applied load causes compression of the continuum element. Members in compression are not supported by fibers, and hence their springs have been removed. In the deformed state, members in compression deform more than members engaged in tension.

Figure 7-5: Types of ELISAs

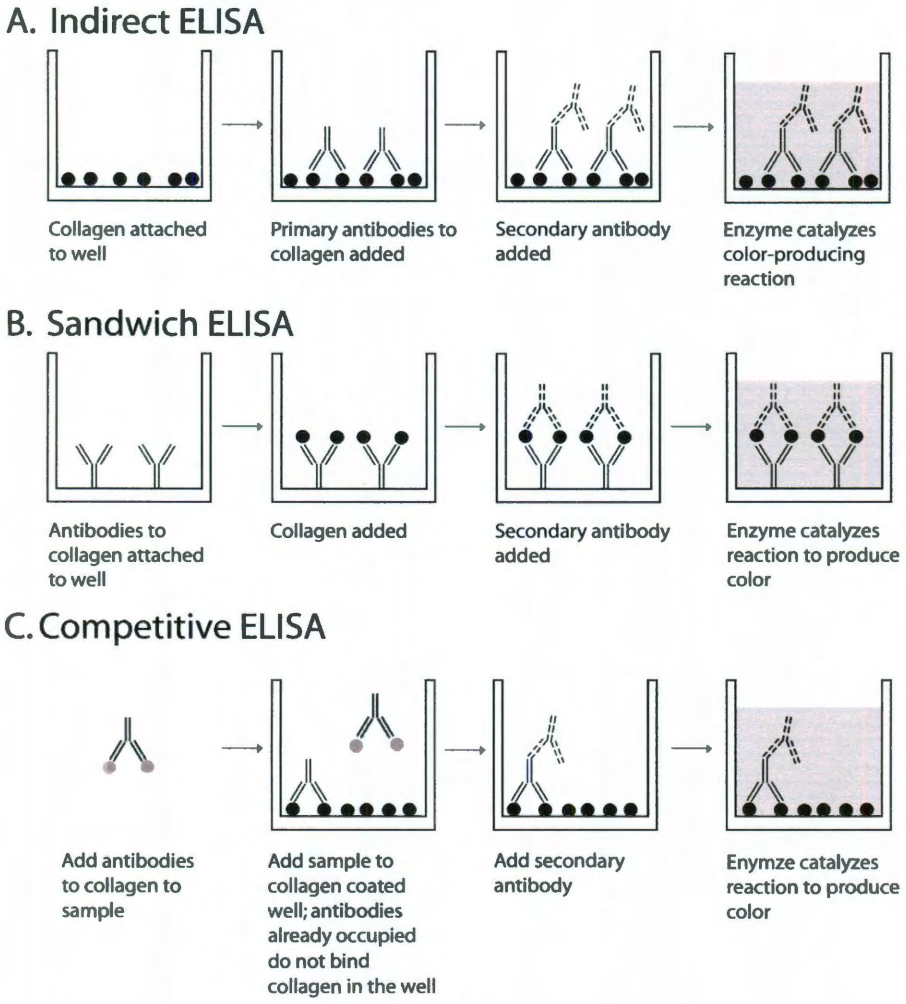

A) Indirect ELISAs detect the presence of sample collagen (dark circle) that is coated onto the well. The primary antibody (solid line) binds to the collagen and then secondary antibodies (dashed line) bind to the primary antibodies. Finally, adding a substrate to activate an enzyme conjugated to the secondary antibody will change the color of the solution (indicated by gray shading). B) Sandwich ELISAs quantify collagen that is retained upon addition to wells coated with collagen antibodies. A secondary antibody is then used to create a "sandwich." Using two antibodies increases the specificity of the assay. C) Competitive ELISAs entail initially incubating primary antibodies with sample collagen (gray circles). Subsequently, samples with more collagen will reduce the amount of free primary antibodies that can bind to the collagen on the well plate (dark circles).

Figure 7-6: TEM image of a self-assembled tissue engineered construct

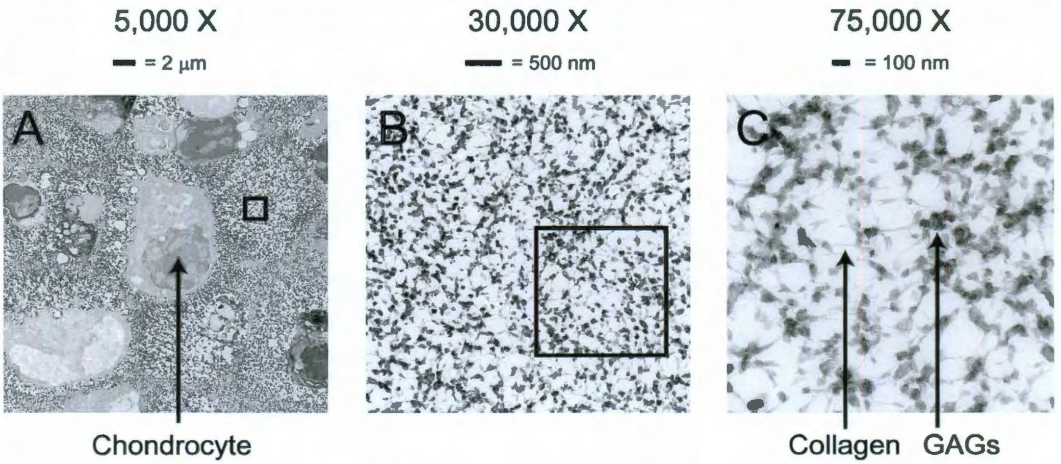

Samples were fixed in paraformaldehyde and then stained with cupromeronic blue for glycosaminoglycan (GAG) distribution. Subsequently, samples were dehydrated in increasing ethanol concentrations and embedded in LX-112 medium. After sectioning, samples were stained with uranyl acetate and lead citrate and examined in a JEM 1010 transmission electron microscope. Boxes indicate the field of view for the image to the right. A) At 5,000X, cells are clearly visible within the matrix. B) At higher magnification, the collagen and glycosaminoglycans become distinguishable. C) At a magnification of 75,000X, glycosaminoglycans and individual collagen fibrils are visible.

Chapter 8: Understanding biomechanics-driven chondrogenesis from embryo to adult*

Abstract

Biomechanics play a pivotal role in cartilage development, pathophysiology, and regeneration. During embryogenesis and cartilage maturation, mechanical stimuli promote chondrogenesis and limb formation. Mechanical loading, which has been characterized using computer modeling and *in vivo* studies, is crucial for maintaining the phenotype of cartilage. However, abnormal loading can have deleterious effects and promote the onset of disease. Informed by the prominent effects of biomechanics, mechanical stimuli have been developed to enhance re-differentiation of chondrocytes and chondroinduction of other cell types, thus providing new chondrocyte cell sources. Biomechanical stimuli have been widely used to enhance the functional properties of neocartilage. In addition to direct mechanical stimulation such as applying hydrostatic pressure or compression, chemical equivalents mimic mechanical signaling and offer exciting new methods for improving neocartilage. Chemical equivalents also elucidate mechanotransduction, which could ultimately improve understanding of cartilage development and how chondrocytes respond to mechanical stimuli. Harnessing mechanics to improve differentiation, maintenance, and regeneration offers a

* Responte DJ, Lee JK, Hu J, Athanasiou KA. Understanding biomechanics-driven chondrogenesis from embryo to adult. *PNAS* (in preparation)

new approach for producing functional neocartilage that could eventually be used to treat cartilage degeneration.

Introduction

Cartilage lines the articulating surfaces of long bones, functioning in the mechanically-demanding environment of the joint space. The extracellular matrix of cartilage primarily includes collagen, proteoglycans, and chondrocytes. Chondrocytes, the only cell type within cartilage, comprise only 1-5% of the tissue by volume.[1] Although chondrocytes represent a small fraction of articular cartilage, they are crucial because they synthesize the matrix that imparts mechanical integrity to the tissue.

The significance of biomechanical stimuli such as hydrostatic pressure, compression, and shear has been well-established for cartilage. Joint loading results in direct compression of chondrocytes, which also experience hydrostatic pressure due to compression of synovial fluid inside the joint capsule.[4-16] This mechanical stimulation produces a signaling cascade, resulting in increased gene expression[55,56] and protein production.[53,54,57,58] Understanding how mechanics influence chondrocytes is crucial because the resulting signaling cascades can alter matrix production and ultimately influence how well the tissue can function in the rigorous joint environment.

As summarized in Fig. 8-1, biomechanics play a significant role throughout an organism's life. Biomechanics contribute to development during embryogenesis and cartilage formation, and maintain the chondrocyte phenotype

in adult tissues. Alternatively, abnormal loading can promote the onset of cartilage degeneration. Informed by these biomechanics studies, various mechanical stimuli have been employed to enhance stem cell differentiation and the development of more robust regeneration therapies. This perspective article highlights the importance of biomechanics in chondrogenesis from the early stages of neocartilage formation to maintenance of adult tissue. In particular, it will describe the role of biomechanics in cartilage development, maintenance, disease, adult cell chondrogenesis, and cartilage regeneration.

Biomechanics in embryogenesis and fetal development

Mechanical stimuli during embryonic and fetal development influence cartilage differentiation and limb morphogenesis. The mechanical microenvironment acts a potent regulator of stem cell fate and contributes to chondrogenesis in the early embryo. Biomechanics also plays a key role in skeletogenesis, which begins with a cartilage blueprint that is later calcified to become bone via a process known as endochondral ossification.[417] Immobilization experiments *in vivo* and computer models of development have shown the central role of mechanical stimuli in proper cartilage development.

Stem cells respond to changing mechanical microenvironment

Much of embryogenesis relies on resident stem cell differentiation into the needed cell types; chondrogenesis occurs in the same manner as progenitor cells undergo pre-cartilaginous condensation to form tightly packed cellular aggregates before differentiating into early chondrocytes.[417] The mechanical mechanisms of this process are currently unknown, as most studies focus on

chemical pathways leading to embryonic cartilage formation. Some groups postulate that mechanical forces influence *de novo* chondrogenesis from early stem cells in addition to growth factor gradients; however, this hypothesis is difficult to test and current studies utilize *in vitro* culture platforms or computer simulations. Biomechanics have been used to characterize single stem cell populations, control differentiation, and further understand development.

At the single cell level, differentiating stem cells exhibit altered mechanical properties. For example, mouse stem cells exhibit increased stiffness after just 6 days of chemical differentiation, exhibiting up to 3-fold higher stiffness values as compared to undifferentiated cells.[418] Similarly, cellular biomechanics can be employed to evaluate differentiation regimens of embryonic[419] and marrow-derived[420] stem cells. Due to the relationship between mechanical properties and differentiation, biomechanics could provide a novel method of stem cell phenotyping and validation of isolation techniques.

The control of stem cell fate via substrate mechanics and mechanical forces is increasingly being explored as a differentiation strategy. By changing the substrate stiffness, researchers can control stem cell lineage commitment. Growing embryonic stem cells substrates of various stiffnesses modulated differentiation expression[421,422] and growth rate kinetics.[422] Furthermore, applying compression enhanced chondrogenesis of progenitor cells, generating 3-fold increases in matrix protein synthesis. The demonstrated ability of both substrate stiffness and mechanical stimulation to differentiate stem cells suggests that biomechanics is a key stimulus during development.

Though the mechanisms underlying pre-cartilaginous condensation have not been fully elucidated, the differential adhesion hypothesis may offer insight into the segregation of cellular sub-populations. Because different stem cell lineages exhibit variable stiffness levels and biochemical marker expression, differential adhesion could lead stem cells to associate with cells of similar lineages. Therefore, pre-cartilaginous condensation may be a result of receptor-mediated aggregation of mesenchymal progenitor cells expressing the same surface receptors. While this hypothesis is untested at the early stages of chondrogenesis, the differential adhesion hypothesis allows researchers to extrapolate findings from embryonic and mesenchymal stem cell studies to *in vivo* embryonic development.

Studying chondrogenesis in embryonic stem cells can inform the mechanisms of *in vivo* cartilage development. As depicted in Fig. 2, five developmental processes are vital to *in vivo* chondrogenesis:[423] 1) cellular condensation, 2) chondrocyte differentiation and initial scaffold formation, 3) extracellular matrix synthesis, 4) selective cellular death and 5) replacement of cartilaginous tissues with bone. Each process necessarily builds upon the prior stage; for example, increased deposition of matrix relies on the presence of the initial scaffold formed in stage 2. While the suggested progression has been studied extensively *in vitro*, *in vivo* validation requires further experimentation.

Stem cell chondrogenesis not only provides a platform for which to study embryonic cartilage tissue formation, but proves dependent upon mechanical forces as differentiation stimuli. Though mechanical stimuli that have been used

experimentally are not guaranteed to be present during *in vivo* development, biomechanics-based studies elucidate various methods with which stem cells may be differentiated into a chondrocyte lineage. The consequential responses of progenitor cells to changes in their mechanical microenvironment suggest a similar pathway *in vivo* and indicate that biomechanics can in fact influence chondrogenesis of stem cells.

Biomechanics drive skeletogenesis

Studies of vertebrate limb development reveal that mechanical stimulation promotes chondrogenesis. For example, compression triggers chondrogenic marker expression—most notably, Sox9, a master gene responsible for activating many of the cartilage genes expressed in terminally differentiated cells.[424] These results indicate mechanical stimulation is a genetic regulator of chondrogenesis.

Because of the difficulties associated with controlling biomechanics during embryogenesis, embryos with impaired limb mobility have been used to determine the effects of mechanics on limb development.[425,426] Strategies such as chemically paralyzing limbs or using animals with skeletal muscle defects have been employed to create abnormal joint loading and subsequently disrupt skeletogenesis. For instance, immobilization of chick limbs [426] resulted in abnormal limb shape and complete failure to form elements of the synovial joint such as the knee meniscus. Muscle paralysis has been shown to hinder articular cartilage development.[427] Immobilization has also been shown to decrease matrix production and subsequently reduce mechanical properties of tissues by

50%.[428] These studies demonstrate that joint mechanics are vital for proper cartilage development.

Computer models corroborate animal studies

While joint immobilization provides insight into *in vivo* cartilage development, the difficulties associated with this procedure have led to computer modeling of joint development.[429] By modeling mechanical stimulation of limb buds, computer simulations can define the stages of limb development and chondrogenesis. Ultimately, comparing computer models to *in vivo* studies has shown the accuracy of these simulations.

The modeling approaches to simulate skeletogenesis under mechanical stimulation vary widely, incorporating stimuli based on muscle contraction,[426] hydrostatic pressure,[430] and shear.[430] Intermittent and cyclic hydrostatic pressure and strain both help regulate matrix protein synthesis to affect macromolecular organization of collagen fibers, which in turn leads to changes in the mechanical properties of the tissue.[430] When the computer simulation was applied to a mesenchymal tissue model, researchers were able to accurately estimate the mechanical properties of different cartilage types. These results reveal a successful cartilage differentiation algorithm based on mechanical forces recapitulative of the native chondrogenic environment.

Alternatively, computer models predict that intermittent compressive hydrostatic pressure inhibits degeneration and ossification of cartilage, preventing cartilage from becoming bone; on the other hand, intermittent strain or shear stresses accelerate ossification and degeneration.[431,432] Such mechanical

forces dictate the progression of what is known as the ossification front, or the line at which cartilage begins to calcify, turning into bone; these forces thus work to maintain a layer of cartilage of suitable thickness during development. Excitingly, the models predict proper limb morphologies progressing through specific embryonic development stages. Ultimately, the algorithms can estimate an anatomically correct long bone shape based on where cartilage will ossify,[433] indicating the accuracy of the chosen stimulation regimen.

Despite the successes of modeling techniques in mimicking chondrogenesis *in vivo* and their contributions to understanding skeletogenesis, the proposed biomechanics responsible for cartilage formation still require validation via animal studies. Animal and computer models must build upon each other to provide insight into the effects of mechanical stimulation during *in vivo* chondrogenesis and development of skeletal tissues.

Maturation of tissue mechanics

In addition to exploring how mechanics drive chondrogenesis, it is important to investigate how these stimuli promote cartilage maturation. Because chondrogenesis is a time-dependent process, various groups have investigated the effects of prolonged mechanical stimulation on cartilage tissue. As skeletal tissues mature, mechanical forces help determine their ultimate tissue strengths. These improvements are often a result of increased matrix synthesis during growth, or of matrix enhancement via matrix organization. Mechanical stimulation thus assists not only in fetal chondrogenesis, but plays a role in cartilage maturation as well.

To study the *in vivo* progression of cartilage development, various studies have examined tissue mechanics at different maturation stages. For example, fetal articular cartilage 20 to 36 weeks old exhibited an age-dependent increase in cartilage tissue stiffness.[434] These increased mechanical properties paralleled biochemical composition: stiffness increased by a factor of 2.5 from age 20 to 36 weeks and collagen content increased 3-fold. Similarly, comparing the mechanical properties of fetal and newborn bovine tissue revealed a correlation between tissue strength and specimen age.[435]

In addition to altered biomechanical properties during tissue maturation, mechanical stimulation also plays a vital role in generating regional variation in cartilage. Although fetal cartilage did not demonstrated regional variation, newborn and adult cartilage exhibited stronger tissues in regions bearing the greatest static or dynamic loads.[436] Similarly, the compressive and tensile properties of bovine fetal, newborn and adult tissues have been shown to exhibit age-dependence and regional variation.[437,438] These results suggest that joint loading is a potent regulator of chondrogenesis.

During chondrogenesis, the mechanical properties of cartilage increase in response to biomechanical stimuli. Although the mechanisms underlying the development of cartilage mechanics have not been fully elucidated, it appears that regional variation stems from joint loading. This presents an exciting research area for understanding cartilage developing as well as developing stimuli to promote in vitro cartilage growth.

Summary

Although the *in vivo* role of biomechanics during embryogenesis has not been fully elucidated, strong evidence exists for biomechanics-driven differentiation and chondrogenesis. Beginning at the embryo stage, biomechanics undoubtedly influences chondrogenesis as demonstrated by inhibiting embryo movement *in utero*. At this point, the role of biomechanics in embryo and fetal chondrogenesis requires more *in vivo* investigations into the mechanisms and types of mechanical stimuli present during differentiation. By understanding the potential role of biomechanics from a developmental biology standpoint, researchers may design methods to differentiate stem cells exploiting biomechanical stimuli as well as better interpret skeletogenesis *in vivo*.

Biomechanics promote maintenance of cartilage phenotype

The effects of mechanics on cartilage maintenance have been assessed using theoretical models of load distributions in cartilage and *in vivo* experiments. The identification of prominent biomechanical forces informed the development of *in vitro* biomechanical stimuli to improve cartilage maintenance *in vitro*.

Assessing native cartilage mechanical forces

Modeling studies have been employed to identify the mechanical forces that maintain tissue properties. Simulations demonstrate that mechanical forces exhibit depth-dependence: forces preserving the upper layers of cartilage are inherently different than those sustaining the lower layers; loading disparities lead to dissimilar cellular phenotypes.[439] Simulations have also been used to model the collagen network[440] and the pericellular matrix[441] to illustrate how the matrix

microenvironment is responsible for transducing tissue-level mechanical loading. Furthermore, models have delineated how loading promotes matrix protein synthesis.[442] Modeling thus represents a useful approach for understanding force transduction at the cellular and tissue levels.

In vivo imaging techniques can help elucidate normal loading kinematics. For example, two-photon laser microscopy has been used to chondrocyte deformation at the single cell level in response to muscle-induced mechanical loading[443] and tissue level[444] during physiological loading. Imaging of articulating surfaces indicates that contact kinematics are vital to maintain in order to prevent cartilage degeneration.[445] Disruption of joint kinematics leads to inappropriate contact points between articulating surfaces, which in turn causes cartilage degradation at these locations. Imaging methods can thus non-invasively examine the normal, *in vivo* cartilage biomechanics that maintain the mechanical properties vital to this load-bearing tissue.

Mechanical stimulation maintains phenotype

Both *in silico* and *in vivo* work has suggested that biomechanics play a key role in cartilage maintenance. To verify the role of mechanics, the effects of substrate stiffness, hydrostatic pressure, and compression have examined *in vitro*. These studies have demonstrated how mechanical stimulation can promote a chondrocytic phenotype.

Substrate stiffness

Though not a traditional form of mechanical stimulation, differences in substrate stiffness have been shown to play a biomechanical role in adult chondrogenesis.

Chondrocyte phenotype in monolayer culture is best maintained on softer as compared to stiffer substrates, validating matrix elasticity as a chondrogenic differentiator.[446] These results may be used to create scaffolds more similar in stiffness to the native chondrocyte microenvironment to actively enhance chondrogenesis. Matrix elasticity acts as a potent regulation of chondrogenesis, promoting the production of cartilage matrix proteins.

Hydrostatic pressure

Hydrostatic pressure has been applied extensively to promote a chondrocytic phenotype. Intermittent application of hydrostatic pressure to chondrocytes up-regulated the expression of genes for cartilage matrix proteins[447,448] and cytoskeletal elements.[449,450] Hydrostatic pressure mechanical stimulation of cells in compromised matrices led to further degeneration of the surrounding matrix, indicating that hydrostatic pressure affects chondrogenesis best in healthy environments.[451] At the cellular level, hydrostatic pressure promotes and maintains appropriate expression levels of cartilage genes, which result in the synthesis of matrix proteins. These results suggest that hydrostatic pressure could promote chondrogenesis *in vivo* by increasing the synthesis of cartilage extracellular matrix components.

Compression

Compression has also been shown to have beneficial effects on cartilage maintenance. For example, chondrocytes increase biosynthesis under physiological levels of dynamic compression, enhancing their cartilage matrix protein production.[452-454] These effects propagate through the depth of the tissue,

with cartilage exhibiting different responses to mechanical loading at various depths.[415,455] Additionally, studies have demonstrated that passaging cells modulates their response to compression, suggesting maturity-dependent responses to mechanical loading.[456] Other factors such as loading duration[442] and magnitude[457] have been shown to alter the response to stimulation, indicating that a specific compression regimen needs to be applied to promote cartilage maintenance.

Summary

Mechanical loading, which has been characterized using computer modeling and *in vivo* studies, plays a pivotal role in maintaining cartilage phenotype. The significance of biomechanics spurred the investigation of mechanical stimuli such as hydrostatic pressure and compression to enhance *in vitro* cartilage gene and protein expression.

Loading can promote disease

Improper loading leads to cartilage degeneration and osteoarthritis

Although biomechanics can have a beneficial role in maintaining cartilage, abnormal loading can promote pathogenesis. Insufficient or excessive mechanical stimulation leads to abnormal expression of chondrogenic markers and ultimately to undesired changes in cartilage at the tissue level. For instance, removing the meniscus increases loading on tibial cartilage.[458] Because the tibial cartilage cannot sustain the increased contact pressures, cartilage thinning and degeneration result.[459] Initiation of osteoarthritis need not be traumatic: slight

changes in the load distribution during trivial activities such as walking may initiate early osteoarthritic effects in even healthy knee joints.[460] Sudden disruptions in joint biomechanics due to ligament or meniscal tear create an improper mechanical loading environment that eventually leads to cartilage degeneration. Proper biomechanical loading can greatly reduce the risk of osteoarthritis and instead promote cartilage maintenance.

Harnessing biomechanics to promote chondrogenesis of adult cells

In addition to promoting chondrogenesis during development, various efforts have focused on harnessing biomechanics to promote the chondrogenesis of adult cells. These efforts aim to combat the deleterious effects of monolayer culture and expand the cell sources that can be used for *in vitro* cartilage formation. In particular, biomechanical stimulation has proven to be an exciting new strategy for effecting chondroinduction and re-differentiation of chondrocytes.

Mechanical loading effects on adult stem cell migration

As previously discussed, stem cell condensation and early chondrocyte differentiation are hallmarks of embryonic cartilage development; alternatively, adult stem cells also exhibit an ability to respond *in vivo* to heal cartilage defects. In addition to chemical factors that promote adult stem cell migration, the mechanical microenvironment influences stem cell recruitment. A rabbit study exceptionally demonstrated the effects of mechanics by grafting periosteal tissue—a source of progenitor cells—in an environment subjected to mechanical

loading.[461] The loaded environment stimulated *in vivo* chondrogenesis of stem cells present in the periosteum, demonstrating how biomechanics can initiate chondro-differentiation. Similarly, simulations of the effects of loading and fluid flow predict that joint motion can prompt stem cell release to heal cartilage defects.[462] These studies illustrate how biomechanics can alter the behavior of adult stem cells and thus influence *in vivo* cartilage regeneration.

Mechanical stimulation to promote re-differentiation

De-differentiation of chondrocytes is problematic in monolayer culture, which limits the potential for expanding cells and conducting large-scale experiments. Chondrocytes exhibit signs of phenotypic loss even after the first passage,[69] which is often manifested by reduced gene and/or protein expression of chondrogenic molecules such as collagen II and aggrecan. In addition, expansion alters cellular mechanical properties[463] and changes the chondrocyte response to mechanical stimulation.[464]

Mechanical stimulation has demonstrated re-differentiation potential, particularly by using hydrostatic pressure. Intermediate hydrostatic pressure during re-differentiation increased synthesis of cartilage-specific matrix molecules.[465] Similarly, applying HP to dedifferentiated chondrocytes in pellet culture up-regulated chondrogenic gene expression and matrix production.[466] However, hydrostatic pressure has also been shown to decrease collagen II production,[467] illustrating that more work needs to be done to understand how hydrostatic pressure can be used as a generic re-differentiation agent.

Compression has also been used to re-differentiate chondrocytes. Applying compression to passaged chondrocytes seeded on a collagen II scaffold increased collagen and proteoglycan production.[468] Another study showed that compression increased GAG production of expanded chondrocytes but did not alter collagen II expression.[456] The parallel responses of compression and hydrostatic pressure indicate that mechanical stimuli can be highly effective re-differentiation agents.

Biomechanics-driven chondroinduction

Biomechanical stimuli are potent chondroinductive agents for various cell types. Applying intermittent HP to murine embryonic fibroblasts resulted in two-fold increases in collagen synthesis and GAG production.[469] Similarly, HP increased chondrogenic gene expression in neonatal human dermal fibroblasts.[470] Mechanical forces have also been postulated to explain chondrogenic gene and protein expression observed in smooth muscle cells following atherosclerotic calcification.[471] Although several studies have shown promising results for using HP to promote chondroinduction, the effects of other forms of mechanical stimulation need to be investigated. Employing biomechanical stimuli to chondroinduce differentiated cells could eventually provide new cell sources to supplement stem cell efforts.

Summary

Biomechanics have been shown to enhance chondrogenesis of adult stem cells, de-differentiated cells, and cells from non-chondrocyte lineages. Thus, biomechanical stimuli could be employed to derive chondrocytes from diverse

cell populations and thus provide new chondrocyte cell sources. Additional refinement of mechanical stimuli for adult cell chondrogenesis will increase the availability of cells sources for applications like tissue regeneration.

Biomechanics drives tissue regeneration

Biomechanical stimuli have been employed to enhance tissue-level chondrogenesis and subsequently promote *de novo* cartilage formation. Several methods of mechanical stimulation including tension, HP, and compression have been used to improve the functional properties of neocartilage. In particular, research has focused on recapitulating the tensile and compressive properties of native cartilage, which could enable neocartilage to function *in vivo*. Additionally, *in vivo* mechanical stimulation has demonstrated chondrogenic potential.

Direct mechanical stimulation

The growing body of working showing the importance of biomechanics in cartilage development and maintenance has spurred investigations *of in vitro* and *in vivo* mechanical stimuli to improve cartilage formation. In particular, HP, direct compression, and shear have been examined.

Hydrostatic pressure

HP has been applied to various cartilage engineering systems to improve neocartilage properties. Studies of chondrocyte-seeded PGA meshes showed that HP increase GAG production 10-fold.[60,61] However, other work has shown that HP increases collagen production but reduces GAG content.[57] The differences in HP effects could be attributed to different chondrocyte culture

techniques, which have been shown to modulate the matrix production resulting from HP application. For example, the anabolic response to dynamic hydrostatic pressure evident for chondrocytes in pellet culture but not for cells cultured in alginate.[58] The widespread use of HP to successfully enhance neotissue suggests that HP is a potent stimulus for *in vitro* cartilage formation.

Despite these promising results, hydrostatic pressure has also been shown to be deleterious. In particular, applying hydrostatic pressure above physiological levels exhibited harmful effects and led to decreased matrix production and increased expression of inflammatory cytokines.[62] Cyclic HP at physiological levels has also been shown to decrease proteoglycan synthesis.[472] These studies showed the necessity of identifying an appropriate HP stimulation regimen to improve neocartilage properties.

Compression

Direct compression has also been used to modulate matrix composition and concomitantly influence neocartilage properties. Early work with cartilage explants demonstrated that compression could act as a catabolic[453,473] or anabolic[452] stimulus. It became clear that dynamic compression was generally more beneficial than static regimens, which tended to produce catabolic effects.[468] More recent efforts, many focusing on tissue engineering applications, have shown that direct compression can be used to improve matrix production and subsequently improve the functional properties of neocartilage. For example, dynamic compression at various frequencies and strain levels has been shown to increase matrix deposition.[53,54] The beneficial role of dynamic compression and

deleterious effects of static compression highlight the importance of selecting an appropriate mechanical stimulation regimen.

Shear

Although most biomechanical stimulation work has focused on HP and compression, shear forces have also been investigated. Treating cartilage explants to dynamic shear increased both collagen and proteoglycan synthesis.[474] Parallel results were observed for neocartilage exposed to shear, which showed 40% more collagen and 35% more proteoglycans than static controls. Excitingly, this shear application also resulted in a 3-fold increase in compressive strength and a 6-fold increase in stiffness.[401] Although there has not been as much work on the effects of shear, results thus far suggest that further investigation is warranted.

Chemically-induced mechanical stimulation

In addition to applying mechanical stimulation, exogenous agents that mimic mechanotransduction have also been identified. Various mechanisms including nuclear deformation,[475,476] α5β1 integrin signaling,[477] hyperosmolarity,[478] and strain-dependent ion channel signaling[479] have been linked to mechanotransduction. Applying exogenous agents such as ionophores and hyper-osmotic media that recapitulate these signaling events have been employed to enhance cartilage regeneration.

Ion channel modulation

Exogenous chemicals can be applied to modulate intracellular ion levels, which are known to vary following compression,[479] shear,[480,481] and hydrostatic

pressure.[478,482,483] To recapitulate these signaling events, one study used ouabain (Na+/K+-ATPase inhibitor) and ionomycin (a Ca^{2+} ionophore) or a combination of the two agents and demonstrated tensile modulus increases of 40-95% for cartilage constructs.[484] Electromagnetic fields, which can also affect ion channels, have been also been applied to increase matrix synthesis.[485] These tissue-level effects suggest that it is possible to apply exogenous agents to mimic biomechanical stimulation and subsequently enhance functional tissue-level properties.

Osmolarity

Applying agents that increase osmolarity mimics the hyper-osmotic environment that is created when compressive loading forces fluid out of cartilage. Hyperosmolarity has been shown to modulate intracellular ion levels,[486] suggesting that it could be employed like ion channel modulators to alter tissue properties. Studies with native cartilage have shown that hyper-osmolarity influences gene expression.[487,488] Although applying hyperosmolarity to tissue engineered constructs has not been studied extensively, expanding chondrocytes in hypertonic medium enhanced construct mechanical properties.[489] These promising results indicate that hyper-osmotic environments need to be further investigated in context of cartilage regeneration.

Summary

Biomechanical stimuli provide many new opportunities for enhancing functional properties during *de novo* cartilage formation. In addition to direct mechanical stimulation, mechanical equivalents offer exciting new methods for improving

neocartilage properties and developing a better understanding of mechanotransduction. Further investigations regarding appropriate stimulation regimens will enable mechanical stimuli to become more consistent among different studies.

Future directions

Biomechanics have been harnessed to improve the study of cartilage development, maintenance, and regeneration. Despite exciting recent advances, several areas need to be further examined to more fully understand biomechanics and develop biomechanics-driven strategies for improving cartilage differentiation and regeneration.

To further develop a biomechanics-driven approach, it will be necessary to develop a better understanding of how mechanics drives chondrogenesis. The load-bearing environment of cartilage influences chondrocyte differentiation will inform stem cell studies that focus on cartilage regeneration. Furthermore, a more thorough understanding of embryogenesis could be used to improve chondroinduction and re-differentiation methods. Although there is strong evidence for biomechanics influencing cartilage development, further *in vivo* work is needed to clarify the role of mechanics in chondrogenesis that occurs in the embryo.

Biomechanical stimuli can be further enhanced by applying them in conjunction with other biochemical and mechanical stimuli. Several studies have already shown the benefits of a multi-stimulus approach. For example, applying TGF-β1 in conjunction with HP had an additive effect on the mechanical

properties, increasing the compressive stiffness by 164% and the tensile stiffness by 231%.[59] A similar effect was observed by applying dynamic compression and TGF-β1 to synergistically increase compressive stiffness by 277%.[141] Additionally, multiple mechanical stimuli could be applied in combination to improve cartilage growth. Because cartilage experiences a complex array of biomechanical and biochemical signals in the joint space, it could be highly advantageous to develop regimens incorporating multiple stimuli.

An appreciation of the multi-level influence of biomechanics, from cellular microenvironment to tissue level, will play a crucial role in cartilage biology and engineering. The most successful efforts will mimic the native cartilage microenvironment and eventually reproduce the tissue-level biomechanics that are crucial for cartilage function. *De novo* cartilage with the functional properties of native tissue could eventually be used to treat cartilage disease and degeneration, which would significantly improve the treatment of conditions like osteoarthritis. Biomechanics research has helped drive recent developments in the field and will continue to be at the frontiers of cartilage biology and regeneration.

Figure 8-1: Role of biomechanics in chondrogenesis

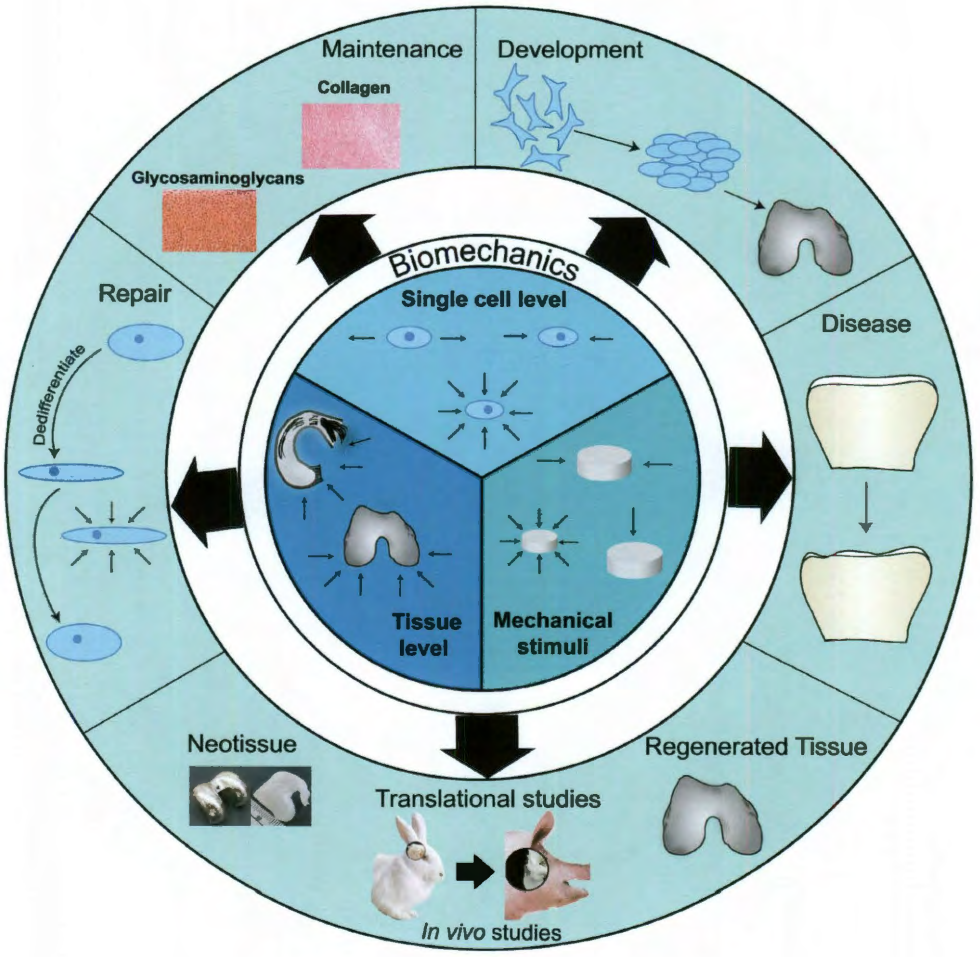

Biomechanics plays a key role in cartilage development by promoting differentiation of stem cells and limb formation. After cartilage has formed, normal mechanical loading is crucial for maintaining cartilage phenotype and prevent pathogenesis. Biomechanics can also be applied exogenously to enhance neocartilage formation.

Figure 8-2: Development of cartilage from embryo to fetal stages

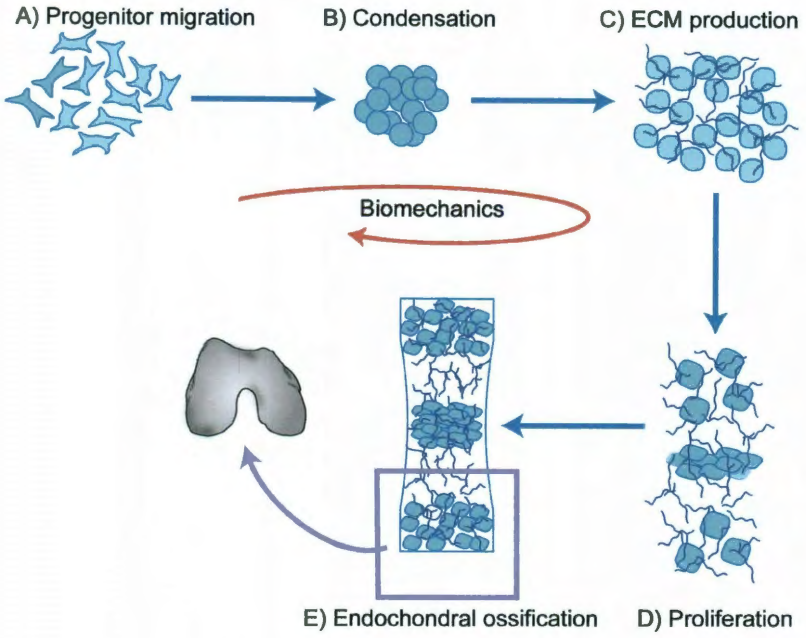

A) Mesenchymal progenitor cells migrate from the early mesoderm to sites of skeletogenesis and B) undergo pre-cartilaginous condensations by increasing expression of cell-cell interaction protein N-cadherin. Compressive forces are thought to initiate this process. C) Chondrocyte progenitors begin secreting cartilage-specific extracellular matrix and decrease expression of cell-cell proteins, thereby increasing their intracellular distance. D) Chondrocyte proliferation continues linearly at the subchondral growth front to create the long bones while endochondral ossification occurs throughout the juvenile stages to transform cartilage into bone. Regions at the long bone ends remain primarily composed of chondrocytes. E) Ends of long bones remain capped with a layer articular cartilage through adulthood.

Figure 8-3: Adult cell chondrogenesis

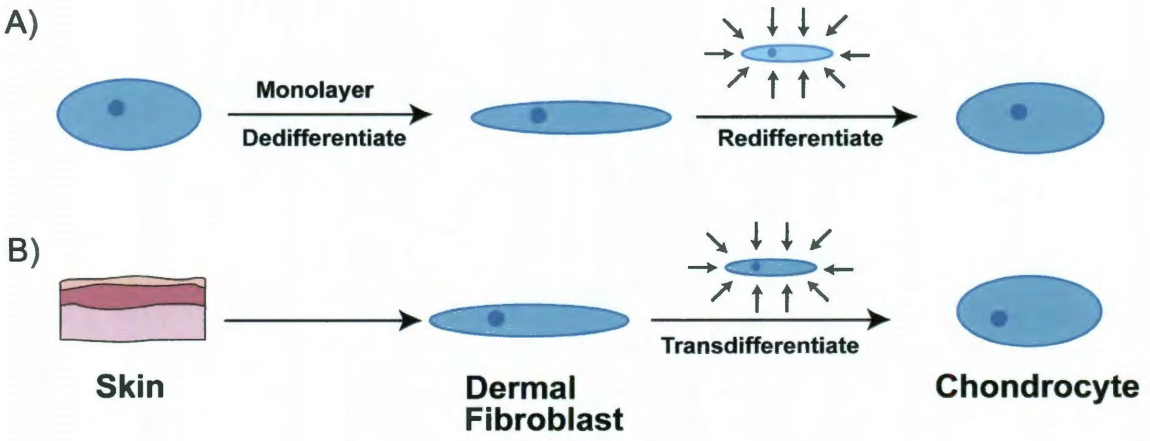

(A) Following monolayer culture, chondrocytes rapidly de-differentiate. Biomechanical stimuli such as hydrostatic pressure can be applied to promote re-differentiation. (B) Mechanical stimulation also can be used to induce transdifferentiation into chondrocytes.

Figure 8-4: Biomechanical stimulation of neocartilage

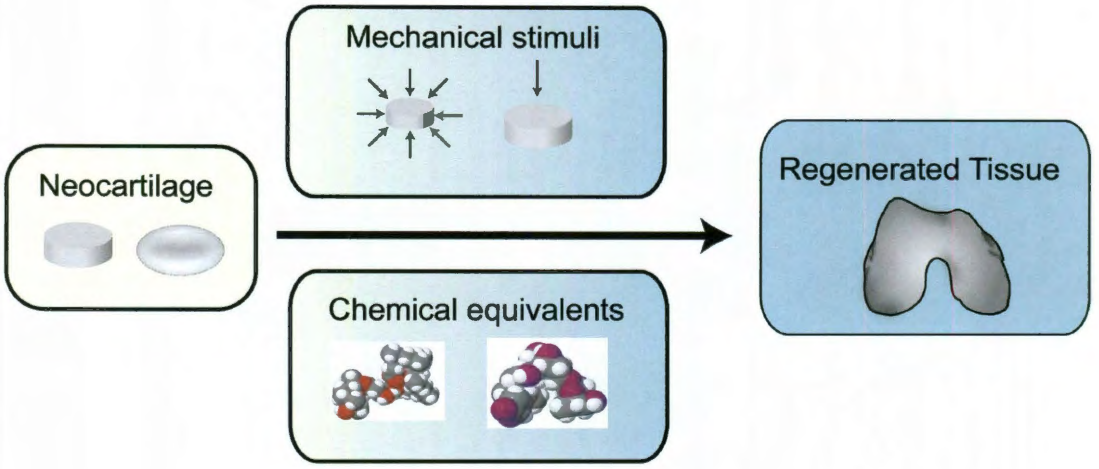

Biomechanical stimuli such as compression and hydrostatic pressure can be applied to enhance neotissue formation. Analogously, chemical equivalents including ionophores and hyperosmotic environments can be applied to mimic mechanotransduction.

Conclusions and future directions

This thesis details work on functional cartilage tissue engineering, investigating the mechanisms underlying responses to various exogenous agents. This dissertation has examined growth factors, enzymes, and matrix molecules that provide simple yet effective methods for improving the functionality of cartilage constructs. Chapters 1-2 focus on the novel catabolic agent C-ABC. Work on hyaluronic acid (Chapters 3-4) showed how exogenously adding this core matrix molecule can enhance tissue-level functional properties. In addition to the central work on exogenous agents, various imaging technologies have been investigated (Chapter 6, Appendix 4) to expand the assessments available for tissue engineering studies. These novel technologies could provide noninvasive assessments to complement the destructive tests typically used in tissue engineering studies.

Chondroitinase-ABC

Work with C-ABC showed that a catabolic agent can be employed to improve the tensile properties of constructs. C-ABC cleaves GAGs, resulting in polysaccharide chains small enough to diffuse out or tissue of neotissue. Although the effects of C-ABC have been shown for explants[47] and constructs,[51,139] the studies of this dissertation aimed to 1) examine multiple treatments to further enhance tensile properties, 2) examine the effects of combining C-ABC with TGF-β1, and 3) elucidate the mechanism underlying C-ABC treatment.

The first study (Chapter 1) examined the effects of multiple C-ABC applications on self-assembled constructs. This study contained both 4 and 6 week cultures, both of which had C-ABC treatment at 2 weeks, 4 weeks, or 2&4 weeks. The 4 wk experiment showed increases in tensile properties for the group treated at 2 weeks. For the 6 week experiment, the tensile stiffness was increased for all C-ABC treatments. The dual 2&4 week treatment enhanced the tensile stiffness more so than the individual C-ABC treatments, providing a strategy for improving C-ABC treatment regimens. Additionally, by 6 weeks the compressive stiffness had returned to control levels despite reduced GAG content. These exciting results were investigated in combination with an anabolic agent in Chapter 2.

The second study (Chapter 2) focused on the effects of combining C-ABC with TGF-β1. This study produced several novel findings including 1) C-ABC and TGF-β1 can be applied to synergistically enhance neotissue, 2) TGF-β1 can be applied to aid the recovery of compressive stiffness following C-ABC treatment, 3) TGF-β1 increases MAPK signaling in self-assembled neocartilage, and 4) C-ABC treatment results in increased collagen fibril diameter. The increased fibril diameter following C-ABC treatment is particularly exciting because it is the first demonstration of a potential mechanism for the effects of C-ABC cartilage constructs. Because C-ABC and TGF-β1 appear to be acting via distinct mechanisms, it makes sense that combining them results in synergistic increases in construct properties.

Constructs treated with C-ABC and TGF-β1 also exhibited stability and maturation *in vivo*. The improvement of functional construct properties after 4 weeks of *in vivo* cultures shows that self-assembled neocartilage has great promise for more extensive *in vivo* work. Although the different responses of constructs and native tissue are not yet fully understood, it is possible that the higher cellularity of constructs influences their response to *in vivo* nutrients and cytokines. Further investigation could help elucidate the differences in responses and also inform future tissue engineering strategies. These exciting *in vivo* results and the promising mechanical properties of constructs post-sacrifice suggest that self-assembled constructs should be studied further using cartilage defect models.

These two studies show significant functional results for a relatively new agent in tissue engineering. Although many tissue regeneration efforts focus on anabolic stimuli, employing a catabolic agent like C-ABC marks a fundamentally different strategy. The success of C-ABC is particularly exciting because it provides an opportunity synergistically enhance the effects of anabolic agents. This was observed in Chapter 2, which illustrated how C-ABC and TGF-β1 had different mechanisms of action and in turn explained the synergistic effects resulting from applying these agents in combination.

Hyaluronic acid

HA work illustrated the ability of HA to improve functional properties of self-assembled constructs and showed its mechanism of action. Two studies were conducted to assess the effects of HA application: an optimization of HA

application and investigation of its mechanism of action (Chapter 3) and an examination of how exogenous HA influences TGF-β1 signaling (Chapter 4).

The first study examined the effects of exogenously applying HA on the biochemical and biomechanical properties of self-assembled articular cartilage. The influence of HA commencement time, concentration, application duration, and molecular weight was assessed in three sequential phases. These results showed that HA application at seeding was optimal, increasing compressive stiffness 1-fold and increasing GAG content by 35%. Furthermore, only higher molecular weight HA at a concentration of 1 mg/ml enhanced the compressive stiffness and GAG content of constructs. These studies illustrated a promising HA application regimen, but the biological and/or biophysical action of HA was not yet clear.

To investigate the mechanism underlying HA treatment, we evaluated the gene expression and GAG retention effects of HA application. Because HA increased GAG retention in self-assembled cartilage, it could be increasing the fixed charge density and thereby increasing water retention in the matrix. This water retention could subsequently enable constructs to resist compressive loading and explain the observed increased compressive properties. Microarray and PCR analyses showed that HA also influenced genetic signaling, up-regulating 503 genes, including multiple genes associated with TGF-β1 signaling.

In chapter 4, additive effects of combining HA and TGF-β1 were observed. This study demonstrated that HA and TGF-β1 increased the GAG content and compressive stiffness of constructs. Additionally, treating with a combination of

HA and TGF-β1 further increased the GAG content and compressive properties, additively enhancing construct properties. Combined HA and TGF-β1 treatment produced neocartilage with a compressive stiffness and GAG content above control values by 150% and 65%, respectively. This study demonstrated that HA does not interfere with TGF-β1 signaling in self-assembled constructs. The additive increases observed with the combination treatment could result from increased retention of the GAGs produced due to growth factor application. Furthermore, HA could sequester TGF-β1 in the matrix and thereby increase its effective dose.

These studies collectively illustrated how exogenous HA application enhances the biochemical and biomechanical properties of cartilage constructs. Gene expression and GAG retention studies showed that HA played biological and biophysical roles, both of which could contribute to the enhanced construct properties. Additionally, the combination of HA and TGF-β1 additively enhanced biochemical and biomechanical properties. Results suggested that HA has great potential for improving future cartilage regeneration efforts, particularly in cases where it is crucial to improve the compressive integrity of the neotissue.

Optical assessments

Studies of optical properties provide exciting new optical measurements to our conventional assessments that could be used for noninvasive evaluation of constructs. Two technologies were investigated for their ability to complement conventional biomechanical and biochemical assessments. The first technology (Chapter 6) was combination of time-resolved fluorescence spectroscopy (TRFS)

and ultrasound backscatter microscopy (UBM). Second harmonic generation (SHG) was also investigated to study the organization of the collagen network.

The effects of matrix composition were examined using TRFS and UBM. To alter matrix composition and mechanical properties, cartilage samples were treated with collagenase, C-ABC, and ribose. UBM was used to discern thicknesses and construct microstructure. Various parameters quantifying fluorescence decay such as the average fluorescence lifetime and decay constants correlated significantly with biochemical and mechanical data. These correlations are exciting because they suggest that noninvasive assessments can be used to infer both the biochemical composition and biomechanical properties of constructs. Refining the optical signal processing and conducting further experiments will enable this technology to be developed as an alternative to traditional destructive assays.

As described in Appendix 4, SHG was used to study zonal variation in patellar cartilage. This work showed that SHG can be used to infer functional properties of cartilage. In particular, the sizes of disordered regions were strongly correlated with tensile strength and stiffness. Although further work will be carried out to fully elucidate the SHG signal origin, the strong correlations are exciting for the development of an optics-based assessment of mechanical properties. Future work focusing on comparing the collagen architecture with SHG data will help clarify what aspects of the collagen network contribute to the differences observed with SHG.

The development of noninvasive technologies that can be used to monitor functional construct properties is an exciting step forward for both *in vitro* and *in vivo* studies. Destructive assays can be time-consuming and require sample loss, limiting the number of assays that can be performed. Similarly, destructive *in vivo* assessments require sacrifice of the experimental animal. Nondestructive assays could be employed to execute more effective animal studies and eventually be used clinically to quantify cartilage degeneration and repair.

Future directions

To build upon the current results, there are several main areas of promising future work: 1) the mechanisms underlying novel stimuli such as C-ABC and HA need to be interrogated in more detail and 2) more extensive *in vivo* work should be undertaken.

Mechanistic studies should go delve into protein-level interactions in addition to the genetic analysis discussed in this work. Because many intermediate signaling events such as Smad cascades depend on post-transcriptional modifications, other analysis modalities will need to be employed to gain a full understanding of intracellular cascades. Other time points could also be used to observe how signaling cascades develop over time in response to stimuli. Additionally, inhibitors of signaling cascades or receptors should be used to demonstrate the effects of blocking stimuli.

Ultimately, *in vivo* studies will validate the functionality of self-assembly and advance the technology. *In vivo* work should first focus on a small animal

model such as rabbit. Because bovine cells are likely to be immunogenic in rabbits, it will be necessary to create leporine constructs. The stimuli that have been developed in this thesis and in other work can be applied to leporine constructs to improve their functionality prior to implantation. These constructs can then be implanted in articular cartilage defects to observe their biological reactivity, including their immunogenicity and integration with surrounding tissue. Post-sacrifice analysis will then illustrate if the constructs have exhibited stability *in vivo* and if they have matured in the *in vivo* environment.

References

1. J.C. Hu & Athanasiou, K.A. in Handbook of Histology Methods for Bone and Cartilage. (eds. Y.H. An & K.L. Martin) (Humana Press Inc., Totowa, NJ; 2003).
2. V.C. Mow, Ratcliffe, A. & Poole, A.R. Cartilage and diarthrodial joints as paradigms for hierarchical materials and structures. *Biomaterials* **13**, 67-97 (1992).
3. D.R. Eyre, Weis, M.A. & Wu, J.J. Articular cartilage collagen: an irreplaceable framework? *Eur Cell Mater* **12**, 57-63 (2006).
4. L. Vaughan et al. D-periodic distribution of collagen type IX along cartilage fibrils. *J Cell Biol* **106**, 991-997 (1988).
5. L. Macri, Silverstein, D. & Clark, R.A. Growth factor binding to the pericellular matrix and its importance in tissue engineering. *Adv Drug Deliv Rev* **59**, 1366-1381 (2007).
6. P.J. Roughley & Lee, E.R. Cartilage proteoglycans: structure and potential functions. *Microsc Res Tech* **28**, 385-397 (1994).
7. M. Costell et al. Perlecan maintains the integrity of cartilage and some basement membranes. *J Cell Biol* **147**, 1109-1122 (1999).
8. E. Arikawa-Hirasawa, Watanabe, H., Takami, H., Hassell, J.R. & Yamada, Y. Perlecan is essential for cartilage and cephalic development. *Nat Genet* **23**, 354-358 (1999).
9. E.B. Hunziker Articular cartilage repair: are the intrinsic biological constraints undermining this process insuperable? *Osteoarthritis Cartilage* **7**, 15-28 (1999).
10. C.J. Campbell The healing of cartilage defects. *Clin Orthop Relat Res* **64**, 45-63 (1969).
11. B.E. Gerber et al. Mechanical resistance of biological repair cartilage: comparative in vivo tests of different surgical repair procedures. *Int J Artif Organs* **25**, 1109-1115 (2002).
12. E. Yelin et al. Medical care expenditures and earnings losses among persons with arthritis and other rheumatic conditions in 2003, and comparisons with 1997. *Arthritis Rheum* **56**, 1397-1407 (2007).
13. J.A. Buckwalter, Saltzman, C. & Brown, T. The impact of osteoarthritis: implications for research. *Clin Orthop Relat Res* **427 Suppl**, S6-15 (2004).
14. J. Samuels, Krasnokutsky, S. & Abramson, S.B. Osteoarthritis: a tale of three tissues. *Bull NYU Hosp Jt Dis* **66**, 244-250 (2008).
15. C.M. Revell & Athanasiou, K.A. Success rates and immunologic responses of autogenic, allogenic, and xenogenic treatments to repair articular cartilage defectst. *Tissue Eng Part B Rev* (2008).
16. S.L. Sledge Microfracture techniques in the treatment of osteochondral injuries. *Clin Sports Med* **20**, 365-377 (2001).
17. J.E. Aston & Bentley, G. Repair of articular surfaces by allografts of articular and growth-plate cartilage. *J Bone Joint Surg Br* **68**, 29-35 (1986).

18. R.T. Burks, Greis, P.E., Arnoczky, S.P. & Scher, C. The use of a single osteochondral autograft plug in the treatment of a large osteochondral lesion in the femoral condyle: an experimental study in sheep. *Am J Sports Med* **34**, 247-255 (2006).
19. L. Hangody & Fules, P. Autologous osteochondral mosaicplasty for the treatment of full-thickness defects of weight-bearing joints: ten years of experimental and clinical experience. *J Bone Joint Surg Am* **85-A Suppl 2**, 25-32 (2003).
20. A. Romaniuk et al. Rejection of cartilage formed by transplanted allogeneic chondrocytes: evaluation with monoclonal antibodies. *Transpl Immunol* **3**, 251-257 (1995).
21. L. Peterson, Brittberg, M., Kiviranta, I., Akerlund, E.L. & Lindahl, A. Autologous chondrocyte transplantation. Biomechanics and long-term durability. *Am J Sports Med* **30**, 2-12 (2002).
22. U. Horas, Pelinkovic, D., Herr, G., Aigner, T. & Schnettler, R. Autologous chondrocyte implantation and osteochondral cylinder transplantation in cartilage repair of the knee joint. A prospective, comparative trial. *J Bone Joint Surg Am* **85-A**, 185-192 (2003).
23. E. Grimaud, Heymann, D. & Redini, F. Recent advances in TGF-beta effects on chondrocyte metabolism. Potential therapeutic roles of TGF-beta in cartilage disorders. *Cytokine Growth Factor Rev* **13**, 241-257 (2002).
24. B. Johnstone, Hering, T.M., Caplan, A.I., Goldberg, V.M. & Yoo, J.U. In vitro chondrogenesis of bone marrow-derived mesenchymal progenitor cells. *Exp Cell Res* **238**, 265-272 (1998).
25. A.M. Mackay et al. Chondrogenic differentiation of cultured human mesenchymal stem cells from marrow. *Tissue Eng* **4**, 415-428 (1998).
26. A.A. Worster, Nixon, A.J., Brower-Toland, B.D. & Williams, J. Effect of transforming growth factor beta1 on chondrogenic differentiation of cultured equine mesenchymal stem cells. *Am J Vet Res* **61**, 1003-1010 (2000).
27. J. Kramer et al. Embryonic stem cell-derived chondrogenic differentiation in vitro: activation by BMP-2 and BMP-4. *Mech Dev* **92**, 193-205 (2000).
28. H.L. Glansbeek, van Beuningen, H.M., Vitters, E.L., van der Kraan, P.M. & van den Berg, W.B. Stimulation of articular cartilage repair in established arthritis by local administration of transforming growth factor-beta into murine knee joints. *Lab Invest* **78**, 133-142 (1998).
29. L.A. Fortier, Nixon, A.J., Mohammed, H.O. & Lust, G. Altered biological activity of equine chondrocytes cultured in a three-dimensional fibrin matrix and supplemented with transforming growth factor beta-1. *Am J Vet Res* **58**, 66-70 (1997).
30. G.J. van Osch, van der Veen, S.W., Buma, P. & Verwoerd-Verhoef, H.L. Effect of transforming growth factor-beta on proteoglycan synthesis by chondrocytes in relation to differentiation stage and the presence of pericellular matrix. *Matrix Biol* **17**, 413-424 (1998).

31. G.J. van Osch, van den Berg, W.B., Hunziker, E.B. & Hauselmann, H.J. Differential effects of IGF-1 and TGF beta-2 on the assembly of proteoglycans in pericellular and territorial matrix by cultured bovine articular chondrocytes. *Osteoarthritis Cartilage* **6**, 187-195 (1998).
32. F.P. Luyten et al. Natural bovine osteogenin and recombinant human bone morphogenetic protein-2B are equipotent in the maintenance of proteoglycans in bovine articular cartilage explant cultures. *J Biol Chem* **267**, 3691-3695 (1992).
33. K.J. Gooch et al. Bone morphogenetic proteins-2, -12, and -13 modulate in vitro development of engineered cartilage. *Tissue Eng* **8**, 591-601 (2002).
34. P. Smith et al. Genetic enhancement of matrix synthesis by articular chondrocytes: comparison of different growth factor genes in the presence and absence of interleukin-1. *Arthritis Rheum* **43**, 1156-1164 (2000).
35. J. Flechtenmacher et al. Recombinant human osteogenic protein 1 is a potent stimulator of the synthesis of cartilage proteoglycans and collagens by human articular chondrocytes. *Arthritis Rheum* **39**, 1896-1904 (1996).
36. R.L. Sah, Chen, A.C., Grodzinsky, A.J. & Trippel, S.B. Differential effects of bFGF and IGF-I on matrix metabolism in calf and adult bovine cartilage explants. *Arch Biochem Biophys* **308**, 137-147 (1994).
37. T. Blunk et al. Differential effects of growth factors on tissue-engineered cartilage. *Tissue Eng* **8**, 73-84 (2002).
38. L.A. Fortier, Lust, G., Mohammed, H.O. & Nixon, A.J. Coordinate upregulation of cartilage matrix synthesis in fibrin cultures supplemented with exogenous insulin-like growth factor-I. *J Orthop Res* **17**, 467-474 (1999).
39. B.D. Elder & Athanasiou, K.A. Systematic assessment of growth factor treatment on biochemical and biomechanical properties of engineered articular cartilage constructs. *Osteoarthritis Cartilage* **18**, 18 (2008).
40. L.J. Bonassar et al. The effect of dynamic compression on the response of articular cartilage to insulin-like growth factor-I. *J Orthop Res* **19**, 11-17 (2001).
41. E.M. Darling & Athanasiou, K.A. Growth factor impact on articular cartilage subpopulations. *Cell Tissue Res* **322**, 463-473 (2005).
42. Y.M. Jenniskens et al. Biochemical and functional modulation of the cartilage collagen network by IGF1, TGFbeta2 and FGF2. *Osteoarthritis Cartilage* **14**, 1136-1146 (2006).
43. P. Galera et al. Effect of transforming growth factor-beta 1 (TGF-beta 1) on matrix synthesis by monolayer cultures of rabbit articular chondrocytes during the dedifferentiation process. *Exp Cell Res* **200**, 379-392 (1992).
44. W.N. Qi & Scully, S.P. Effect of type II collagen in chondrocyte response to TGF-beta 1 regulation. *Exp Cell Res* **241**, 142-150 (1998).
45. P.A. Guerne, Sublet, A. & Lotz, M. Growth factor responsiveness of human articular chondrocytes: distinct profiles in primary chondrocytes, subcultured chondrocytes, and fibroblasts. *J Cell Physiol* **158**, 476-484 (1994).

46. V. Prabhakar et al. The catalytic machinery of chondroitinase ABC I utilizes a calcium coordination strategy to optimally process dermatan sulfate. *Biochemistry* **45**, 11130-11139 (2006).
47. A. Asanbaeva, Masuda, K., Thonar, E.J., Klisch, S.M. & Sah, R.L. Mechanisms of cartilage growth: modulation of balance between proteoglycan and collagen in vitro using chondroitinase ABC. *Arthritis Rheum* **56**, 188-198 (2007).
48. L. Bian et al. in Trans Orthopaedic Res, Vol. 33 601San Francisco; 2008).
49. A.K. Williamson, Chen, A.C., Masuda, K., Thonar, E.J. & Sah, R.L. Tensile mechanical properties of bovine articular cartilage: variations with growth and relationships to collagen network components. *J Orthop Res* **21**, 872-880 (2003).
50. A.K. Williamson, Masuda, K., Thonar, E.J. & Sah, R.L. Growth of immature articular cartilage in vitro: correlated variation in tensile biomechanical and collagen network properties. *Tissue Eng* **9**, 625-634 (2003).
51. R. Natoli, Revell, C.M. & Athanasiou, K. Chondroitinase ABC Treatment Results in Increased Tensile Properties of Self-Assembled Tissue Engineered Articular Cartilage. *Tissue Eng Part A*, doi:10.1089/ten.TEA.2008.0478 (2009).
52. F. Guilak et al. The role of biomechanics and inflammation in cartilage injury and repair. *Clin Orthop Relat Res*, 17-26 (2004).
53. R.L. Mauck et al. Functional tissue engineering of articular cartilage through dynamic loading of chondrocyte-seeded agarose gels. *J Biomech Eng* **122**, 252-260 (2000).
54. M. Pei et al. Bioreactors mediate the effectiveness of tissue engineering scaffolds. *Faseb J* **16**, 1691-1694 (2002).
55. A.C. Aufderheide & Athanasiou, K.A. A direct compression stimulator for articular cartilage and meniscal explants. *Ann Biomed Eng* **34**, 1463-1474 (2006).
56. R.L. Smith et al. Time-dependent effects of intermittent hydrostatic pressure on articular chondrocyte type II collagen and aggrecan mRNA expression. *J Rehabil Res Dev* **37**, 153-161 (2000).
57. J.C. Hu & Athanasiou, K.A. The effects of intermittent hydrostatic pressure on self-assembled articular cartilage constructs. *Tissue Eng* **12**, 1337-1344 (2006).
58. S.H. Elder et al. Chondrocyte response to cyclic hydrostatic pressure in alginate versus pellet culture. *J Orthop Res* **24**, 740-747 (2006).
59. B.D. Elder & Athanasiou, K.A. Synergistic and additive effects of hydrostatic pressure and growth factors on tissue formation. *PLoS ONE* **3** (2008).
60. S.E. Carver & Heath, C.A. Increasing extracellular matrix production in regenerating cartilage with intermittent physiological pressure. *Biotechnol Bioeng* **62**, 166-174 (1999).

61. S.E. Carver & Heath, C.A. Semi-continuous perfusion system for delivering intermittent physiological pressure to regenerating cartilage. *Tissue Eng* **5**, 1-11 (1999).
62. K. Takahashi et al. Hydrostatic pressure induces expression of interleukin 6 and tumour necrosis factor alpha mRNAs in a chondrocyte-like cell line. *Ann Rheum Dis* **57**, 231-236 (1998).
63. L.A. Solchaga et al. Repair of osteochondral defects with hyaluronan- and polyester-based scaffolds. *Osteoarthritis Cartilage* **13**, 297-309 (2005).
64. L.A. Solchaga et al. Hyaluronan-based polymers in the treatment of osteochondral defects. *J Orthop Res* **18**, 773-780 (2000).
65. S. Hofmann et al. Cartilage-like tissue engineering using silk scaffolds and mesenchymal stem cells. *Tissue Eng* **12**, 2729-2738 (2006).
66. F. Barry, Boynton, R.E., Liu, B. & Murphy, J.M. Chondrogenic differentiation of mesenchymal stem cells from bone marrow: differentiation-dependent gene expression of matrix components. *Exp Cell Res* **268**, 189-200 (2001).
67. S. Ichinose, Yamagata, K., Sekiya, I., Muneta, T. & Tagami, M. Detailed examination of cartilage formation and endochondral ossification using human mesenchymal stem cells. *Clin Exp Pharmacol Physiol* **32**, 561-570 (2005).
68. Y. Takemitsu The effect of age upon sulfate-S35 fixation of chondroitin sulfate in cartilage and bone of the normal white rats and S35-autoradiographic study of these tissues. *Kyushu J Med Sci*, 251-281 (1961).
69. E.M. Darling & Athanasiou, K.A. Rapid phenotypic changes in passaged articular chondrocyte subpopulations. *J Orthop Res* **23**, 425-432 (2005).
70. D.A. Grande, Halberstadt, C., Naughton, G., Schwartz, R. & Manji, R. Evaluation of matrix scaffolds for tissue engineering of articular cartilage grafts. *J Biomed Mater Res* **34**, 211-220 (1997).
71. O. Lupi Prions in dermatology. *J Am Acad Dermatol* **46**, 790-793 (2002).
72. L. Benedetti et al. Biocompatibility and biodegradation of different hyaluronan derivatives (Hyaff) implanted in rats. *Biomaterials* **14**, 1154-1160 (1993).
73. R. Cortivo, Brun, P., Rastrelli, A. & Abatangelo, G. In vitro studies on biocompatibility of hyaluronic acid esters. *Biomaterials* **12**, 727-730 (1991).
74. S. Nehrer et al. Three-year clinical outcome after chondrocyte transplantation using a hyaluronan matrix for cartilage repair. *Eur J Radiol* **57**, 3-8 (2006).
75. A.P. Hollander, Dickinson, S.C., Sims, T.J., Soranzo, C. & Pavesio, A. Quantitative analysis of repair tissue biopsies following chondrocyte implantation. *Novartis Found Symp* **249**, 218-229; discussion 229-233, 234-218, 239-241 (2003).
76. A. Gobbi et al. Patellofemoral full-thickness chondral defects treated with Hyalograft-C: a clinical, arthroscopic, and histologic review. *Am J Sports Med* **34**, 1763-1773 (2006).

77. K. Lindenhayn et al. Retention of hyaluronic acid in alginate beads: aspects for in vitro cartilage engineering. *J Biomed Mater Res* **44**, 149-155 (1999).
78. F. Allemann et al. Effects of hyaluronan on engineered articular cartilage extracellular matrix gene expression in 3-dimensional collagen scaffolds. *J Biomed Mater Res* **55**, 13-19 (2001).
79. H.S. Yoo, Lee, E.A., Yoon, J.J. & Park, T.G. Hyaluronic acid modified biodegradable scaffolds for cartilage tissue engineering. *Biomaterials* **26**, 1925-1933 (2005).
80. D.A. Hendrickson et al. Chondrocyte-fibrin matrix transplants for resurfacing extensive articular cartilage defects. *J Orthop Res* **12**, 485-497 (1994).
81. G. Kaplonyi, Zimmerman, I., Frenyo, A.D., Farkas, T. & Nemes, G. The use of fibrin adhesive in the repair of chondral and osteochondral injuries. *Injury* **19**, 267-272 (1988).
82. G.A. Paletta, Arnoczky, S.P. & Warren, R.F. The repair of osteochondral defects using an exogenous fibrin clot. An experimental study in dogs. *Am J Sports Med* **20**, 725-731 (1992).
83. H.K. Kjaergard & Weis-Fogh, U.S. Important factors influencing the strength of autologous fibrin glue; the fibrin concentration and reaction time--comparison of strength with commercial fibrin glue. *Eur Surg Res* **26**, 273-276 (1994).
84. A. Atala, Kim, W., Paige, K.T., Vacanti, C.A. & Retik, A.B. Endoscopic treatment of vesicoureteral reflux with a chondrocyte-alginate suspension. *J Urol* **152**, 641-643; discussion 644 (1994).
85. K.T. Paige, Cima, L.G., Yaremchuk, M.J., Vacanti, J.P. & Vacanti, C.A. Injectable cartilage. *Plast Reconstr Surg* **96**, 1390-1398; discussion 1399-1400 (1995).
86. K.T. Paige et al. De novo cartilage generation using calcium alginate-chondrocyte constructs. *Plast Reconstr Surg* **97**, 168-178; discussion 179-180 (1996).
87. H.J. Hauselmann et al. Phenotypic stability of bovine articular chondrocytes after long-term culture in alginate beads. *J Cell Sci* **107 (Pt 1)**, 17-27 (1994).
88. B. Kulseng et al. Transplantation of alginate microcapsules: generation of antibodies against alginates and encapsulated porcine islet-like cell clusters. *Transplantation* **67**, 978-984 (1999).
89. C.A. Vacanti, Kim, W., Schloo, B., Upton, J. & Vacanti, J.P. Joint resurfacing with cartilage grown in situ from cell-polymer structures. *Am J Sports Med* **22**, 485-488 (1994).
90. C.R. Chu et al. Articular cartilage repair using allogeneic perichondrocyte-seeded biodegradable porous polylactic acid (PLA): a tissue-engineering study. *J Biomed Mater Res* **29**, 1147-1154 (1995).
91. C.D. Sims et al. Injectable cartilage using polyethylene oxide polymer substrates. *Plast Reconstr Surg* **98**, 843-850 (1996).

92. K.S. Furukawa et al. Rapid and large-scale formation of chondrocyte aggregates by rotational culture. *Cell Transplant* **12**, 475-479 (2003).
93. M.C. Stewart, Saunders, K.M., Burton-Wurster, N. & Macleod, J.N. Phenotypic stability of articular chondrocytes in vitro: the effects of culture models, bone morphogenetic protein 2, and serum supplementation. *J Bone Miner Res* **15**, 166-174 (2000).
94. J.C. Hu & Athanasiou, K.A. A self-assembling process in articular cartilage tissue engineering. *Tissue Eng* **12**, 969-979 (2006).
95. Y. Deng, Zhao, K., Zhang, X.F., Hu, P. & Chen, G.Q. Study on the three-dimensional proliferation of rabbit articular cartilage-derived chondrocytes on polyhydroxyalkanoate scaffolds. *Biomaterials* **23**, 4049-4056 (2002).
96. G. Schulze-Tanzil et al. Redifferentiation of dedifferentiated human chondrocytes in high-density cultures. *Cell Tissue Res* **308**, 371-379 (2002).
97. Y. Kato, Iwamoto, M., Koike, T., Suzuki, F. & Takano, Y. Terminal differentiation and calcification in rabbit chondrocyte cultures grown in centrifuge tubes: regulation by transforming growth factor beta and serum factors. *Proc Natl Acad Sci U S A* **85**, 9552-9556 (1988).
98. Z. Zhang, McCaffery, J.M., Spencer, R.G. & Francomano, C.A. Hyaline cartilage engineered by chondrocytes in pellet culture: histological, immunohistochemical and ultrastructural analysis in comparison with cartilage explants. *J Anat* **205**, 229-237 (2004).
99. I. Sekiya, Vuoristo, J.T., Larson, B.L. & Prockop, D.J. In vitro cartilage formation by human adult stem cells from bone marrow stroma defines the sequence of cellular and molecular events during chondrogenesis. *Proc Natl Acad Sci U S A* **99**, 4397-4402 (2002).
100. R.D. Graff, Lazarowski, E.R., Banes, A.J. & Lee, G.M. ATP release by mechanically loaded porcine chondrons in pellet culture. *Arthritis Rheum* **43**, 1571-1579 (2000).
101. N. Indrawattana et al. Growth factor combination for chondrogenic induction from human mesenchymal stem cell. *Biochem Biophys Res Commun* **320**, 914-919 (2004).
102. G.M. Hoben, Hu, J.C., James, R.A. & Athanasiou, K.A. Self-assembly of fibrochondrocytes and chondrocytes for tissue engineering of the knee meniscus. *Tissue Eng* **13**, 939-946 (2007).
103. G. Ofek et al. Matrix development in self-assembly of articular cartilage. *PLoS ONE* **3**, e2795 (2008).
104. B.D. Elder & Athanasiou, K.A. Systematic assessment of growth factor treatment on biochemical and biomechanical properties of engineered articular cartilage constructs. *Osteoarthritis Cartilage* **17**, 114-123 (2009).
105. B.D. Elder & Athanasiou, K.A. Effects of Temporal Hydrostatic Pressure on Tissue-Engineered Bovine Articular Cartilage Constructs. *Tissue Eng Part A* **15**, 1151-1158 (2008).
106. R.A. Kandel, Chen, H., Clark, J. & Renlund, R. Transplantation of cartilagenous tissue generated in vitro into articular joint defects. *Artif Cells Blood Substit Immobil Biotechnol* **23**, 565-577 (1995).

107. B.D. Elder & Athanasiou, K.A. Synergistic and additive effects of hydrostatic pressure and growth factors on tissue formation. *PLoS ONE* **3**, e2341 (2008).
108. B.D. Elder & Athanasiou, K.A. Systematic assessment of growth factor treatment on biochemical and biomechanical properties of engineered articular cartilage constructs. *Osteoarthritis Cartilage* (2008).
109. L.E. Freed et al. Chondrogenesis in a cell-polymer-bioreactor system. *Exp Cell Res* **240**, 58-65 (1998).
110. W. Kafienah et al. Lumican inhibits collagen deposition in tissue engineered cartilage. *Matrix Biol* (2008).
111. K.W. Ng et al. Culture duration modulates collagen hydrolysate-induced tissue remodeling in chondrocyte-seeded agarose hydrogels. *Ann Biomed Eng* **35**, 1914-1923 (2007).
112. M. Wong et al. Collagen fibrillogenesis by chondrocytes in alginate. *Tissue Eng* **8**, 979-987 (2002).
113. Y.M. Bastiaansen-Jenniskens et al. Contribution of collagen network features to functional properties of engineered cartilage. *Osteoarthritis Cartilage* **16**, 359-366 (2008).
114. B.D. Elder & Athanasiou, K.A. Effects of confinement on the mechanical properties of self-assembled articular cartilage constructs in the direction orthogonal to the confinement surface. *J Orthop Res* **26**, 238-246 (2008).
115. J.D. Kisiday, Kurz, B., DiMicco, M.A. & Grodzinsky, A.J. Evaluation of medium supplemented with insulin-transferrin-selenium for culture of primary bovine calf chondrocytes in three-dimensional hydrogel scaffolds. *Tissue Eng* **11**, 141-151 (2005).
116. L.W. Fisher, Stubbs, J.T., 3rd & Young, M.F. Antisera and cDNA probes to human and certain animal model bone matrix noncollagenous proteins. *Acta Orthop Scand Suppl* **266**, 61-65 (1995).
117. A.J. Almarza & Athanasiou, K.A. Seeding techniques and scaffolding choice for tissue engineering of the temporomandibular joint disk. *Tissue Eng* **10**, 1787-1795 (2004).
118. V.C. Mow, Kuei, S.C., Lai, W.M. & Armstrong, C.G. Biphasic creep and stress relaxation of articular cartilage in compression? Theory and experiments. *J Biomech Eng* **102**, 73-84 (1980).
119. V.C. Mow, Gibbs, M.C., Lai, W.M., Zhu, W.B. & Athanasiou, K.A. Biphasic indentation of articular cartilage--II. A numerical algorithm and an experimental study. *J Biomech* **22**, 853-861 (1989).
120. K.A. Athanasiou et al. Biomechanical properties of hip cartilage in experimental animal models. *Clin Orthop* **316**, 254-266 (1995).
121. C.Y. Huang, Soltz, M.A., Kopacz, M., Mow, V.C. & Ateshian, G.A. Experimental verification of the roles of intrinsic matrix viscoelasticity and tension-compression nonlinearity in the biphasic response of cartilage. *J Biomech Eng* **125**, 84-93 (2003).
122. A.C. Aufderheide & Athanasiou, K.A. Assessment of a bovine co-culture, scaffold-free method for growing meniscus-shaped constructs. *Tissue Eng* **13**, 2195-2205 (2007).

123. B.K. Slinker The statistics of synergism. *J Mol Cell Cardiol* **30**, 723-731 (1998).
124. P.S. Khalsa & Eisenberg, S.R. Compressive behavior of articular cartilage is not completely explained by proteoglycan osmotic pressure. *J Biomech* **30**, 589-594 (1997).
125. A.K. Williamson, Chen, A.C. & Sah, R.L. Compressive properties and function-composition relationships of developing bovine articular cartilage. *J Orthop Res* **19**, 1113-1121 (2001).
126. M.B. Schmidt, Mow, V.C., Chun, L.E. & Eyre, D.R. Effects of proteoglycan extraction on the tensile behavior of articular cartilage. *J Orthop Res* **8**, 353-363 (1990).
127. M.H. Schwartz, Leo, P.H. & Lewis, J.L. A microstructural model for the elastic response of articular cartilage. *J Biomech* **27**, 865-873 (1994).
128. G.E. Kempson, Muir, H., Pollard, C. & Tuke, M. The tensile properties of the cartilage of human femoral condyles related to the content of collagen and glycosaminoglycans. *Biochim Biophys Acta* **297**, 456-472 (1973).
129. T. Douglas, Heinemann, S., Bierbaum, S., Scharnweber, D. & Worch, H. Fibrillogenesis of collagen types I, II, and III with small leucine-rich proteoglycans decorin and biglycan. *Biomacromolecules* **7**, 2388-2393 (2006).
130. Z. Ferdous, Wei, V.M., Iozzo, R., Hook, M. & Grande-Allen, K.J. Decorin-transforming Growth Factor- Interaction Regulates Matrix Organization and Mechanical Characteristics of Three-dimensional Collagen Matrices. *J Biol Chem* **282**, 35887-35898 (2007).
131. H.D. Adkisson, Gillis, M.P., Davis, E.C., Maloney, W. & Hruska, K.A. In vitro generation of scaffold independent neocartilage. *Clin Orthop Relat Res*, S280-294 (2001).
132. M.M. Fedewa, Oegema, T.R., Jr., Schwartz, M.H., MacLeod, A. & Lewis, J.L. Chondrocytes in culture produce a mechanically functional tissue. *J Orthop Res* **16**, 227-236 (1998).
133. C.V. Gemmiti & Guldberg, R.E. Fluid flow increases type II collagen deposition and tensile mechanical properties in bioreactor-grown tissue-engineered cartilage. *Tissue Eng* **12**, 469-479 (2006).
134. B.E. Koop, Lewis, J.L., Fedewa, M.M. & Oegema, T.R., Jr. The effects of displacement rate and proteoglycan digestion on the fracture resistance of tissue grown from chondrocyte culture. *J Mater Sci Mater Med* **13**, 823-828 (2002).
135. J.L. Lewis, Johnson, S.L. & Oegema, T.R., Jr. Interfibrillar collagen bonding exists in matrix produced by chondrocytes in culture: evidence by electron microscopy. *Tissue Eng* **8**, 989-995 (2002).
136. N.K. Simha, Fedewa, M., Leo, P.H., Lewis, J.L. & Oegema, T. A composites theory predicts the dependence of stiffness of cartilage culture tissues on collagen volume fraction. *J Biomech* **32**, 503-509 (1999).
137. C.M. Revell, Reynolds, C.E. & Athanasiou, K.A. Effects of initial cell seeding in self assembly of articular cartilage. *Ann Biomed Eng* **36**, 1441-1448 (2008).

138. R.M. Natoli, Responte, D.J., Lu, B.Y. & Athanasiou, K.A. Effects of multiple chondroitinase ABC applications on tissue engineered articular cartilage *Journal of Orthopaedic Research*, 10.1002/jor.20821 (2009).
139. L. Bian et al. Influence of Temporary Chondroitinase ABC-Induced Glycosaminoglycan Suppression on Maturation of Tissue-Engineered Cartilage. *Tissue Eng Part A* (2009).
140. R.M. Natoli, Responte, D.J., Lu, B.Y. & Athanasiou, K.A. Effects of multiple chondroitinase ABC applications on tissue engineered articular cartilage. *J Orthop Res* (2009).
141. R.L. Mauck, Nicoll, S.B., Seyhan, S.L., Ateshian, G.A. & Hung, C.T. Synergistic action of growth factors and dynamic loading for articular cartilage tissue engineering. *Tissue Eng* **9**, 597-611 (2003).
142. D.J. Responte, Natoli, R.M. & Athanasiou, K.A. Collagens of articular cartilage: structure, function, and importance in tissue engineering. *Crit Rev Biomed Eng* **35**, 363-411 (2007).
143. R.K. Studer & Chu, C.R. p38 MAPK and COX2 inhibition modulate human chondrocyte response to TGF-beta. *J Orthop Res* **23**, 454-461 (2005).
144. C.D. Oh et al. Opposing role of mitogen-activated protein kinase subtypes, erk-1/2 and p38, in the regulation of chondrogenesis of mesenchymes. *J Biol Chem* **275**, 5613-5619 (2000).
145. Y.M. Yoon et al. Epidermal growth factor negatively regulates chondrogenesis of mesenchymal cells by modulating the protein kinase C-alpha, Erk-1, and p38 MAPK signaling pathways. *J Biol Chem* **275**, 12353-12359 (2000).
146. A.D. Weston, Chandraratna, R.A., Torchia, J. & Underhill, T.M. Requirement for RAR-mediated gene repression in skeletal progenitor differentiation. *J Cell Biol* **158**, 39-51 (2002).
147. T.K. Langsjo et al. Electron microscopic stereological study of collagen fibrils in bovine articular cartilage: volume and surface densities are best obtained indirectly (from length densities and diameters) using isotropic uniform random sampling. *J Anat* **195 (Pt 2)**, 281-293 (1999).
148. C. Weiss, Rosenberg, L. & Helfet, A.J. An ultrastructural study of normal young adult human articular cartilage. *J Bone Joint Surg Am* **50**, 663-674 (1968).
149. D.L. Christiansen, Huang, E.K. & Silver, F.H. Assembly of type I collagen: fusion of fibril subunits and the influence of fibril diameter on mechanical properties. *Matrix Biol* **19**, 409-420 (2000).
150. A. Asanbaeva et al. Articular cartilage tensile integrity: modulation by matrix depletion is maturation-dependent. *Arch Biochem Biophys* **474**, 175-182 (2008).
151. S. Calve, Lytle, I.F., Grosh, K., Brown, D.L. & Arruda, E.M. Implantation increases tensile strength and collagen content of self-assembled tendon constructs. *J Appl Physiol* **108**, 875-881 (2010).
152. K.A. Athanasiou, Agarwal, A. & Dzida, F.J. Comparative study of the intrinsic mechanical properties of the human acetabular and femoral head cartilage. *J Orthop Res* **12**, 340-349 (1994).

153. K.A. Athanasiou, Niederauer, G.G. & Schenck, R.C., Jr. Biomechanical topography of human ankle cartilage. *Ann Biomed Eng* **23**, 697-704 (1995).
154. J.P. Urban, Maroudas, A., Bayliss, M.T. & Dillon, J. Swelling pressures of proteoglycans at the concentrations found in cartilaginous tissues. *Biorheology* **16**, 447-464 (1979).
155. S.L. Woo, Akeson, W.H. & Jemmott, G.F. Measurements of nonhomogeneous, directional mechanical properties of articular cartilage in tension. *J Biomech* **9**, 785-791 (1976).
156. S.J. Bryant, Chowdhury, T.T., Lee, D.A., Bader, D.L. & Anseth, K.S. Crosslinking density influences chondrocyte metabolism in dynamically loaded photocrosslinked poly(ethylene glycol) hydrogels. *Ann Biomed Eng* **32**, 407-417 (2004).
157. J.M. Anderson Biological responses to materials. *Annual Reviews in Materials Research* **31**, 81-110 (2001).
158. C.B. Knudson & Knudson, W. Cartilage proteoglycans. *Semin Cell Dev Biol* **12**, 69-78 (2001).
159. S.P. Frean, Abraham, L.A. & Lees, P. In vitro stimulation of equine articular cartilage proteoglycan synthesis by hyaluronan and carprofen. *Res Vet Sci* **67**, 183-190 (1999).
160. K. Kawasaki, Ochi, M., Uchio, Y., Adachi, N. & Matsusaki, M. Hyaluronic acid enhances proliferation and chondroitin sulfate synthesis in cultured chondrocytes embedded in collagen gels. *J Cell Physiol* **179**, 142-148 (1999).
161. T. Kikuchi, Yamada, H. & Shimmei, M. Effect of high molecular weight hyaluronan on cartilage degeneration in a rabbit model of osteoarthritis. *Osteoarthritis Cartilage* **4**, 99-110 (1996).
162. K. Fukuda et al. Hyaluronic acid increases proteoglycan synthesis in bovine articular cartilage in the presence of interleukin-1. *J Pharmacol Exp Ther* **277**, 1672-1675 (1996).
163. R. Takeuchi et al. Effects of vibration and hyaluronic acid on activation of three-dimensional cultured chondrocytes. *Arthritis Rheum* **54**, 1897-1905 (2006).
164. M.W. Holmes, Bayliss, M.T. & Muir, H. Hyaluronic acid in human articular cartilage. Age-related changes in content and size. *Biochem J* **250**, 435-441 (1988).
165. B. Mansson, Wenglen, C., Morgelin, M., Saxne, T. & Heinegard, D. Association of chondroadherin with collagen type II. *J Biol Chem* **276**, 32883-32888 (2001).
166. H.A. Leddy, Awad, H.A. & Guilak, F. Molecular diffusion in tissue-engineered cartilage constructs: effects of scaffold material, time, and culture conditions. *J Biomed Mater Res B Appl Biomater* **70**, 397-406 (2004).
167. A.I. Caplan Tissue engineering designs for the future: new logics, old molecules. *Tissue Eng* **6**, 1-8 (2000).

168. C.B. Knudson Hyaluronan receptor-directed assembly of chondrocyte pericellular matrix. *J Cell Biol* **120**, 825-834 (1993).
169. S. Ohno, Im, H.J., Knudson, C.B. & Knudson, W. Hyaluronan oligosaccharides induce matrix metalloproteinase 13 via transcriptional activation of NFkappaB and p38 MAP kinase in articular chondrocytes. *J Biol Chem* **281**, 17952-17960 (2006).
170. A. Shimazu et al. Effects of hyaluronic acid on the release of proteoglycan from the cell matrix in rabbit chondrocyte cultures in the presence and absence of cytokines. *Arthritis Rheum* **36**, 247-253 (1993).
171. E.A. Morris, Wilcon, S. & Treadwell, B.V. Inhibition of interleukin 1-mediated proteoglycan degradation in bovine articular cartilage explants by addition of sodium hyaluronate. *Am J Vet Res* **53**, 1977-1982 (1992).
172. G. Abatangelo et al. Intraarticular sodium hyaluronate injections in the Pond-Nuki experimental model of osteoarthritis in dogs. I. Biochemical results. *Clin Orthop Relat Res*, 278-285 (1989).
173. Y. Kato, Mukudai, Y., Okimura, A., Shimazu, A. & Nakamura, S. Effects of hyaluronic acid on the release of cartilage matrix proteoglycan and fibronectin from the cell matrix layer of chondrocyte cultures: interactions between hyaluronic acid and chondroitin sulfate glycosaminoglycan. *J Rheumatol Suppl* **43**, 158-159 (1995).
174. L. Haglund et al. Identification and characterization of the integrin alpha2beta1 binding motif in chondroadherin mediating cell attachment. *J Biol Chem* **286**, 3925-3934 (2011).
175. K. Ishiguro et al. Syndecan-4 deficiency leads to high mortality of lipopolysaccharide-injected mice. *J Biol Chem* **276**, 47483-47488 (2001).
176. W. Knudson & Loeser, R.F. CD44 and integrin matrix receptors participate in cartilage homeostasis. *Cell Mol Life Sci* **59**, 36-44 (2002).
177. L.Y. Bourguignon, Singleton, P.A., Zhu, H. & Zhou, B. Hyaluronan promotes signaling interaction between CD44 and the transforming growth factor beta receptor I in metastatic breast tumor cells. *J Biol Chem* **277**, 39703-39712 (2002).
178. B.D. Elder & Athanasiou, K.A. Systematic assessment of growth factor treatment on biochemical and biomechanical properties of engineered articular cartilage constructs. *Osteoarthritis Cartilage* **17**, 114-123 (2009).
179. T. Ito, Williams, J.D., Fraser, D.J. & Phillips, A.O. Hyaluronan regulates transforming growth factor-beta1 receptor compartmentalization. *J Biol Chem* **279**, 25326-25332 (2004).
180. C.M. McKee et al. Hyaluronan (HA) fragments induce chemokine gene expression in alveolar macrophages. The role of HA size and CD44. *J Clin Invest* **98**, 2403-2413 (1996).
181. D. Huang, Sherman, BT, Lempicki, RA Systematic and integrative analysis of large gene lists using DAVID Bioinformatics Resources. *Nature Protoc.* **4**, 44-57 (2009).
182. J.M. Hootman & Helmick, C.G. Projections of US prevalence of arthritis and associated activity limitations. *Arthritis Rheum* **54**, 226-229 (2006).

183. J.P. Urban The chondrocyte: a cell under pressure. *Br J Rheumatol* **33**, 901-908 (1994).
184. M.J. Kujawa, Carrino, D.A. & Caplan, A.I. Substrate-bonded hyaluronic acid exhibits a size-dependent stimulation of chondrogenic differentiation of stage 24 limb mesenchymal cells in culture. *Dev Biol* **114**, 519-528 (1986).
185. W. Knudson & Knudson, C.B. Assembly of a chondrocyte-like pericellular matrix on non-chondrogenic cells. Role of the cell surface hyaluronan receptors in the assembly of a pericellular matrix. *J Cell Sci* **99 (Pt 2)**, 227-235 (1991).
186. N.J. Goodstone, Cartwright, A. & Ashton, B. Effects of high molecular weight hyaluronan on chondrocytes cultured within a resorbable gelatin sponge. *Tissue Eng* **10**, 621-631 (2004).
187. D.J. Huey & Athanasiou, K.A. Maturational growth of self-assembled, functional menisci as a result of TGF-beta1 and enzymatic chondroitinase-ABC stimulation. *Biomaterials* **32**, 2052-2058 (2011).
188. A. Maroudas, Wachtel, E., Grushko, G., Katz, E.P. & Weinberg, P. The effect of osmotic and mechanical pressures on water partitioning in articular cartilage. *Biochim Biophys Acta* **1073**, 285-294 (1991).
189. I.S. Kovach & Athanasiou, K.A. Small-angle HeNe laser light scatter and the compressive modulus of articular cartilage. *J Orthop Res* **15**, 437-441 (1997).
190. S.H. Lee & Shin, H. Matrices and scaffolds for delivery of bioactive molecules in bone and cartilage tissue engineering. *Adv Drug Deliv Rev* **59**, 339-359 (2007).
191. B.K. Mann, Schmedlen, R.H. & West, J.L. Tethered-TGF-beta increases extracellular matrix production of vascular smooth muscle cells. *Biomaterials* **22**, 439-444 (2001).
192. D.M. Yoon, Curtiss, S., Reddi, A.H. & Fisher, J.P. Addition of hyaluronic acid to alginate embedded chondrocytes interferes with insulin-like growth factor-1 signaling in vitro and in vivo. *Tissue Eng Part A* **15**, 3449-3459 (2009).
193. G.A. Homandberg, Ummadi, V. & Kang, H. The role of insulin-like growth factor-I in hyaluronan mediated repair of cultured cartilage explants. *Inflamm Res* **53**, 396-404 (2004).
194. J.A. Buckwalter Articular cartilage: injuries and potential for healing. *J Orthop Sports Phys Ther* **28**, 192-202 (1998).
195. H. Kurosawa, Fukubayashi, T. & Nakajima, H. Load-bearing mode of the knee joint: physical behavior of the knee joint with or without menisci. *Clinical orthopaedics and related research*, 283-290 (1980).
196. S.L. Woo et al. Injury and repair of ligaments and tendons. *Annu Rev Biomed Eng* **2**, 83-118 (2000).
197. A.J. Almarza & Athanasiou, K.A. Design characteristics for the tissue engineering of cartilaginous tissues. *Ann Biomed Eng* **32**, 2-17 (2004).
198. J.R. Ralphs & Benjamin, M. The joint capsule: structure, composition, ageing and disease. *Journal of anatomy* **184 (Pt 3)**, 503-509 (1994).

199. D.J. Responte, Natoli, R.M. & Athanasiou, K.A. Collagens of articular cartilage: structure, function, and importance in tissue engineering. *Critical reviews in biomedical engineering* **35**, 363-411 (2007).
200. N.D. Broom Further insights into the structural principles governing the function of articular cartilage. *J Anat* **139 (Pt 2)**, 275-294 (1984).
201. in American Academy of Orthopaedic SurgeonsRosemount, IL; 2008).
202. L.S. Lohmander, Englund, P.M., Dahl, L.L. & Roos, E.M. The long-term consequence of anterior cruciate ligament and meniscus injuries: osteoarthritis. *The American journal of sports medicine* **35**, 1756-1769 (2007).
203. K.L. Ong, Lau, E., Suggs, J., Kurtz, S.M. & Manley, M.T. Risk of subsequent revision after primary and revision total joint arthroplasty. *Clin Orthop Relat Res* **468**, 3070-3076 (2010).
204. S.A. Barbour & King, W. The safe and effective use of allograft tissue--an update. *Am J Sports Med* **31**, 791-797 (2003).
205. C.J. Walsh, Goodman, D., Caplan, A.I. & Goldberg, V.M. Meniscus regeneration in a rabbit partial meniscectomy model. *Tissue Eng* **5**, 327-337 (1999).
206. D.L. Butler et al. Functional tissue engineering for tendon repair: A multidisciplinary strategy using mesenchymal stem cells, bioscaffolds, and mechanical stimulation. *J Orthop Res* **26**, 1-9 (2008).
207. S. Calve et al. Engineering of functional tendon. *Tissue Eng* **10**, 755-761 (2004).
208. J.W. Hayami, Surrao, D.C., Waldman, S.D. & Amsden, B.G. Design and characterization of a biodegradable composite scaffold for ligament tissue engineering. *J Biomed Mater Res A* **92**, 1407-1420 (2010).
209. A.M. Reginato, Iozzo, R.V. & Jimenez, S.A. Formation of nodular structures resembling mature articular cartilage in long-term primary cultures of human fetal epiphyseal chondrocytes on a hydrogel substrate. *Arthritis Rheum* **37**, 1338-1349 (1994).
210. F.T. Moutos, Freed, L.E. & Guilak, F. A biomimetic three-dimensional woven composite scaffold for functional tissue engineering of cartilage. *Nat Mater* **6**, 162-167 (2007).
211. F. Van Eijk et al. Tissue engineering of ligaments: a comparison of bone marrow stromal cells, anterior cruciate ligament, and skin fibroblasts as cell source. *Tissue Eng* **10**, 893-903 (2004).
212. Q.A. Louw, Manilall, J. & Grimmer, K.A. Epidemiology of knee injuries among adolescents: a systematic review. *Br J Sports Med* **42**, 2-10 (2008).
213. G.M. Hoben & Athanasiou, K.A. Creating a spectrum of fibrocartilages through different cell sources and biochemical stimuli. *Biotechnol Bioeng* **100**, 587-598 (2008).
214. R.L. Sah, Trippel, S.B. & Grodzinsky, A.J. Differential effects of serum, insulin-like growth factor-I, and fibroblast growth factor-2 on the maintenance of cartilage physical properties during long-term culture. *J Orthop Res* **14**, 44-52 (1996).

215. J.J. Lim, Scott, L., Jr. & Temenoff, J.S. Aggregation of bovine anterior cruciate ligament fibroblasts or marrow stromal cells promotes aggrecan production. *Biotechnology and bioengineering* **108**, 151-162 (2011).
216. R.A. Bank et al. Sensitive fluorimetric quantitation of pyridinium and pentosidine crosslinks in biological samples in a single high-performance liquid chromatographic run. *J Chromatogr B Biomed Sci Appl* **703**, 37-44 (1997).
217. J.A. Merida-Velasco et al. Development of the human knee joint ligaments. *The Anatomical record* **248**, 259-268 (1997).
218. T. Fukubayashi & Kurosawa, H. The contact area and pressure distribution pattern of the knee. A study of normal and osteoarthrotic knee joints. *Acta Orthop Scand* **51**, 871-879 (1980).
219. Y. Hoshikawa, Kurosawa, H., Fukubayashi, T., Nakajima, H. & Watarai, K. The prognosis of meniscectomy in athletes. The simple meniscus lesions without ligamentous instabilities. *The American journal of sports medicine* **11**, 8-13 (1983).
220. W.M. Elbjeirami, Yonter, E.O., Starcher, B.C. & West, J.L. Enhancing mechanical properties of tissue-engineered constructs via lysyl oxidase crosslinking activity. *J Biomed Mater Res A* **66**, 513-521 (2003).
221. S. Tanimori, Fukubayashi, K. & Kirihata, M. Synthesis of the spirosuccinimide moiety of Asperparaline A. *Biosci Biotechnol Biochem* **64**, 1758-1760 (2000).
222. M.Y. Berezin & Achilefu, S. Fluorescence lifetime measurements and biological imaging. *Chem Rev* **110**, 2641-2684.
223. C.A. Chorvat D Multi-wavelength fluorescence lifetime spectroscopy: a new approach to the study of endogenous fluorescence in living cells and tissues. . *Laser Phys Lett.* **6**, 175-193 (2009).
224. K. Svanberg et al. Laser-based spectroscopic methods in tissue characterization. *Ann N Y Acad Sci* **838**, 123-129 (1998).
225. G.E. Kochiadakis et al. The role of laser-induced fluorescence in myocardial tissue characterization: an experimental in vitro study. *Chest* **120**, 233-239 (2001).
226. L.J. Albrecht C Principles of fluorescence spectroscopy. *Analytical and Bioanalytical Chemistry* **390**, 1223-1224 (2008).
227. D. Elson et al. Time-domain fluorescence lifetime imaging applied to biological tissue. *Photochem Photobiol Sci* **3**, 795-801 (2004).
228. P. Ashjian et al. Noninvasive in situ evaluation of osteogenic differentiation by time-resolved laser-induced fluorescence spectroscopy. *Tissue Eng* **10**, 411-420 (2004).
229. B.Z. Fite et al. Noninvasive multimodal evaluation of bioengineered cartilage constructs combining time-resolved fluorescence and ultrasound imaging. *Tissue Eng Part C Methods* **17**, 495-504.
230. F.S. Foster et al. Principles and applications of ultrasound backscatter microscopy. *IEEE Trans Ultrason Ferroelectr Freq Control* **40**, 608-617 (1993).

231. D. McPherson Tissue Characterization by Ultrasound: What is Possible Now? What Will be Possible? *Echocardiography* **8**, 77-91 (1991).
232. T.H. Kawasaki M, Noda T, Ito Y, Kunishima A, Arai M Noninvasive quantitative tissue characterization and two-dimensional color-coded map of human atherosclerotic lesions using ultrasound integrated backscatter: Comparison between histology and integrated backscatter images. . *J Am Coll Cardiol* **38**, 486-492 (2001).
233. R.D. Langevin HM, Fox JR, Badger GJ, Wu J, Konofagou EE, Stevens-Tuttle D, Bouffard NA, Krag MH Dynamic morphometric characterization of local connective tissue network structure in humans using ultrasound. *BMC Systems Biology* **1** (2007).
234. S.L. Bridal, Fournier, C., Coron, A., Leguerney, I. & Laugier, P. Ultrasonic backscatter and attenuation (11-27 MHz) variation with collagen fiber distribution in ex vivo human dermis. *Ultrason Imaging* **28**, 23-40 (2006).
235. D.N. Stephens, Park, J., Sun, Y., Papaioannou, T. & Marcu, L. Intraluminal fluorescence spectroscopy catheter with ultrasound guidance. *J Biomed Opt* **14**, 030505 (2009).
236. Y. Sun et al. Development of a dual-modal tissue diagnostic system combining time-resolved fluorescence spectroscopy and ultrasonic backscatter microscopy. *Rev Sci Instrum* **80**, 065104 (2009).
237. H.Y. Wang SZ, Saarakkala S, Zheng YP Quantitative Assessment of Articular Cartilage with Morphologic, Acoustic and Mechanical Properties Obtained Using High-Frequency Ultrasound. *Ultrasound Med Biol* **36**, 512-527 (2010).
238. D.R. Richards-Kortum R, Sokolov K, Pavlova I, Pollen M in Handbook of Biomedical Fluorescence (CRC Press, 2003).
239. W.S. Saarakkala S, Huang YP, Zheng YP Quantification of the optical surface reflection and surface roughness of articular cartilage using optical coherence tomography. *Phys Med Biol* **54**, 6837-6852 (2009).
240. M.D. Forman, Malamet, R. & Kaplan, D. A survey of osteoarthritis of the knee in the elderly. *J Rheumatol* **10**, 282-287 (1983).
241. C.G. Armstrong & Mow, V.C. Variations in the intrinsic mechanical properties of human articular cartilage with age, degeneration, and water content. *J Bone Joint Surg Am* **64**, 88-94 (1982).
242. C.G. Peterfy Scratching the surface: articular cartilage disorders in the knee. *Magn Reson Imaging Clin N Am* **8**, 409-430 (2000).
243. J. Lakowicz Principles of fluorescence spectroscopy, Edn. 2. (Kluwer Academic/Plenum, New York; 1999).
244. J.Y. Reginster The prevalence and burden of arthritis. *Rheumatology (Oxford)* **41 Supp 1**, 3-6 (2002).
245. J. Borrelli, Jr. & Ricci, W.M. Acute effects of cartilage impact. *Clin Orthop* **423**, 33-39 (2004).
246. S.E. Carver & Heath, C.A. Influence of intermittent pressure, fluid flow, and mixing on the regenerative properties of articular chondrocytes. *Biotechnol Bioeng* **65**, 274-281 (1999).

247. I. Martin et al. Modulation of the mechanical properties of tissue engineered cartilage. *Biorheology* **37**, 141-147 (2000).
248. S.D. Waldman, Grynpas, M.D., Pilliar, R.M. & Kandel, R.A. Characterization of cartilagenous tissue formed on calcium polyphosphate substrates in vitro. *J Biomed Mater Res* **62**, 323-330 (2002).
249. D.J. Kelly et al. Biochemical markers of the mechanical quality of engineered hyaline cartilage. *J Mater Sci Mater Med* **18**, 273-281 (2007).
250. E. Reichenberger, Aigner, T., von der Mark, K., Stoss, H. & Bertling, W. In situ hybridization studies on the expression of type X collagen in fetal human cartilage. *Dev Biol* **148**, 562-572 (1991).
251. C. Yang et al. Apoptosis of chondrocytes in transgenic mice lacking collagen II. *Exp Cell Res* **235**, 370-373 (1997).
252. J.J. Wu, Woods, P.E. & Eyre, D.R. Identification of cross-linking sites in bovine cartilage type IX collagen reveals an antiparallel type II-type IX molecular relationship and type IX to type IX bonding. *J Biol Chem* **267**, 23007-23014 (1992).
253. B.R. Olsen Collagen IX. *Int J Biochem Cell Biol* **29**, 555-558 (1997).
254. F. Mwale, Tchetina, E., Wu, C.W. & Poole, A.R. The assembly and remodeling of the extracellular matrix in the growth plate in relationship to mineral deposition and cellular hypertrophy: an in situ study of collagens II and IX and proteoglycan. *J Bone Miner Res* **17**, 275-283 (2002).
255. R. Dreier, Opolka, A., Grifka, J., Bruckner, P. & Grassel, S. Collagen IX-deficiency seriously compromises growth cartilage development in mice. *Matrix Biol* **30**, 30 (2008).
256. A. Opolka et al. Collagen IX is indispensable for timely maturation of cartilage during fracture repair in mice. *Matrix Biol* **26**, 85-95 (2007).
257. Y. Muragaki et al. A mutation in the gene encoding the alpha 2 chain of the fibril-associated collagen IX, COL9A2, causes multiple epiphyseal dysplasia (EDM2). *Nat Genet* **12**, 103-105 (1996).
258. K.E. Gregory et al. Structural organization of distinct domains within the non-collagenous N-terminal region of collagen type XI. *J Biol Chem* **275**, 11498-11506 (2000).
259. R. Seegmiller, Fraser, F.C. & Sheldon, H. A new chondrodystrophic mutant in mice. Electron microscopy of normal and abnormal chondrogenesis. *J Cell Biol* **48**, 580-593 (1971).
260. C.A. Poole, Ayad, S. & Schofield, J.R. Chondrons from articular cartilage: I. Immunolocalization of type VI collagen in the pericellular capsule of isolated canine tibial chondrons. *J Cell Sci* **90 (Pt 4)**, 635-643 (1988).
261. P. Bonaldo, Russo, V., Bucciotti, F., Doliana, R. & Colombatti, A. Structural and functional features of the alpha 3 chain indicate a bridging role for chicken collagen VI in connective tissues. *Biochemistry* **29**, 1245-1254 (1990).
262. F. Guilak et al. The pericellular matrix as a transducer of biomechanical and biochemical signals in articular cartilage. *Ann N Y Acad Sci* **1068**, 498-512 (2006).

263. R. Quarto, Dozin, B., Bonaldo, P., Cancedda, R. & Colombatti, A. Type VI collagen expression is upregulated in the early events of chondrocyte differentiation. *Development* **117**, 245-251 (1993).
264. E.H. Morrison, Ferguson, M.W., Bayliss, M.T. & Archer, C.W. The development of articular cartilage: I. The spatial and temporal patterns of collagen types. *J Anat* **189 (Pt 1)**, 9-22 (1996).
265. Y.S. Bland & Ashhurst, D.E. The hip joint: the fibrillar collagens associated with development and ageing in the rabbit. *J Anat* **198**, 17-27 (2001).
266. T. Furukawa, Eyre, D.R., Koide, S. & Glimcher, M.J. Biochemical studies on repair cartilage resurfacing experimental defects in the rabbit knee. *J Bone Joint Surg Am* **62**, 79-89 (1980).
267. X. Wei, Gao, J. & Messner, K. Maturation-dependent repair of untreated osteochondral defects in the rabbit knee joint. *J Biomed Mater Res* **34**, 63-72 (1997).
268. P.D. Benya & Shaffer, J.D. Dedifferentiated chondrocytes reexpress the differentiated collagen phenotype when cultured in agarose gels. *Cell* **30**, 215-224 (1982).
269. T. Kirsch & von der Mark, K. Isolation of human type X collagen and immunolocalization in fetal human cartilage. *Eur J Biochem* **196**, 575-580 (1991).
270. G.D. Walker, Fischer, M., Gannon, J., Thompson, R.C., Jr. & Oegema, T.R., Jr. Expression of type-X collagen in osteoarthritis. *J Orthop Res* **13**, 4-12 (1995).
271. I. Girkontaite et al. Immunolocalization of type X collagen in normal fetal and adult osteoarthritic cartilage with monoclonal antibodies. *Matrix Biol* **15**, 231-238 (1996).
272. P. Castagnola, Moro, G., Descalzi-Cancedda, F. & Cancedda, R. Type X collagen synthesis during in vitro development of chick embryo tibial chondrocytes. *J Cell Biol* **102**, 2310-2317 (1986).
273. R.C. Siegel Collagen cross-linking. Synthesis of collagen cross-links in vitro with highly purified lysyl oxidase. *J Biol Chem* **251**, 5786-5792 (1976).
274. A.P. Hollander et al. Maturation of tissue engineered cartilage implanted in injured and osteoarthritic human knees. *Tissue Eng* **12**, 1787-1798 (2006).
275. P. Ulrich & Cerami, A. Protein glycation, diabetes, and aging. *Recent Prog Horm Res* **56**, 1-21 (2001).
276. A.C. Chen et al. Induction of advanced glycation end products and alterations of the tensile properties of articular cartilage. *Arthritis Rheum* **46**, 3212-3217 (2002).
277. N. Verzijl et al. Age-related accumulation of Maillard reaction products in human articular cartilage collagen. *Biochem J* **350 Pt 2**, 381-387 (2000).
278. R.A. Bank, Bayliss, M.T., Lafeber, F.P., Maroudas, A. & Tekoppele, J.M. Ageing and zonal variation in post-translational modification of collagen in normal human articular cartilage. The age-related increase in non-enzymatic glycation affects biomechanical properties of cartilage. *Biochem J* **330 (Pt 1)**, 345-351 (1998).

279. D.R. Eyre, Dickson, I.R. & Van Ness, K. Collagen cross-linking in human bone and articular cartilage. Age-related changes in the content of mature hydroxypyridinium residues. *Biochem J* **252**, 495-500 (1988).
280. J. Riesle, Hollander, A.P., Langer, R., Freed, L.E. & Vunjak-Novakovic, G. Collagen in tissue-engineered cartilage: types, structure, and crosslinks. *J Cell Biochem* **71**, 313-327 (1998).
281. H.K. Graham, Holmes, D.F., Watson, R.B. & Kadler, K.E. Identification of collagen fibril fusion during vertebrate tendon morphogenesis. The process relies on unipolar fibrils and is regulated by collagen-proteoglycan interaction. *J Mol Biol* **295**, 891-902 (2000).
282. D.F. Holmes, Graham, H.K., Trotter, J.A. & Kadler, K.E. STEM/TEM studies of collagen fibril assembly. *Micron* **32**, 273-285 (2001).
283. D. Eyre Collagen of articular cartilage. *Arthritis Res* **4**, 30-35 (2002).
284. H. Muir, Bullough, P. & Maroudas, A. The distribution of collagen in human articular cartilage with some of its physiological implications. *J Bone Joint Surg Br* **52**, 554-563 (1970).
285. A. Benninghoff Form und Bau der Gelenkknorpel in ihren Beziehungen zur Funktion. *Cell and Tissue Research* **2**, 783-862 (1925).
286. C.J. Moger et al. Regional variations of collagen orientation in normal and diseased articular cartilage and subchondral bone determined using small angle X-ray scattering (SAXS). *Osteoarthritis Cartilage* **15**, 682-687 (2007).
287. M. Wong & Carter, D.R. Articular cartilage functional histomorphology and mechanobiology: a research perspective. *Bone* **33**, 1-13 (2003).
288. F. Guilak & Mow, V.C. The mechanical environment of the chondrocyte: a biphasic finite element model of cell-matrix interactions in articular cartilage. *J Biomech* **33**, 1663-1673 (2000).
289. F. Guilak, Jones, W.R., Ting-Beall, H.P. & Lee, G.M. The deformation behavior and mechanical properties of chondrocytes in articular cartilage. *Osteoarthritis Cartilage* **7**, 59-70 (1999).
290. L.G. Alexopoulos, Haider, M.A., Vail, T.P. & Guilak, F. Alterations in the mechanical properties of the human chondrocyte pericellular matrix with osteoarthritis. *J Biomech Eng* **125**, 323-333 (2003).
291. L.G. Alexopoulos, Setton, L.A. & Guilak, F. The biomechanical role of the chondrocyte pericellular matrix in articular cartilage. *Acta Biomater* **1**, 317-325 (2005).
292. E. Ruoslahti & Yamaguchi, Y. Proteoglycans as modulators of growth factor activities. *Cell* **64**, 867-869 (1991).
293. S.K. de Visser et al. Anisotropy of collagen fibre alignment in bovine cartilage: comparison of polarised light microscopy and spatially resolved diffusion-tensor measurements. *Osteoarthritis Cartilage* **16**, 16 (2007).
294. M.J. Kaab, Gwynn, I.A. & Notzli, H.P. Collagen fibre arrangement in the tibial plateau articular cartilage of man and other mammalian species. *J Anat* **193 (Pt 1)**, 23-34 (1998).
295. J.M. Clark The organisation of collagen fibrils in the superficial zones of articular cartilage. *J Anat* **171**, 117-130 (1990).

296. P. Bullough & Goodfellow, J. The significance of the fine structure of articular cartilage. *J Bone Joint Surg Br* **50**, 852-857 (1968).
297. G. Meachim, Denham, D., Emery, I.H. & Wilkinson, P.H. Collagen alignments and artificial splits at the surface of human articular cartilage. *J Anat* **118**, 101-118 (1974).
298. S. Below, Arnoczky, S.P., Dodds, J., Kooima, C. & Walter, N. The split-line pattern of the distal femur: A consideration in the orientation of autologous cartilage grafts. *Arthroscopy* **18**, 613-617 (2002).
299. Y.S. Bland & Ashhurst, D.E. Development and ageing of the articular cartilage of the rabbit knee joint: distribution of the fibrillar collagens. *Anat Embryol (Berl)* **194**, 607-619 (1996).
300. J.M. Clark, Norman, A. & Notzli, H. Postnatal development of the collagen matrix in rabbit tibial plateau articular cartilage. *J Anat* **191 (Pt 2)**, 215-221 (1997).
301. J. Foolen et al. Collagen orientation in periosteum and perichondrium is aligned with preferential directions of tissue growth. *J Orthop Res* **26**, 1263-1268 (2008).
302. W. Wilson, Driessen, N.J., van Donkelaar, C.C. & Ito, K. Prediction of collagen orientation in articular cartilage by a collagen remodeling algorithm. *Osteoarthritis Cartilage* **14**, 1196-1202 (2006).
303. D.R. Henshaw, Attia, E., Bhargava, M. & Hannafin, J.A. Canine ACL fibroblast integrin expression and cell alignment in response to cyclic tensile strain in three-dimensional collagen gels. *J Orthop Res* **24**, 481-490 (2006).
304. Y. Nabeshima, Grood, E.S., Sakurai, A. & Herman, J.H. Uniaxial tension inhibits tendon collagen degradation by collagenase in vitro. *J Orthop Res* **14**, 123-130 (1996).
305. J.W. Ruberti & Hallab, N.J. Strain-controlled enzymatic cleavage of collagen in loaded matrix. *Biochem Biophys Res Commun* **336**, 483-489 (2005).
306. H. Watanabe, Yamada, Y. & Kimata, K. Roles of aggrecan, a large chondroitin sulfate proteoglycan, in cartilage structure and function. *J Biochem* **124**, 687-693 (1998).
307. E. Hedbom et al. Cartilage matrix proteins. An acidic oligomeric protein (COMP) detected only in cartilage. *J Biol Chem* **267**, 6132-6136 (1992).
308. K. Rosenberg, Olsson, H., Morgelin, M. & Heinegard, D. Cartilage oligomeric matrix protein shows high affinity zinc-dependent interaction with triple helical collagen. *J Biol Chem* **273**, 20397-20403 (1998).
309. L. Cao et al. beta-Integrin-collagen interaction reduces chondrocyte apoptosis. *Matrix Biol* **18**, 343-355 (1999).
310. M.Y. Lo & Kim, H.T. Chondrocyte apoptosis induced by collagen degradation: inhibition by caspase inhibitors and IGF-1. *J Orthop Res* **22**, 140-144 (2004).
311. B. Beekman, Verzijl, N., Bank, R.A., von der Mark, K. & TeKoppele, J.M. Synthesis of collagen by bovine chondrocytes cultured in alginate;

posttranslational modifications and cell-matrix interaction. *Exp Cell Res* **237**, 135-141 (1997).

312. P.M. van der Kraan, Buma, P., van Kuppevelt, T. & van den Berg, W.B. Interaction of chondrocytes, extracellular matrix and growth factors: relevance for articular cartilage tissue engineering. *Osteoarthritis Cartilage* **10**, 631-637 (2002).
313. H.J. Kim & Kirsch, T. Collagen/annexin V interactions regulate chondrocyte mineralization. *J Biol Chem* **283**, 10310-10317 (2008).
314. W. Wang, Xu, J. & Kirsch, T. Annexin V and terminal differentiation of growth plate chondrocytes. *Exp Cell Res* **305**, 156-165 (2005).
315. T. Bengtsson et al. Loss of alpha10beta1 integrin expression leads to moderate dysfunction of growth plate chondrocytes. *J Cell Sci* **118**, 929-936 (2005).
316. D. Garciadiego-Cazares, Rosales, C., Katoh, M. & Chimal-Monroy, J. Coordination of chondrocyte differentiation and joint formation by alpha5beta1 integrin in the developing appendicular skeleton. *Development* **131**, 4735-4742 (2004).
317. C.Y. Huang, Stankiewicz, A., Ateshian, G.A. & Mow, V.C. Anisotropy, inhomogeneity, and tension-compression nonlinearity of human glenohumeral cartilage in finite deformation. *J Biomech* **38**, 799-809 (2005).
318. M.A. Soltz & Ateshian, G.A. A Conewise Linear Elasticity mixture model for the analysis of tension-compression nonlinearity in articular cartilage. *J Biomech Eng* **122**, 576-586 (2000).
319. Z.P. Luo, Sun, Y.L., Fujii, T. & An, K.N. Single molecule mechanical properties of type II collagen and hyaluronan measured by optical tweezers. *Biorheology* **41**, 247-254 (2004).
320. M.D. Wang, Yin, H., Landick, R., Gelles, J. & Block, S.M. Stretching DNA with optical tweezers. *Biophys J* **72**, 1335-1346 (1997).
321. S. Cusack & Miller, A. Determination of the elastic constants of collagen by Brillouin light scattering *Journal of Molecular Biology* **135**, 39-51 (1979).
322. R. Harley, James, D., Miller, A. & White, J.W. Phonons and the elastic moduli of collagen and muscle. *Nature* **267**, 285-287 (1977).
323. N. Sasaki & Odajima, S. Stress-strain curve and Young's modulus of a collagen molecule as determined by the X-ray diffraction technique. *J Biomech* **29**, 655-658 (1996).
324. R.C. Haut & Little, R.W. A constitutive equation for collagen fibers. *J Biomech* **5**, 423-430 (1972).
325. L.P. Li & Herzog, W. The role of viscoelasticity of collagen fibers in articular cartilage: theory and numerical formulation. *Biorheology* **41**, 181-194 (2004).
326. F.H. Silver, Bradica, G. & Tria, A. Elastic energy storage in human articular cartilage: estimation of the elastic modulus for type II collagen and changes associated with osteoarthritis. *Matrix Biol* **21**, 129-137 (2002).

327. T. Farquhar, Dawson, P.R. & Torzilli, P.A. A microstructural model for the anisotropic drained stiffness of articular cartilage. *J Biomech Eng* **112**, 414-425 (1990).
328. M. Fortin, Soulhat, J., Shirazi-Adl, A., Hunziker, E.B. & Buschmann, M.D. Unconfined compression of articular cartilage: nonlinear behavior and comparison with a fibril-reinforced biphasic model. *J Biomech Eng* **122**, 189-195 (2000).
329. J.J. Garcia & Cortes, D.H. A biphasic viscohyperelastic fibril-reinforced model for articular cartilage: formulation and comparison with experimental data. *J Biomech* **40**, 1737-1744 (2007).
330. P. Julkunen, Kiviranta, P., Wilson, W., Jurvelin, J.S. & Korhonen, R.K. Characterization of articular cartilage by combining microscopic analysis with a fibril-reinforced finite-element model. *J Biomech* **40**, 1862-1870 (2007).
331. R.K. Korhonen et al. Fibril reinforced poroelastic model predicts specifically mechanical behavior of normal, proteoglycan depleted and collagen degraded articular cartilage. *J Biomech* **36**, 1373-1379 (2003).
332. L. Li, Shirazi-Adl, A. & Buschmann, M.D. Investigation of mechanical behavior of articular cartilage by fibril reinforced poroelastic models. *Biorheology* **40**, 227-233 (2003).
333. L.P. Li, Buschmann, M.D. & Shirazi-Adl, A. A fibril reinforced nonhomogeneous poroelastic model for articular cartilage: inhomogeneous response in unconfined compression. *J Biomech* **33**, 1533-1541 (2000).
334. L.P. Li & Herzog, W. Strain-rate dependence of cartilage stiffness in unconfined compression: the role of fibril reinforcement versus tissue volume change in fluid pressurization. *J Biomech* **37**, 375-382 (2004).
335. L.P. Li, Korhonen, R.K., Iivarinen, J., Jurvelin, J.S. & Herzog, W. Fluid pressure driven fibril reinforcement in creep and relaxation tests of articular cartilage. *Med Eng Phys* **30**, 182-189 (2008).
336. L.P. Li, Soulhat, J., Buschmann, M.D. & Shirazi-Adl, A. Nonlinear analysis of cartilage in unconfined ramp compression using a fibril reinforced poroelastic model. *Clin Biomech (Bristol, Avon)* **14**, 673-682 (1999).
337. R. Shirazi & Shirazi-Adl, A. Analysis of articular cartilage as a composite using nonlinear membrane elements for collagen fibrils. *Med Eng Phys* **27**, 827-835 (2005).
338. R. Shirazi & Shirazi-Adl, A. Deep vertical collagen fibrils play a significant role in mechanics of articular cartilage. *J Orthop Res* **26**, 608-615 (2008).
339. J. Soulhat, Buschmann, M.D. & Shirazi-Adl, A. A fibril-network-reinforced biphasic model of cartilage in unconfined compression. *J Biomech Eng* **121**, 340-347 (1999).
340. W. Wilson, van Donkelaar, C.C., van Rietbergen, B. & Huiskes, R. A fibril-reinforced poroviscoelastic swelling model for articular cartilage. *J Biomech* **38**, 1195-1204 (2005).
341. W. Wilson, van Donkelaar, C.C., van Rietbergen, B., Ito, K. & Huiskes, R. Stresses in the local collagen network of articular cartilage: a

poroviscoelastic fibril-reinforced finite element study. *J Biomech* **37**, 357-366 (2004).
342. R.M. Aspden Fibre reinforcing by collagen in cartilage and soft connective tissues. *Proc Biol Sci* **258**, 195-200 (1994).
343. R.M. Aspden Fibre stress and strain in fibre-reinforced composites. *Journal of Material Science* **29**, 1310-1318 (1994).
344. L.P. Li, Buschmann, M.D. & Shirazi-Adl, A. Strain-rate dependent stiffness of articular cartilage in unconfined compression. *J Biomech Eng* **125**, 161-168 (2003).
345. P. Julkunen, Korhonen, R.K., Herzog, W. & Jurvelin, J.S. Uncertainties in indentation testing of articular cartilage: a fibril-reinforced poroviscoelastic study. *Med Eng Phys* **30**, 506-515 (2008).
346. B. Cohen, Lai, W.M. & Mow, V.C. A transversely isotropic biphasic model for unconfined compression of growth plate and chondroepiphysis. *J Biomech Eng* **120**, 491-496 (1998).
347. S. Federico, Grillo, A., La Rosa, G., Giaquinta, G. & Herzog, W. A transversely isotropic, transversely homogeneous microstructural-statistical model of articular cartilage. *J Biomech* **38**, 2008-2018 (2005).
348. C.Y. Huang, Mow, V.C. & Ateshian, G.A. The role of flow-independent viscoelasticity in the biphasic tensile and compressive responses of articular cartilage. *J Biomech Eng* **123**, 410-417 (2001).
349. P. Bursac, McGrath, C.V., Eisenberg, S.R. & Stamenovic, D. A microstructural model of elastostatic properties of articular cartilage in confined compression. *J Biomech Eng* **122**, 347-353 (2000).
350. P.L. Chandran & Barocas, V.H. Affine versus non-affine fibril kinematics in collagen networks: theoretical studies of network behavior. *J Biomech Eng* **128**, 259-270 (2006).
351. T.M. Quinn & Morel, V. Microstructural modeling of collagen network mechanics and interactions with the proteoglycan gel in articular cartilage. *Biomech Model Mechanobiol* **6**, 73-82 (2007).
352. A. Verteramo & Seedhom, B.B. Zonal and directional variations in tensile properties of bovine articular cartilage with special reference to strain rate variation. *Biorheology* **41**, 203-213 (2004).
353. A. Asanbaeva, Masuda, K., Thonar, E.J., Klisch, S.M. & Sah, R.L. Cartilage growth and remodeling: modulation of balance between proteoglycan and collagen network in vitro with beta-aminopropionitrile. *Osteoarthritis Cartilage* **16**, 1-11 (2008).
354. P.J. Basser, Schneiderman, R., Bank, R.A., Wachtel, E. & Maroudas, A. Mechanical properties of the collagen network in human articular cartilage as measured by osmotic stress technique. *Arch Biochem Biophys* **351**, 207-219 (1998).
355. P. Kiviranta et al. Collagen network primarily controls Poisson's ratio of bovine articular cartilage in compression. *J Orthop Res* **24**, 690-699 (2006).
356. D.L. Butler, Goldstein, S.A. & Guilak, F. Functional tissue engineering: the role of biomechanics. *J Biomech Eng* **122**, 570-575 (2000).

357. G.K. Reddy & Enwemeka, C.S. A simplified method for the analysis of hydroxyproline in biological tissues. *Clin Biochem* **29**, 225-229 (1996).
358. N.Y. Ignat'eva et al. Determination of hydroxyproline in tissues and the evaluation of the collagen content of the tissues *Journal of Analytical Chemistry* **62**, 51-57 (2007).
359. L.C. Junqueira, Bignolas, G. & Brentani, R.R. Picrosirius staining plus polarization microscopy, a specific method for collagen detection in tissue sections. *Histochem J* **11**, 447-455 (1979).
360. J.A. Ramos-Vara Technical aspects of immunohistochemistry. *Vet Pathol* **42**, 405-426 (2005).
361. S.J. Bryant & Anseth, K.S. Controlling the spatial distribution of ECM components in degradable PEG hydrogels for tissue engineering cartilage. *J Biomed Mater Res A* **64**, 70-79 (2003).
362. D.L. Nettles, Elder, S.H. & Gilbert, J.A. Potential use of chitosan as a cell scaffold material for cartilage tissue engineering. *Tissue Eng* **8**, 1009-1016 (2002).
363. J. Aigner et al. Cartilage tissue engineering with novel nonwoven structured biomaterial based on hyaluronic acid benzyl ester. *J Biomed Mater Res* **42**, 172-181 (1998).
364. B. Bierer, Margulies, D., Shevach, E., Strober, W. & Coico, R. Current Protocols in Immunology. (John Wiley & Sons, 2005).
365. C.M. Revell, Reynolds, C.E. & Athanasiou, K.A. Effects of Initial Cell Seeding in Self Assembly of Articular Cartilage. *Ann Biomed Eng* **24**, 24 (2008).
366. R.J. Minns & Steven, F.S. The collagen fibril organization in human articular cartilage. *J Anat* **123**, 437-457 (1977).
367. D.E. Birk, Zycband, E.I., Woodruff, S., Winkelmann, D.A. & Trelstad, R.L. Collagen fibrillogenesis in situ: fibril segments become long fibrils as the developing tendon matures. *Dev Dyn* **208**, 291-298 (1997).
368. B. Engfeldt, Reinholt, F.P., Hultenby, K., Widholm, S.M. & Muller, M. Ultrastructure of hypertrophic cartilage: histochemical procedures compared with high pressure freezing and freeze substitution. *Calcif Tissue Int* **55**, 274-280 (1994).
369. R.G. Richards & Kaab, M.J. Microwave-enhanced fixation of rabbit articular cartilage. *J Microsc* **181**, 269-276 (1996).
370. I. ap Gwynn, Wade, S., Ito, K. & Richards, R.G. Novel aspects to the structure of rabbit articular cartilage. *Eur Cell Mater* **4**, 18-29 (2002).
371. L.C. Hughes, Archer, C.W. & ap Gwynn, I. The ultrastructure of mouse articular cartilage: collagen orientation and implications for tissue functionality. A polarised light and scanning electron microscope study and review. *Eur Cell Mater* **9**, 68-84 (2005).
372. F. Ortolani, Giordano, M. & Marchini, M. A model for type II collagen fibrils: distinctive D-band patterns in native and reconstituted fibrils compared with sequence data for helix and telopeptide domains. *Biopolymers* **54**, 448-463 (2000).

373. S.M. Kuo, Wang, Y.J., Weng, C.L., Lu, H.E. & Chang, S.J. Influence of alginate on type II collagen fibrillogenesis. *J Mater Sci Mater Med* **16**, 525-531 (2005).
374. W. Kafienah et al. Lumican inhibits collagen deposition in tissue engineered cartilage. *Matrix Biol* **24**, 24 (2008).
375. C.A. Poole, Flint, M.H. & Beaumont, B.W. Morphological and functional interrelationships of articular cartilage matrices. *J Anat* **138 (Pt 1)**, 113-138 (1984).
376. E.S. Reynolds The use of lead citrate at high pH as an electron-opaque stain in electron microscopy. *J Cell Biol* **17**, 208-212 (1963).
377. P.A. Cattini & Davies, H.G. Kinetics of lead citrate staining of thin sections for electron microscopy. *Stain Technol* **58**, 29-40 (1983).
378. J.P. Arokoski et al. Decreased birefringence of the superficial zone collagen network in the canine knee (stifle) articular cartilage after long distance running training, detected by quantitative polarised light microscopy. *Ann Rheum Dis* **55**, 253-264 (1996).
379. Y. Xia Averaged and depth-dependent anisotropy of articular cartilage by microscopic imaging. *Semin Arthritis Rheum* **37**, 317-327 (2008).
380. T.A. Kelly, Ng, K.W., Wang, C.C., Ateshian, G.A. & Hung, C.T. Spatial and temporal development of chondrocyte-seeded agarose constructs in free-swelling and dynamically loaded cultures. *J Biomech* **39**, 1489-1497 (2006).
381. R. Meder, de Visser, S.K., Bowden, J.C., Bostrom, T. & Pope, J.M. Diffusion tensor imaging of articular cartilage as a measure of tissue microstructure. *Osteoarthritis Cartilage* **14**, 875-881 (2006).
382. L. Filidoro et al. High-resolution diffusion tensor imaging of human patellar cartilage: feasibility and preliminary findings. *Magn Reson Med* **53**, 993-998 (2005).
383. S.K. de Visser, Crawford, R.W. & Pope, J.M. Structural adaptations in compressed articular cartilage measured by diffusion tensor imaging. *Osteoarthritis Cartilage* **16**, 83-89 (2008).
384. Y. Xia & Elder, K. Quantification of the graphical details of collagen fibrils in transmission electron micrographs. *J Microsc* **204**, 3-16 (2001).
385. S. Thomopoulos, Fomovsky, G.M. & Holmes, J.W. The development of structural and mechanical anisotropy in fibroblast populated collagen gels. *J Biomech Eng* **127**, 742-750 (2005).
386. B.K. Wicker, Hutchens, H.P., Wu, Q., Yeh, A.T. & Humphrey, J.D. Normal basilar artery structure and biaxial mechanical behaviour. *Comput Methods Biomech Biomed Engin*, 1 (2008).
387. A. Boskey & Pleshko Camacho, N. FT-IR imaging of native and tissue-engineered bone and cartilage. *Biomaterials* **28**, 2465-2478 (2007).
388. K. Potter, Kidder, L.H., Levin, I.W., Lewis, E.N. & Spencer, R.G. Imaging of collagen and proteoglycan in cartilage sections using Fourier transform infrared spectral imaging. *Arthritis Rheum* **44**, 846-855 (2001).
389. D.R. Eyre, Weis, M.A. & Wu, J.J. Advances in collagen cross-link analysis. *Methods* **45**, 65-74 (2008).

390. P.C. Trackman, Zoski, C.G. & Kagan, H.M. Development of a peroxidase-coupled fluorometric assay for lysyl oxidase. *Anal Biochem* **113**, 336-342 (1981).
391. A.H. Palamakumbura & Trackman, P.C. A fluorometric assay for detection of lysyl oxidase enzyme activity in biological samples. *Anal Biochem* **300**, 245-251 (2002).
392. R.M. Natoli, Responte, D.J., Lu, B.Y. & Athanasiou, K.A. Effects of multiple chondroitinase ABC applications on tissue engineered articular cartilage *Journal of Orthopaedic Research* **in press** (2008).
393. M. Fuss, Ehlers, E.M., Russlies, M., Rohwedel, J. & Behrens, P. Characteristics of human chondrocytes, osteoblasts and fibroblasts seeded onto a type I/III collagen sponge under different culture conditions. A light, scanning and transmission electron microscopy study. *Ann Anat* **182**, 303-310 (2000).
394. M.C. Ronziere et al. Ascorbate modulation of bovine chondrocyte growth, matrix protein gene expression and synthesis in three-dimensional collagen sponges. *Biomaterials* **24**, 851-861 (2003).
395. S. Nehrer et al. Canine chondrocytes seeded in type I and type II collagen implants investigated in vitro. *J Biomed Mater Res* **38**, 95-104 (1997).
396. F.J. O'Brien, Harley, B.A., Yannas, I.V. & Gibson, L.J. The effect of pore size on cell adhesion in collagen-GAG scaffolds. *Biomaterials* **26**, 433-441 (2005).
397. A.I. Caplan, Elyaderani, M., Mochizuki, Y., Wakitani, S. & Goldberg, V.M. Principles of cartilage repair and regeneration. *Clin Orthop Relat Res* **342**, 254-269 (1997).
398. S. Wakitani et al. Mesenchymal cell-based repair of large, full-thickness defects of articular cartilage. *J Bone Joint Surg Am* **76**, 579-592 (1994).
399. S. Nehrer et al. Chondrocyte-seeded collagen matrices implanted in a chondral defect in a canine model. *Biomaterials* **19**, 2313-2328 (1998).
400. A.E. Sams, Minor, R.R., Wootton, J.A., Mohammed, H. & Nixon, A.J. Local and remote matrix responses to chondrocyte-laden collagen scaffold implantation in extensive articular cartilage defects. *Osteoarthritis Cartilage* **3**, 61-70 (1995).
401. S.D. Waldman, Spiteri, C.G., Grynpas, M.D., Pilliar, R.M. & Kandel, R.A. Long-term intermittent shear deformation improves the quality of cartilaginous tissue formed in vitro. *J Orthop Res* **21**, 590-596 (2003).
402. G.M. Williams, Klein, T.J. & Sah, R.L. Cell density alters matrix accumulation in two distinct fractions and the mechanical integrity of alginate-chondrocyte constructs. *Acta Biomater* **1**, 625-633 (2005).
403. T.B. Woodfield et al. Polymer scaffolds fabricated with pore-size gradients as a model for studying the zonal organization within tissue-engineered cartilage constructs. *Tissue Eng* **11**, 1297-1311 (2005).
404. S.D. Waldman, Grynpas, M.D., Pilliar, R.M. & Kandel, R.A. The use of specific chondrocyte populations to modulate the properties of tissue-engineered cartilage. *J Orthop Res* **21**, 132-138 (2003).

405. M.B. Aydelotte & Kuettner, K.E. Differences between sub-populations of cultured bovine articular chondrocytes. I. Morphology and cartilage matrix production. *Connect Tissue Res* **18**, 205-222 (1988).
406. S.A. Fraser et al. Localization of type VI collagen in tissue-engineered cartilage on polymer scaffolds. *Tissue Eng* **12**, 569-577 (2006).
407. J. Chang & Poole, C.A. Sequestration of type VI collagen in the pericellular microenvironment of adult chrondrocytes cultured in agarose. *Osteoarthritis Cartilage* **4**, 275-285 (1996).
408. M.A. Dimicco, Kisiday, J.D., Gong, H. & Grodzinsky, A.J. Structure of pericellular matrix around agarose-embedded chondrocytes. *Osteoarthritis Cartilage* **15**, 1207-1216 (2007).
409. M.B. Sporn, Roberts, A.B., Wakefield, L.M. & Assoian, R.K. Transforming growth factor-beta: biological function and chemical structure. *Science* **233**, 532-534 (1986).
410. C. Englert et al. Bonding of articular cartilage using a combination of biochemical degradation and surface cross-linking. *Arthritis Res Ther* **9**, R47 (2007).
411. S.Y. Chuang, Odono, R.M. & Hedman, T.P. Effects of exogenous crosslinking on in vitro tensile and compressive moduli of lumbar intervertebral discs. *Clin Biomech (Bristol, Avon)* **22**, 14-20 (2007).
412. N. Verzijl et al. Crosslinking by advanced glycation end products increases the stiffness of the collagen network in human articular cartilage: a possible mechanism through which age is a risk factor for osteoarthritis. *Arthritis Rheum* **46**, 114-123 (2002).
413. M.A. Derby & Pintar, J.E. The histochemical specificity of Streptomyces hyaluronidase and chondroitinase ABC. *Histochem J* **10**, 529-547 (1978).
414. S.S. Chen, Falcovitz, Y.H., Schneiderman, R., Maroudas, A. & Sah, R.L. Depth-dependent compressive properties of normal aged human femoral head articular cartilage: relationship to fixed charge density. *Osteoarthritis Cartilage* **9**, 561-569 (2001).
415. A.C. Chen, Bae, W.C., Schinagl, R.M. & Sah, R.L. Depth- and strain-dependent mechanical and electromechanical properties of full-thickness bovine articular cartilage in confined compression. *J Biomech* **34**, 1-12 (2001).
416. B.D. Elder & Athanasiou, K.A. Hydrostatic pressure in articular cartilage tissue engineering: from chondrocytes to tissue regeneration. *Tissue Eng Part B Rev* **15**, 43-53 (2009).
417. V. Lefebvre & Bhattaram, P. in Current Topics in Developmental Biology, Vol. Volume 90. (ed. K. Peter) 291-317 (Academic Press, 2010).
418. A. Pillarisetti et al. Mechanical Phenotyping of Mouse Embryonic Stem Cells: Increase in Stiffness with Differentiation. *Cellular Reprogramming* **13**, 371-380 (2011).
419. G. Ofek et al. Mechanical characterization of differentiated human embryonic stem cells. *J Biomech Eng* **131**, 061011 (2009).
420. H. Chiang et al. Differences Between Chondrocytes and Bone Marrow-Derived Chondrogenic Cells. *Tissue Engineering Part A* (2011).

421. A.J. Engler, Sen, S., Sweeney, H.L. & Discher, D.E. Matrix Elasticity Directs Stem Cell Lineage Specification. *Cell* **126**, 677-689 (2006).
422. N.D. Evans et al. Substrate Stiffness Affects Early Differentiation Events in Embryonic Stem Cells. *European Cells and Materials* **18**, 1-14 (2009).
423. A. Yamashita, Nishikawa, S. & Rancourt, D.E. Identification of Five Developmental Processes during Chondrogenic Differentiation of Embryonic Stem Cells. *PLoS ONE* **5**, e10998 (2010).
424. I. Takahashi et al. Compressive force promotes Sox9, type II collagen and aggrecan and inhibits IL-1 beta expression resulting in chondrogenesis in mouse embryonic limb bud mesenchymal cells. *J. Cell Sci.* **111**, 2067-2076 (1998).
425. N.C. Nowlan, Sharpe, J., Roddy, K.A., Prendergast, P.J. & Murphy, P. Mechanobiology of embryonic skeletal development: Insights from animal models. *Birth Defects Research Part C: Embryo Today: Reviews* **90**, 203-213 (2010).
426. K.A. Roddy, Prendergast, P.J. & Murphy, P. Mechanical Influences on Morphogenesis of the Knee Joint Revealed through Morphological, Molecular and Computational Analysis of Immobilised Embryos. *PLoS ONE* **6**, e17526 (2011).
427. R.C. Solem, Eames, B.F., Tokita, M. & Schneider, R.A. Mesenchymal and mechanical mechanisms of secondary cartilage induction. *Developmental Biology* **356**, 28-39 (2011).
428. B. Mikic, Isenstein, A.L. & Chhabra, A. Mechanical Modulation of Cartilage Structure and Function During Embryogenesis in the Chick. *Annals of Biomedical Engineering* **32**, 18-25 (2004).
429. N.C. Nowlan, Murphy, P. & Prendergast, P.J. Mechanobiology of Embryonic Limb Development. *Annals of the New York Academy of Sciences* **1101**, 389-411 (2007).
430. E.G. Loboa, Wren, T.A.L., Beaupré, G.S. & Carter, D.R. Mechanobiology of soft skeletal tissue differentiation—a computational approach of a fiber-reinforced poroelastic model based on homogeneous and isotropic simplifications. *Biomechanics and Modeling in Mechanobiology* **2**, 83-96 (2003).
431. D.R. CARTER, ORR, T.E., FYHRIE, D.P. & SCHURMAN, D.J. Influences of Mechanical Stress on Prenatal and Postnatal Skeletal Development. *Clinical Orthopaedics and Related Research* **219**, 237-250 (1987).
432. D.R. Carter & Wong, M. Mechanical stresses and endochondral ossification in the chondroepiphysis. *Journal of Orthopaedic Research* **6**, 148-154 (1988).
433. D.R. Carter & Wong, M. The role of mechanical loading histories in the development of diarthrodial joints. *Journal of Orthopaedic Research* **6**, 804-816 (1988).
434. R. Mahmoodian et al. Changes in mechanics and composition of human talar cartilage anlagen during fetal development. *Osteoarthritis and Cartilage* **19**, 1199-1209 (2011).

435. T.J. Klein, Chaudhry, M., Bae, W.C. & Sah, R.L. Depth-dependent biomechanical and biochemical properties of fetal, newborn, and tissue-engineered articular cartilage. *Journal of Biomechanics* **40**, 182-190 (2007).
436. H. Brommer et al. Functional adaptation of articular cartilage from birth to maturity under the influence of loading: a biomechanical analysis. *Equine Veterinary Journal* **37**, 148-154 (2005).
437. A.K. Williamson, Chen, A.C., Masuda, K., Thonar, E.J.M.A. & Sah, R.L. Tensile mechanical properties of bovine articular cartilage: Variations with growth and relationships to collagen network components. *Journal of Orthopaedic Research* **21**, 872-880 (2003).
438. A.K. Williamson, Chen, A.C. & Sah, R.L. Compressive properties and function—composition relationships of developing bovine articular cartilage. *Journal of Orthopaedic Research* **19**, 1113-1121 (2001).
439. D.R. Carter & Wong, M. Modelling cartilage mechanobiology. *Philosophical Transactions of the Royal Society of London. Series B: Biological Sciences* **358**, 1461-1471 (2003).
440. R. Korhonen et al. Collagen Network of Articular Cartilage Modulates Fluid Flow and Mechanical Stresses in Chondrocyte. *Biomechanics and Modeling in Mechanobiology* **5**, 150-159 (2006).
441. E. Kim, Guilak, F. & Haider, M.A. An Axisymmetric Boundary Element Model for Determination of Articular Cartilage Pericellular Matrix Properties In Situ via Inverse Analysis of Chondron Deformation. *Journal of Biomechanical Engineering* **132**, 031011-031013 (2010).
442. N.M. Bachrach et al. Changes in proteoglycan synthesis of chondrocytes in articular cartilage are associated with the time-dependent changes in their mechanical environment. *Journal of Biomechanics* **28**, 1561-1569 (1995).
443. Z. Abusara, Seerattan, R., Leumann, A., Thompson, R. & Herzog, W. A novel method for determining articular cartilage chondrocyte mechanics in vivo. *Journal of Biomechanics* **44**, 930-934 (2011).
444. F. Eckstein, Reiser, M., Englmeier, K.-H. & Putz, R. In vivo morphometry and functional analysis of human articular cartilage with quantitative magnetic resonance imaging - from image to data, from data to theory. *Anatomy and Embryology* **203**, 147-173 (2001).
445. G. Li, DeFrate, L.E., Park, S.E., Gill, T.J. & Rubash, H.E. In Vivo Articular Cartilage Contact Kinematics of the Knee. *The American Journal of Sports Medicine* **33**, 102-107 (2005).
446. E. Schuh et al. Effect of Matrix Elasticity on the Maintenance of the Chondrogenic Phenotype. *Tissue Engineering Part A* **16**, 1281-1290 (2009).
447. T. Ikenoue et al. Mechanoregulation of human articular chondrocyte aggrecan and type II collagen expression by intermittent hydrostatic pressure in vitro. *Journal of Orthopaedic Research* **21**, 110-116 (2003).

448. T. Toyoda et al. Hydrostatic pressure modulates proteoglycan metabolism in chondrocytes seeded in agarose. *Arthritis & Rheumatism* **48**, 2865-2872 (2003).
449. Y.-M. Juang et al. Proteomic analysis of chondrocytes exposed to pressure. *Biomedical Chromatography* **24**, 1273-1282 (2010).
450. M.M. Knight, Toyoda, T., Lee, D.A. & Bader, D.L. Mechanical compression and hydrostatic pressure induce reversible changes in actin cytoskeletal organisation in chondrocytes in agarose. *Journal of Biomechanics* **39**, 1547-1551 (2006).
451. T. Kunitomo et al. Influence of extracellular matrix on the expression of inflammatory cytokines, proteases, and apoptosis-related genes induced by hydrostatic pressure in three-dimensionally cultured chondrocytes. *Journal of Orthopaedic Science* **14**, 776-783 (2009).
452. R.L. Sah et al. Biosynthetic response of cartilage explants to dynamic compression. *J Orthop Res* **7**, 619-636 (1989).
453. F. Guilak, Meyer, B.C., Ratcliffe, A. & Mow, V.C. The effects of matrix compression on proteoglycan metabolism in articular cartilage explants. *Osteoarthritis Cartilage* **2**, 91-101 (1994).
454. S. Park, Hung, C.T. & Ateshian, G.A. Mechanical response of bovine articular cartilage under dynamic unconfined compression loading at physiological stress levels. *Osteoarthritis and Cartilage* **12**, 65-73 (2004).
455. R.M. Schinagl, Gurskis, D., Chen, A.C. & Sah, R.L. Depth-dependent confined compression modulus of full-thickness bovine articular cartilage. *Journal of Orthopaedic Research* **15**, 499-506 (1997).
456. O. Démarteau et al. Dynamic compression of cartilage constructs engineered from expanded human articular chondrocytes. *Biochemical and Biophysical Research Communications* **310**, 580-588 (2003).
457. A.M. Loening et al. Injurious Mechanical Compression of Bovine Articular Cartilage Induces Chondrocyte Apoptosis. *Archives of Biochemistry and Biophysics* **381**, 205-212 (2000).
458. J.M. Haemer, Song, Y., Carter, D.R. & Giori, N.J. Changes in articular cartilage mechanics with meniscectomy: A novel image-based modeling approach and comparison to patterns of OA. *Journal of Biomechanics* **44**, 2307-2312 (2011).
459. M.A. LeRoux et al. Simultaneous changes in the mechanical properties, quantitative collagen organization, and proteoglycan concentration of articular cartilage following canine meniscectomy. *Journal of Orthopaedic Research* **18**, 383-392 (2000).
460. T.P. Andriacchi & Mundermann, A. The role of ambulatory mechanics in the initiation and progression of knee osteoarthritis. *Current Opinion in Rheumatology* **18**, 514-518 (2006).
461. D. Moukoko, Pourquier, D., Pithioux, M. & Chabrand, P. Influence of cyclic bending loading on in vivo skeletal tissue regeneration from periosteal origin. *Orthopaedics & Traumatology: Surgery & Research* **96**, 833-839 (2010).

462. D.J. Kelly & Prendergast, P.J. Mechano-regulation of stem cell differentiation and tissue regeneration in osteochondral defects. *Journal of Biomechanics* **38**, 1413-1422 (2005).
463. E. Darling et al. Mechanical Properties and Gene Expression of Chondrocytes on Micropatterned Substrates Following Dedifferentiation in Monolayer. *Cellular and Molecular Bioengineering* **2**, 395-404 (2009).
464. R.H. Das et al. In vitro expansion affects the response of chondrocytes to mechanical stimulation. *Osteoarthritis Cartilage* **16**, 385-391 (2008).
465. J. Heyland et al. Redifferentiation of chondrocytes and cartilage formation under intermittent hydrostatic pressure. *Biotechnol Lett* **28**, 1641-1648 (2006).
466. M. Kawanishi et al. Redifferentiation of dedifferentiated bovine articular chondrocytes enhanced by cyclic hydrostatic pressure under a gas-controlled system. *Tissue Eng* **13**, 957-964 (2007).
467. C. Domm, Fay, J., Schunke, M. & Kurz, B. [Redifferentiation of dedifferentiated joint cartilage cells in alginate culture. Effect of intermittent hydrostatic pressure and low oxygen partial pressure]. *Orthopade* **29**, 91-99 (2000).
468. C.R. Lee, Grodzinsky, A.J. & Spector, M. Biosynthetic response of passaged chondrocytes in a type II collagen scaffold to mechanical compression. *J Biomed Mater Res A* **64**, 560-569 (2003).
469. S.H. Elder, Fulzele, K.S. & McCulley, W.R. Cyclic hydrostatic compression stimulates chondroinduction of C3H/10T1/2 cells. *Biomech Model Mechanobiol* **3**, 141-146 (2005).
470. M. Singh, Pierpoint, M., Mikos, A.G. & Kasper, F.K. Chondrogenic differentiation of neonatal human dermal fibroblasts encapsulated in alginate beads with hydrostatic compression under hypoxic conditions in the presence of bone morphogenetic protein-2. *J Biomed Mater Res A* **98**, 412-424 (2011).
471. L.C. Doehring et al. Myeloid CD34+CD13+ precursor cells transdifferentiate into chondrocyte-like cells in atherosclerotic intimal calcification. *Am J Pathol* **177**, 473-480 (2010).
472. J.J. Parkkinen et al. Effects of cyclic hydrostatic pressure on proteoglycan synthesis in cultured chondrocytes and articular cartilage explants. *Arch Biochem Biophys* **300**, 458-465 (1993).
473. N. Burton-Wurster, Vernier-Singer, M., Farquhar, T. & Lust, G. Effect of compressive loading and unloading on the synthesis of total protein, proteoglycan, and fibronectin by canine cartilage explants. *J Orthop Res* **11**, 717-729 (1993).
474. M. Jin, Frank, E.H., Quinn, T.M., Hunziker, E.B. & Grodzinsky, A.J. Tissue shear deformation stimulates proteoglycan and protein biosynthesis in bovine cartilage explants. *Arch Biochem Biophys* **395**, 41-48 (2001).
475. N.D. Leipzig & Athanasiou, K.A. Static compression of single chondrocytes catabolically modifies single-cell gene expression. *Biophys J* **94**, 2412-2422 (2008).

476. M.D. Buschmann, Hunziker, E.B., Kim, Y.J. & Grodzinsky, A.J. Altered aggrecan synthesis correlates with cell and nucleus structure in statically compressed cartilage. *J Cell Sci* **109 (Pt 2)**, 499-508 (1996).
477. T.T. Chowdhury, Salter, D.M., Bader, D.L. & Lee, D.A. Integrin-mediated mechanotransduction processes in TGFbeta-stimulated monolayer-expanded chondrocytes. *Biochem Biophys Res Commun* **318**, 873-881 (2004).
478. J.A. Browning, Saunders, K., Urban, J.P. & Wilkins, R.J. The influence and interactions of hydrostatic and osmotic pressures on the intracellular milieu of chondrocytes. *Biorheology* **41**, 299-308 (2004).
479. P. D'Andrea et al. Intercellular Ca2+ waves in mechanically stimulated articular chondrocytes. *Biorheology* **37**, 75-83 (2000).
480. M. Edlich, Yellowley, C.E., Jacobs, C.R. & Donahue, H.J. Oscillating fluid flow regulates cytosolic calcium concentration in bovine articular chondrocytes. *J Biomech* **34**, 59-65 (2001).
481. C.E. Yellowley, Jacobs, C.R. & Donahue, H.J. Mechanisms contributing to fluid-flow-induced Ca2+ mobilization in articular chondrocytes. *J Cell Physiol* **180**, 402-408 (1999).
482. S. Mizuno A novel method for assessing effects of hydrostatic fluid pressure on intracellular calcium: a study with bovine articular chondrocytes. *Am J Physiol Cell Physiol* **288**, C329-337 (2005).
483. A.C. Hall Differential effects of hydrostatic pressure on cation transport pathways of isolated articular chondrocytes. *J Cell Physiol* **178**, 197-204 (1999).
484. R.M. Natoli et al. Intracellular Na(+) and Ca(2+) modulation increases the tensile properties of developing engineered articular cartilage. *Arthritis Rheum* **62**, 1097-1107.
485. A. Ongaro et al. Chondroprotective effects of pulsed electromagnetic fields on human cartilage explants. *Bioelectromagnetics* **32**, 543-551 (2011).
486. C.E. Yellowley, Hancox, J.C. & Donahue, H.J. Effects of cell swelling on intracellular calcium and membrane currents in bovine articular chondrocytes. *J Cell Biochem* **86**, 290-301 (2002).
487. S.R. Tew et al. Hyperosmolarity regulates SOX9 mRNA posttranscriptionally in human articular chondrocytes. *Am J Physiol Cell Physiol* **297**, C898-906 (2009).
488. G.D. Palmer et al. Time-dependent aggrecan gene expression of articular chondrocytes in response to hyperosmotic loading. *Osteoarthritis Cartilage* **9**, 761-770 (2001).
489. E.S. Oswald et al. Effects of Hypertonic (NaCl) Two-Dimensional and Three-Dimensional Culture Conditions on the Properties of Cartilage Tissue Engineered from an Expanded Mature Bovine Chondrocyte Source. *Tissue Eng Part C Methods* (2011).
490. I. Freund, Deutsch, M. & Sprecher, A. Connective tissue polarity. Optical second-harmonic microscopy, crossed-beam summation, and small-angle scattering in rat-tail tendon. *Biophys J* **50**, 693-712 (1986).

491. P. Stoller, Reiser, K.M., Celliers, P.M. & Rubenchik, A.M. Polarization-modulated second harmonic generation in collagen. *Biophys J* **82**, 3330-3342 (2002).
492. A.T. Yeh et al. Nonlinear optical microscopy of articular cartilage. *Osteoarthritis Cartilage* **13**, 345-352 (2005).
493. I. Rocha-Mendoza et al. Sum frequency vibrational spectroscopy: the molecular origins of the optical second-order nonlinearity of collagen. *Biophys J* **93**, 4433-4444 (2007).

Appendix 1: Genes differentially expressed due to C-ABC and TGF-β1

C-ABC		TGF		TGF+C-ABC		Gene Symbol	human Entrez ID
4.9015756	up	1.0403095	up	1.0091964	down		3643
3.6445346	down	1.0832741	up	1.0428727	up	LOC616969	64283
3.1834419	up	1.1570461	up	1.048409	down	FOSL2	2355
2.1836698	up	1.157017	up	1.0712886	down		not found yet
2.0065997	down	1.2738936	up	1.0725881	up	DTYMK	1841
6.6061444	down	1.076887	up	1.0735799	up	TTC36	143941
2.6536276	down	1.0896107	up	1.079404	up	CHST2	9435
2.4148612	down	1.0546892	up	1.084452	up		80775
2.3879619	up	1.2759495	down	1.0869504	down		5286
2.4231634	down	1.1586796	up	1.0901477	up	ACOT2	10965
2.0777082	down	1.0542128	down	1.1150856	down		not found yet
2.279873	up	1.1059803	up	1.1289849	up	PIM1	5292
2.3799655	up	1.0623609	down	1.1787587	down	ARHGAP21	57584
2.6392217	up	1.0520011	down	1.1794683	down	RALGDS	5900
3.0405967	down	1.2100194	up	1.1847044	up	UCHL1	7345
4.7605104	up	1.112944	up	1.2097858	up		not found yet
2.662217	up	1.1783559	down	1.2279336	down		not found yet
2.4334786	down	1.1244112	down	1.2384548	down	GNG2	54331
3.2531354	up	1.1740832	up	1.2554867	up		not found yet
2.4242969	up	1.3502362	up	1.3096834	up	STK3	6788
2.9527056	up	1.7144948	up	1.313285	up	KRTCAP3	200634
3.3123212	down	1.5462247	down	1.3376262	down	PTPLAD2	401494
2.268236	down	1.1770442	down	1.3558139	down		not found yet
3.3141582	down	1.3444972	down	1.3762094	down	GPR143	4935
2.5297132	up	1.2099886	down	1.3797472	down	KCTD7	154881
4.2787204	up	1.3469323	up	1.3858787	up	RIN2	54453
2.1111155	down	1.1948843	down	1.401657	down	HOXA9	not found yet
2.7156503	down	1.5361385	down	1.4124867	down	KCTD1	not found yet
2.358832	up	1.4502801	up	1.4246473	up	RASSF8	11228
2.387816	up	1.523363	down	1.4372935	up	ARHGAP18	93663
2.5910487	up	1.4257276	down	1.4873735	down		not found yet
2.467413	up	1.2352266	down	1.5830711	down		8844
2.0980406	down	1.5881585	down	1.6170659	down	C25H16OR	116028
7.710766	up	1.9033235	down	1.6181289	down		not found yet

C-ABC		TGF		TGF+C-ABC		Gene Symbol	human Entrez ID
1.2698736	down	2.0545468	up	1.6203291	up	APLP2	334
5.757525	up	1.8390882	up	1.6237885	up	RGS1	5996
3.0886679	up	2.0294733	down	1.6726714	down	HRH1	3269
2.582046	up	1.6868291	down	1.6947392	down		not found yet
2.0365717	down	1.7529999	down	1.6969494	down	RANGRF	29098
2.219547	down	1.631639	down	1.6995617	down	TP53I3	9540
1.0202878	up	2.083397	up	1.7121162	up	GBGT1	26301
1.4002259	up	2.0009165	up	1.7153105	up	CDKL4	344387
3.8801126	up	1.6483566	up	1.7167046	up	TSPAN13	27075
2.1056504	up	1.6107342	up	1.7170373	up	ZBTB43	23099
2.2413926	up	1.8650888	up	1.7241894	up		not found yet
1.024952	down	2.072654	up	1.7464159	up		not found yet
1.0092305	down	2.0025196	up	1.7545491	up	LOC78943	not found yet
1.2969291	up	2.0310533	up	1.7622942	up		not found yet
4.2454605	up	1.9621024	up	1.766288	up	NFATC1	4772
1.1433569	up	3.6961887	up	1.7751596	up	TMEM132E	124842
2.1382291	up	2.0011594	up	1.7756317	up	POLR1D	51082
2.0853052	down	1.6589415	down	1.7899919	down		not found yet
1.150062	down	2.0350637	up	1.8348933	up		not found yet
1.0250725	down	2.001905	up	1.835938	up	LDHA	3939
1.4449745	down	2.0311692	down	1.8359752	down	RGS7	6000
2.1381638	down	2.144713	down	1.8460011	down		not found yet
9.323849	down	2.2108417	down	1.8572714	down	LOC61482	not found yet
1.4071224	up	2.072172	up	1.8611709	up	SLK	9748
1.3071691	up	2.0074022	up	1.8707045	up	MFSD9	84804
1.1773912	up	2.1309576	up	1.8789455	up	ITPKC	80271
1.2407342	down	2.1077657	down	1.8814342	down	NSMCE1	197370
1.2495337	down	2.0440948	up	1.8865193	up	NFX1	4799
1.0227376	down	2.1494243	up	1.8979813	up	C14H8orf	65265
2.6292682	up	1.9165483	up	1.9007959	up		734
1.3519865	down	2.0001912	down	1.901896	down	OSBPL1A	114876
1.4314009	down	2.0958352	up	1.9192401	up	NMI	9111
2.4341502	down	2.0122235	down	1.9375664	down		not found yet
1.0323571	up	2.123672	up	1.9390423	up		not found yet
1.0499125	down	2.0992274	up	1.9421153	up	ANKRD54	129138
2.328048	up	1.8754404	up	1.9481441	up	MAP2K4	6416
1.0405006	up	2.5238194	down	1.952007	down	SCNN1A	6337
1.1430696	up	2.1898403	up	1.9596405	up	ITGA5	3678
1.6382186	down	2.2766705	up	1.959958	up	TMEM120A	83862

C-ABC		TGF		TGF+C-ABC		Gene Symbol	human Entrez ID
1.0738645	down	2.0096188	down	1.9619429	down	PRKD3	23683
1.2716118	up	2.0408506	down	1.9737242	down		not found yet
1.211432	up	2.0340095	down	1.9767976	down		not found yet
1.0987617	down	2.0165653	up	1.9774314	up	VAMP3	9341
1.5321649	down	2.197055	up	1.9820287	up		not found yet
1.2326775	up	2.076399	up	1.9825537	up	NGRN	51335
1.1310698	up	2.2471929	up	1.9827988	up	TMEM11	8834
1.393504	up	2.1094813	up	1.9833035	up	HIP1R	9026
1.3772234	up	2.750556	up	1.9931641	up	NEK9	91754
2.0655665	down	1.9641404	down	1.9996179	down	MMP23B	8510
1.1286536	down	2.1140273	down	2.001297	down		not found yet
1.7305224	up	2.059546	down	2.0034006	down	PFKFB3	5209
1.1143031	down	2.1261003	up	2.005346	up	SLC15A4	121260
1.2164307	down	1.8807808	down	2.0129297	down		not found yet
1.0950947	down	2.1581628	up	2.0146935	up		not found yet
1.0591428	down	2.2286847	up	2.016651	up		not found yet
1.0696607	down	2.2311568	up	2.0323944	up		not found yet
1.2077997	up	1.9493029	up	2.0350845	up	PTRH2	51651
1.1909176	down	2.4998538	down	2.0409586	down	TCEA3	6920
1.418723	up	1.8513179	up	2.045131	up	MKI67IP	84365
1.1687165	up	2.281919	up	2.0464835	up	TNFAIP1	7126
2.1767335	down	2.2753336	up	2.0519114	up	FANCE	2178
1.5154134	down	2.342698	down	2.0535254	down	KCTD15	79047
1.3013417	down	2.0903437	up	2.0572288	up	PSMA1	5682
1.2509115	down	2.1306384	up	2.0607917	up	SUSD4	55061
1.3398112	up	2.0590696	up	2.0870898	up	MAPK13	5603
1.2333162	up	1.9579817	down	2.089843	down		166647
1.8149283	up	1.8621416	up	2.0910833	up	DNTTIP2	30836
1.4322599	up	1.9511508	up	2.0950732	up	CCDC85B	11007
1.4917597	down	2.078183	down	2.0973306	down		not found yet
1.3352706	down	2.3142018	up	2.0992513	up	TOP3B	8940
2.3574698	up	2.2684314	up	2.1005137	up	LOC51163	not found yet
1.1581705	up	2.9805024	up	2.1018317	up	EIF3F	8665
1.0776464	down	1.9401795	up	2.1043231	up		not found yet
1.040704	up	2.7067525	up	2.1134758	up	JAKMIP2	9832
1.0742064	up	2.234418	up	2.1181145	up	SRRT	51593
1.2016991	up	2.0137947	down	2.1242156	down		not found yet
1.1035868	up	1.9920549	up	2.1312492	up	C10H15or	81556

C-ABC		TGF		TGF+C-ABC		Gene Symbol	human Entrez ID
1.3504026	down	2.3870413	up	2.1348176	up	TAF6L	10629
1.0354674	down	2.1626034	down	2.1394618	down		not found yet
1.1814162	up	1.936651	up	2.1424315	up	LBH	81606
1.7910793	up	2.8944652	up	2.145998	up	RBM22	none
1.1020904	down	2.182597	down	2.1535091	down		not found yet
1.2573025	up	2.2952964	up	2.1557317	up	UBTF	7343
1.6107242	down	2.0605295	down	2.1561933	down	IRAK4	51135
1.1718096	up	1.989224	up	2.1562097	up	UNC50	25972
1.1752428	up	1.8163778	up	2.1567411	up		not found yet
3.720657	up	2.3451266	down	2.158956	down	ANKRD37	353322
1.4689589	down	1.8643689	down	2.1594906	down	ARHGAP22	58504
1.5320667	down	2.3976977	down	2.162716	down	ZNF32	7580
1.1348641	up	1.900795	down	2.1676471	down		not found yet
1.2183964	up	2.6208737	up	2.1683164	up	PROSC	11212
1.0139945	up	1.2217233	up	2.1712306	up	ZBTB5	9925
1.8697323	up	1.9139298	down	2.1714013	down		not found yet
2.3177526	down	2.1790917	up	2.1714835	up	FAM129A	116496
1.2596956	up	2.040952	up	2.1776123	up	PSMD6	9861
4.4040995	up	2.698971	up	2.1849384	up		not found yet
1.1091124	up	2.755864	up	2.1876853	up	KCNQ3	3786
1.1108452	down	1.8541149	down	2.1916778	down	CDH3	1001
1.247224	up	1.8590497	up	2.1929138	up	MED6	10001
1.0792893	down	2.1201332	down	2.1968975	down	USP9X	8239
1.4857253	down	2.307843	up	2.1983004	up	PRDX1	5052
1.3454791	down	2.5601377	up	2.2024953	up	TXNRD3	none
1.2006079	up	2.1285164	up	2.2036312	up	GMDS	2762
1.6278675	up	2.2468617	up	2.2109077	up	KCTD5	54442
1.0236837	up	2.345092	up	2.213217	up	TBRG1	not found yet
1.3195492	down	2.413385	up	2.2148957	up	SPON2	10417
1.0124848	down	2.6112764	up	2.2171817	up	SENP3	26168
1.0042065	down	3.643015	up	2.2183323	up	PKP3	11187
1.0647688	up	2.5935724	up	2.2218354	up	LRP8	7804
2.1008217	up	2.1386085	up	2.2220256	up	RASA2	5922
1.1704376	up	2.1556697	down	2.2249506	down	HSD17B4	3295
1.421185	down	2.2234964	down	2.2294497	down		not found yet
2.0027559	down	2.3694777	down	2.2298656	down	ACSL5	51703
1.2272127	up	2.3513403	up	2.2434998	up	ARHGAP26	23092
1.237074	up	2.3626919	up	2.2449124	up	FKBPL	not found yet
1.187632	down	2.412843	up	2.246164	up	POLR2J	5439
1.3133228	down	2.6611476	up	2.2491248	up	CHST11	50515
1.1123184	up	2.1273403	down	2.2499003	down	NDRG2	57447

C-ABC		TGF		TGF+C-ABC		Gene Symbol	human Entrez ID
1.6664172	up	2.0305965	down	2.2512445	down	GAS7	8522
1.2076786	down	1.9183267	down	2.2528334	down		not found yet
1.9293876	down	2.868439	up	2.2531333	up	ACSL6	23305
1.2083362	up	2.3684509	up	2.2559464	up	C3orf39	84892
3.1715612	down	2.0669487	down	2.273674	down	APOA1	335
1.3563006	down	2.1789138	down	2.2765071	down		not found yet
1.983315	down	2.1077878	down	2.290807	down		not found yet
1.1988106	down	2.0368447	down	2.2932296	down	ZNF532	55205
1.1084356	up	2.0968473	down	2.301958	down		not found yet
1.1583425	down	2.0097072	down	2.3033688	down		not found yet
1.6714807	down	2.493926	down	2.3035157	down	TSPYL4	23270
1.6101749	down	2.249273	down	2.3050134	down	MFAP2	4237
1.5907756	up	2.599245	up	2.3092244	up	GRB7	2886
1.1435785	down	2.403123	down	2.3113093	down	ME1	4199
1.1424454	down	2.3281274	up	2.3193634	up	FUS	2521
1.0652771	up	2.7198768	down	2.3200746	down		not found yet
1.466776	down	2.066089	down	2.3275898	down	IGF2	3481
2.0526717	up	1.9885459	up	2.3343098	up		not found yet
1.6415204	up	2.7670908	up	2.3359704	up	DIP2B	57609
1.5068405	up	1.9112371	up	2.339905	up	MKNK1	8569
4.050903	up	2.019834	up	2.3420155	up	GPR68	8111
1.5015069	up	2.4098008	up	2.3474042	up		not found yet
1.2888963	down	2.6330204	down	2.3665276	down	MST4	51765
1.325751	down	2.8618252	up	2.367214	up	ABHD11	83451
1.1913924	down	2.159122	down	2.371023	down	TGFB3	7043
1.1673371	down	2.7237163	up	2.3724535	up		not found yet
1.0959351	down	2.4473052	up	2.3756042	up	MRPL49	740
1.7554717	up	2.4641943	up	2.3825464	up	CAMLG	819
1.4979506	up	1.6284522	up	2.3890631	up	C16H1ORF	163859
1.2022715	up	2.349902	up	2.3895886	up		not found yet
2.2395308	down	2.0342534	down	2.3904939	down	MAP1A	4130
2.2410932	down	2.3798542	down	2.396234	down	NFU1	27247
1.3692697	up	2.5838375	up	2.397329	up	TCF7	6932
1.5048778	up	2.3840442	up	2.4006138	up	PRKRIP1	79706
2.440888	up	2.631391	up	2.401925	up	DSE	29940
1.1371698	up	2.791733	up	2.4048095	up	LOC53959	not found yet
1.3634651	down	2.3212967	down	2.4176514	down		not found yet
1.1879445	up	2.7448325	up	2.4245808	up	MORG1	84292
1.2968701	down	4.152734	down	2.4260643	down		not found

C-ABC		TGF		TGF+C-ABC		Gene Symbol	human Entrez ID
1.0358844	down	2.714399	up	2.4266007	up	STIP1	10963
1.3946375	down	1.8743402	down	2.428181	down		not found yet
1.8104963	up	2.3121433	up	2.4382339	up	PIGA	5277
1.0195549	up	2.5296292	up	2.4404163	up		not found yet
1.6490428	down	2.0890446	down	2.442919	down	LOC508015	not found yet
1.159661	down	2.5762708	up	2.4484603	up	PSMD14	10213
1.0735195	up	3.1131701	up	2.4570093	up	PITPNB	23760
2.139502	up	2.5500758	up	2.459456	up		not found yet
1.0252186	down	2.7415202	up	2.462911	up	HABP4	22927
2.8784652	up	2.3323138	down	2.463459	down	LOXL4	84171
1.2541357	up	2.1639345	down	2.466271	down	CACNB3	784
1.1140985	down	2.2701235	down	2.4694157	down	SDC3	9672
1.0175054	up	2.3264687	up	2.4744303	up	SQRDL	not found yet
1.3039547	up	2.2647321	up	2.474709	up	TSNAX	not found yet
1.3295789	down	2.4397235	down	2.4864612	down		not found yet
1.0303869	up	2.224381	up	2.4884584	up	UBE2B_HU	not found yet
1.0699071	down	2.549118	up	2.5044029	up		not found yet
1.7097763	up	2.7502174	up	2.504579	up	NKRF	not found yet
1.0934718	up	2.0537937	down	2.509598	down		not found yet
1.2798603	down	2.488982	down	2.5096436	down	EFEMP2	30008
1.462542	up	2.2302551	up	2.509902	up		not found yet
1.4102297	down	2.368238	down	2.5104382	down		not found yet
1.8860523	down	2.301686	down	2.515596	down	DDB2	1643
1.9958661	down	2.5939136	down	2.517772	down	CYP39A1	51302
1.4564852	up	2.3977807	up	2.5205498	up	TP53I11	9537
1.6225696	down	2.3281386	down	2.521655	down	SFXN3	81855
1.7482036	up	2.4404957	up	2.5248542	up	DYRK3	8444
2.604903	up	2.1666887	up	2.526468	up	B3GNT2	10678
1.0994741	down	2.7208567	up	2.5270915	up	NOP16	51491
2.5654593	up	2.8330016	up	2.5312576	up	DUSP4	not found yet
2.614989	up	2.673643	up	2.5323186	up	LOC10014	not found yet
1.4692864	down	2.4125311	down	2.5383263	down		not found yet
1.6253155	up	2.3957942	up	2.5389605	up		not found yet
1.2440169	up	2.2418215	down	2.542093	down		not found

C-ABC		TGF		TGF+C-ABC		Gene Symbol	human Entrez ID
2.8180707	up	2.4757597	up	2.5472147	up	BOLA-N	not found yet
1.554106	up	3.1221828	up	2.5490866	up	SF1	7536
1.2014999	up	2.377746	up	2.5501838	up		not found yet
1.1850991	down	2.4115653	up	2.5508053	up	SCG2	7857
2.5096455	down	2.7947512	down	2.5534146	down		not found yet
1.0291198	down	2.3924696	up	2.5582092	up	PQBP1	10084
1.0707166	up	3.5939844	up	2.5619557	up	MAPK8IP1	9479
1.9345593	down	2.5022843	down	2.5671625	down		not found yet
1.0097018	up	3.4857788	up	2.5749109	up	SLURP1	57152
1.5591538	down	2.4215734	down	2.5838223	down	PIGP	51227
1.4093169	down	2.4127426	down	2.5900342	down	GATSL3	652968
1.635167	up	2.7409897	up	2.5924506	up		not found yet
1.4496231	down	2.632667	up	2.5938132	up	PPCDC	60490
2.263011	up	2.5612733	down	2.5994782	down	SLC6A14	11254
1.3240415	down	2.4586844	down	2.601335	down	RBPJ	3516
1.5491153	up	2.6138058	up	2.601829	up	TBP	6908
1.3224908	down	2.6829712	down	2.603372	down	FAM115A	9747
1.1594895	down	2.4480958	down	2.6036885	down	EXT2	2132
2.2393806	down	2.3935761	down	2.6096923	down	FBLN5	10516
1.0423334	up	2.1849225	down	2.6122794	down	PLCE1	51196
5.663506	up	3.2219908	up	2.6155717	up	JUNB	3726
1.5142583	down	2.400985	down	2.619251	down	MANSC1	54682
2.5881414	down	2.646018	down	2.6223853	down		not found yet
1.183004	down	2.866338	up	2.6293645	up		not found yet
2.3786123	up	3.038464	up	2.6338377	up		not found yet
1.1524073	down	3.2378407	down	2.6398067	down	MAP3K5	4217
1.1724197	up	2.9055235	up	2.6400616	up	DDX56	54606
1.1775446	up	2.444821	up	2.641342	up		not found yet
1.5756801	down	1.5146326	up	2.6491396	up	MYLK	4638
2.7845385	down	2.0308828	down	2.6581671	down		none
1.0313165	up	2.7671804	up	2.6607559	up	ORMDL1	94101
1.4024034	down	3.5309722	down	2.6627097	down	MST4	51765
1.5705991	up	2.5405223	up	2.6711872	up	RCHY1	25898
1.7289288	down	3.4107652	up	2.6752129	up	TLR7	51284
1.0109245	up	2.1241984	down	2.6764119	down		not found yet
1.3193097	up	2.5928278	up	2.6771662	up		not found yet
2.4477792	up	2.715759	up	2.6785057	up	UBE2H	7328
1.0173111	down	2.5759518	up	2.6803572	up	SLC25A22	79751
1.5228544	up	2.642589	down	2.6840947	down	TGFBR2	7048

C-ABC		TGF		TGF+C-ABC		Gene Symbol	human Entrez ID
1.3494971	down	3.7625754	up	2.6852372	up	POP1	10940
6.373607	down	2.8433473	down	2.6898022	down	AKAP3	10566
1.6902938	down	2.5423536	down	2.6914165	down	MAGEF1	64110
1.0047361	up	2.6946597	up	2.6975718	up	RBM4	5936
1.7289723	up	2.8540814	down	2.7044663	down	LMO7	4008
3.1186552	down	2.030994	down	2.7063782	down	SLC6A12	none
1.2040496	down	2.5671792	down	2.7094786	down	DNMBP	23268
1.355325	up	2.7185903	up	2.712614	up	TJP3	27134
1.3613573	down	2.7948723	down	2.7362437	down	IFIT5	24138
1.282987	down	2.4781709	down	2.7433863	down		not found yet
1.0528868	up	2.5878441	down	2.7464004	down		not found yet
1.9344132	up	2.7409682	up	2.7514856	up	TOE1	114034
1.0029378	down	2.8847094	up	2.7527537	up	ABCF2	10061
1.3745375	up	3.1808543	up	2.7566466	up	MYL4	4635
1.154493	down	2.6143477	up	2.7582977	up	NUP85	79902
1.0466037	down	2.592014	up	2.7614913	up	E2F4	1874
2.013666	down	2.7902744	down	2.7779233	down	TTC8	123016
2.3016937	up	3.1157095	up	2.7814727	up		79798
1.8480738	down	2.5820956	up	2.7965033	up	PAK1	5058
2.0749416	down	2.8537126	down	2.7976227	down	EFCAB1	79645
1.2918354	down	2.533671	down	2.8065743	down	CUEDC1	404093
13.1872425	down	2.9083717	up	2.8098698	up	CATHL1	820
1.1082803	down	2.3069777	down	2.8119843	down		not found yet
2.2801986	up	2.7725427	up	2.818499	up	C4orf32	132720
1.1350935	up	2.2597258	up	2.8472166	up	SESN2	83667
1.7060609	down	3.1293845	down	2.851912	down	LOC53021	167359
1.3757409	down	2.935798	down	2.8675966	down		not found yet
1.2092056	up	2.6850197	up	2.875018	up	GAL3ST3	89792
1.5593632	up	3.4776094	up	2.892076	up	CCDC151	115948
1.0475821	up	2.7861416	down	2.8952677	down	EFNA1	1942
1.1225343	down	3.1325798	down	2.903698	down	LOC50955	388341
1.3213458	up	3.3391654	up	2.905848	up	CASK	8573
1.1071916	up	3.2307189	up	2.9065025	up	SLC37A1	54020
1.0503942	up	2.8001566	up	2.9106617	up	PAQR9	344838
2.2527761	up	1.3579719	up	2.9245694	up	UTP3	not found yet
1.535865	down	2.2419598	down	2.9345944	down	GPR173	54328
1.6872048	down	2.650158	down	2.9383204	down	TCEA2	6919
1.0935609	down	2.8823385	up	2.9410617	up	SNRPC	6631
1.2729754	down	2.610434	up	2.949077	up	EIF2S1	1965
2.0206134	down	3.5530193	down	2.9522688	down	S100A9	6280
6.786773	up	3.1627035	down	2.9544806	down	PTGES	9536
1.0572647	down	2.9063723	down	2.9753795	down	ENOSF1	55556
2.498345	down	3.2950635	down	2.9778662	down	TPD52L1	7164
1.2944517	up	3.3113568	down	2.9912195	down		not found yet

C-ABC		TGF		TGF+C-ABC		Gene Symbol	human Entrez ID
1.0171213	up	3.2197945	up	2.9967856	up		not found yet
1.5222762	down	3.0872855	up	3.0034716	up	GSR	2936
1.0645467	up	2.7449343	down	3.0099277	down	ADAMTSL2	9719
1.706997	up	3.1029277	up	3.0253143	up	RPAIN	84268
1.6436144	up	2.0103576	down	3.040507	down		not found yet
1.1470275	up	3.4615738	up	3.0425148	up	MRAS	22808
3.5998442	up	2.8440244	up	3.0439718	up		not found yet
1.1392188	down	2.2549202	down	3.0514061	down	IGF2R	3482
1.4400855	down	3.2597315	down	3.0540686	down	TST	none
2.507685	up	3.9714868	up	3.058635	up		not found yet
1.3162374	up	3.2813785	up	3.0649276	up	CDA	978
3.8624952	up	3.0706077	up	3.067854	up	SGK1	6446
2.9732668	up	2.7706516	up	3.069435	up	PGF	not found yet
1.0536393	down	2.0542078	up	3.0862892	up	SAR1B	51128
4.9132676	up	2.9648468	up	3.0945923	up	THSD1	55901
4.0812416	up	3.6961637	up	3.1038983	up		not found yet
1.3582988	up	3.6137476	up	3.105273	up	CAMTA1	not found yet
1.3374321	up	3.1069398	up	3.1126585	up	RCAN3	11123
1.9302014	up	2.7011766	up	3.1227937	up	ECT2	1894
1.277453	up	4.5986457	up	3.1354046	up	CHD4	1108
1.0947918	down	3.1505322	down	3.140971	down	B3GNT9	84752
1.3665565	down	5.327489	up	3.1469862	up		57642
1.2931242	up	3.4445279	down	3.1717286	down	RRAGD	58528
1.3956175	up	3.793012	up	3.1770632	up	CHRNA10	57053
2.4026654	up	3.2321677	up	3.185317	up	SIK1	150094
1.1569903	up	2.2829976	up	3.1931899	up	FGF18	8817
1.0169852	down	3.0644739	up	3.1999838	up		338657
1.0385623	down	3.7386317	up	3.211961	up		not found yet
1.5516782	up	3.3334298	up	3.2521477	up	ITFG2	55846
1.3989775	up	6.4452868	up	3.2603595	up	LOC524694	27143
1.2289053	down	4.745711	down	3.2741516	down		not found yet
1.7656565	up	3.5877528	up	3.2772574	up		not found yet
3.7852402	up	5.4661636	up	3.288583	up	PTPN7	5778
1.9406823	up	3.091763	up	3.332797	up	TP53INP1	94241
1.2557672	down	2.944683	up	3.3520975	up	KCNK7	10089
2.3748977	up	3.5875654	up	3.355734	up	BCAS2	10286
1.0748934	up	4.468307	up	3.3586102	up		not found yet
1.8905472	down	3.1622655	up	3.3615441	up	FGF13	2258
1.1949329	up	3.1581414	up	3.3630111	up	DOHH	83475

C-ABC		TGF		TGF+C-ABC		Gene Symbol	human Entrez ID
1.4712131	up	2.6368139	up	3.3699903	up	KLHL25	64410
1.3863946	down	3.0862787	down	3.3881478	down		not found yet
1.0113295	down	4.38441	up	3.4156332	up	MMP15	4324
3.0386994	up	4.453125	up	3.4237907	up	CLDN4	1364
1.3633215	down	2.3601031	down	3.4488301	down	ZBTB7B	51043
1.3675708	up	4.3549075	up	3.4526787	up	LOC539609	27094
1.3138007	up	4.783742	up	3.4533546	up	LOC530472	none
1.1928498	down	3.4320154	up	3.4598837	up	PCBD1	5092
1.3604134	up	3.6046312	up	3.4746754	up	NXF1	10482
1.2611979	down	3.5325148	down	3.484802	down		not found yet
1.4051749	up	2.4342942	up	3.4989543	up	COL6A1	1291
1.5068434	up	3.6751702	up	3.504516	up	Bos taur	1647
1.1356875	up	1.5575407	up	3.5317233	up	BBS4	585
4.5004563	down	3.4371061	down	3.5323806	down		not found yet
1.7576377	up	3.5629237	up	3.5352762	up		3858
2.5327806	down	2.7785249	down	3.5367632	down	ODZ4	26011
1.1524539	down	3.0343683	down	3.5384545	down	TCFL5	none
1.227667	up	7.536936	up	3.5389214	up		not found yet
2.4536686	down	2.8981876	down	3.5426679	down	ZNF84	7637
1.9237865	down	3.6975787	down	3.5562801	down	CDK5RAP2	55755
1.3766019	up	4.556256	up	3.5660882	up		not found yet
1.4182881	up	3.948201	up	3.579726	up	MDM2	4193
1.1013724	down	4.147421	up	3.579798	up		not found yet
2.8802633	up	3.115038	up	3.5823262	up	RABGAP1L	not found yet
1.3597994	down	7.7407527	down	3.5831466	down		not found yet
1.4700658	down	3.2448008	down	3.583776	down	PGC	5225
1.1288188	down	3.756585	down	3.5913644	down	VAV3	10451
1.3032715	down	3.1553357	down	3.591542	down	PDGFRA	5156
1.6562916	down	3.9022677	up	3.6143284	up	NFE2L3	9603
1.3294446	down	3.6400201	down	3.6248896	down	PLCE1	51196
1.1746292	up	3.8721755	down	3.6365178	down		not found yet
1.3390449	up	2.9708447	up	3.6368892	up	SLC25A4	291
2.2384346	up	2.7726078	up	3.6373808	up	LTBP2	4053
1.1689352	down	4.977705	up	3.6405952	up	RECQL4	9401
3.9253683	down	2.7055082	down	3.6548493	down		not found yet
2.6867158	down	3.068712	down	3.659204	down	MS4A8B	83661
1.9606739	up	3.634362	up	3.6592324	up	CENPE	not found yet
1.0533085	up	3.3435814	down	3.6673074	down	OGT	8473

C-ABC		TGF		TGF+C-ABC		Gene Symbol	human Entrez ID
1.2163312	up	3.8034656	up	3.6704507	up		5599
2.0842566	up	4.010074	up	3.6773603	up	GPR162	27239
1.8353796	down	4.171599	down	3.6793618	down		not found yet
1.202141	up	3.2885532	down	3.6869571	down	KCNMA1	3778
1.1202505	up	3.7255461	up	3.7556872	up		not found yet
2.496803	up	4.0607533	up	3.778193	up		not found yet
1.0896423	up	3.5714028	down	3.7990608	down		not found yet
1.7271354	down	3.3532825	down	3.7997644	down	LOC61679	not found yet
1.218612	up	3.2031016	up	3.8003051	up		not found yet
1.6619626	down	4.020443	down	3.840271	down	NFIA	4774
1.2962128	up	4.6099606	up	3.8869188	up		5800
1.0279901	up	2.9200935	up	3.8933516	up	SYT5	6861
1.0204479	up	4.1571374	down	3.8955693	down	SERPINA1	5265
2.1014924	up	4.5720778	up	3.8988805	up	MAPK8IP1	9479
4.7588577	up	4.2980046	up	3.9095008	up		not found yet
6.046609	up	5.6565204	up	3.9210854	up		not found yet
1.0881543	up	3.573831	up	3.9213157	up	BIRC5	332
1.957142	up	4.627286	up	3.9304435	up	HSPH1	10808
1.8017187	up	3.712933	up	3.9455285	up	ST8SIA1	6489
2.286553	up	4.157042	up	3.952745	up	MAP2K3	5606
3.020998	up	3.5885441	up	3.9717622	up		not found yet
1.6557907	down	3.3278458	down	3.9726975	down		not found yet
1.0571743	down	3.2556405	down	3.9744673	down	RASL11B	65997
1.4000032	down	4.0416183	down	3.992534	down	GAB1	2549
1.6490785	up	3.7360551	up	3.9938915	up	SLBP	7884
1.3654764	down	3.7851398	down	4.000058	down	LHFPL2	10184
1.7718093	down	3.5993505	down	4.0290613	down	SLC11A2	4891
1.4164734	up	2.8061097	up	4.0875387	up	EIF3J	8669
1.2698401	up	4.2409053	up	4.0974293	up	LOC10017	not found yet
1.6646079	down	3.2310705	down	4.123896	down	PLCE1	51196
2.6102667	up	4.0230417	up	4.1342745	up	FGF2	2247
3.7997396	up	4.232461	up	4.140013	up	TGIF1	7050
1.2529715	up	4.437685	up	4.143091	up	C18H19or	56006
5.165703	up	3.3635867	up	4.151217	up	SLC30A1	7779
1.9410077	up	4.181233	up	4.1861644	up	CD68	968
4.4187393	up	3.8408976	up	4.2083244	up	ADRB2	154
1.740131	up	4.459207	up	4.2338185	up	IGFBP3	3486
2.2762842	up	5.037452	up	4.235868	up	SNAPC5	10302
1.1398602	up	3.4486198	up	4.266538	up	PAQR5	54852

C-ABC		TGF		TGF+C-ABC		Gene Symbol	human Entrez ID
2.0842047	down	4.0483055	down	4.3020124	down	SIRT3	23410
1.6240525	up	2.655072	up	4.3388515	up	BAMBI	25805
4.8896613	up	5.301905	up	4.3499055	up	ITPRIP	85450
2.5629761	down	4.7870603	up	4.3512645	up	E2F1	1869
1.1740124	up	4.397139	up	4.3740897	up	RASSF7	not found yet
1.9269323	up	5.240814	up	4.3747835	up		not found yet
2.3885117	down	5.515665	up	4.435285	up	EPHB2	2048
1.3626428	up	4.3493433	up	4.438893	up	TUBB2C	10383
2.2283068	up	4.2495008	up	4.4941034	up	SMURF2	64750
1.3726611	up	4.358388	up	4.5205503	up		not found yet
1.2354732	down	4.480074	down	4.556166	down	FKBP10	60681
1.0638231	down	3.9097722	down	4.5729413	down	THBS4	7060
1.0729396	down	3.3754218	up	4.6012373	up	LAMB3	3914
1.9845389	up	5.6068325	up	4.6203957	up	NLRP6	171389
1.164265	down	4.371583	down	4.622005	down		not found yet
2.6785371	up	4.6505103	up	4.623603	up	LAPTM5	7805
1.0287519	down	4.5528507	up	4.642802	up	LOC614669	not found yet
2.729713	up	4.3826413	up	4.675583	up	IFRD1	3475
1.0471861	up	5.164725	down	4.689234	down	AE000785	not found yet
1.6632512	down	6.3105545	up	4.7116714	up	GCG	2641
4.2411284	up	4.8122106	up	4.715147	up	TGIF1	7050
1.1412283	down	5.330548	down	4.7217956	down	STAC2	342667
1.9117992	down	3.727457	up	4.7292776	up	PROC	5624
3.0934255	down	4.0913544	down	4.7333097	down	PLCD4	84812
1.2288761	up	5.8435264	up	4.778885	up		not found yet
1.4417832	up	5.475371	up	4.797967	up		not found yet
1.270624	up	5.051258	up	4.81373	up	ISYNA1	51477
1.0829424	down	4.1570663	down	4.832486	down		not found yet
1.461919	down	3.9084842	down	4.882957	down	GLB1L	79411
4.789552	up	4.8926497	down	4.883491	down		not found yet
1.0164498	up	4.9275756	down	4.8889756	down	ADCY2	108
1.364317	up	5.110558	up	4.962964	up	RASL10A	10633
1.0930865	up	4.5320354	up	4.97764	up	COL11A1	1301
1.3672736	down	4.580678	down	5.0668054	down		not found yet
1.8264153	up	5.364406	up	5.0857797	up	ZNF750	79755
1.1656871	up	3.9557645	down	5.1523824	down	PIK3R1	5295
2.1955793	down	4.564729	down	5.212081	down	GLI3	2737
1.9992377	down	4.6247163	down	5.282652	down	LOC61596	54586
2.1434767	up	6.298757	up	5.2909393	up	CENPK	64105

C-ABC		TGF		TGF+C-ABC		Gene Symbol	human Entrez ID
3.4820526	up	6.0919657	up	5.2952433	up	ST3GAL1	6482
1.3976505	up	6.2721977	up	5.312982	up	ITPKA	3706
1.0248469	up	4.3529677	down	5.3608384	down		not found yet
2.8549964	up	3.983416	down	5.3677125	down		117248
1.8706241	up	5.150632	up	5.3787465	up	MAP3K6	9064
1.3521882	down	5.1360292	up	5.419618	up	GDAP1	54332
1.0010103	down	6.392243	up	5.4676433	up	CCNF	899
2.6401532	down	5.407202	down	5.5548897	down	ANXA9	8416
2.4861133	down	5.3150907	down	5.566002	down	CXHXORF4	139212
1.1142812	down	4.9383082	down	5.5839243	down	COL12A1	not found yet
1.1703227	down	2.9916117	up	5.590863	up		not found yet
1.0097867	up	4.137005	down	5.5976205	down	DMTF1	9988
1.8540739	up	5.7503858	up	5.619072	up	CCRN4L	25819
1.5729865	down	5.5316615	down	5.6230764	down	SOX8	30812
1.0823025	down	6.1471324	down	5.6307416	down	SPON1	10418
1.216774	down	6.4675226	up	5.6735997	up	RAB26	25837
1.5211424	up	4.5794306	down	5.6925807	down		not found yet
1.6992375	down	5.707675	down	5.708976	down		not found yet
1.5896442	down	5.785146	down	5.7421412	down	CARD11	84433
1.3628274	down	4.9254174	down	5.747124	down	MAN1C1	57134
1.496253	up	7.00452	up	5.756747	up		not found yet
2.6251798	up	5.4166007	up	5.7742596	up	PREX2	80243
1.0676433	down	5.453607	down	5.774538	down	NRP2	8828
11.911834	up	6.3820887	up	5.7745657	up	HSPB3	8988
2.4760218	up	6.4447756	up	5.8937426	up	B3GNT8	374907
2.3303094	down	6.4225683	up	5.903876	up	C1QL1	10882
1.2621373	down	6.329532	down	5.939477	down	TGFBR3	7049
1.1253759	up	4.683143	down	5.9859614	down	ATP8	not found yet
1.2587955	down	4.525118	down	6.1018987	down	ACAN	176
1.5425686	down	6.121172	down	6.102947	down	CERCAM	51148
1.6502489	down	7.7599626	down	6.125916	down	IFI16	3428
1.0770255	up	6.8752613	up	6.171526	up	PBX4	80714
1.5191065	down	5.947346	down	6.182932	down	MAPRE2	10982
2.2492502	down	7.0700274	down	6.2494655	down		not found yet
1.509992	down	5.932147	down	6.2814765	down	SLC22A16	85413
1.3065306	up	6.914314	up	6.300955	up		not found yet
2.3967214	up	5.667539	up	6.3117166	up	RPAP2	79871
1.0272484	up	7.340063	up	6.3768024	up	GPR84	53831
1.0182298	up	6.680339	up	6.4098535	up	ACBD7	414149
1.0750619	up	5.4539695	up	6.4963174	up	DGAT2	84649
1.4345999	down	6.8017325	down	6.666559	down	NFIB	none

C-ABC		TGF		TGF+C-ABC		Gene Symbol	human Entrez ID
1.0613542	up	6.043587	up	6.7314095	up	ARHGAP25	9938
2.656527	down	5.855164	up	6.815524	up	COL16A1	1307
2.423109	down	6.603288	down	6.864555	down		none
2.8553715	up	5.4450817	up	6.875869	up		not found yet
1.4276327	up	6.8605084	up	6.9169607	up	TXNRD1	7296
1.1884139	up	7.1678576	up	6.924168	up		not found yet
1.339659	up	5.3308806	down	6.9609904	down	ND1	none
2.1115835	up	6.5890865	up	6.978598	up	TGFB1	not found yet
2.0876596	up	7.1473007	up	7.1031647	up	RHOV	171177
1.925435	down	9.264734	down	7.1560636	down	TOX	9760
1.0947837	down	4.831062	up	7.1669006	up	NAAA	27163
1.6026946	up	7.901762	up	7.194202	up	HIST1H2B	8341
4.321536	down	4.7767816	down	7.237031	down	CLDN7	1366
1.7858223	up	6.7679176	up	7.290616	up	MC1R	4157
2.1776254	up	6.943243	up	7.3371177	up	RCAN1	none
1.0391849	down	6.6171727	down	7.376043	down		not found yet
2.3996716	down	8.731816	down	7.565273	down	EFEMP1	2202
3.3997722	up	6.3904243	up	7.650434	up	DLL4	54567
1.2581141	down	7.554394	down	7.665854	down	PAK3	5063
2.0074582	down	4.7893553	down	7.6852756	down		not found yet
3.0413463	up	5.994275	up	7.7264347	up	SH2D3C	10044
1.3183197	down	7.8271756	down	7.772719	down	LPL	4023
2.3215787	up	6.8984423	up	7.8038197	up	GRASP	160622
1.4535302	down	8.752241	down	7.8567166	down		not found yet
2.2111766	up	7.3043013	up	7.8745756	up		54498
2.9922938	down	6.8156004	down	7.9079084	down	PLA2R1	22925
3.0914476	down	9.382526	down	7.9236627	down	BCO2	83875
1.5611192	up	7.189873	up	7.953059	up	TAGAP	117289
1.7863861	down	7.717103	down	7.985852	down	PDGFRL	5157
2.8927777	down	8.827048	down	7.9895835	down	TMEM90B	79953
1.6419544	down	5.7487564	down	8.044555	down	PRM1	not found yet
2.4081178	up	9.032786	up	8.093484	up		not found yet
1.3162274	up	6.1380715	down	8.205122	down		not found yet
1.7994679	up	5.189304	up	8.308894	up	IL1RL2	8808
1.617134	up	13.119147	up	8.333474	up	GPR157	80045
1.0232939	up	8.354948	up	8.4446535	up		not found yet
2.351486	up	8.171648	up	8.600302	up	BCL2L11	not found yet
1.7203656	up	9.01704	up	8.613381	up	CSPG5	10675
1.5222696	up	8.563685	up	8.62703	up	GALNT10	55568

C-ABC		TGF		TGF+C-ABC		Gene Symbol	human Entrez ID
1.3917518	up	17.978193	up	8.650253	up		not found yet
1.2889426	down	7.1168013	up	8.721611	up	PKIB	not found yet
1.7753866	down	9.410274	down	8.999549	down	RARRES2	5919
1.3187244	up	12.304173	up	9.019645	up	NRIP3	56675
3.4757938	up	11.500069	up	9.18707	up	GPRC5A	9052
2.1551843	down	3.9088671	down	9.321633	down		4916
1.2822757	down	10.945822	down	9.322531	down	MGST2	4258
1.4115542	up	5.744077	up	9.538851	up	IFIT1	3434
1.0953921	up	8.811695	down	9.5760565	down		not found yet
1.1747012	up	10.436025	up	9.619276	up	CAMKV	79012
1.0909197	down	10.134245	down	9.697239	down	F2R	2149
1.8988444	down	9.545914	down	9.808312	down	CSGALNACT1	55790
1.6676607	up	6.395044	up	9.811101	up		not found yet
2.5430977	up	11.966972	down	9.839919	down		not found yet
3.049745	up	5.7851386	up	9.871931	up		not found yet
2.0109463	up	10.407687	up	9.883663	up	PTPRE	5791
4.813546	up	9.947744	up	9.915726	up	CYB561	1534
1.3469199	down	9.004676	down	9.928766	down		not found yet
1.27794	up	8.5754795	up	9.971019	up	PKIB	not found yet
1.0478247	down	8.820894	down	10.017535	down		not found yet
2.4757378	down	8.444028	down	10.0971365	down		not found yet
2.8092756	up	9.679538	up	10.103738	up		not found yet
6.4416122	down	8.997313	down	10.13726	down		not found yet
1.4920088	up	12.448486	down	10.2072525	down	KCNJ8	3764
2.9075103	up	12.186936	up	10.707724	up	CCL2	6347
2.320356	up	9.1362505	up	10.969729	up	LOC618708	not found yet
2.7346618	down	8.217133	down	11.137622	down	FNDC1	84624
1.6005067	down	11.540692	down	11.320967	down	PPAP2B	8613
1.3304777	up	12.310799	down	11.403743	down	SFRP4	6424
1.2384831	down	11.372253	up	11.687462	up	TNFSF13B	10673
1.8963207	down	13.417542	up	11.729195	up	KCNT1	57582
1.7423487	down	11.902527	down	11.771932	down	VCAM1	7412
3.1124148	down	10.969009	down	11.791678	down	ANG	283
1.6451237	up	6.4411683	up	11.823164	up		not found yet
2.7262433	up	14.978828	up	12.104685	up	GPRC5A	9052
1.9152048	down	9.218979	down	12.283286	down	RGS13	6003
1.5072047	down	18.381298	down	13.045399	down	AHSG	197

C-ABC		TGF		TGF+C-ABC		Gene Symbol	human Entrez ID
3.8262036	down	12.315087	down	13.118096	down		not found yet
2.4884028	up	12.445648	down	13.333374	down	S100G	795
1.1474786	up	10.34427	down	13.355462	down	COX2	1E+08
1.1668326	up	14.866286	up	13.496918	up		not found yet
1.561023	up	14.027843	up	13.526388	up	MFSD6L	162387
1.0734468	down	14.366854	up	13.690345	up	PTPN5	84867
4.673984	down	12.437477	up	13.702984	up	ISG15	9636
1.0847207	down	18.470402	up	14.063114	up	GABRD	2563
1.3595139	down	24.168238	down	14.214198	down	B3GALNT1	8706
2.598093	down	14.822899	up	14.308889	up	SCRG1	11341
1.0337337	up	12.657353	down	15.119983	down	CYTB	none
2.1291625	down	14.424986	down	15.519769	down		not found yet
1.4537166	up	19.05149	up	15.597991	up	CHRNA7	1139
1.2402269	up	13.38799	down	16.26207	down		not found yet
2.100859	up	13.997187	down	16.314499	down		not found yet
3.1339912	up	16.463484	up	16.576937	up	RND1	27289
6.498768	up	20.344517	up	17.134975	up		not found yet
1.3483279	up	19.872509	down	17.372868	down		not found yet
5.1296496	up	14.10521	up	17.49387	up		not found yet
1.6714151	up	16.939123	up	18.354124	up	GDF15	9518
1.1749309	down	22.828346	down	18.70133	down	KCNE4	23704
1.6558633	up	18.469852	up	19.298754	up		not found yet
1.3066667	up	19.889647	up	20.065443	up		not found yet
10.870654	down	10.452961	down	22.452724	down	COLEC11	78989
1.6208721	down	22.71264	down	23.228792	down		not found yet
1.3580009	down	26.60113	up	25.921827	up	PRSS16	10279
1.7512186	down	27.468958	up	28.13812	up	COL28A1	340267
1.3670394	up	30.50448	up	30.372225	up		not found yet
5.3727684	down	34.30109	down	32.708134	down	ITGBL1	not found yet
2.6015403	down	37.863586	down	32.954426	down		not found yet
2.3243833	up	30.317844	up	33.40616	up	FAM83D	81610
7.1131577	down	39.74648	down	39.027416	down	COL1A2	1278
3.1975613	up	36.345272	up	39.221916	up	KCNN4	not found yet
2.6915343	up	37.401512	up	41.044163	up	KRT13	3860
9.393338	down	48.18166	down	44.74362	down	COL1A1	1277
27.317495	up	45.60362	up	47.97852	up	FOSL1	8061

10.196195	up	74.78285	up	72.677376	up	GJB3	2707
1.2307239	up	157.54912	up	171.10565	up		4741
1.3520703	up	221.1537	up	208.04163	up	DRD2	1813

Appendix 2: Genes differentially expressed due to hyaluronic acid

Gene	FC	Regulation	Gene	FC	Regulation
EFEMP2	3.114134	up	RARRES2	5.336247	up
CCDC64B	3.123814	up	MYC	5.342393	up
VAMP2	3.127333	up	TMEM130	5.350016	up
ATP6V0C	3.166901	up	ST3GAL3	5.362597	up
SH3GL1	3.172893	up	FBLN7	5.3653	up
AHCY	3.173209	up	ANKRD9	5.406378	up
PER2	3.181076	up	SPLUNC2B	5.456031	up
VILL	3.183418	up	CCNL1	5.45869	up
SLA	3.190728	up	NOV	5.469276	up
APBA3	3.193908	up	STAR	5.484474	up
ITPKC	3.212448	up	CATHL1	5.495899	up
MYOD1	3.214046	up	DNM1	5.504668	up
TMEM201	3.215399	up	SDC4	5.522861	up
MYO9B	3.220082	up	SMOC2	5.530566	up
TRIM15	3.226252	up	DLK1	5.534524	up
PHLDA2	3.243244	up	GADD45B	5.546174	up
LOC615935	3.243289	up	LOC528939	5.557385	up
NOMO2	3.260491	up	CYTL1	5.569976	up
SLC12A9	3.285481	up	LOC510193	5.58086	up
PHF13	3.296038	up	CATHL1	5.581614	up
LIPG	3.316718	up	OLFM1	5.584549	up
MMP2	3.316891	up	RHOU	5.594534	up
LOC781123	3.326981	up	ZFP36L1	5.596132	up
AGTR1	3.336225	up	SYTL2	5.608112	up
IGHMBP2	3.350734	up	RAB9A	5.630354	up
LOC506470	3.351745	up	PFKFB3	5.638695	up
COL3A1	3.354212	up	RHOV	5.661543	up
LAPTM5	3.368565	up	CD1A	5.662686	up
PTMS	3.372933	up	LOC781311	6.407356	up
LOC788112	3.383465	up	FOS	6.424679	up
NEPN	3.397535	up	IL1RAP	6.437739	up
CEBPD	3.398838	up	G0S2	6.49481	up
MXRA8	3.405266	up	HSPA1A	6.595901	up
COL3A1	3.415606	up	CABP2	6.608299	up
LOC615291	3.432834	up	DYRK3	6.608676	up
DLK1	3.433493	up	PI3	6.610308	up
KIF3C	3.434818	up	NPEPPS	6.636694	up
ANGPTL6	3.438558	up	ARRDC2	6.665806	up
DNM1	3.440338	up	APOBEC3B	6.671162	up
SLC38A3	3.45249	up	IVNS1ABP	6.713525	up
TCN2	3.455155	up	GEM	6.7734	up
ZNF358	3.462085	up	RAB15	6.782245	up
RNF19B	3.477796	up	INHBA	6.820276	up

Gene	FC	Regulation	Gene	FC	Regulation
SERPING1	3.478325	up	THBS4	6.82103	up
TRMT61A	3.486873	up	COL16A1	6.87392	up
FERMT1	3.49078	up	GPR182	6.875762	up
KDM5C	3.495404	up	BHLHE41	6.879804	up
GTLF3B	3.513406	up	LOC100297155	6.888501	up
NDUFA6	3.514897	up	G0S2	6.940129	up
TSTA3	3.515673	up	SOCS1	6.945253	up
KLK9	3.524472	up	ATP2A2	6.972224	up
BUB1B	3.893257	up	DYRK3	6.975043	up
NOS2	3.896367	up	TRIM2	7.032845	up
FAM174B	3.896538	up	F3	7.040987	up
B9D1	3.900384	up	CECR1	7.070349	up
MARCKSL1	3.90271	up	CPZ	7.084812	up
C1R	3.904908	up	HIST1H2BN	7.102291	up
RGP1	3.909194	up	CCK	7.166775	up
IFT80	3.913821	up	HSPC159	7.18218	up
MYO19	3.925459	up	TPPP3	7.255092	up
ENHO	3.92661	up	FBLN7	7.269387	up
COBL	3.927865	up	DEGS2	7.325464	up
LOC787788	3.937935	up	NFKBIA	7.335706	up
TOP1	3.94752	up	OXT	7.382643	up
SLC41A3	3.953745	up	JUN	7.484951	up
GPR56	3.96527	up	PARD6B	7.575008	up
UBAP1	3.972372	up	IRF1	7.692354	up
TCF7	3.980768	up	TMEM49	7.749526	up
DUSP1	3.984211	up	CSRNP1	7.806801	up
AQP4	3.984848	up	SF3B3	7.878956	up
PDLIM7	3.999578	up	TPPP3	7.889803	up
INHBA	4.003334	up	ELF1	7.897074	up
SUPT3H	4.016495	up	HSPA1A	7.914533	up
C1S	4.03461	up	ZFP36	7.924141	up
FOXL2	4.037437	up	C28H10ORF10	7.985926	up
CFB	4.038267	up	TMEM158	8.056785	up
LDOC1	4.050761	up	CCL5	8.094933	up
TNFRSF18	4.055958	up	TMEM49	8.124417	up
FNDC5	4.056771	up	ANKRD37	8.155333	up
ITGA7	4.065326	up	IL6	13.90824	up
CITED2	4.074863	up	HSPA6	14.39829	up
LOC618617	4.076769	up	NFIL3	14.71455	up
PFAS	4.08242	up	LOC790889	14.87002	up
CCNI	4.090396	up	IGFBP3	14.95146	up
FAM174B	4.097991	up	MT3	15.10529	up
CAMK1D	4.104024	up	CCL5	15.24592	up
NOV	4.118534	up	PLAT	15.63222	up
HIST1H1D	4.119286	up	NFIL3	15.63792	up
DLK1	4.126021	up	MT3	15.91723	up
CSNK1E	4.131059	up	CXCR7	16.1135	up
EVL	4.132863	up	CCL5	16.22842	up
GGT7	4.13391	up	MMP3	18.71563	up

Gene	FC	Regulation	Gene	FC	Regulation
NPDC1	4.134587	up	PIM1	18.72436	up
NOS2	4.137818	up	MMP3	19.93427	up
VNN1	4.142443	up	NOS2	21.78343	up
CPXM1	4.143405	up	IER3	21.81434	up
BAMBI	4.145873	up	IER3	22.12448	up
RCN1	4.158174	up	MMP3	22.7386	up
WAC	4.165419	up	MMP3	24.5752	up
CD40	4.173619	up	DRD1	29.05235	up
ARRDC2	4.182496	up	MMP1	34.83856	up
ZYG11B	4.188269	up	CSF3	51.37992	up
NOMO2	4.516851	up	MMP1	97.79984	up
ZFP36L1	4.520244	up	MMP1	104.4976	up
CMTM8	4.521695	up	FABP4	82.27321	down
RCN1	4.541266	up	LOC527068	17.42143	down
MUSTN1	4.551707	up	AKR1C4	9.713958	down
SMOC2	4.561538	up	C28H10ORF116	8.687338	down
LBP	4.57437	up	ID1	8.5725	down
VPREB3	4.588874	up	C29H11orf54	7.879276	down
CASK	4.60929	up	LYRM7	7.264526	down
LOC531776	4.615991	up	ACADM	7.052514	down
PCDH1	4.616793	up	FAIM	6.664464	down
RYBP	4.618319	up	LIG4	6.540285	down
EPAS1	4.62966	up	CETN3	6.322228	down
CITED2	4.629825	up	LOC519309	6.302485	down
TMEM98	4.636385	up	GTF2H2	6.264545	down
MAML3	4.639368	up	LY96	6.248935	down
MEG3	4.643378	up	PUS10	6.221768	down
DPF1	4.646753	up	CCDC90B	6.197324	down
TUBA1C	4.646847	up	PPIL5	6.150221	down
OSGIN1	4.65273	up	CDC25A	6.135601	down
HEXA	4.66391	up	CCBL2	6.053514	down
ID2	4.671534	up	ACOT13	5.892866	down
ACTL6B	4.672018	up	CRYZL1	5.864327	down
S1PR5	4.68331	up	ACADM	5.690349	down
TCP11	4.686401	up	COX2	5.621278	down
C1orf35	4.700328	up	ZNF570	5.470599	down
AHSG	4.704005	up	NLK	5.445201	down
CHI3L1	4.70421	up	SLC30A6	5.346192	down
SOCS1	4.707557	up	PIN4	5.282741	down
PRMT8	4.711311	up	MGC140340	5.227598	down
NUAK2	4.753817	up	HDC	5.215012	down
ZNF667	4.75695	up	CISD1	5.212131	down
OTUD1	4.772456	up	FGL2	5.201345	down
COL9A2	4.772885	up	DUSP19	5.183243	down
E2F4	4.776411	up	ACADM	5.164629	down
ALOX12B	4.805715	up	TTC35	5.159855	down
HAGHL	4.827222	up	ERGIC2	5.132423	down
AHSG	4.828063	up	SCP2	5.120106	down
LECT1	4.885042	up	CISD1	5.018009	down

Gene	FC	Regulation	Gene	FC	Regulation
GALNT13	4.89353	up	PAAF1	4.950032	down
CPXM1	4.908038	up	COL1A1	4.917915	down
THBS1	4.929988	up	HIBCH	4.888956	down
HOMER2	4.93372	up	LOC617365	4.861082	down
LOC786034	4.938739	up	ZNF45	4.843883	down
EPHB2	4.947095	up	TERF1	4.785919	down
NEUROG1	4.948686	up	MANF	4.773417	down
RCN1	4.956459	up	ALDH3B1	4.758535	down
SLC5A5	4.956598	up	HOPX	4.739635	down
OR4N5	4.959062	up	GPR89	4.734633	down
CNKSR1	4.961392	up	FAM33A	4.702982	down
C1S	4.970248	up	C9H6ORF203	4.673188	down
SYT5	5.671103	up	LOC790576	4.670548	down
INTS5	5.683684	up	FAM55C	4.657504	down
ARRDC2	5.684059	up	PDSS2	3.989857	down
RALGDS	5.738509	up	MON1A	3.989083	down
TAP1	5.742827	up	MRPS14	3.988718	down
MRC2	5.749599	up	JKAMP	3.983036	down
PDK4	5.768647	up	HSBP1	3.958594	down
DYRK3	5.772271	up	NDUFAF2	3.958105	down
NFKBIA	5.792005	up	C23H6orf129	3.957848	down
LOC100139238	5.800545	up	COPB2	3.946307	down
CTSC	5.804622	up	SNAP23	3.94504	down
LTBP3	5.832209	up	SEC22A	3.944591	down
LRRC32	5.840722	up	TAF12	3.929604	down
DIO3	5.842606	up	HSBP1	3.925867	down
MSRA	5.846904	up	ACAT1	3.909122	down
RARRES2	5.857441	up	TMCO1	3.908627	down
CCK	5.859914	up	ASF1A	3.899491	down
TFPI2	5.860603	up	MGC148355	3.891568	down
BHLHE41	5.86465	up	PEX3	3.88103	down
PACSIN2	5.910937	up	SEC22B	3.857293	down
KRT19	5.948271	up	C10H14ORF169	3.856819	down
ABCA3	6.003136	up	ZNF679	3.849454	down
SERPINA3	6.004657	up	DECR1	3.847653	down
ZNF282	6.033475	up	ISOC2	3.844383	down
LOC526547	6.053746	up	INVS	3.842454	down
VIT	6.055173	up	LOC618360	3.827295	down
HIST2H2AC	6.060773	up	NUDT18	3.821577	down
CD79A	6.064678	up	NUDCD2	3.809828	down
LTBP3	6.070079	up	F2RL2	3.803153	down
SNN	6.074573	up	MR1	3.79494	down
MSRA	6.080097	up	LIN7C	3.777147	down
ADRB2	6.101583	up	DEM1	3.75459	down
CNGB1	6.113863	up	COL1A1	3.754417	down
FKBP2	6.128055	up	DLD	3.752985	down
IGFBP3	6.153936	up	EXOSC6	3.74926	down
SPRY1	6.159435	up	FKBP3	3.739859	down
TFPI2	6.163176	up	RMI2	3.737547	down

Gene	FC	Regulation	Gene	FC	Regulation
CSNK1E	6.192606	up	IFT80	3.727095	down
LOC784866	6.193188	up	C17H12ORF65	3.719115	down
C2CD4B	6.210067	up	COG4	3.699608	down
SIK1	6.210187	up	WDR89	3.697491	down
SOX14	6.234561	up	ECHDC1	3.697172	down
HKDC1	6.237713	up	IKBIP	3.697029	down
LOC789453	6.239328	up	TRIM38	3.693888	down
NFKBIA	6.256089	up	TAF12	3.690125	down
EAF1	6.303177	up	LOC790145	3.689718	down
CA2	6.350652	up	ALG8	3.68716	down
NPDC1	6.36291	up	ORC4	3.683722	down
C17H12orf43	6.375712	up	PTX3	3.677576	down
NFKBIA	6.376849	up	NQO1	3.664299	down
MYBPH	6.388492	up	WDR61	3.658443	down
THBS2	8.217781	up	ZNF212	3.648185	down
WC1.3	8.248548	up	SLC35B3	3.645502	down
HSPA1A	8.267817	up	RPAP3	3.348476	down
SLC18A1	8.329465	up	DNAJC19	3.336782	down
TRIB1	8.369038	up	BCAP29	3.332476	down
PABPN1	8.436981	up	MLF1IP	3.329613	down
ARIH1	8.469493	up	FASTKD2	3.327411	down
DOK5	8.470063	up	C8H9orf82	3.326499	down
ISG15	8.633556	up	DAD1	3.314407	down
CAMK2N2	8.646427	up	LOC509351	3.312666	down
PENK	8.702706	up	CCBL2	3.303083	down
CORO6	8.728603	up	M6PR	3.301267	down
COCH	8.931233	up	CNPY2	3.293272	down
VIPR2	9.0446	up	S100B	3.291978	down
TXNIP	9.055558	up	NEDD8	3.285314	down
BHLHE40	9.059837	up	ORC4	3.279729	down
DUSP2	9.085271	up	SPIN2	3.278208	down
F3	9.112331	up	IGFBP6	3.269127	down
MGC128424	9.394942	up	MOBKL2C	3.266382	down
DNAJB1	9.412842	up	COMMD5	3.265207	down
GPR143	9.441118	up	SEC24A	3.259661	down
IGFBP3	9.745452	up	USP3	3.25718	down
NFIL3	9.751995	up	MEGF10	3.248936	down
ABCC5	9.770067	up	TXN	3.248487	down
SLC6A12	10.05488	up	SEC24A	3.247972	down
HSPA1A	10.18999	up	PDCD10	3.235048	down
CD83	10.21416	up	SCFD1	3.23246	down
JUN	10.31015	up	C19H17orf59	3.229274	down
PPP1R15A	10.45808	up	NDUFA12	3.227958	down
ANKRD37	10.53529	up	VRK1	3.227353	down
FOXC2	10.56122	up	RP2	3.22672	down
PIM1	10.79375	up	SRBD1	3.223807	down
LOC781225	10.82594	up	DHRS7B	3.22126	down
KLF6	11.10566	up	HIBCH	3.218236	down
HIST3H2A	11.25192	up	OSTM1	3.211916	down

Gene	FC	Regulation	Gene	FC	Regulation
ATF3	11.5361	up	MAGED2	3.203118	down
SIRPB1	11.95384	up	NUP37	3.202151	down
EDN2	11.99311	up	ANXA4	3.197249	down
NR1D1	12.19705	up	ZNF583	3.197115	down
TTLL1	12.25681	up	LOC507750	3.192091	down
IL6	12.29486	up	AP3M1	3.183748	down
TMEM201	12.40948	up	C29H11orf54	3.182208	down
TTLL1	12.59335	up	HSDL2	3.181174	down
CXCR7	12.68297	up	NUP35	3.174443	down
ABCA3	12.72033	up	TM4SF18	3.160268	down
LOC539246	13.12961	up	NSUN3	3.159656	down
HIST3H2A	13.13226	up	GOSR2	3.159473	down
PPP1R15A	13.21102	up	ANAPC13	3.156304	down
CHAD	13.41516	up	OSGEPL1	3.143615	down
HHAT	13.78577	up	BNIP1	3.142914	down
UNC5B	13.89304	up	NEDD8	3.138902	down
TNIP2	3.005433	up	MTRF1	3.132261	down
FBXW11	3.005953	up	FMC1	3.131933	down
THRAP3	3.00726	up	PIGV	4.656295	down
NUCB1	3.013866	up	NUDT12	4.641157	down
ARG2	3.025374	up	C24H18orf19	4.610604	down
BGN	3.035267	up	FAM33A	4.590575	down
CLU	3.050675	up	TTC35	4.5864	down
LOC514257	3.057187	up	DIXDC1	4.583977	down
TMEM2	3.059981	up	IFT81	4.56812	down
MMP2	3.065241	up	ELP3	4.552411	down
CELF1	3.069309	up	ZFYVE19	4.548154	down
ACOT11	3.075295	up	GEMIN6	4.537964	down
PMP22	3.08949	up	UGP2	4.500171	down
PTGDS	3.099971	up	LOC100139010	4.481614	down
CTU1	3.114043	up	BDH2	4.437852	down
OSBPL10	3.527234	up	FAM33A	4.411434	down
FES	3.533298	up	GOSR1	4.411247	down
ZFP36L1	3.53613	up	HOPX	4.404112	down
ACOT11	3.547875	up	IFT74	4.401402	down
PELI1	3.550364	up	LOC790145	4.397867	down
LOC100139804	3.557612	up	MRPL1	4.379288	down
MT1A	3.564599	up	RPS19BP1	4.358896	down
IFT80	3.568703	up	ORC5	4.358825	down
TMEM37	3.569978	up	TMEM69	4.358188	down
SEMA4A	3.57003	up	CDC26	4.324949	down
DYRK1B	3.574329	up	NSUN3	4.296114	down
NECAP1	3.576426	up	MED7	4.292007	down
TRIB2	3.577234	up	XRCC4	4.257215	down
COL9A2	3.583751	up	ATG7	4.251924	down
ZFP36L1	3.586739	up	CCBL2	4.251091	down
CHI3L1	3.59329	up	LRRC8E	4.246186	down
FBXL2	3.601454	up	DAD1	4.233543	down
PID1	3.603112	up	MRPL13	4.21195	down

Gene	FC	Regulation	Gene	FC	Regulation
AEBP1	3.605375	up	SMARCA4	4.192433	down
CRTC2	3.632599	up	CHCHD7	4.183427	down
LOC521525	3.633227	up	C23H6ORF47	4.166932	down
EVL	3.642021	up	C8H9ORF85	4.148521	down
MXRA8	3.647827	up	ACTR6	4.146216	down
KCNJ9	3.651811	up	LOC790576	4.142726	down
MT2A	3.660033	up	NPM3	4.141362	down
SDC4	3.668364	up	NDUFC1	4.135549	down
IFT80	3.676864	up	ACAT1	4.132094	down
TNFRSF6B	3.689817	up	DECR1	4.091567	down
C20orf111	3.690375	up	ANXA1	4.090646	down
ECRG4	3.694305	up	SERPINI1	4.089996	down
TGM2	3.701644	up	PPP2R3C	4.079665	down
TMEM55B	3.701872	up	PTX3	4.07661	down
SRSF1	3.70805	up	TXNDC9	4.075418	down
RASSF8	3.724096	up	C23H6orf129	4.069323	down
SDC4	3.739374	up	MED7	4.054468	down
BGN	3.741939	up	ZUFSP	4.0383	down
SHISA2	3.747012	up	CUL7	4.033473	down
LOC785034	3.774395	up	ADAL	4.003998	down
C2CD4B	3.794694	up	VCAM1	3.634909	down
NOXA1	3.798554	up	BDH2	3.622305	down
PITPNM1	3.817486	up	NUDCD1	3.618385	down
GAL	3.820223	up	LNPEP	3.600666	down
MGC152278	3.823275	up	MGC157372	3.599697	down
LOC514257	3.8261	up	CCDC56	3.597535	down
CERCAM	3.828667	up	CETN3	3.591166	down
CKB	3.828687	up	DLD	3.58827	down
TMEM132A	3.839545	up	LSM3	3.585655	down
SERPINE2	3.84178	up	COL1A1	3.582285	down
PAOX	3.848381	up	ERGIC2	3.581946	down
LTBP3	3.866936	up	TTC5	3.581138	down
GPRC5A	3.887951	up	BDH2	3.576943	down
PGF	4.194395	up	NPM3	3.57642	down
HSPA1A	4.198737	up	TMEM128	3.572492	down
MGC127492	4.201395	up	C16H1orf93	3.568938	down
ACTC1	4.208372	up	PDHX	3.565717	down
PDK4	4.210336	up	DIXDC1	3.554141	down
LOC618633	4.212641	up	ZNF189	3.55031	down
STRC	4.215305	up	TPRKB	3.540622	down
PAOX	4.216295	up	MRPL47	3.537328	down
SERPING1	4.229056	up	USO1	3.52868	down
CAMK1D	4.23078	up	CCDC86	3.521197	down
LECT1	4.236096	up	WDR61	3.513664	down
LGALS9	4.236411	up	C16H1orf156	3.507061	down
PAK4	4.241145	up	C9H6ORF203	3.507011	down
YOD1	4.245889	up	CNPY2	3.506887	down
ANKRD9	4.251147	up	SEC62	3.490794	down
TLE1	4.254692	up	JKAMP	3.483456	down

Gene	FC	Regulation	Gene	FC	Regulation
PREX1	4.254959	up	TXNDC9	3.481243	down
EXOC3L2	4.259448	up	ITGB1BP1	3.474314	down
THBS3	4.260544	up	PSMA4	3.470595	down
C1S	4.27444	up	RWDD2A	3.426783	down
CEBPB	4.27594	up	NUP37	3.42411	down
MPPED2	4.276982	up	GIN1	3.418056	down
ELF3	4.287345	up	GPX8	3.415606	down
SMOC2	4.294398	up	HRSP12	3.404223	down
CKB	4.295063	up	ZNF521	3.394173	down
ID2	4.307009	up	COMMD6	3.392332	down
LOC787315	4.312689	up	PPWD1	3.386303	down
CFB	4.316038	up	TM2D1	3.383726	down
SOCS2	4.319769	up	ZNF187	3.380747	down
RMND5A	4.326815	up	JKAMP	3.378612	down
MFAP2	4.334281	up	DCTN5	3.378608	down
SOCS1	4.352686	up	CPNE8	3.367283	down
NUAK2	4.362635	up	FARSB	3.366696	down
LOC539596	4.366135	up	MRPL22	3.361334	down
ZFP36L1	4.382076	up	VCAM1	3.359486	down
AHSG	4.389936	up	INSIG2	3.355151	down
NCF1	4.403068	up	C16H1orf156	3.354657	down
RAB15	4.41229	up	NDUFS4	3.352199	down
WWTR1	4.412438	up	CCDC56	3.126912	down
ACTC1	4.412507	up	NIF3L1	3.124021	down
GADD45B	4.420004	up	LYPLAL1	3.118687	down
FOXJ1	4.423711	up	RPL7L1	3.116196	down
CPXM2	4.439729	up	ARV1	3.114181	down
RHOB	4.448938	up	WRN	3.109585	down
COL2A1	4.471056	up	ISOC2	3.103268	down
DDX3X	4.473314	up	ARV1	3.103001	down
IFI6	4.477788	up	POT1	3.100881	down
NPPC	4.488915	up	NIPSNAP1	3.093173	down
PMEPA1	4.502809	up	OSTF1	3.081111	down
PPP6R3	4.504335	up	CCDC132	3.077971	down
PI3	4.515165	up	LINS	3.077036	down
DUSP10	4.995005	up	ZNF830	3.074852	down
COL11A2	5.007313	up	ACTR2	3.072552	down
EPYC	5.00984	up	NDUFA2	3.072021	down
ACSM2A	5.021521	up	CCL25	3.071394	down
HIST1H1D	5.032537	up	ALG10	3.070998	down
DPF1	5.076459	up	ALG11	3.066288	down
LOC616942	5.079365	up	AASDH	3.05837	down
CD40	5.089731	up	GGPS1	3.056568	down
CLK3	5.124697	up	CCDC90B	3.056387	down
CFB	5.142702	up	ZNF323	3.053176	down
NOV	5.150844	up	NFU1	3.051242	down
LOC614284	5.157355	up	TRMT5	3.050756	down
FUBP1	5.175399	up	C17H12ORF65	3.045974	down
TIMP3	5.176029	up	MED6	3.045792	down

Gene	FC	Regulation	Gene	FC	Regulation
BHLHE40	5.177926	up	C11H2ORF7	3.043979	down
PABPN1	5.187668	up	GTF2H3	3.041368	down
OLFM1	5.195365	up	COL16A1	3.040849	down
PPP2CA	5.205952	up	PAAF1	3.031732	down
PAOX	5.223555	up	ZNF266	3.017759	down
C3	5.22476	up	COQ7	3.011555	down
COL18A1	5.254467	up	ISOC2	3.004399	down
PPM1M	5.310961	up	C12H13orf27	3.003012	down
FOSB	5.322266	up	ORMDL2	3.0002	down

Appendix 3: HPLC for pyridinoline quantification

General methodology

An HPLC protocol was developed to quantify pyridinoline and pentosidine crosslinks based on a protocol reported previsouly.[216] Samples were digested in 200 µL of 6N HCl at 100°C for 20h on a heating block and then using a vacuum concentrator. For native cartilage samples with masses of approximately 20mg, samples were re-suspended in 100µL of an aqueous solution containing 10 nmol pyridoxine/mL and 2.4 µmol homoarginine/mL and then diluted fivefold with an aqueous solution of 0.5% HFBA acetonitrile in 10% acetonitrile. 10 µL of each sample was injected into the reverse phase column and eluted using a solvent profile described previously.[216] To use less tissue or to assay samples with lower crosslink densities, it is possible to use larger injection volumes and/or smaller resuspension volumes.

Pyridinoline detection

Initially, various emission wavelengths were scanned to ensure that pyridinoline signal was maximized, showing that maximum emission at approximately 400 nm. Both immature and mature bovine cartilage was used as positive controls because they are known to produce crosslinks.

Pyridinoline eluted between 5-10 minutes, yielding chromatograms as shown in Fig. A3-2. To validate the pyridinoline peak, samples were spike and areas were computed (Fig. A3-3), showing that the target peak was indeed

pyridinoline. Variation in elution was probably due to differences in HFBA and/or HCl concentrations. Based on the work of Bank *et. al*,[216] it is known that even 0.01% variation in HFBA concentration can alter elution profiles. This shows the importance of careful solvent preparation for this method.

Pentosidine detection

Pentosidine detection could be employed to quantify crosslinks induced by ribose treatment or to evaluate the formation of advanced glycation end products in native tissue. A pentosidine standard was also purchased and assayed based on the ability of the Banks protocol to detect pyridinoline and pentosidine in a single HPLC run. Standards were eluting at 20 minutes. Because we primarily tested immature tissue, pentosidine was not assessed in most samples. However, uture work with different exogenous stimuli or different native tissue sources could benefit from pentosidine quantification.

Figure A3-1: Emission wavelength spectrum for pyridinoline detection.

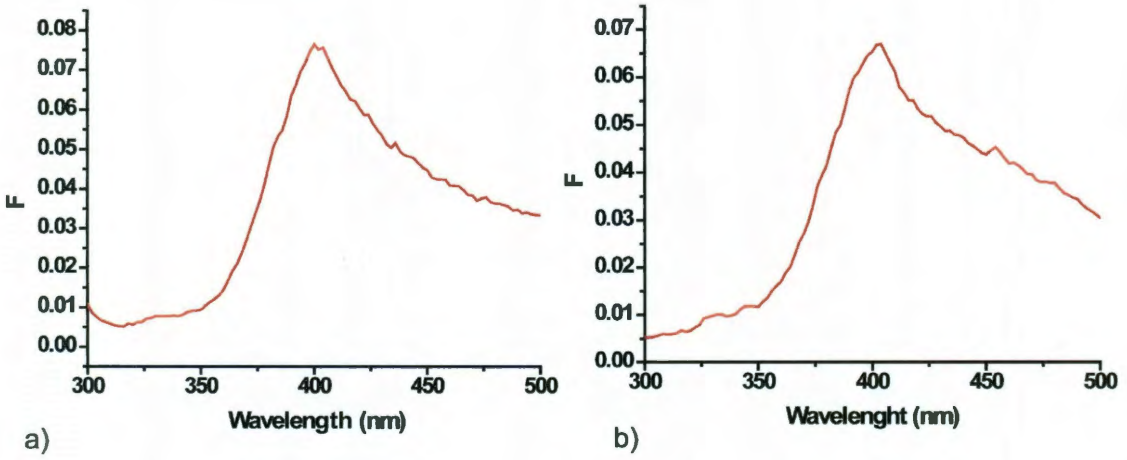

(a) Emission spectrum of mature bovine cartilage based on 295 nm excitation. (b) Emission spectrum of immature bovine cartilage based on 295 nm excitation. The y-axis is fluorescence intensity based on HPLC elution. Both immature and mature bovine cartilage exhibited maximum emission at approximately 400 nm, so this emission wavelength was carried forward.

Figure A3-2: Representative chromatogram of native tissue

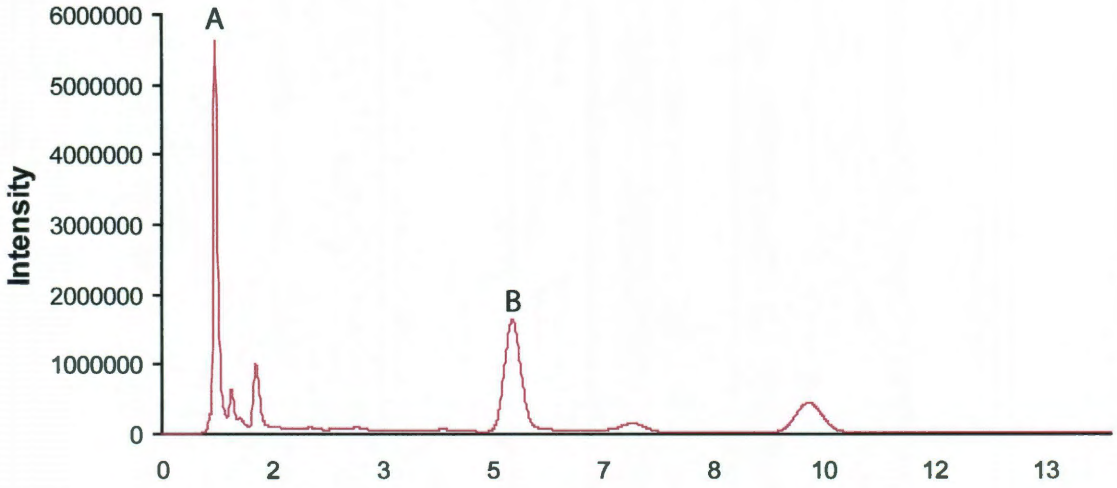

Species with low binding affinities typically elute within the first 1-2 minutes. The internal standard (pyridoxine, marked as A) also eluted during the first several minutes. Pyridinoline (peak B) eluted at 5-10 minutes; its elution time could vary depending on solvent composition. The peak shows pyridinoline from articular cartilage.

Figure A3-3: Validation of pyridinoline standard

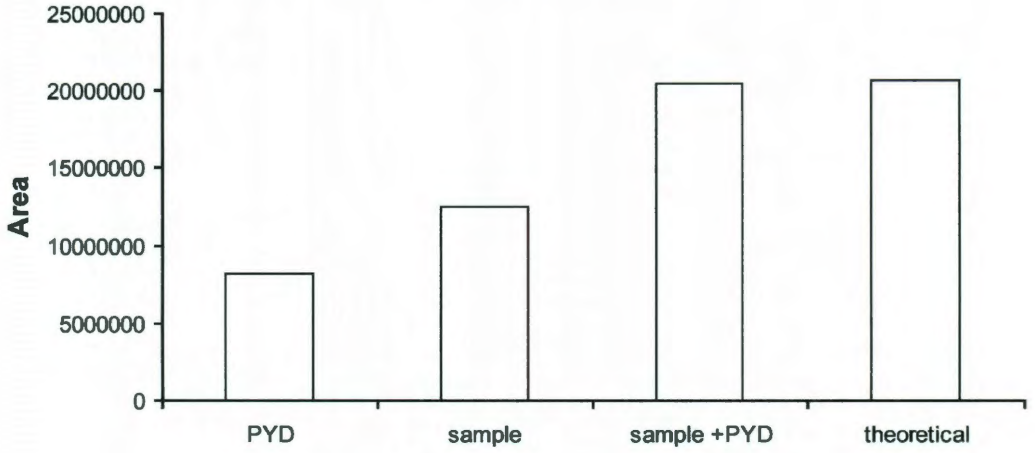

To validate the observed peaks, a sample was spiked with a standard. The construct area, pyridinoline (PYD) area, spiked sample area are shown. The theoretical area sum (construct area + PYD area) corresponds with the area of the spiked sample, suggesting that the samples contained pyridinoline.

Figure A3-4: Pentosidine detection with HPLC

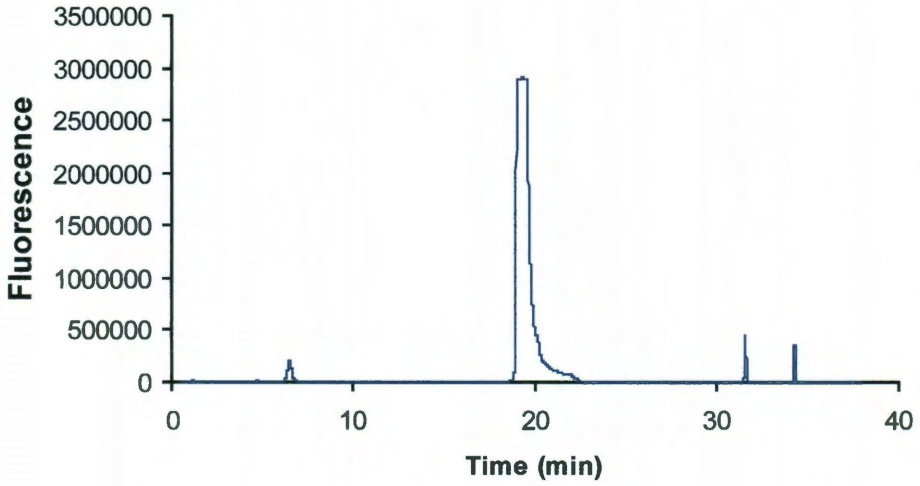

In addition detecting pyridinoline, the HPLC protocol is capable of quantifying the amount of pentosidine. This crosslink elutes later, at approximately 20 min, so there is not overlap with any pyridinoline peaks in the same run. Thus, pentosidine and pyridinoline can be detected during a single HPLC run.

Appendix 4: Nonlinear optical analysis of patella

Introduction

Cartilage has a zonal collagen organization that has been characterized for the different layers of cartilage. The superficial zone, which is closest to the articulating surface, has collagen aligned parallel to the surface. Collagen abundance is also highest in the superficial zone.[284] The deep zone, which is near the calcified bone, has fibrils oriented perpendicularly to the surface. The middle zone of cartilage has intermediate organization of fibrils rather than exhibiting dominant parallel or perpendicular alignment.

Collagen organization has practical importance because it influences tissue mechanics, which are crucial for normal cartilage function. For instance, split-line orientation has been shown to dictate tensile properties.[128,155] The effects of orientation can be dramatic: the tensile modulus is 42.2 MPa when tested parallel to the collagen orientation but only 15.6 MPa when tested perpendicularly.[2] One of the major challenges in biomechanics has been rigorously quantifying the orientation, which is often assessed using indirect methods such as split lines. Quantifying collagen organization could enable better elucidation of structure-function relationships and provide a method for evaluating the quality of tissue engineered cartilage.

Various methods have been employed to quantify collagen organization. Polarized light microscopy can be used to observe organization because collagen is birefringent. In general, highly oriented fibers will increase the phase difference between the orthogonal components of the light.[379] Diffusion tensor imaging (DTI) has also been used to examine orientation.[293,381-383] DTI is based on quantifying water molecule movement, which can be quantified using DTI. Collagen anisotropy can alter water movement such that DTI can differentiate matrix organization.[293] Although polarized light microscopy is widely used and DTI is quantitative, a prevalent, quantitative technique has not yet emeraged.

SHG provides a uniquely specific method of examining collagen organization in tissues and has been extensively employed to study collagen in cartilage. Collagen organization was first studied using SHG analysis of the tendon[490] and various other tissues including fascia, cornea, and cartilage have been extensively characterized.[491,492] It has been shown that nonlinear optical properties of articular cartilage exhibit depth-dependence.[492] However, how SHG properties relate to biomechanical properties, which are crucial to cartilage function, has not been clearly delineated.

This study evaluated the relationships among biochemical, biomechanical, and nonlinear optical properties of patella cartilage. Different zones of immature and mature patella were examined to observe any potential effects of maturation. This work tested the hypotheses that 1) biochemical, biomechanical, and nonlinear optical properties vary depending on depth and 2) optical properties can be used to infer biochemical and biomechanical properties.

Methods

Tissue acquisition/sectioning

Full thickness cartilage was removed with a 4 mm biopsy punch from [region] immature and mature patella. Immature (4 week old) bovine patellae were purchased from Research 87. Mature bovine patellae, from steers approximately one year old, were acquired from the UC Davis Meat Lab. Immature patella samples were tested in three different zones (Fig. A4-1). Mature patella samples were tested in two different zones due to the reduced thickness of cartilage. Split lines were employed to assess collagen orientation prior to removing.

Biochemistry

Following freezing -20°C, each sample was lyophilized to enable dry weight determination. Each sample was digested using papain for 18h.[187] To assess collagen abundances, samples were assayed using a chloramine-T hydroxyproline assay.[117]

Tensile testing

Prior to conducting tensile tests, samples were cut into dog-bone shapes and glued to paper tabs for gripping.[122] ImageJ was used to examine the width, gauge length, and thickness of samples. All tensile tests were conducted to failure by pulling at a strain rate of 1% of the gauge length per second. Tensile tests were conducted on a materials testing system (Instron Model 5565). The

maximum stress was reported as the ultimate tensile strength (UTS). The Young's modulus (E_Y) was determined by computing the slope of the linear region of the stress-strain curves.

SHG data collection

In order to obtain scans from a similar region of each section, a punch was used to remove a circular section from an opaque cloth. The hole was centered over the circular section, so that no samples edges were included in the scan. Samples varied considerably in SHG intensity. Initial scans were performed on a 500 x 500 μm region with 5 μm steps to ensure that a representative region of the tissue was being examined. The final scan was performed on a 200 x 200 μm region using 0.5 μm steps. The optical set up and method for data acquisition has been described in detail in earlier papers. An algorithm for assessing disorder in fibrillar collagens has been described in detail in an earlier paper: disorder is expressed as the percent of maximum disorder possible. The original algorithm has since been extended; several additional methods are now included for analyzing parameters potentially related to structural disorder: these include calculation of local director angles, calculation deviation from the director, as well as parameters related to liquid crystal structure. In addition, the distribution of peak angles were assessed for the presence of multiple Gaussian distributions, using probability density plots. Finally, the size of the largest fibril within the scan region was determined during the analysis of disorder: a "fibril" was defined by the presence of at least three lines of pixels varying less than 5% in orientation

with no breaks. Although this procedure may underestimate the true size of fibrils since they are known to be interwoven, this calculation provides a uniquely useful way of assessing another aspect of cartilage structure.

Results

Tensile properties and collagen content varied significantly depending on zone. The UTS was 12.2±3.7 and 21.8±6.5 MPa for the lower and upper zones, respectively. Similarly, the tensile stiffness was 21.8±6.5 and 46.5±20.7 MPa for the lower and upper zones, respectively. Collagen content was highest in the upper zone and lowest in the deeper zone, exhibiting respective values of 12.8±2.2% and 7.5±0.6% for the lower and upper zones, respectively. Col/dw was not significantly different among the various zones. Similarly, both tensile strength and stiffness were highest in the upper zone and lowest in the lower zone.

For SHG, at least three scans were performed on each sample. The standard disorder parameter was based on a nearest-neighbor analysis designed for application to fibrillar collagen and has been described in detail previously.[493] The alternative disorder parameter was based on the degree to which a given pixel deviates from the neighborhood director with respect to orientation, and was expressed in degrees. The size of the ordered area within the scanned region was defined as the length over which at least 3 parallel lines of pixels extended with less than 10% change in orientation.

SHG scans showed clear differences among zones as summarized in Figure 4. Quiver diagrams of fibril orientation (Fig. A4-4A, Fig. A4-4C) were represented in histograms of the fibril orientation distribution (Fig. A4-4B, Fig. A4-4D). Interestingly, the histograms revealed 2 distinct organization populations in the upper zone. In contrast, the lower zone did not display preferential organization. This suggested that the upper zone had two ordered populations whereas the deeper zone did not exhibit ordered regions.

Analyses of ordered region size and disorder percentage were examined to observe relationships with biomechanical properties. The ordered region size was generally greater in the upper zone, which had an area size almost 5 times greater than the lower zone (Fig. A4-5A). Ordered region size was correlated with both tensile stiffness and tensile strength (Fig. A4-5C, A4-5D). Although the disorder parameter exhibited a trend that was inversely related to biomechanical properties (Fig. 4-5B), the correlation were not significant. The disorder parameter was, however, significantly correlated with zone, with the highest level of disorder associated with lower zone and the least disorder in upper zone. Correlation analysis of all the parameters confirms that the disordered region size was most strongly correlated with Young's Modulus and UTS.

Discussion

This study confirmed the hypothesis that SHG can be used to infer functional properties of cartilage. The core novelty of this work is the use of SHG to quantitatively assess biomechanical properties of the patella.

The finding that the disordered region size was strongly correlated with Young's Modulus and UTS is particularly exciting because it provides a new method of assessing mechanical properties. Because biomechanical tests are destructive, time-consuming, and require special equipment, developing an SHG methodology could be enormously useful. The core question is what exact matrix components or organization SHG is measuring to infer mechanical properties. Further work will be carried out to understand the basis of SHG differences in the patella, which could be used to further understand the collagen architectures and develop SHG as a novel testing modality.

The next step towards understanding the basis of the SHG results will be differentiating the effects of collagen abundance and collagen organization. Although biochemistry assays can be employed to quantify the amount of collagen, it will also be necessary to quantify the collagen organization. SEM or TEM could potentially be employed to more rigorously compare collagen orientation and SHG parameters. Conducting SEM in conjunction with collagen quantification will develop the SHG technology platform.

One of they key limitations of this work was the lack on knowledge concerning the collagen architecture of the immature patella. Attempts to discern split lines were unsuccessful, suggesting that the collagen may not yet be oriented in the superficial zone. Future work with mature patella will help confirm any results seen in this experiment and also provide a system with more well-document collagen organization. Additionally, the mature samples will provide

information regarding how biomechanical, optical, and biochemical properties change during maturation.

Figure A4-1: Patella sectioning schematic

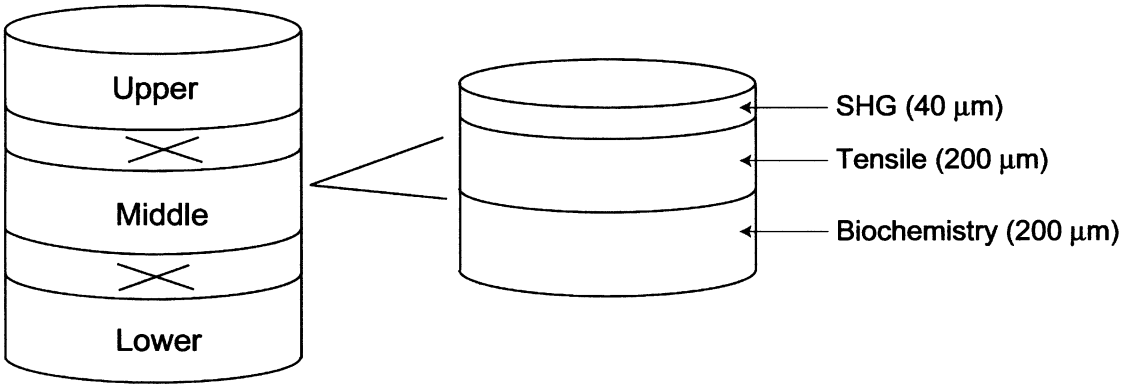

Patella samples were removed with biopsy punches and then sectioned parallel to the surface to evaluate three different zones. From each zone, a 40 μm slice was placed on a slide and evaluated using SHG. 200 μm slices were used for biochemistry and mechanical assays.

Figure A4-2: Zonal variation of tensile stiffness and tensile strength.

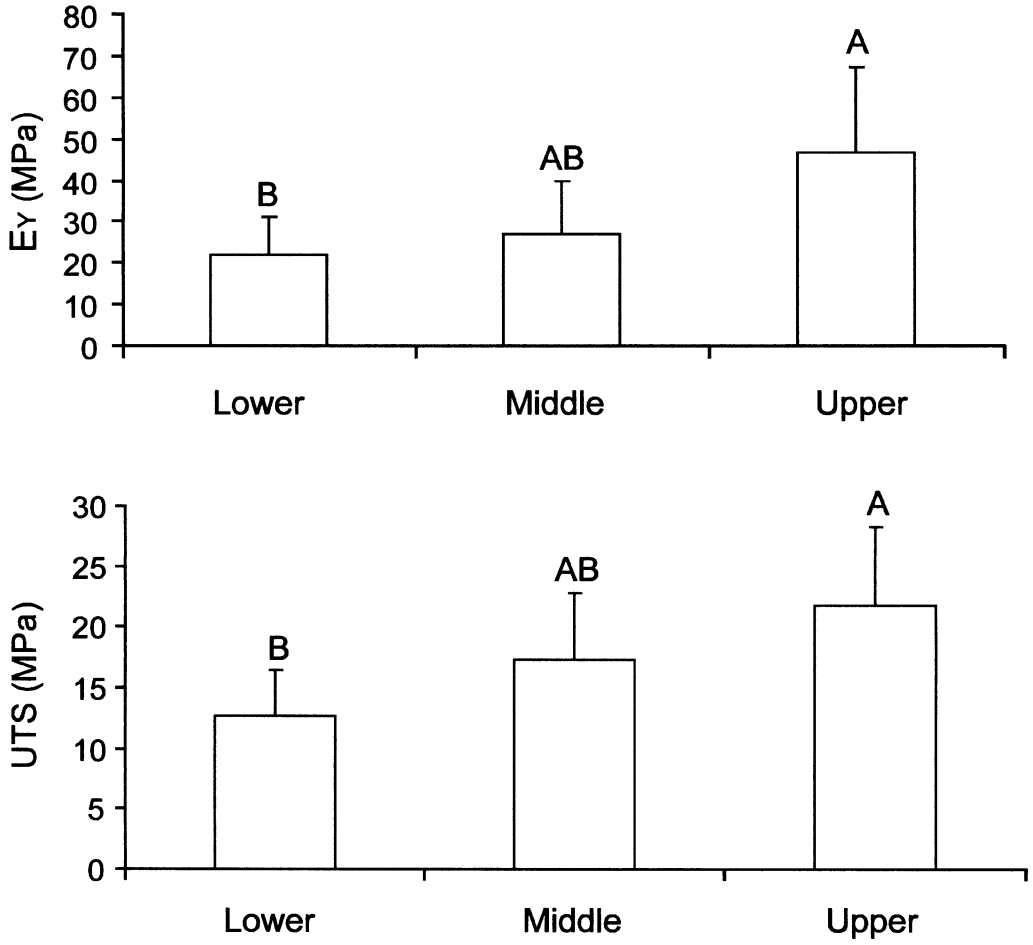

Tensile stiffness and strength were highest for the upper zone and lowest for the lower zone. Bars labeled with different letters exhibit significant differences ($p < 0.05$).

Figure A4-3: Zonal variation of collagen content.

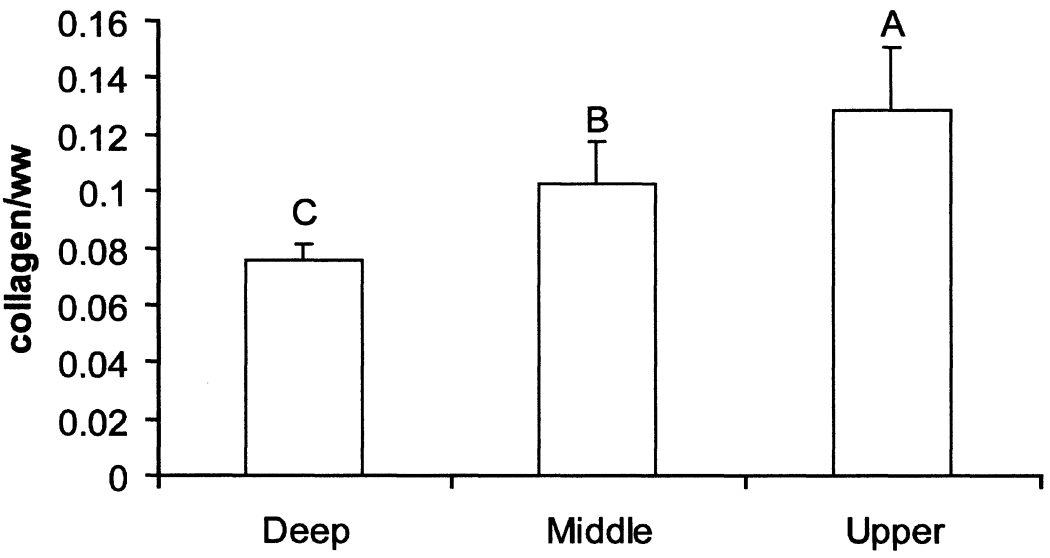

Collagen content was highest for the upper zone and lowest for the lower zone. The middle zone had intermediate collagen content. Bars labeled with different letters exhibit significant differences ($p < 0.05$).

Figure A4-4: SHG evaluation of upper and lower zones

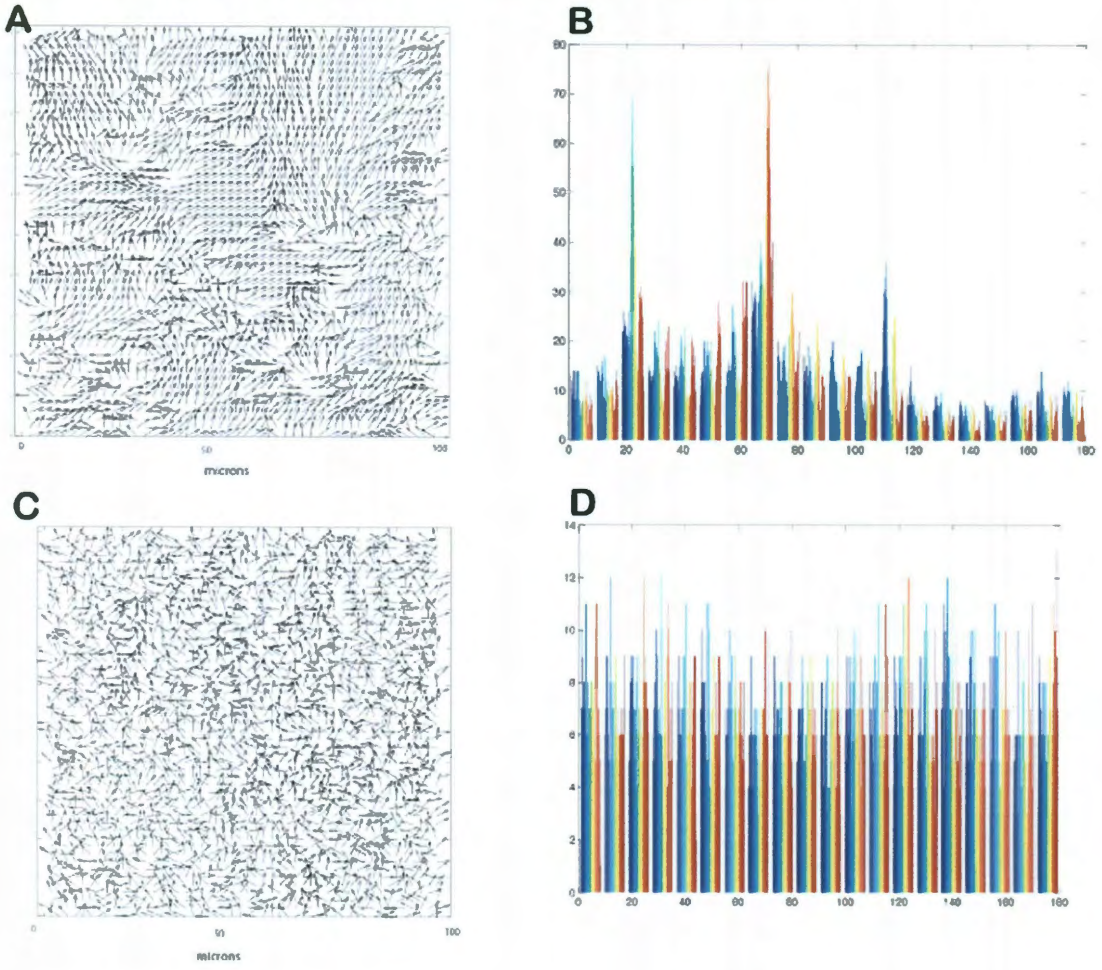

(A) Quiver map of collagen order in upper zone. (B) Histogram of counts for different orientation angles in upper zone illustrates two distinct populations around 20° and 70°. (C) Quiver map of collagen order in lower zone. (D) Histogram of counts for different orientation angles in lower zone illustrates lack of distinct populations.

Figure A4-5: Relationship between SHG parameters and mechanics

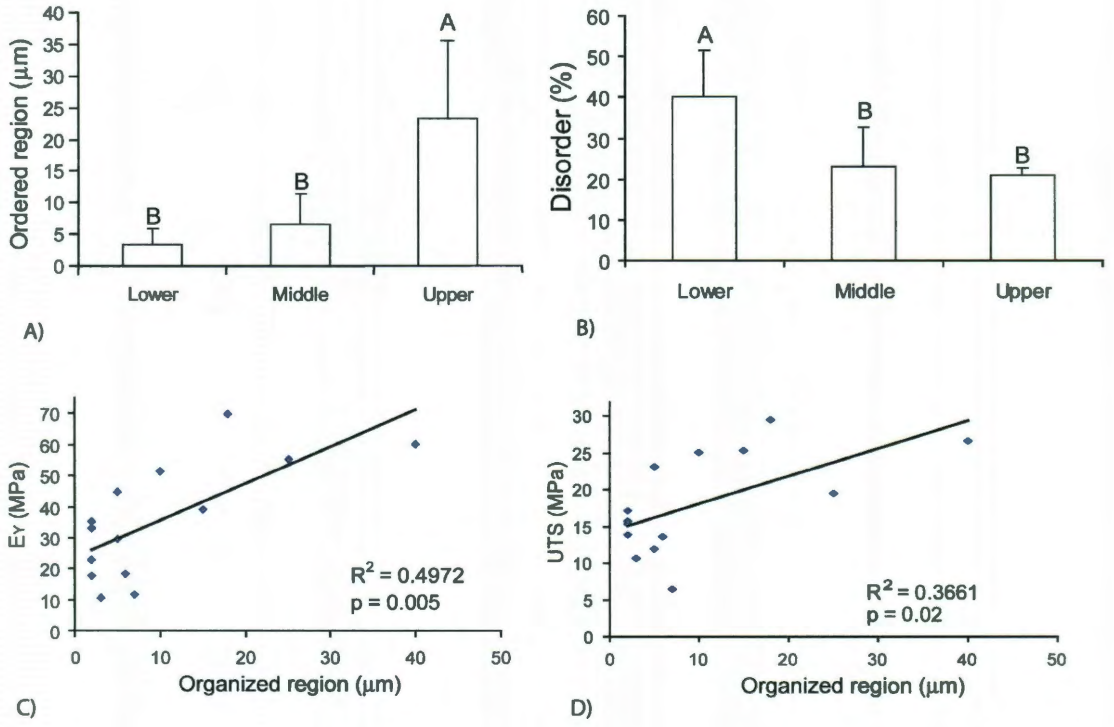

(A) Ordered region size of three zones. (B) Disorder quantification of three zones. (C) Significant correlation between the tensile stiffness and organized region size. (D) Significant correlation between the tensile stiffness and organized region size.